Network dynamics and origin of anastomosis, upper Columbia River, British Columbia, Canada

Network dynamics and origin of anastomosis, upper Columbia River, British Columbia, Canada

Tjalling de Haas

Student nr.: 3021378

August-March 2009/2010

Final version: 22-10-2010

MSc thesis Physical Geography

Faculty of Geosciences,

Universiteit Utrecht

Supervisor: Dr. M.G. Kleinhans (UU)

Preface and Acknowledgements

This thesis on network dynamics and the origin of anastomosis of the upper Columbia River was written for the Master of Science degree programme in Earth Sciences, direction Physical Geography at the Utrecht University. This thesis is written under supervision of Dr. Maarten G. Kleinhans.

The report covers a literature research, field research and a modelling research. The fieldwork is performed in the upper Columbia River, in the reach between Spillimacheen and Castledale, from August 17 to October 1, 2009. The fieldwork has been performed in cooperation with Eva Lavooi, who also performed the fieldwork as part of her MSc research. The objective of both the thesis of Eva Lavooi and mine was to solve questions about the origin of anastomosis of the upper Columbia River. Eva Lavooi investigated this by a geological reconstruction of the upper 8m of the valley-fill, whereas I addressed it with a process-based method.

I would like to thank Dr. Maarten G. Kleinhans for his help, time, enthusiasm and great discussions during the research. Eva Lavooi for her cooperation during the fieldwork and help during the further research. I would like to thank Dr. Bart Makaske and Wout van Dijk for their help and support during the fieldwork. Special thanks go out to Prof. Derald G. Smith, who picked us up from the airport, accommodated us in his house the first night, brought us to the fieldwork area and last but not least provided us with all equipment needed.

Finally I would like to thank Barb and Oley, who accommodated us for the entire fieldwork period in one of their great cabins. Barb and Oley took great care of both Eva Lavooi and me. They cooked us some Canadian specialties, introduced us to Canadian Football and Ice Hockey and they let us use the internet whenever we wanted.

Tjalling de Haas,

Utrecht, October 2010

Abstract

The upper Columbia River is an anastomosing river. Anastomosing rivers consist of a network of channels enclosing floodbasins. The factors that determine the configuration of river networks such as the upper Columbia River are unknown. Additionally the origin of anastomosing rivers is unclear. Two main theories exist on the origin of anastomosis; Nanson and Knighton (1996) state that it is hydraulically more efficient to transport flow and sediment in multiple channels instead of a single channel, for rivers that are unable to adjust their slope. Makaske (2001) states that frequent avulsion and/or slow abandonment of old channels leads to continuing coexistence of multiple channels. The Nanson and Knighton (1996) hypothesis on the origin of anastomosis implicates that anastomosis is an equilibrium channel pattern, whereas Makaske (2001) states that it is a disequilibrium channel pattern. The aim of this research was to explain the network dynamics and origin of anastomosis in the upper Columbia River.

Field measurements were performed in the upper Columbia River to collect model input and to test model concepts. A river network model was developed to address the factors that determine the configuration of river networks, and to test the current hypotheses on the origin of anastomosis.

The discharge distribution through a river network is mainly determined by the network topology. Additionally, the bifurcation (morpho)dynamics affect the discharge distribution through a river network. The bifurcation dynamics are determined by downstream slope differences between bifurcates, upstream bend effect and amount of downstream confluences and bifurcations.

When a constant Chézy roughness is assumed to represent bed roughness, it is more efficient to transport flow and sediment in multiple channels than in a single channel. When a constant Nikuradse roughness length is assumed to represent bed roughness, it is more efficient to transport flow and sediment in a single channel. The effect on network configuration is largest for the latter roughness assumption. Additionally, in natural rivers the constant Nikuradse roughness length assumption is more plausible since the wall friction is relatively large in small channels compared to large channels. Hence the Nanson and Knighton (1996) hypothesis on the origin of anastomosis does not hold for the upper Columbia River.

A network model is applied to a 21km reach of the upper Columbia River that is characterized by well developed anastomosis. The steepest part of this reach is characterized by the best developed anastomosis. Model results indicate that a sediment pulse of 150yr of on average 3 times the transport capacity is able to reproduce the bed slope of this steep reach. It follows that the Makaske (2001) hypothesis on the origin of anastomosis explains anastomosis in the upper Columbia River. Sediment pulses induce a high avulsion rate, and therefore cause the coexistence of multiple channels on the floodplain. In the absence of a new sediment pulse the river network will most likely evolve towards a single main channel again. Consequently anastomosis in the upper Columbia River is a disequilibrium

channel pattern. The cause of anastomosis in other anastomosing river systems might possibly also be a constant overload of sediment or a temporary sediment pulse.

Table of contents

Appendices

1. DVD with all data

1. Introduction

1.1. Problem definition and thesis objective

On many floodplains and river deltas, river channels split, join and avulse, meanwhile shaping the landscape, distributing drinking water, building fertile agricultural land and forming transportation pathways. Unfortunately, also flooding risk is distributed over river floodplains and deltas. Over time flooding has led to numerous disasters all over the globe. In order to minimize the risks of living and building in river floodplains and deltas the evolution of single river channels has been extensively investigated over the last decades.

Yet, many systems consist of a network of interconnected river channels. Discharge and sediment in these systems are divided by bifurcations, whereas flow and sediment of two upstream channels is combined to form a new channel at confluences. Bifurcations originate by avulsion, the formation of new channels on the floodplain. Bifurcations are the key to understand the evolution of river networks. In a natural situation, bifurcations do not experience a stable configuration. Bifurcations evolve over time, consequently the division of discharge and sediment evolves over time. It follows that due to evolving bifurcations river networks have a changing configuration over time. Since bifurcations are unstable, the question is raised whether river networks are stable, and thus occur as equilibrium channel pattern, or that river networks are disequilibrium channel patterns.

Wang et al. (1995) showed that the evolution of bifurcations can be modelled by simple 1D models, referred to as nodal point relations, which are computationally less expensive than more detailed 3D models. However, the nodal point relation of Wang et al. (1995) requires a separate calibration for each individual bifurcation. Bolla Pittaluga et al. (2003) obtained a process-based 1D model to predict the evolution of bifurcations. Their nodal point relation was especially derived for braided rivers. To overcome this problem, Kleinhans et al. (2008) added bend effects and variable width to the Bolla Pittaluga et al. (2003) nodal point relation, making it suitable for predicting the evolution of meandering river bifurcations and avulsions.

Since the 1D nodal point relations are computationally far less expensive than 3D models, it has become possible to model the evolution of complete river networks or deltas over millennia. No published attempt has ever been made to do so however. In this thesis a river network model is employed to explain the network dynamics and origin of anastomosis in the upper Columbia River.

The upper Columbia River in British Columbia, Canada, is a river with multiple channels on the floodplain (anastomosing river) with 2-6 parallel channels over a reach of approximately 100km. This river is confined by two mountain ranges, bounding a floodplain of only 1.5km in width. This makes this river accessible for fieldwork. Additionally, much previous research has been performed in this river, so that a large amount of data is already available on this river, e.g. Smith (1983), Locking

(1983), Makaske et al., (1998; 2002; 2009), Tabata and Hickin (2003) and Abbado et al. (2005). This previous research has raised multiple questions regarding the dynamics and origin of anastomosis in the upper Columbia River, which might be solved by analysis of field measurements and/or modelling. In summary, due to the recent development of 1D nodal point relations for the prediction of the flow and sediment division at bifurcations, it has become possible to model the evolution of river networks on geological timescales. Such a model is used to gain insight into the dynamics of the anastomosing upper Columbia River, and is used to investigate the origin of anastomosis. Hence the objective of this thesis is formulated as follows:

- To explain the network dynamics and origin of anastomosis of the upper Columbia River.

1.2. Methodology and thesis outline

This research is based on three components: a review (section 2), fieldwork (section 3) and modelling (section 4). These components are combined in order to gain insight into the dynamics and origin of river networks, in this case the anastomosing upper Columbia River (section 5).

The analysed literature comprises literature on the upper Columbia River, anastomosing rivers, avulsions, bifurcations and confluences.

The main objective of the fieldwork campaign was to test the model concepts, by measuring inlet step and area ratio at bifurcations, transverse bed slope in bends, residual channel fill and confluence scour depth. Additionally, input parameters for the network model were collected.

Modelling was performed in order to gain insight in the evolution of river networks, to address the dominant forcings, and to explore the necessary conditions for anastomosis in the upper Columbia River. The first part of the modelling consists of a sensitivity analysis performed on a bifurcation, in order to obtain information on the processes influencing flow and sediment division at bifurcations. In the second part, bifurcation equilibrium configurations are calculated for a range of Shields stresses, as done by Bertoldi and Tubino (2005) for experimental braided river bifurcations. The third part is an analysis of simple river networks, in order to address the dominant forcings for the division of flow and sediment in river networks. Finally, the complete network of the upper Columbia River is modelled, in order to test to what extent the river network model is able to reproduce the current discharge division over the channels of the investigated upper Columbia River reach, and to explain anastomosis in this reach.

2. Review

2.1. Introduction

In this section, the physical setting of the study site and earlier research that is performed at the study site is described (section 2.2). Secondly, anabranching rivers are reviewed (section 2.3), starting with their general classification (section 2.3.1), followed by a review on the origin of anastomosis (section 2.3.2) and a review on the dominant mechanism causing anastomosis according to Makaske (2001): avulsion (section 2.3.3).

Bifurcations are reviewed in section 2.4, starting with dynamics associated with river bifurcations (section 2.4.1), followed by field, experimental and modelling observations on river bifurcations in section 2.4.2. In section 2.4.3, nodal point relations, 1D relations that specify the division of flow and sediment at a bifurcation, are discussed. Finally, confluences are reviewed in section 2.5.

2.2. Study site

2.2.1. Physical setting

The upper Columbia River is located in British Columbia, Canada (figure 2.1). The Columbia River finds its origin in the Columbia Lake. Between the Columbia Lake and Radium Hot Springs, the river consists of a single channel. Between Radium Hot Springs and Golden an anastomosed reach is present over a length of approximately 50km. Downstream of Golden a braided reach is present where the river flows across the alluvial fan of a tributary, the Kicking Horse River. Finally, the river turns west and south-west and consists of a single channel again (Abbado et al., 2005). Anastomosing morphology is best developed within the lower part of the anastomosing reach, between Spillimacheen and Golden (Makaske et al., 2002; Smith, 1983). Therefore this reach will be discussed in more detail in section 2.2.2.

The upper Columbia River valley is part of the Rocky Mountain Trench and separates the Rocky Mountains in the north-east from the Purcell Mountains in the south-west (figure 2.1). Major tributaries of the upper Columbia River drain the Purcell Mountains. The two largest tributaries are Bugaboo Creek and Spillimacheen River (Tabata and Hickin, 2003). Only minor creeks drain the Rocky Mountains, in the upper Columbia River.
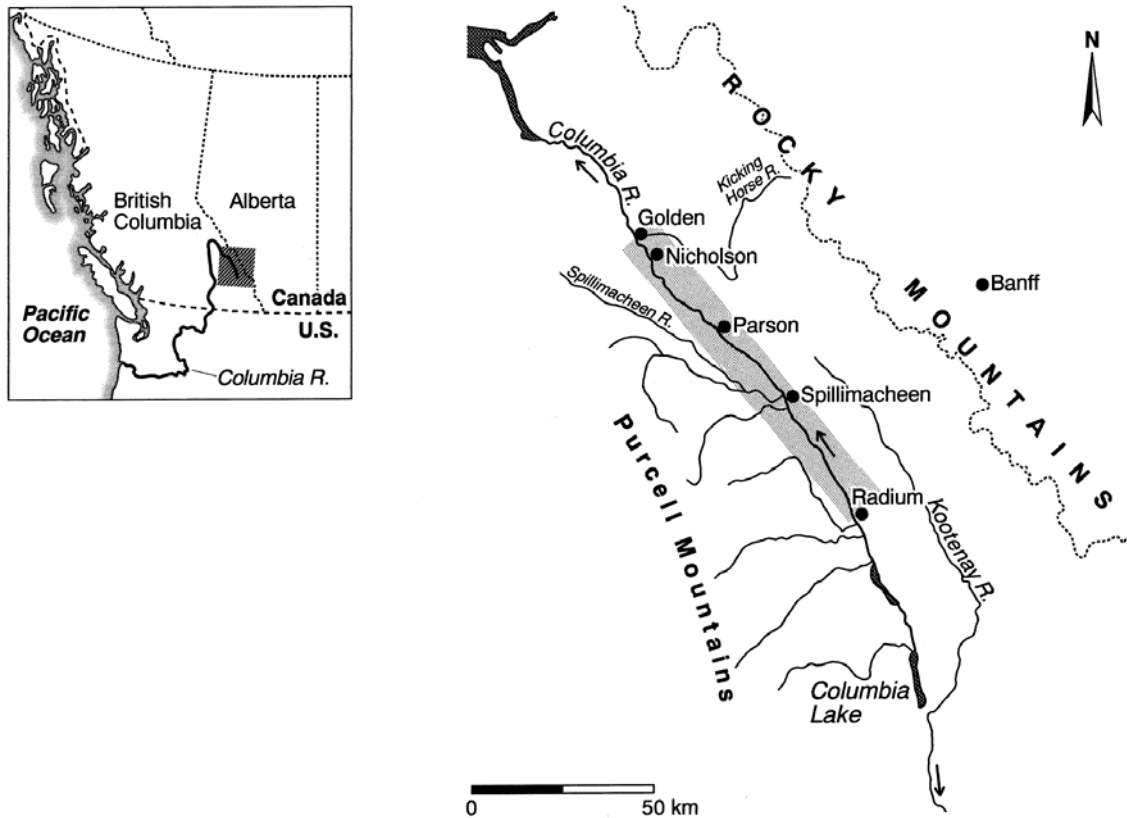
Fig. 2.1: Location of the upper Columbia River (Makaske et al., 2002).

The Purcell Mountains consist primarily of Proterozoic shales, sandstones, conglomerates and slates (Makaske et al., 2002; Makaske, 1998). They rise above 3000m amsl, and glaciers surround the highest peaks. The Rocky Mountains are free of ice, with a number of summits close to 2700m amsl. The Rocky Mountains are mainly composed of calcareous slates and shales, limestones and dolomites of Palaeozoic age (Makaske et al., 2002).

Tributaries originating in both mountain ranges act as sediment feeder for the upper Columbia River. Especially the Spillimacheen River delivers a large amount of sediment to the upper Columbia River at Spillimacheen (Makaske et al., 2009).

Due to these surrounding mountain ranges, the upper Columbia River system is laterally restricted, with a mean valley width of 1.5km, mainly by valley sides and alluvial fans protruding from tributary valleys. Over most its anastomosing reach, the upper Columbia River consists of a main channel and a variable number of smaller parallel channels. The alluvial valley floor in this reach has a mean elevation of around 790m amsl and a generally gentle slope, averaging 11.5cm/km (Makaske et al., 2009).

The upper Columbia River valley has a Quaternary fill, consisting of silts, sands and gravels, partly of glacial, glaciofluvial and glaciolacustrine origin (Makaske et al., 2002). The thickness of this Quaternary fill is probably about 20m (Makaske et al., 2009).

11

The upper Columbia River at Golden has an annual temperature range of 39.3°C. Temperatures reach a mean monthly low of -10.1°C in January and a mean monthly high of 17.2°C in July. The annual average precipitation is 490.7mm. Precipitation (mostly snow) peaks in December and January, but significant amounts are also recorded during the remainder of the year with a broad secondary peak centered in July (Tabata and Hickin, 2003). Annual mean precipitation gradually declines in a south-easterly direction and Invermere receives about 300mm (Makaske, 1998). In the adjacent mountains, particularly the Purcell Mountains, precipitation is markedly greater and provides most of the flow to the upper Columbia River (Tabata and Hickin, 2003).

Above the Nicholson gauging station (figure 2.1), the drainage area of the upper Columbia River is 6600km^2, with an annual mean discharge of 107m^3 s^{-1} (Makaske et al., 2009). Discharge measurements from the Nicholson gauging station for the upper Columbia River (1917-2008) indicate that discharge is highly seasonal (figure 2.2). This is caused by snow melt from the Purcell- and Rocky Mountains. Minimum monthly mean discharge occurs in February, at an average of 23m^3 s^{-1}, and maximum monthly mean discharge occurs in June and July, at an average of 310m^3 s^{-1}, with overbank discharge 45 days per year on average occurring almost every year (Locking, 1983).
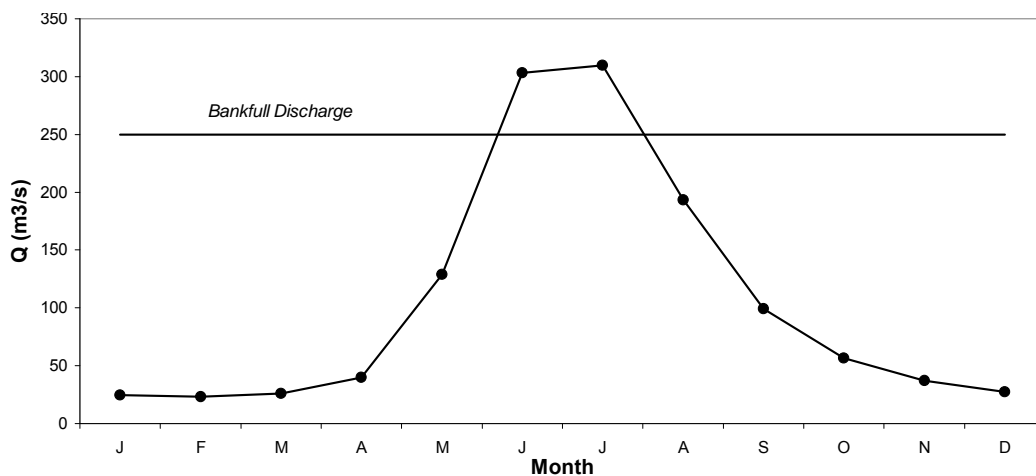

Fig. 2.2: Monthly average discharge, from 1917-2008, at the Nicholson gauging station, downstream of the Spillimacheen-Castledale reach.

2.2.2. Morphology and sedimentation dynamics of the Spillimacheen-Golden reach

All research to the anastomosing upper Columbia River has been performed in the Spillimacheen-Golden reach, since this is the reach characterized by the best developed anastomosis (Makaske et al., 2002; Smith, 1983) (figure 2.3).

Fig. 2.3: Part of the Spillimacheen-Golden reach of the upper Columbia River. View from Castledale in an upstream direction (copyright Patrice Halley, www.patricehalley.com).

This research was sedimentological (Smith, 1983; Makaske et al., 2002) as well as morphological (Makaske et al., 2002;2009, Locking, 1983; Tabata and Hickin, 2003; Abbado et al., 2005). Relevant findings of this research in the upper Columbia River are summarized below.

Abbado et al. (2005) distinguished two contrasting anastomosing reaches between Spillimacheen and Golden based on valley slope: (1) a relatively steep upper reach from Spillimacheen, where the Spillimacheen River enters the Columbia valley, to Castledale (maximum $S = 2.1*10^{-4}$), characterized by well-developed anastomosis with three to five parallel channels, (2) a relatively gentle sloped reach between Castledale and Golden ($S = 6.8*10^{-5}$), with typically one to three parallel channels (see figure 2.6 for location). They used this knowledge to present a hypothesis on the origin of anastomosis in the upper Columbia River. This hypothesis is described in detail in section 2.3.2.

Makaske et al. (2002) investigated the floodplain lithofacies in a cross-valley transect located near the break in slope found by Abbado et al. (2005) near Castledale (figure 2.4).
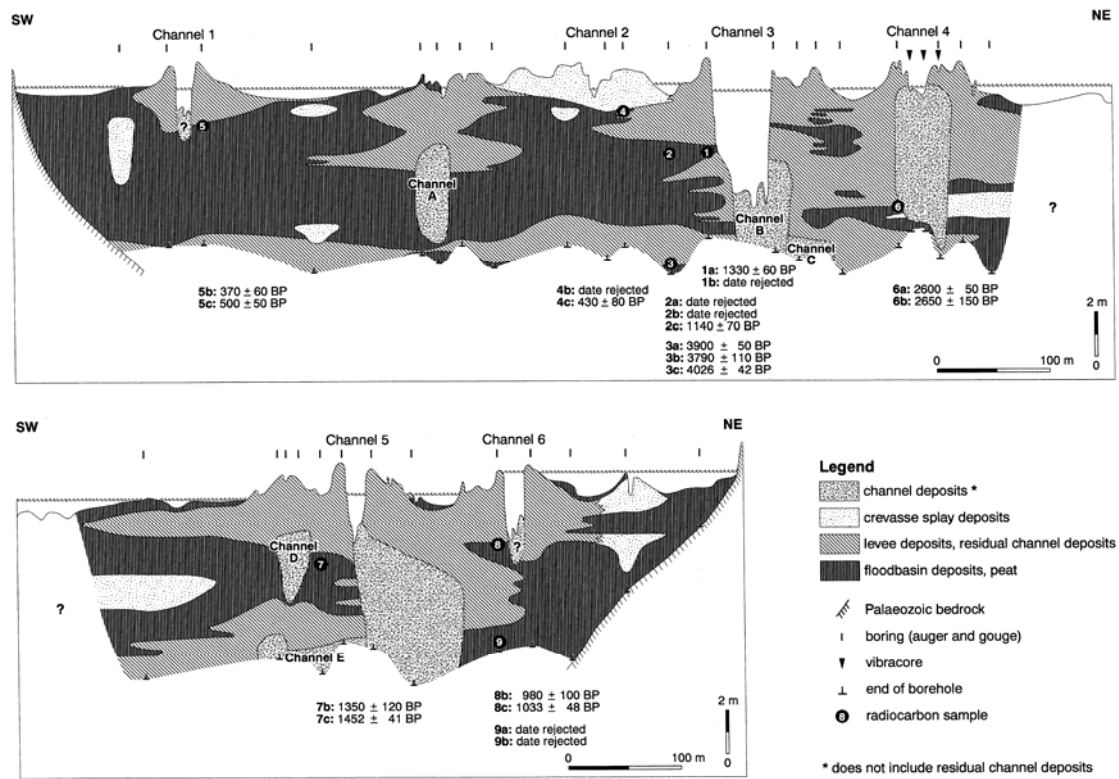
Fig. 2.4: Genetic interpretation of the lithofacies in a cross-section near Castledale. Sample locations are shown, and accepted ages are given ^{14}C years BP (Makaske et al., 2002).

Discharge measurements and sediment transport calculations by Makaske (1998) showed that channel 3 in this transect was by far the most dominant, accounting for 87% of the total flow and 99% of the total sediment transport at high stage. In general the width/depth ratios of the channels in this transect were below 10, although channel 2 and 4 had a greater width/depth ratio of around 20.

Tabata and Hickin (2003) investigated the hydraulic geometry of the channels of the anastomosing reach between Spillimacheen and Castledale in more detail. They determined the width, depth and flow velocity of 16 channels downstream of Spillimacheen. They concluded that the hydraulic geometry of the upper Columbia River can in general adequately be described by power functions based on bankfull discharge. The highest rate of change in channel geometry is found in bankfull width, followed by bankfull depth and bankfull velocity:

$$w_{bf} = 3.24 Q_{bf}^{0.64} \tag{2.1}$$

$$h_{bf} = 1.04 Q_{bf}^{0.19} \tag{2.2}$$

14

$$u_{bf} = 0.30Q_{bf}^{0.17} \qquad\qquad\qquad\qquad\qquad\qquad (2.3)$$

wherein Q_{bf} is bankfull discharge (m³/s), w_{bf} is the bankfull width (m), h_{bf} is the bankfull depth (m) and u_{bf} is the bankfull velocity (m/s). However, they measured both hydraulic geometry in the steep reach distinguished by Abbado et al. (2005) and upstream of this reach close to Spillimacheen (figure 2.6). This might affect the power functions, since hydraulic geometry might differ between the steep and relatively gentle sloped reaches.

Based on ^{14}C data, Makaske et al. (2002) concluded that channel lifetimes in the upper Columbia River are approximately between 800-3000 yr from formation to abandonment. In the past 3000 yr, the formation of nine new channels by avulsion occurred within the studied transect, while older channels were abandoned. Important reasons for avulsion in the upper Columbia River are log jams and beaver dams (Makaske et al., 2002; Smith, 1983).

Channel bed aggradation rates in the transect between Spillimacheen and Golden are higher than levee aggradation rates. This difference is most pronounced in the Spillimacheen-Castledale reach (Makaske et al., 2009). This finding is highly relevant for the avulsion rate in the upper Columbia River which on its turn is highly relevant for the origin of anastomosis in the upper Columbia River, as will be discussed in section 2.3.

Based on morphological observations and chronological data, Makaske et al. (2002) propose a four-stage model for channel evolution in the upper Columbia River (figure 2.5).

The first stage in the model is the formation of a shallow channel on a crevasse splay. The second stage is reached when the channel has become deep enough and the banks have become steep enough to allow widening of the channel by bank slumping following continued bank-toe bed scour. In the third stage, in-channel sedimentation becomes dominant. Two different stages of channel-filling can be observed in the upper Columbia River. In gradually abandoning channels, which are inadequately supplied with coarse bedload, channel narrowing by lateral accretion of banks is the dominant sedimentation process. This narrowing might cause very low width/depth ratios. Alternatively, where abundant coarse sediment is available, old channel reaches may fill vertically with sand and become shallow. This type of channel-filling might lead to a high width/depth ratio, since the vertical deposition of coarse sediment occurs rapidly relative to the channel narrowing proces. Work of Kleinhans et al. (2008) suggests that vertical channel-filling might occur in inner bend bifurcates, while channel narrowing might occur in outer bend bifurcates.

The fourth stage is that of fully abandoned channels, termed residual channels, in which only suspended/wash load deposition takes place.
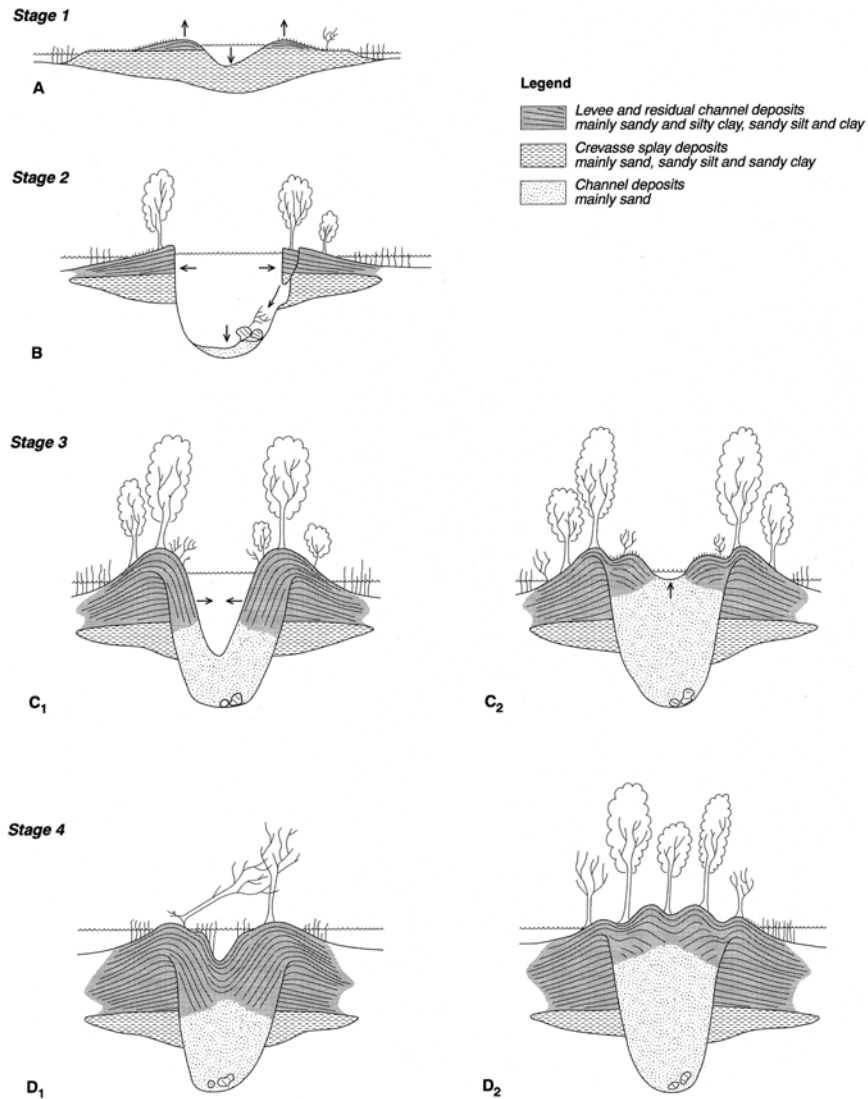
Fig. 2.5: Conceptual model for channel evolution in the upper Columbia River (from Makaske et al., 2002).

2.2.3. Overview of available data

Thanks to research of Makaske (1998), Tabata and Hickin (2003), Abbado et al. (2005) and Locking (1983), a large amount of hydraulic measurements have already been performed in the upper Columbia River. In this section these measurements are presented.

Makaske (1998), Tabata and Hickin (2003) and Abbado et al. (2005) all measured bankfull hydraulic geometry of individual branches of the upper Columbia River. Makaske (1998) and Tabata and Hickin (2003) also measured bankfull discharge and bankfull mean velocity. Abbado et al. (2005) measured median grain size, as did Makaske (1998). Makaske (1998) also measured hydraulic radius, cross-sectional area and sinuosity index of the individual channels.

Makaske (1998) defined bankfull stage by the break in slope between the steep channel bank and the flatter surface of the levee. It is unknown how Tabata and Hickin (2003) and Abbado et al. (2005) defined bankfull stage but here the same method is assumed. The locations of these measurements are shown in figure 2.6. An overview of the measured values is given in table 2.1.

Locking (1983) measured river stage, corresponding discharge and suspended- and bedload transport in the upper Columbia River at Spillimacheen (see figure 5 for location) and Nicholson from the beginning of May to the end of August in 1982. Additionally, Locking (1983) measured river width, mean depth, flow area, hydraulic radius, mean velocity and unit stream power. These measurements are summarized in table 2.2 and 2.3.

Peak flows at Spillimacheen were about 14 percent higher at Nicholson than at Spillimacheen. This is due to flow in two small parallel channels to the side of the Spillimacheen station that were not measured. Additionally, a small amount of flow may have been added between the two stations from small ephemeral tributaries and groundwater. However, Locking (1983) estimated that the amount was less than three percent of the total discharge.

Locking (1983) compared the discharge values with the permanent Nicholson gauging station of the water survey of Canada, which was located approximately 7 km downriver of the temporary gauging station of Locking (1983). Discharge values from the Water Survey of Canada permanent gauging station appeared to be approximately 5 percent higher than for the temporary Nicholson gauging station of Locking (1983). This is due to input from Canyon Creek, which is downstream of the Locking (1983) station but upstream of the Water Survey station.

So, between the two temporary gauging stations at Spillimacheen and Nicholson no significant discharge input of secondary channels occurs. Hence, discharge data from the temporary Nicholson gauging station of Locking (1983) is representative for the discharge in the Spillimacheen-Castledale reach. Additionally, data from the permanent Nicholson gauging station can be used to represent the discharge in the Spillimacheen-Castledale reach when the 5 percent deviation is taken into account.
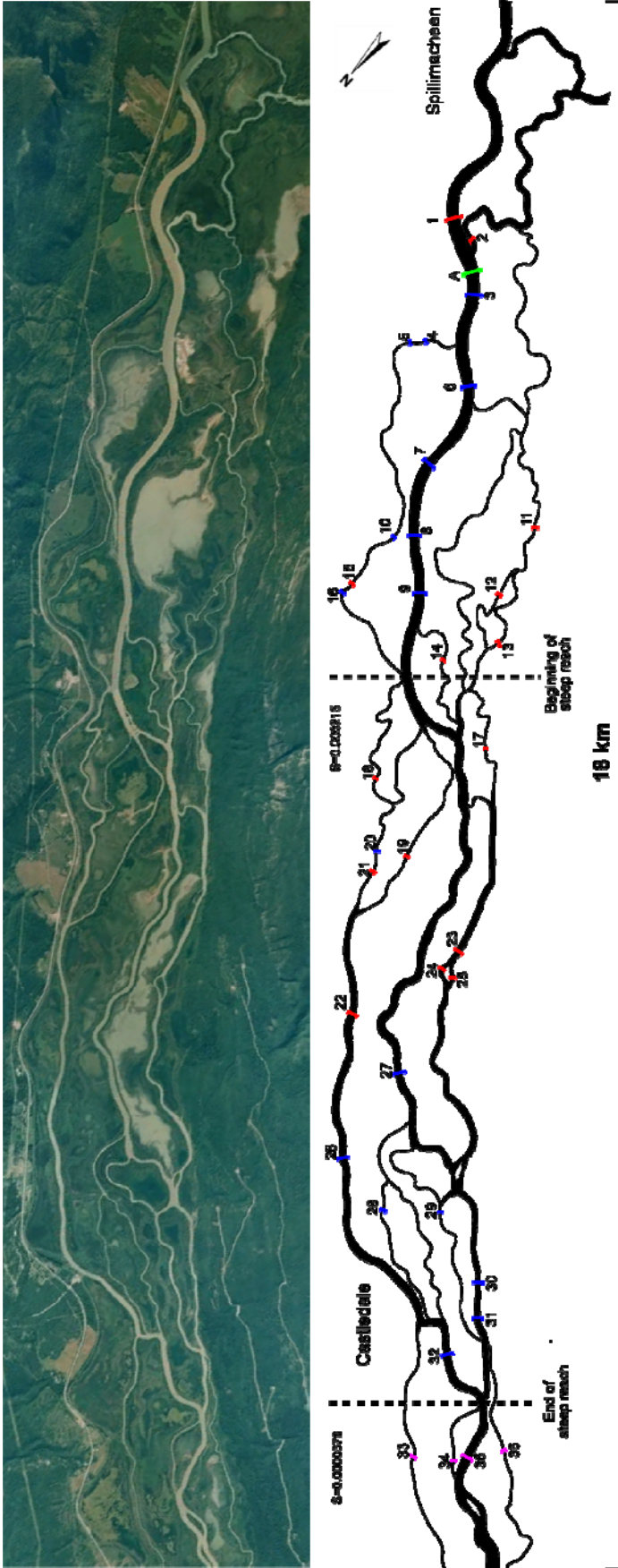
Fig. 2.6: Satellite image of the anastomosing upper Columbia River, between Spillimacheen and Castledale, and a channel map of this reach, wherein measurement locations are indicated. Numbers at measurement locations refer to the numbers in table 1. Red lines indicate measurement locations of Tabata and Hickin (2003), blue lines indicate measurement locations of Abbado et al. (2005), purple lines indicate measurement locations of Makaske et al. (2002) and the green line indicates the location of the Spillimacheen gauging station of Locking (1983).

Tbl. 2.1: Data of Makaske et al. (2002), Tabata and Hickin (2003) and Abbado et al. (2005). Locations of measurements are indicated in figure 2.6.

Location	W_{bf} (m)	D_{bf} (m)	W/D	v_{bf} (m/s)	Q_{bf} (m³/s)	Additional data	Source
1	41.7	2.0	20.7	0.51	42.5		Tabata & Hickin, 2003
2	131.2	2.2	60.8	0.69	200.6		Tabata & Hickin, 2003
3	125.7	2.9	44.0			D50, not published	Abbado et al., 2005
4	19.0	2.0	9.7			D50, not published	Abbado et al., 2005
5	18.7	2.2	8.4			D50, not published	Abbado et al., 2005
6	125.0	2.9	43.1			D50, not published	Abbado et al., 2005
7	88.9	2.9	31.0			D50, not published	Abbado et al., 2005
8	88.0	2.9	30.6			D50, not published	Abbado et al., 2005
9	90.0	3.0	30.5			D50, not published	Abbado et al., 2005
10	23.2	2.1	11.2			D50, not published	Abbado et al., 2005
11	23.9	3.3	7.3	0.49	34.6		Tabata & Hickin, 2003
12	14.9	2.4	6.2	0.47	15.8		Tabata & Hickin, 2003
13	18.0	2.6	6.8	0.37	15.9		Tabata & Hickin, 2003
14	25.7	3.0	8.6	0.62	44.7		Tabata & Hickin, 2003
15	15.1	1.9	7.8	0.46	12.8		Tabata & Hickin, 2003
16	13.7	2.3	6.1			D50, not published	Abbado et al., 2005
17	13.4	1.9	7.1	0.49	11.1		Tabata & Hickin, 2003
18	29.8	2.2	13.3	0.68	43.9		Tabata & Hickin, 2003
19	24.8	1.1	22.3	0.47	10.8		Tabata & Hickin, 2003
20	38.0	3.0	12.9			D50, not published	Abbado et al., 2005
21	46.1	2.3	20.5	0.56	63.5		Tabata & Hickin, 2003
22	52.5	2.7	19.7	0.66	87.8		Tabata & Hickin, 2003
23	50.1	2.1	24.0	0.54	46.1		Tabata & Hickin, 2003
24	20.8	2.1	9.8	0.48	16.7		Tabata & Hickin, 2003
25	23.8	1.5	15.8	0.44	15.7		Tabata & Hickin, 2003
26	55.0	2.8	19.5			D50, not published	Abbado et al., 2005
27	67.7	2.6	26.0			D50, not published	Abbado et al., 2005
28	30.4	1.6	19.2			D50, not published	Abbado et al., 2005
29	38.9	2.9	13.4			D50, not published	Abbado et al., 2005
30	31.0	3.6	8.5			D50, not published	Abbado et al., 2005
31	35.0	3.5	10.0			D50, not published	Abbado et al., 2005
32	84.5	2.9	28.7			D50, not published	Abbado et al., 2005
33	18.6	3.2	5.9	0.40	14.8	R, A, D50, D90, Pind	Makaske et al., 2002
34	20.7	1.1	19.7	0.35	5.4	R, A, D50, D90, Pind	Makaske et al., 2002
35	56.0	5.9	9.6	0.79	193.5	R, A, D50, D90, Pind	Makaske et al., 2002
36	19.3	2.1	9.2	0.32	9.5	R, A, D50, D90, Pind	Makaske et al., 2002

Tbl. 2.2: Data of Locking (1983) for the Spillimacheen gauging station, locations of measurements is indicated in figure 2.6. Measurements are performed in 1982.

Date	h (m)	w (m)	A (m^2)	R (m)	u_m (m/s)	Q (m^3/s)	c_s (mg/l)	Q_s (kg/s)	Q_b (kg/s)	Q_t (kg/s)	ω (kg/m/s)
10-5	2.10					37.70					
16-5	2.54					75.15	69.56	5.80			
17-5	2.63					83.16					
19-5	2.89					107.58	154.60	18.46			
21-5	2.96					115.18	180.72	23.10			
23-5	3.18					131.70	120.95	17.68			
25-5	3.30					148.32					
28-5	3.37					157.34					
29-5	3.28					150.21	140.37	23.40			
1-6	3.21	98	191	1.87	0.73	139.03	135.29	20.88	4.24	25.12	0.142
4-6	3.58					181.41	213.25	42.94			
5-6	3.63	100	235	2.24	0.79	186.36	109.10	22.57	7.09	29.66	0.186
8-6	3.55					177.38					
15-6	4.21	103	307	2.82	0.90	276.25	505.02	154.85	7.95	162.80	0.268
17-6	4.34	102	310	2.87	0.95	294.76	402.17	131.57	16.37	147.95	0.288
19-6	4.39	104	332	3.01	0.94	312.28	411.73	142.71	7.36	150.07	0.300
21-6	4.50					321.69	371.47	132.64	13.12	145.76	
26-6	4.47	100	326	3.06	0.96	313.59	115.45	40.19	8.31	48.49	0.313
2-7	4.50					321.69	239.35	85.47			
6-7	4.23					269.58	80.18	23.99			
10-7	4.09					273.59	129.53	39.34	9.42	48.75	
15-7	4.09	122	346	2.71	0.88	273.59	72.27	21.95	18.74	40.68	0.249
22-7	4.07					250.45	127.14	35.34	15.41	50.75	
29-7	3.74					200.00	62.88	13.96	19.62	33.57	
6-8	3.58	122	278	2.20	0.70	175.97	67.37	13.16	5.05	18.21	0.160
10-8	3.55	122	282	2.23	0.73	184.27	94.39	19.31	8.68	27.99	0.168
18-8	3.15	114	217	1.84	0.63	122.34	44.20	6.00	7.15	13.15	0.119

Tbl. 2.3: *Data of Locking (1983) for the Nicholson gauging station, locations of measurements is indicated in figure 2.6. Measurements are performed in 1982.*

Date	h (m)	w (m)	A (m^2)	R (m)	u_m (m/s)	Q (m^3/s)	c_s (mg/l)	Q_s (kg/s)	Q_b (kg/s)	Q_t (kg/s)	ω (kg/m/s)
22-5	4.50					131.55	78.55	10.33			
2-6	2.54	90	306	3.16	0.55	166.63	135.23	22.53	0.24	22.77	0.186
7-6	5.64	95	371	3.61	0.67	246.99	50.57	12.49	1.20	13.69	0.260
15-6	5.73	2.9	375	3.81	0.70	261.01	186.20	48.60	0.35	48.95	0.290
18-6	6.27	93	435	4.25	0.80	347.45	56.63	19.68	1.43	21.11	0.373
21-6	6.89					395.00	12.26	4.84	1.24	6.08	
22-6	7.05					403.62					
25-6	7.29	90	521	5.13	0.80	416.29	41.86	17.43	2.49	19.92	0.462
3-7	7.26					414.00	29.39	12.17	0.96	13.13	
7-7	6.86	90	479	4.76	0.85	406.15	31.34	12.73	2.78	15.51	0.451
13-7	6.25					349.00	38.15	13.31	0.99	14.30	
16-7	6.16	87	404	4.20	0.85	343.23	62.20	21.35	1.70	23.05	0.394
23-7	5.97					309.00	22.44	6.93	2.23	9.16	
30-7	5.71	87	357	4.10	0.75	265.80	59.38	15.78	1.53	17.31	0.306
7-8	5.60	87	346	3.64	0.68	237.23	32.27	7.66	0.81	8.46	0.272
20-8	4.90	84	286	3.15	0.55	159.94	26.22	4.19	1.02	5.21	0.187

2.3. Anastomosing rivers

The Spillimacheen-Golden reach in the upper Columbia River is characterized by its multi-branched morphology. In this section a review on anabranching rivers is presented. A classification and overview of different sorts of anabranching rivers is given in section 2.3.1. In section 2.3.2 the origin of anastomosis, the type of anabranching river the upper Columbia River is agreed to be, is discussed. Finally, in section 2.3.3 avulsions are discussed, as they are hypothesized to be the driving mechanism behind anastomosis.

2.3.1. Classification of anabranching rivers

There is much discussion about the definition of anabranching rivers. It is not the scope of this review to discuss these different definitions. Therefore only the descriptive classification of Nanson and Knighton (1996) as used in this research is presented.

Nanson and Knighton (1996) classify river systems that consist of multiple channels separated by vegetated semi-permanent alluvial islands, formed by within-channel or deltaic accretion as anabranching rivers. Six different types of anabranching rivers are recognized. They can be classified from low energy, organic or fine-sediment textured systems, to relatively high-energy gravel- or boulder transporting systems.

Type 1: Cohesive sediment anabranching rivers
These are anabranching rivers of relatively uniform and narrow width, with low gradients and stable cohesive banks. Channels are often, but not always, sinuous, exhibit no lateral migration and relocate by avulsion. Stream power is characteristically very low due to small slopes, and channels are frequently canal-like in cross-section. On the basis of environment and associated sediment type they are divided into three subprofiles; (a) organic systems, (b) organo-clastic systems and (c) mud-dominated systems. These systems are commonly referred to as anastomosing rivers. Examples of these river systems are. the upper Columbia River (Canada), the Attawapiskat River (Canada) and the Diamantian River and Cooper Creek (Australia).

Type 2: sand-dominated, island-forming anabranching rivers
In terms of discharge and slope these rivers are the same as type 1 rivers, their sediments are much less cohesive and their channels tend to be subparallel with intermittent, relatively wide and sometimes braided reaches. Because of the generally non-cohesive nature of sand, this type requires the

combination of stabilizing vegetation and low stream energy to prevent the channel from braiding or meandering. An example of this anabranching river type is Magela Creek (Australia).

Type 3: mixed-load, laterally active anabranching rivers
These are meandering multichannel rivers that migrate laterally across a portion of their floodplain. They represent a diverse group that is difficult to define as a single type carrying a mixed sediment load of sand and mud, and in some cases fine gravel. Examples are the Thompson and Murray River in Australia.

Type 4: sand-dominated, ridge-forming anabranching rivers
Linear and curvilinear ridged systems. Like the type 2 rivers, they are strongly dominated by sand deposition where vegetation is crucial for developing non-compliant banks. Stream powers are significantly higher than for otherwise similar type 2 rivers. Hence streamlined ridges rather than islands are formed. An example is the Durack River (Australia).

Type 5: gravel-dominated, laterally active anabranching rivers
These are relatively energetic wandering gravel-bed rivers. They often exhibit a dominant channel accompanied by several anabranches, but may also alternate downstream between multi- and single-channelled reaches. The dominant channel commonly braids. An example of such an anabranching river type is the Bella Coola River (Canada).

Type 6: gravel-dominated, stable anabranching rivers
A number of small, steep drainage basins that respond to rapid rainfall events exhibit anabranching channels with well-vegetated gravel, coarse-gravel or boulder islands.

The upper Columbia River as described by Makaske (2001), Makaske et al. (2002), Smith (1983), Tabata and Hickin (2003) and Abbado et al. (2005), is clearly a type 1b anabranching river, from now on referred to as anastomosing river, as it exhibits resistant, well-vegetated banks (Smith, 1983; Makaske, 2001; Makaske et al., 2002) that protect swampy, levee-banked islands commonly with central depressions that may produce lacustrine sedimentary facies. Although the upper Columbia River is transporting sand and sometimes gravel as bedload, it is characterized by abundant overbank fine-sediment deposition, causing resistant well-vegetated banks (Makaske et al., 2002) on a rapidly accreting low-gradient floodplain (Makaske, 2002; Abbado et al., 2005).

2.3.2. Origin of anastomosis

There are two main hypotheses on the origin of anastomosis, one presented by Nanson and Knighton (1996) and one presented by Makaske (2001). Both will be reviewed in this section.

A river in a state of dynamic equilibrium adjusts its channel pattern, cross-sectional geometry, slope and roughness in order to balance the available sediment load with an ability to transport this load (Nanson and Knighton, 1996). Therefore the temporal and spatial persistence of anabranching systems indicates that in certain situations they must exhibit considerable advantages over their single-thread counterparts. In cases where river gradients cannot easily be increased or sinuosity can be reduced to carry a larger sediment load, then an increase in the sediment/water discharge ratio must be accommodated by an increase in the rate of work being done per unit area of the bed. This can be accomplished by a shift from single to multiple channels, which leads to an increase in sediment transport rate per unit discharge (Nanson and Knighton, 1996; Nanson and Huang, 1999).

Recently, this hypothesis has been criticized by Tabata and Hickin (2003) and Abbado et al. (2005). Tabata and Hickin (2003) developed empirical hydraulic geometry relations for a reach of the multi-channelled upper Columbia River (section 2.2.2). Based on these relations Tabata and Hickin (2003) calculated flow resistance for single- and multi-branched river systems. From these calculations it became clear that a single channel has smaller flow resistance than a multiple channel system (see table 3 in Tabata and Hickin (2003)), which contradicts with the hypothesis of Nanson and Knighton (1996).

Abbado et al. (2005) calculated sediment transport rates for single and multiple channel systems, both transporting the same amount of discharge, with two methods: (i) the Bagnold (1977) bedload predictor coupled with the Rouse (1937) suspended sediment formulation, and (ii) the Van Rijn predictors for bedload and suspended load (Van Rijn, 1984a,b). Total sediment load was reduced as the flow was divided into additional channels. However, both authors used empirical friction relations, leaving their results still debatable. Hence, a comparison between the efficiency of single- and multi-channelled river systems still has to be made based on more advanced friction relations. In response to the findings of Tabata and Hickin (2003) and Abbado et al. (2005), Huang and Nanson (2007) state that only in some rivers it is hydraulically more efficient to transport sediment in multiple channels.

The second hypothesis on the origin of anastomosis is that of Makaske (2001). Makaske (2001) states that frequent avulsions and/or slow abandonment of old channels lead to continuing coexistence of younger deepening channels and old vertically infilling channels, composing an anastomosing system. Thus, if the avulsion duration exceeds the interavulsion period multiple channels occur on a floodplain giving rise to the existence of an anastomosing river pattern (figure 2.7).
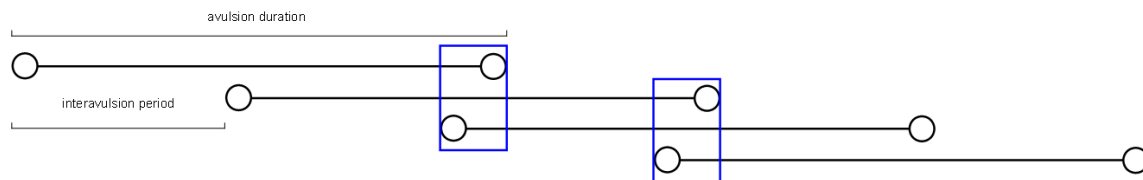
Fig. 2.7: Avulsion duration and interavulsion period. The avulsion duration exceeds the interavulsion period leading to the coexistence of two and sometimes three channels (indicated in blue).

According to this point of view, the fluvial system exists in a perpetual transition state consisting of multiple coexisting channels. Anastomosis is thus a non-equilibrium form according to the Makaske (2001) hypothesis, whereas it is an equilibrium form according to the Nanson and Knighton (1996) hypothesis (Abbado et al., 2005).

According to Makaske (2001), the possible causes of frequent avulsions are a rise in base-level, subsidence (Smith, 1983), and high rates of aggradation, in the channel belt or within the channel. However, Abbado et al. (2005) and Makaske et al. (2009) indicate that avulsion of the upper Columbia River is mainly caused by the upstream sediment supply, as is often observed on alluvial fans (Slingerland and Smith, 2004). The immediate cause of slow abandonment is conjectured to be low stream power according to Makaske (2001). However, from the work of Kleinhans et al. (2008) it becomes clear that slow abandonment of an avulsion channel can also be explained by bifurcation dynamics, as they concluded that the evolution of a bifurcation is mainly dependent upon the presence of an upstream bend and the downstream gradient of the bifurcates. Therefore avulsions and bifurcation dynamics will be discussed in more detail in section 2.3.3 and 2.4 respectively.

2.3.3. Avulsions

Makaske (2001) defines an avulsion as the diversion of flow from an existing channel onto the floodplain, eventually resulting in a new channel belt.

Many conditions favouring avulsions have been mentioned, these can roughly be divided into local and regional conditions. Regional factors commonly are external as they comprise the boundary conditions that are unaffected by the local evolution. The local factors commonly are internal because they evolve as a result of the internal system dynamics. Examples of local conditions are: high in-channel aggradation rate (Makaske, 2001; Makaske et al., 2002, 2009; Nanson and Knighton, 1996), obstructions like log jams (Smith, 1983), beaver dams (Smith, 1983; Makaske, 2002), ice jams in cold climates and dunes in arid climates (Makaske, 1998) and resistant banks (Nanson and Knighton, 1996). Examples of regional conditions are: low gradient floodplain (Makaske, 2001), tectonics (Makaske, 2001; Stouthamer and Berendsen, 2000), variable flooding (Nanson and Knighton, 1996;

Makaske 2001) and rising base level (Stouthamer and Berendsen, 2000; Törnqvist, 1994; Smith, 1983).

Overall, the mechanisms causing avulsions are site dependent. For example, in the Rhine-Meuse delta in the Netherlands the location and shifting of Holocene avulsion sites in space and time are related to the following factors: (1) rising base level, by sea level rise, (Stouthamer and Berendsen, 2000; Törnqvist, 1994) causing aggradation in the Holocene Rhine-Meuse delta. (2) Neotectonics, the location of avulsions sites seems to have been influenced by neotectonic movements of the Peel Horst between 4900-1700 yr BP, where four of the six avulsions of this period were located. (3) Increased discharge and/or within-channel sedimentation (Stouthamer and Berendsen, 2000).

Anastomosis, and thus frequent avulsion, of the upper Columbia River was initially understood to result from a downstream rise in base-level caused by aggrading cross-valley alluvial fans (Smith, 1983). However, Abbado et al. (2005) and Makaske et al. (2009) argue that the amount of upstream sediment supply, rather than a downstream rise in base level causes anastomosis in the upper Columbia River. This idea is based on the fact that anastomosis is best developed in a reach between Spillimacheen and Golden, where aggradation rates are highest as inferred from valley gradient (Abbado et al., 2005) and sediment budget calculations (Makaske et al., 2009). Further downstream, the aggradation rate decreases, and consequently the degree of anastomosis decreases, from 6 to 2-3 tributaries.

Avulsion duration (=channel lifetime, figure 2.7) is highly variable. The avulsion in the Yellow River in 1855 happened in one day. Data from the Rhine-Meuse delta (Stouthamer and Berendsen, 2000; Törnqvist, 1994) reveals examples of rapid avulsions, which occurred within 200 yr, as well as more gradual avulsions, which occurred within 500-1000 year. The period of activity of the former lower Saskatchewan River channel belts ranged from 700-2900 years (Makaske et al., 2002). Channel lifetimes of the upper-Columbia River range between 800 and 3000 year. This high variability in channel lifetime can be explained by bifurcation dynamics (Kleinhans et al., 2008), this will be discussed in section 2.4.

An avulsion starts with the break-through of a levee, and the formation of a crevasse. Under certain conditions a crevasse might turn into an avulsion, by cutting a new channel through the levee. The entrance of a newly formed crevasse channel is located high in a river's water column. Hence, water entering the crevasse channel contains a low concentration of sediment, as most sediment is transported near the river bed. Consequently, the flow into the crevasse channel is able to entrain a relatively large amount of sediment, causing the crevasse entrance to erode depending on the erodibility of the lip. Deepening of the crevasse entrance increases the crevasse-channel discharge and the concentration of sediment, because water is tapped closer to the bed. The crevasse entrance will

further deepen until its transport capacity is satisfied by the suspended solids entering from the main channel (Slingerland and Smith, 1998). From this point in time onwards, the further evolution of the crevasse/avulsion can be explained by bifurcation dynamics, which is discussed in the following section.

2.4. Bifurcations

A bifurcation is unstable if one of the bifurcates receives more or less sediment than the transport capacity (Wang et al., 1995; Kleinhans et al., 2008). The division of flow and sediment is influenced by a combination of processes; these will be briefly addressed in section 2.4.1. In section 2.4.2 a review of laboratory, field and modelling observations on bifurcations is presented.

Since 3D models are computationally too expensive to study complete river networks, or bifurcations on geological time-scales 1D bifurcation models are needed. For 1D models, a relation describing the sediment division is necessary, known as nodal point relation. Therefore, nodal point relations are discussed in section 2.4.3.

2.4.1. Dynamics associated with river bifurcations

A slope difference between two bifurcates, gives the bifurcate with the largest slope an advantage as flow rate and sediment transport are larger. Ultimately this leads to the silting up of the other bifurcate if more sediment enters this bifurcate than can be transported.

Another important factor is the length of the branches. The larger the length of a branch is, the smaller the influence of the backwater effect in rivers with subcritical flow. Where bifurcates reach a sea, lake or engineering structure (like a bridge or weir) water decelerates strongly, causing a backwater effect upstream, which leads to flow deceleration there also. So, the shortest bifurcate experiences the largest backwater effect. Hence, more water is forced into the other bifurcate.

When flow towards a bifurcation is asymmetrically, due to a meander bend, water is forced towards the outer bend due to the centrifugal force. Due to this force, the water table shows a slope in cross direction, with the highest water level in the outer bend. This causes a difference in hydrostatic pressure, which in combination with the centrifugal force leads to flow circulation in cross direction, known as spiral flow (figure 2.8).
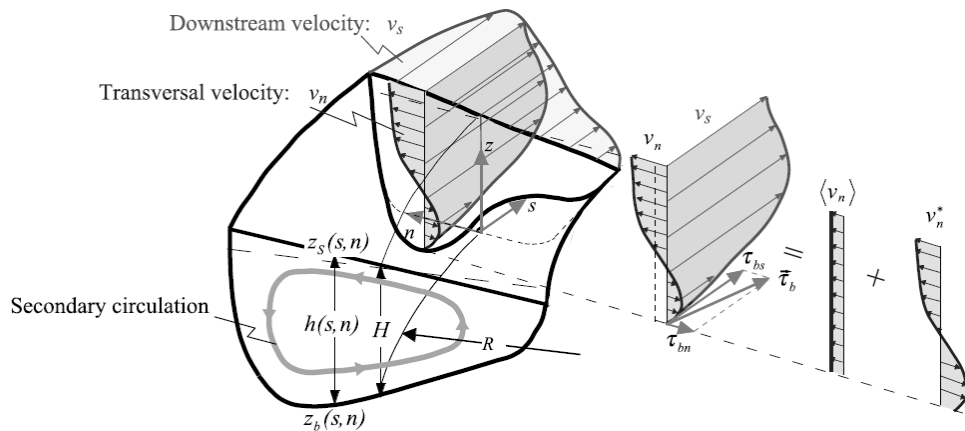
27

Fig. 2.8: Centrifugal force leading to spiral flow in meander bends (Blanckaert and de Vriend, 2003).

As illustrated in figure 2.8, spiral flow leads to flow towards the inner bend at the bottom and flow to the outer bend at the water surface. Sediment concentration is highest close to the bed, consequently sediment is eroded at the outer bend and transported towards the inner bend. This leads to a transverse slope in the bend. This is balanced by the gravitational force. In a bifurcation located just downstream of a bend, sediment is forced into the inner bend due to spiral flow, but this effect might be balanced by the transverse slope effect. Which process dominates depends upon the specific conditions of the bifurcation.

In sharply curved meander bends flow separation occurs (Ferguson and Parsons, 2003; Kleinhans et al., 2009). This alters the locations of strongest and weakest flow and thus has important implications for sedimentation and meander migration. However, the radius of curvature relative to channel width is not the primary cause of flow separation; it is the abruptness whereby the inner bank changes direction (Ferguson and Parsons, 2003).

Flow separates near the most sharply curved point on the inner bank, and a recirculation eddy occurs. Here a "dead zone" of small downstream velocity is present. This "dead zone" causes deposition, and hence a lateral expansion (Ferguson and Parsons, 2003; Kleinhans et al., 2009).

Consequently, flow separation might have a pronounced effect on river bifurcations with an upstream meander bend that experience flow separation. In the first place the helical motion is restricted to the outer part of the channel, due to the presence of a recirculation eddy in the inner bend (Ferguson and Parsons, 2003). In the second place, the transverse slope increases due to sedimentation at the inner bend. Both the restrictions of helical flow and an increase in transverse slope favour sediment supply towards the outer bend. Additionally, the dead zone in front of the inner bend bifurcate favours discharge into the outer bend bifurcate, as flow velocities are higher in the outer bend compared to the inner bend. Whether this leads to smaller avulsion duration depends on the ratio between discharge and sediment supply increase in the outer bend bifurcate induced by flow separation.

2.4.2. Field, experimental and modelling observations

There has been much experimental research on bifurcations. The first experiment carried out on river bifurcations is that of Bulle (1926), recently reconsidered by De Heer and Mosselman (2004). Bulle (1926) performed experiments measuring flow and bed load distribution in a bifurcation with fixed sidewalls. He observed that close to the bifurcation fluid particles were moving in helical trajectories. This caused a so called "Bulle effect"; a disproportionate amount of bedload feed into the diverting channel. Additionally, an eddy was present downstream of the bifurcation, most likely enhanced by the sharp deviation of the sidewall, causing flow separation (section 2.4.1).

Most experimental research on river bifurcations concerns braided gravel bed bifurcations (Bertoldi et al., 2001, 2002; Bertoldi and Tubino, 2005, 2007). In experiments with erodible banks, due to the initial migration of alternate bars a weakly sinuous channel displaying periodic oscillations of bank profile developed. Once a migrating alternate bar became fixed in a channel, flow was diverted, causing a bifurcation to occur. Bertoldi and Tubino (2005) present a detailed quantitative analysis of the above process.

Bertoldi and Tubino (2007) performed measurements on bifurcation equilibrium configuration in a flume. The bifurcations in the flume had fixed banks. The geometry and bed sediment was chosen in such a way that a braided river bifurcation was simulated. The main outcome of the experimental observations is the recognition that for given slope, grain size and channel width the ability of the bifurcation to keep a more or less balanced discharge partition depends on flow discharge. In particular, the smaller the discharge of the incoming flow, the larger the observed imbalance at the node. In dimensionless form this implies that the node can keep balanced (i.e. discharge ratio ≈ 1 and dimensionless inlet step ≈ 0) only for relatively large values of upstream Shields stress, or equivalently for small values of aspect ratio (note that due to the fixed width of the branches, higher values of Shields stress correspond to lower values of aspect ratio) (figure 2.9). Furthermore, the discharge ratio becomes smaller and the amplitude of inlet step larger for decreasing/increasing values of Shields stress/aspect ratio. In other words, more mobile bifurcations remain more symmetric.

However, in braided gravel bed rivers, significant upstream bends are never present and flow depth is relatively small due to highly erodible banks. Therefore it is reasonable to expect that both helical flow and flow separation are less intense in braided river bifurcations compared to meandering/anastomosing river bifurcations (Miori et al., 2006). Hence, the above results are most likely only slightly representative for meandering/anastomosing river bifurcations.
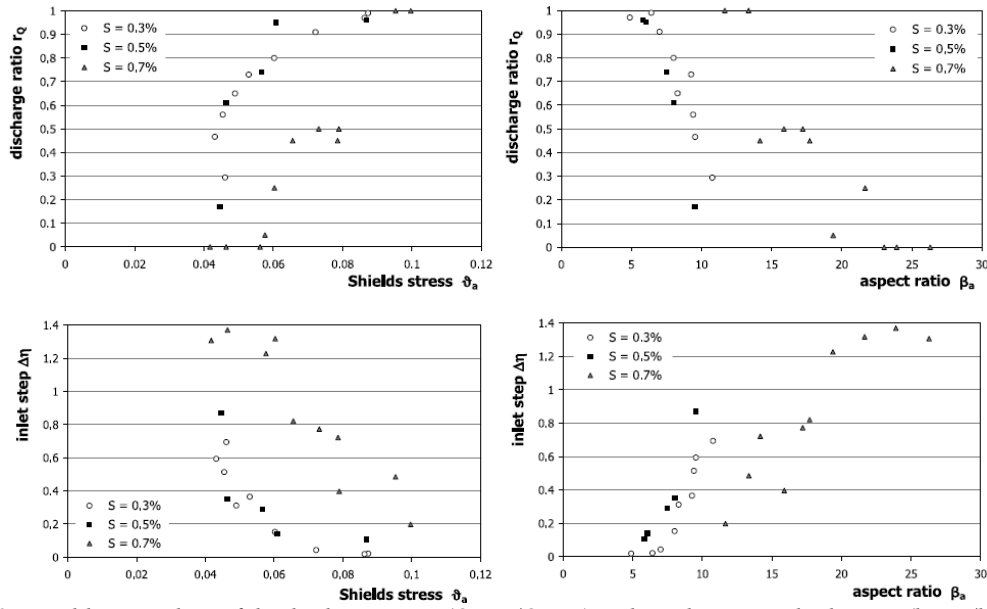
Fig. 2.9: Equilibrium values of the discharge ratio (Q_{down1}/Q_{down2}) and nondimensional inlet step (h_{down1}/h_{up}) versus Shields stress and aspect ratio ($w_{up}/2h_{up}$) of the upstream channel (Bertoldi and Tubino, 2005).
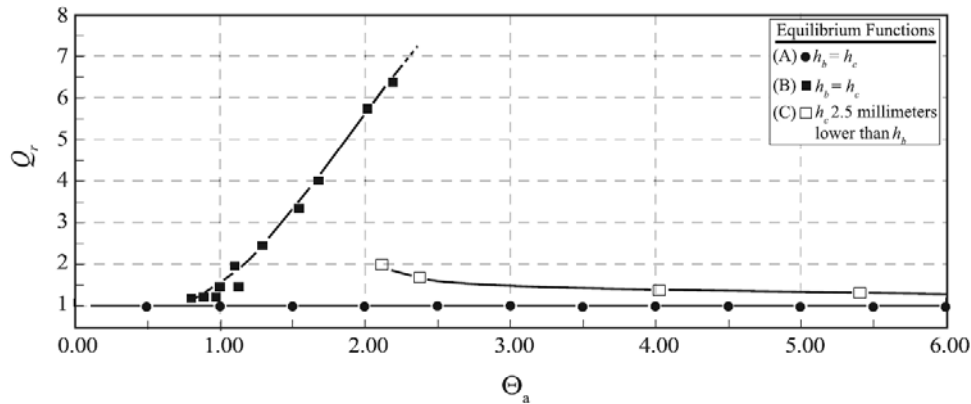

Fig. 2.10: Equilibrium diagram for fine-grained cohesive deltaic bifurcations (Edmonds and Slingerland, 2008). Note that the discharge ratio is taken as major bifurcate/minor bifurcate opposite to Bertoldi and Tubino (2005).
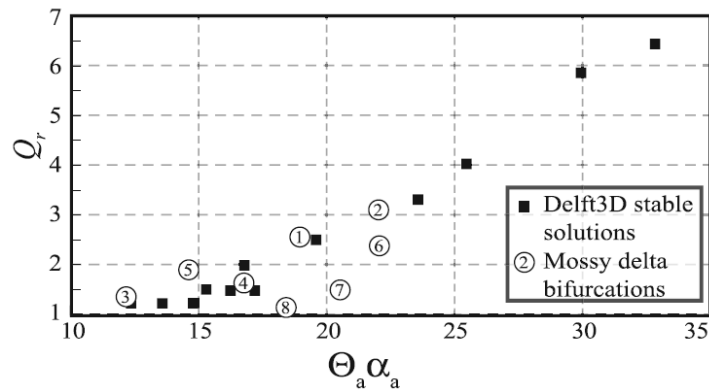

Fig. 2.11: Measured equilibrium values of the Mossy delta compared to modelled equilibrium solutions with Delft3D. The measured equilibrium solutions all behave conform scenario A in figure 2.10 (Edmonds and Slingerland, 2008). The discharge ratio is taken opposite to Bertoldi and Tubino (2005).

30

Delta distributary networks are composed of bifurcating channels. Edmonds and Slingerland (2008) schematically modelled the origin and stability of the asymmetrical fine-grained cohesive bifurcations. The model results were compared to bifurcations of the Mossey Delta, located at the Cumberland marshes, Alberta, Canada. Edmonds and Slingerland (2008) modelled the evolution of deltaic bifurcations with Delft3D. They found three different equilibrium functions (figure 2.10): (A) at all values of Shields stress above transport and with equal water level, there is an equilibrium function with discharge ratio = 1. (B) At relatively low values of Shields stress and with equal water levels, there is an equilibrium function with discharge ratio ≠ 1. (C) At relatively high values of Shields stress and with unequal water levels, there is an equilibrium function with discharge ratio ≠ 1. Note that in contrary to Bertoldi and Tubino (2007), Edmonds and Slingerland (2008) divided the major bifurcate by the minor bifurcate, so that the higher the discharge ratio, the more asymmetric the discharge division at the bifurcation. Field equilibrium configurations of bifurcations in the Mossey delta all behave conform equilibrium function 2 (figure 2.11); bifurcations become more asymmetric with increasing upstream Shields stress.

The results of bifurcations becoming more asymmetric with increasing upstream Shields stress contradicts the model and flume results of Bertoldi and Tubino, 2007. To explain the contradiction in equilibrium configuration between gravel- and sand bed rivers, Edmonds and Slingerland (2008) computed the static flow and sediment transport fields at various values of discharge ratio (or bed ramp height) while holding Shields stress constant. The bed was not allowed to deform. An increase in bed ramp height causes an increase in discharge ratio and sediment discharge ratio, because more discharge and sediment flows into the major bifurcate than into the minor bifurcate with high inlet step. An increase in inlet step also increases the water surface slope in the minor bifurcate. A steeper water surface slope in the minor bifurcate requires more bed load to be delivered to the entrance of the minor bifurcate to remain in equilibrium, and this can only happen if the Shields stress is larger.

This results in a counterintuitive, inverse relationship between water and bed load discharge in the smaller discharge channel of equilibrium bifurcations, because an increase in discharge ratio simultaneously causes an increase in water surface slope (and hence bed load transport) and a decrease in discharge in that channel. Therefore the trend of this equilibrium function is a consequence of the elevated and depressed water surface around the bifurcation point that allows for equilibrium asymmetrical energy slopes and sediment transport rates in the bifurcate arms (Edmonds and Slingerland, 2008).

Kleinhans et al. (2008) presented model results, obtained with the Delft3D model, that help understanding bifurcations. These are the competition between an upstream bend with a downstream gradient advantage of the bifurcate in the inner bend, the length of the bifurcates relative to the backwater adaptation curve, variable versus constant discharge, the effects of upstream width/depth ratio and the length of the upstream bend. The general morphological development of bifurcations

with an upstream bend is described by Kleinhans et al. (2008) as follows: in the first few years, alternating bars develop from the plane bed and migrate downstream. Then a fixed bar develops at the inner bend upstream of the bifurcation. Meanwhile, a bar and pool migrate side by side into the bifurcates and become fixed in position as well. If the downstream conditions in both bifurcates are equal, the outer-bend becomes dominant. This is caused by helical flow, forcing sediment into the inner bend, so that deposition will take place in the inner bend and erosion in the outer bend. Initially, the division of sediment is fairly similar to that of flow. Later flow and discharge are increasingly discharged into one bifurcate. Finally, the sediment transport declines more rapidly than the discharge. This is caused by the increasing transverse slope of the bed into the closing bifurcate, which deflects the sediment transport into the larger bifurcate and the increasing relative roughness due to the decrease in water depth. Consequently, the discharge in the closing bifurcate then stabilizes at a small but nonzero value. For sharper bends, the silting up of one bifurcate occurs more rapidly.

The effect of an upstream bend can be counteracted by increasing the gradient of the inner-bend bifurcate. If the gradient of the inner-bend bifurcate is 30 percent higher than the gradient of the outer bend the inner bend always becomes the major bifurcate. For a difference in gradient of 10 percent, the inner-bend bifurcate dominates for gentle bends, while the outer-bend bifurcate dominates for sharp bends. In conclusion, a gradient advantage can be counteracted by an upstream bend. Hence combinations exist of bend radius and downstream gradient for which a bifurcation remains quasi-balanced for a longer time.

Longer bifurcates cause silting up to occur more slowly. Analysis of relatively long bifurcates clarified one important aspect: sharp bends initially silt up more rapidly than gentle bends, but bars become fixed less rapidly, so that eventually the silting up occurs more slowly.

The effect of varying discharge with respect to constant discharge is nearly negligible in rivers with a relatively small width/depth ratio, because the morphological adaptation timescale of a closing bifurcate is of the order of decades whereas a flood takes place within a month. Hence, rivers with a relatively small width/depth ratio that experience a highly seasonal discharge regime can be modelled by using their channel forming discharge.

In bifurcations with small width/depth ratios bar behaviour is damped. In contrast, bifurcations with large width/depth ratios show underdamped bar behaviour. Consequently, a large width/depth ratio causes bars to emerge and extent making the bifurcation evolution fairly unpredictable. The upper Columbia River is characterized by a small width/depth ratio (Locking, 1983; Makaske et al., 2002; Tabata and Hickin, 2003; Abbado et al., 2005), hence the bar behaviour will most likely be damped so that the influence of bars on bifurcations is smaller. Bar dynamics is described in more detail in section 2.4.3.1.

2.4.3 Flow division at bifurcations

In this section nodal point relations describing the division of flow and sediment at bifurcations are described (section 2.4.3.1). Migrating alternating bars have a pronounced effect on bifurcation evolution, therefore theory on alternating bars is described in section 2.4.3.2.

2.4.3.1 Nodal point relations

In order to be able to predict bifurcation networks and bifurcation evolution in 1D models, nodal point relations are needed. Here, the Wang et al. (1995), Bolla Pittaluga et al. (2003), Miori et al. (2006) and Kleinhans et al. (2008) nodal point relations are described.

Wang et al. (1995)
Wang et al. (1995) presented an empirical relation for the division of sediment over two bifurcates:

$$\frac{Q_{s2}}{Q_{s3}} = \left(\frac{Q_2}{Q_3}\right)^k \left(\frac{w_2}{w_3}\right)^{1-k} \qquad (2.4)$$

where k is an empirical power, Q_{s2} and Q_{s3} are the sediment discharges (m³/s) into bifurcate 2 and 3 respectively, Q_2 and Q_3 are the discharges into bifurcate 2 an 3 respectively and w_2 and w_3 are the widths (m) of bifurcate 2 and 3 respectively. The power k depends on the local geometry and has to be calibrated for each bifurcation separately. Wang et al. (1995) found that bifurcations are stable for $k > n/3$ and unstable for $k < n/3$ where n is the effective power on flow velocity u to calculate the sediment transport as $q_s = mu^n$. For all transport equations $n \geq 3$.

In words, the findings of Wang et al. (1995) can be described as follows: if the discharge of a bifurcate decreases, a k larger than $n/3$ would cause an even larger decrease of sediment transport capacity. Hence, the bed of the closing branch is scoured to some extent, which increases the flow discharge capacity of this channel, so a k larger than $n/3$ stabilizes the bifurcation (Kleinhans et al., 2006). The Wang et al. (1995) nodal point relation does not take into account transverse slopes, upstream bends and spiral flow.

Bolla Pittaluga et al. (2003)
Bolla Pittaluga et al. (2003) presented a nodal point that is based on a physical basis, where Wang et al. (1995) used a specified k.
The velocity upstream of the bifurcation (u, in m/s), in the main flow direction, is calculated as:

$$u = \frac{Q_1}{h_1 w_1} \tag{2.5}$$

wherein w_1 is the width of branch 1, h_1 is the water depth taken at the end of branch 1, where the upstream discharge (Q_1) is assumed to be uniformly distributed over the cross-section. The transverse flow velocity, caused by the transverse slope, is then calculated from the flow discharge Q_y that crosses the division between the upstream channel of the two bifurcates (equation 2.6):

$$Q_y = \frac{1}{2}\left(Q_2 - Q_3 - Q_1 \frac{w_2 - w_3}{w_2 + w_3} \right) \tag{2.6}$$

from equation 2.6, the transverse flow velocity v is calculated as follows:

$$v = \frac{Q_y}{h_1 \alpha_w w_1} \tag{2.7}$$

herein $\alpha_w w_1$ is defined as the length upstream of the bifurcation where the flow and sediment cross the dividing line between two bifurcates. In other words, $\alpha_w w_1$ is the maximum distance upstream where a transverse slope is still present. According to Bolla Pittaluga et al. (2003), $1 < \alpha_w w_1 < 3$. Additionally, they found that the bifurcation stability is not sensitive to α_w. Sediment transport in the transverse direction q_{sy} (m^2/s) can then be calculated:

$$q_{sy} = \frac{\tan \beta_s Q_{s1}}{w_1} \tag{2.8}$$

wherein $\tan(\beta_s)$ is:

$$\tan \beta_s = \sin \beta_\tau - \frac{r}{\sqrt{\theta}} \frac{\partial z}{\partial y} \tag{2.9}$$

where $\delta z / \delta y$ = transverse bed slope, $r = 0.3\text{-}1$ is specified, β_τ is defined as:

$$\beta_\tau = \arctan \frac{v}{u} \tag{2.10}$$

34

where θ is the nondimensional bed shear stress (Shields stress),:

$$\theta = \frac{\tau_b}{\rho(s-1)gD_{50}} = \frac{u^2}{C'^2(s-1)gD_{50}} \qquad (2.11)$$

wherein the former is the total Shields stress, and the latter is the grain related shields stress. D_{50} denotes the median grain size of the bed (m), g denotes the acceration of gravity (m/s^2), ρ is the water density (kg/m^3), s-1 is the submerged sediment density (kg/m^3) and τ_b denotes the bed shear stress (N/m^2), given as:

$$\tau_b = \rho g R_r S \qquad (2.12)$$

wherein S is the bed slope (-) and R_r is the hydraulic radius (m) here calculated for assuming rectangular channels:

$$R_r = \frac{wh}{w+2h} \qquad (2.13)$$

C denotes the Chézy coefficient (m$^{0.5}$/s) which indicates bed roughness:

$$C = 18.02\log\left(\frac{12.2R_r}{k_s}\right) \qquad (2.14)$$

wherein k_s is the Nikuradse roughness length (m), if C', then $k_s' = D_{90}$. Now, the transverse transport rate is subtracted from one bifurcate and added to the other:

$$Q_{s2} = \frac{w_2}{w_2+w_3}Q_{s1} + q_{sy}\alpha_w w_1 \qquad (2.15)$$

It follows from continuity that $Q_{s3} = Q_{s1}$-Q_{s2}. Bolla Pittaluga et al. (2003) present a numerical solution to calculate the transverse slope:

$$\frac{\Delta z}{\Delta y} = \frac{z_{2,1} - z_{3,1}}{0.5w_1} \qquad (2.16)$$

where $z_{\text{bifurcate},1}$ is the bed level of the first cell of bifurcate $i = 2,3$.

35

At relatively high Shields stress ($\theta/\theta_{cr} > 1$), one equilibrium solution is found by the Bolla Pittaluga et al. (2003) nodal point relation with both branches open; this solution is found to be invariably stable. For low values of the Shields parameter below the above threshold two other equilibrium configurations appear, which are characterized by different values of water discharge flowing into the two downstream branches. Under these conditions the two new solutions are stable while the previous solution becomes unstable. Stabilization often occurs with the Bolla Pittaluga et al. (2003) nodal point relation because the transverse slope decreases the sediment transport into the closing bifurcate.

Recently, Bertoldi and Tubino (2007) tested the Bolla Pittaluga et al. (2003) nodal point relation, and confirmed its correctness to braided river bifurcations, at least in a qualitative way. Due to the transverse slope effect of bifurcations, modelled by Bolla Pittaluga et al. (2003), bifurcations often stabilize, because the transverse slope counteracts the sediment transport into the closing bifurcate. Upstream meander bend effects, spiral flow and backwater effects are neglected by the Bolla Pittaluga et al. (2003) model.

Miori et al. (2006)

Miori et al. (2006) noted that a gravel bed channel widens when the discharge is increased. Hence, they extended the model of Bolla Pittaluga et al. (2003) with erodible banks. They proposed the usage of either a rational or empirical regime relation.

The adoption of any of the regime relationships to evaluate the width of a channel evolving in time assumes an instantaneous adaption of channel width to flow conditions, which is an assumption which need not be true in natural rivers. In order to preserve the evolutionary character of the width adaptation process, Miori et al. (2006) developed a further differential equation for channel width:

$$\frac{dw}{dt} = \frac{1}{T_w}(w_r - w) \qquad (2.17)$$

where T_w denotes the time scale of the width adaptation process and w_r is computed by a regime relationship. Modelling results point out that results do not differ qualitatively, whatever the value of T_w.

Field evidence and results of laboratory experiments (Bertoldi et al., 2005) indicate that channel narrowing as a consequence of decreasing discharge is not physically justified by regime relations, at least not at a relatively short timescale. As a result of the increasing width, the system only admits of stable configurations which are strongly asymmetrical.

Kleinhans et al. (2008)

As becomes clear in section 2.4.1, spiral flow caused by an upstream meander bend might have a large effect on bifurcation dynamics, therefore Kleinhans et al. (2008) presented a nodal point relation, including transverse slope, upstream meander bend, and thus spiral flow effects. They did so by extending the Bolla Pittaluga et al. (2003) relation with the deflection by bend flow based on simplified theory for flow and sediment transport in bends of Struiksma et al. (1985).

In the Kleinhans et al. (2008) nodal point relation, $\tan\beta_s$ is not calculated with equation 2.9 from Bolla Pittaluga et al. (2003), but by a formulation including both transverse slope and spiral flow effects from Struiksma et al. (1985):

$$\tan\beta_s = \frac{\sin\beta_\tau - \dfrac{1}{f(\theta)}\dfrac{\delta z}{\delta y}}{\cos\beta_\tau - \dfrac{1}{f(\theta)}\dfrac{\delta z}{\delta x}}$$

(2.18)

with:

$$\beta_\tau = \arctan\frac{v}{u} - \arctan A\frac{h}{R}$$

(2.19)

wherein R is meander bend radius (m), the second part of the equation defines the influences of the bend effect. The spiral flow coefficient A is:

$$A = \frac{2\varepsilon}{\kappa^2}\left(1 - \frac{\sqrt{g}}{\kappa C}\right)$$

(2.20)

wherein κ is the Kármán's constant and ε = calibration coefficient. The bed slope effect on sediment transport is calculated as follows:

$$f(\theta) = 9\left(\frac{D_{50}}{h}\right)^{0.3}\sqrt{\theta}$$

(2.21)

It should be noted that the Bolla Pittaluga et al. (2003) nodal point relation was developed for braided rivers. Compared to meandering rivers, braided rivers have relatively straight, shallow channels where spiral flow can perhaps be neglected (Kleinhans et al., 2008). In meandering rivers, and anastomosing rivers such as the upper Columbia River, spiral flow in bends cannot be neglected. Therefore the

Kleinhans et al. (2008) nodal point relation is of most interest for this review. Hence, a review of a comparison between Delft3D and the Kleinhans et al. (2008) 1D model done in Kleinhans et al. (2008) is presented below.

The Kleinhans et al. (2008) nodal point relation always predicts development to a stable, highly asymmetrical discharge division.

Flow and sediment become increasingly discharged into one bifurcate and the bifurcates silt up or scour along their whole length, but mostly in their upstream parts. In the final stages the sediment transport declines more rapidly than the discharge. This is caused by the increasing transverse slope of the bed into the closing bifurcate, which forces sediment transport into the larger bifurcate. Secondly, the relative roughness k_s/h increases as k_s is constant while the water depth decreases due to silting up of the bifurcate, which affects sediment transport rate. This leads to stabilization of the closing bifurcate at a small but nonzero value.

Kleinhans et al. (2008) found that their nodal point relation behaves qualitatively similar to the 3D model. However, they found that there are large quantitative differences in the initial stages, the adaptation path to equilibrium and the equilibrium attained due to the complexities present in the 3D model but absent in the 1D model. The initial differences are due to the formation of local bars and scour at the bifurcation in the 3D model. The differences in adaptation and final equilibrium discharge division are caused by the three-dimensionality of the flow and the bed (local bars and scour at the bifurcation, and nonlinear transverse bed slopes) in the 3D model, and the adaptation of the spiral flow for infinite ideal bends as represented in the 1D model. This discrepancy is larger for high width/depth ratios.

So summarizing, the main differences between the 3D and 1D model are caused by bar dynamics at the bifurcation. In example Miori et al. (2006) describes quasistable bifurcations with a fluctuating discharge division due to migration of alternating bars. Hirose et al. (2003) describes a switch bifurcation (main flow switching to the opposite bifurcate). Especially for bifurcations that are balanced by opposing factors, such as an upstream bend effect opposed by an increased slope of the inner bend bifurcate bar dynamics may have a pronounced effect on the bifurcation evolution. For these bifurcates, the direction of evolution is very sensitive to minor changes of topography (bars and scoures) at the bifurcation.

Bar dynamics are especially large in wide shallow rivers, where bars are underdamped. In narrow, deep channels the bars are mostly overdamped, causing the effects of bar dynamics on bifurcation in narrow, deep channels to be small. The upper Columbia River is composed of narrow, deep channels (Locking, 1983; Makaske et al., 2002; Tabata and Hickin, 2003; Abbado et al., 2005). Hence, bifurcations in this anastomosing system are most likely only slightly influenced by bars. Consequently, the 1D model will most likely be applicable here. A rivers bar regime can be

determined using Struiksma's theory (Struiksma et al., 1985) This theory is described in the next section.

2.4.3.2 Bar regime and applicability of nodal point relations

As described in the previous section, migrating alternating bars have a pronounced effect on bifurcation evolution. Therefore, understanding of the bar regime in the upper Columbia River is crucial when attempting to model bifurcation evolution with 1D nodal point relations. In this section the theory behind bar regime in alluvial rivers is described, and equations that enable the determination of a rivers bar regime are presented.

The bar regime in alluvial rivers can be predicted with Struiksma's theory (Struiksma et al., 1985). Struiksma et al. (1985) distinguished three bar regimes: underdamped bars, overdamped bars and unstable, spatially growing bars. The bar regime depends on the interaction parameter IP, which is the ratio between the adaptation length of a bed disturbance λ_s and the adaptation length of the flow λ_w. The interaction parameter depends strongly on the channel width-depth ratio (figure 2.12). In the overdamped regime, a river responds quickly to a perturbation, causing only a single bar to form in the lee side of the perturbation. In the underdamped regime, a perturbation leads to the formation of several bars that decrease in size in downstream direction and eventually are damped out completely. In the unstable, spatially growing, bar regime, a perturbation causes bars to emerge and to grow without being damped, leading to the emergence of bars everywhere on the riverbed downstream of the perturbation. The 1D nodal relations do not take into account the effect of alternating bars on the bifurcation evolution, therefore the nodal point relations of Wang et al. (1995), Bolla Pittaluga et al. (2002), Miori et al. (2006) and Kleinhans et al. (2008) are only suitable for the prediction of bifurcation evolution in overdamped rivers. Therefore it is important to determine a river's bar regime prior to modelling bifurcation evolution. A river's bar regime can be obtained with the following equations.

Struiksma et al. (1985) identified four characteristic length scales to identify the bar regime, namely the adaptation length of the flow λ_w (m):

$$\lambda_w = \frac{C^2 h}{2g} \tag{2.22}$$

the adaptation length of a bed disturbance λ_s (m):

$$\lambda_s = \frac{1}{\pi^2} h \left(\frac{W}{h}\right)^2 f(\theta)$$ (2.23)

the wavelength of the bar L_p (m):

$$2\pi \frac{\lambda_w}{L_p} = \frac{1}{2} \sqrt{(n+1)\frac{\lambda_w}{\lambda_s} - \left(\frac{\lambda_w}{\lambda_s}\right)^2 - \left(\frac{n-3}{2}\right)^2}$$ (2.24)

and the damping length L_D (m):

$$\frac{\lambda_w}{L_D} = \frac{1}{2}\left(\frac{\lambda_w}{\lambda_s} - \frac{n-3}{2}\right)$$ (2.25)

wherein n is the power of unit sediment transport rate to flow velocity.
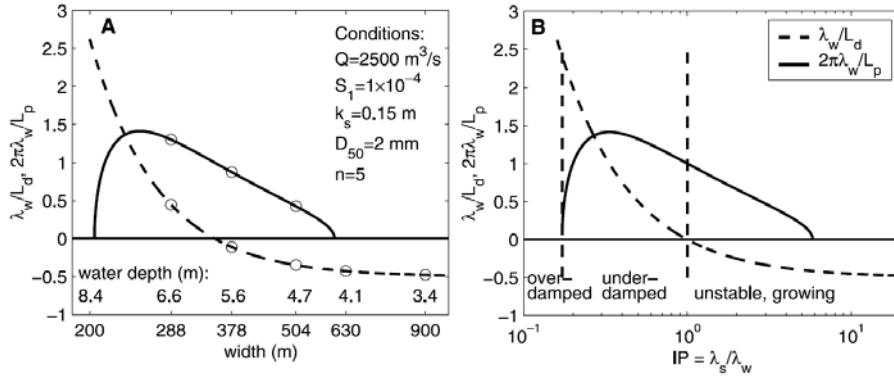
Fig. 2.12: Bar regime as a function of width/depth ratio (left) and IP (right) (Kleinhans et al., 2008, after Struiksma et al., 1985).

The interaction parameter determines whether an alluvial river channel is characterized by an overdamped, underdamped or unstable bar regime. Struiksma and Klaassen (1988) defined the occurrence of the three bar regimes as follows:

$$\frac{\lambda s}{\lambda w} \leq \frac{2}{n+1+2\sqrt{2n-2}}$$ overdamped (2.26a)

$$\frac{2}{n+1+2\sqrt{2n-2}} < \frac{\lambda s}{\lambda w} \leq \frac{2}{n-3}$$ underdamped (2.26b)

$$\frac{2}{n-3} < \frac{\lambda s}{\lambda w}$$ unstable (2.26c)

40

2.5. Confluences

In a river network, confluences are a frequent occurring phenomenon. Confluences are less complex than bifurcations. At a confluence, the flow and sediment discharge in the downstream channel is simply the sum of flow and sediment discharge from both upstream channels.

The joining of two upstream channels at a confluence leads to friction between the water masses from both upstream channels. This leads to highly complex three-dimensional patterns of flow and sediment transport (Rhoads and Kenworthy, 1998; Best and Reid,1985; Best and Roy, 1991; Biron et al., 2002; 2004). The two dominant controls on these three-dimensional patterns are confluence angle and the ratio of discharge of the confluent channels (Best, 1986). The confluence planform also modifies the distribution and magnitude of processes present and this subsequently affects the bed morphology. Mosley (1975) distinguished two basic types of confluence planform: (1) junctions in which the post confluence channel forms a linear extension of the mainstream and (2) junctions that are more 'Y' shaped in planform, termed asymmetrical and symmetrical confluences respectively (Best, 1986).

The bed morphology induced by the three-dimensional patterns of flow and sediment transport can be divided into three elements: (1) a distinct, commonly steep, avalanche face that forms at the entrance of the confluent channels, (2) a region experiencing pronounced scour within the centre of the junction and (3) bars of sediment, originating from the scour hole, which are formed in the post-confluence channel (Best, 1986) (figure 2.13).
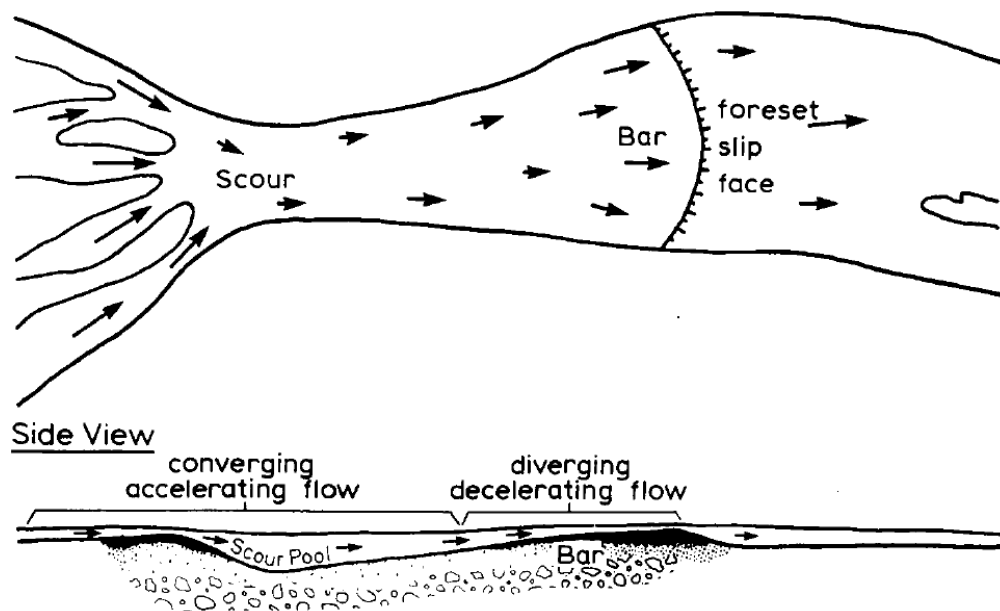

Fig. 2.13: Bed morphology of a braided river confluence (Best, 1986).

In both symmetrical and asymmetrical planform confluences, the scour hole originates at the upstream corner of the junction and stretches downstream. The orientation of the scour varies with both confluence angle and channel discharge ratio. The origin of the scour is complex. It involves both

41

initial erosion and distinctive sediment transport pathways within the confluence. Erosion of the bed occurs along the turbulent shear layer between the two flows. This generates vertical vortices within the flow which erode the bed sediment (Best, 1986; Rhoads and Kenworthy, 1998). A secondary flow pattern emerges. This secondary flow pattern is characterized by flow towards the middle at the surface and flow towards the side of the channel at the bottom. Consequently, material that is being eroded by the vertical vortices is transported towards the side of the channel, leading to the formation of the scour hole. This secondary flow pattern leading to the formation of a scour hole is illustrated by Rhoads and Kenworthy (1998), who measured secondary velocities in the Copper Slough – Kaskaskia River confluence in the central United States (figure 2.14).
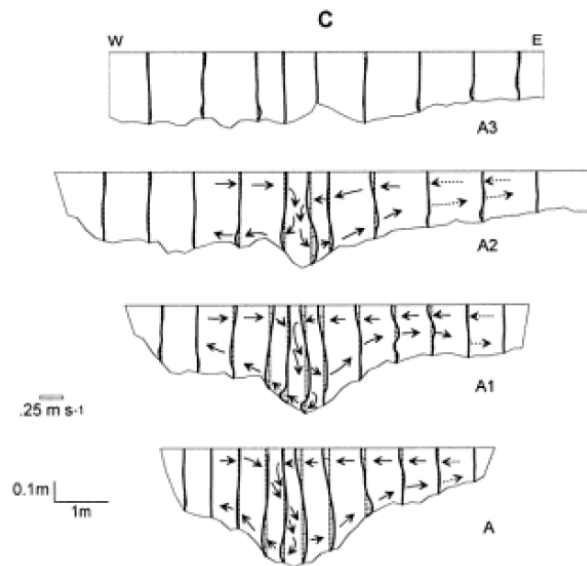
Fig. 2.14: Cross-stream components of cross-stream velocities and patterns of secondary velocity. A3 is the most upstream transect, just in front of the confluence point, C is the most downstream point where al turbulence, and thus secondary velocity, is damped (from Rhoads and Kenworthy, 1998).

The higher the confluence angle, the larger is the friction and consequently the vertical vortices and the secondary velocity. So the scour hole depth is larger for high confluence angles than for low confluence angles.

The steepness of the avalanche face is determined by the depth of the scour hole. Ashmore and Parker (1983), Best, (1985) and Kjerfve et al. (1979) (in Best, 1986) developed a scour hole depth predictor based on confluence angle α. The Ashmore and Parker (1983) predictor reads as:

$$d_s = 2.235 + 0.0308\alpha \qquad\qquad (2.27)$$

the Best (1985) predictor as:

$$d_s = -3.262 + 1.589 \ln \alpha \tag{2.28}$$

and the Kjerfve et al. (1979) predictor as:

$$d_s = -0.40 + 0.04\alpha \tag{2.29}$$

where d_s is the dimensionless scour depth:

$$d_s = \frac{h}{\left(\left(Y_m + Y_t\right)/2\right)} \tag{2.30}$$

wherein h_m is mean depth of the main channel (m) and h_t is mean depth of the tributary channel (m).

3. Fieldwork

3.1. Introduction

In this section the fieldwork methods are described and the results are analysed. In section 3.2 the methods employed are described. In section 3.3 the fieldwork data is presented. The collected field data is analyzed in section 3.4 in order to (1) obtain model input and (2) to test model concepts. The interpretation and discussion of the fieldwork data are performed in combination with the interpretation and discussion of the model results (section 5).

3.2. Methods

In this section the methods employed during the fieldwork are described. First, the period and site of the fieldwork is described (section 3.2.1). Second, the instrumentation is discussed (section 3.2.2). Finally, the methods employed for the different measurements is described (section 3.2.3).

3.2.1. Period and site

All measurements obtained for this research were performed in the Spillimacheen – Castledale reach of the upper Columbia River, between the Spillimacheen bridge and the cross-valley transect of Makaske (1998) (figure 2.6) .

Fieldwork in the upper Columbia River was performed from August 17 to September 30, 2009. In this period the upper Columbia River was characterized by a gradually falling discharge stage, the fall in water level at the Spillimacheen bridge in this period was 0.7m.

During the fieldwork campaign, measurements were performed for this research project as well as for the research of Lavooi (2010). Approximately 2 weeks were used for the process-based morphological measurements employed in this research and 4 weeks were used for the sedimentological measurements employed in the research of Lavooi (2010). The measurements performed for this research span the period August 22 to September 11.

3.2.2. Instrumentation

The measuring instruments used for this research were a level and stadia rod, echo sounder, laser range finder, grab sampler, sand ruler, open gouge, vibra-corer and shear vane.

The level and stadia rod were used to obtain the planform of bifurcations, confluences, crevasses and bars. Additionally, the level and stadia rod were used to obtain cross-profiles of bars that were located above the water surface to complete the echo sounding measurements that were performed under the water surface in order to obtain full channel cross-profiles. The precision of the level and stadia rod was approximately 1cm in 100m.

An echo sounder and laser range finder were used to obtain cross- and long-profiles of bifurcations, confluences, crevasses and bars. The precision of the echo sounder was 0.1m. The laser range finder had an precision of 1m.

The grab sampler was used to obtain bottom sediment samples, of which the median grain size was determined with a sand ruler and the sorting according to the method of Berendsen and Stouthamer (2001). The sand ruler had an accuracy of approximately 100μm. To account for the spatial variability of the bed sediment, three samples were taken each time to obtain an average value for median grain size.

The open gouge and vibra-corer were used to perform borings in residual channels. The depth of each sample had an precision of approximately 1cm for the open gouge. The depth control of the vibra-corer was less accurate. The recovery of the sampling was 50 percent. The shear vane was used to determine bank strength.

3.2.3. Methods of analysis

In this section the procedure employed to process the field data is described. In section 3.2.3.1, procedure employed to obtain planform is described. In section 3.2.3.2, the procedure used to obtain long-profiles is described. The procedure used to obtain cross-profiles is described in section 3.2.3.3. In section 3.2.3.4 the procedure used to obtain bank strength is described. Finally, the procedure employed for boring in residual channels is described in section 3.2.3.5.

3.2.3.1. Planform

The planform of bifurcations, confluences and sharp bends was measured by level and stadia rod and laser range finder measurements of the water level position along banklines at bifurcations, confluences and sharp bends. Level and stadia rod were used to measure angle. The laser range finder was used to measure distance. The exact planform could then be obtained by triangulating the measured positions in a x-y coordinate system.

3.2.3.2. Long-profiles

Long profiles were derived by navigating down- or upstream following the channel's thalweg. Approximately every 8m, the distance to a reference point was measured as well as the water depth. After obtaining the water depth, the levee height was added to the water depth to obtain the bankfull water depth. The reference point for measuring distance was either the bifurcation or confluence point. When passing the bifurcation or confluence point, a new reference point was chosen along the side of the channel. Note that an error was made by using the bifurcation of confluence point as reference point (figure 3.1). In figure 3.1 an example is given with a bifurcation point as reference point. For the situation where the long-profile is obtained over the dashed line, the intersection between the line D_0 (m) and the dashed line is the location of the bifurcation in the long-profile. The line $D_{measured}$ (m) is the distance measured to the bifurcation. This length overestimates the real distance to the bifurcation, $D_{corrected}$ (m). Note that closer to the bifurcation point, the overestimation increases. To overcome this problem, an angle of 90 degrees is assumed between the line $D_{corrected}$ and D_0. According to the law of Phytagoras the true distance to the bifurcation $D_{corrected}$ can now be calculated as:

$$D_{corrected} = \sqrt{D_{measured}^2 - \frac{D_0^2}{2}}$$
(3.1)

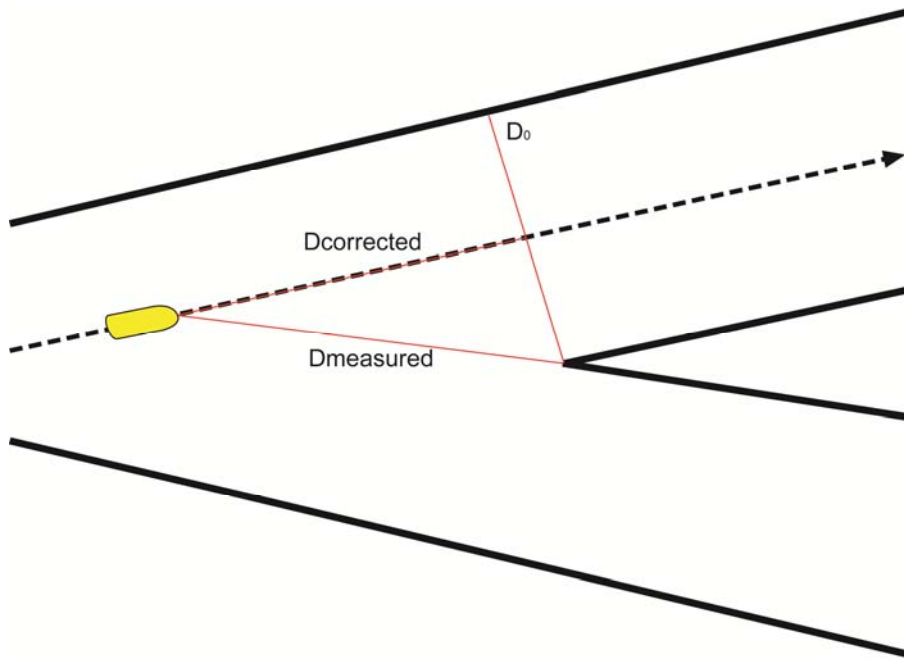where $(D_0)/2$ is $D_{measured}$ at the moment the boat navigates across the line D_0.

Fig. 3.1 Illustration of the difference between the measured distance to the bifurcation point (D $_{measured}$) and the real distance to the bifurcation point (D$_{corrected}$) when measuring a long-profile at a bifurcation.

3.2.3.4. Cross-profiles

Cross-profiles of the bed surface were collected by navigating from one side of the channel to the other, perpendicular to the flow direction. The laser range finder was used to measure the distance to one side of the channel. Each time the distance to one side of the channel was measured, the water depth was measured with the echo sounder. Approximately every 5m a measurement was performed. To enable conversion of measured water depth to bankfull depth the difference in height and distance between waterline and levee top was measured. In some cases, especially on bars, the distance from waterline to levee top was relatively large. In these cases the level and stadia rod were used to obtain sufficient measurements between the position of the water level and the levee top. This was mostly the case in sharp bends, where bars were present at the inner bend above the water surface during the moderate discharge stage in September. The distance from the water line was measured by using a measuring tape. This distance is not the true distance ($D_{corrected}$), but is measured along the surface of the bar ($D_{measured}$). The true distance can be calculated by assuming an angle of 90 degrees between *height (m)* and $D_{corrected}$ so that an equation similar to equation 2.6 can be used to calculate the corrected distance (figure 3.2).
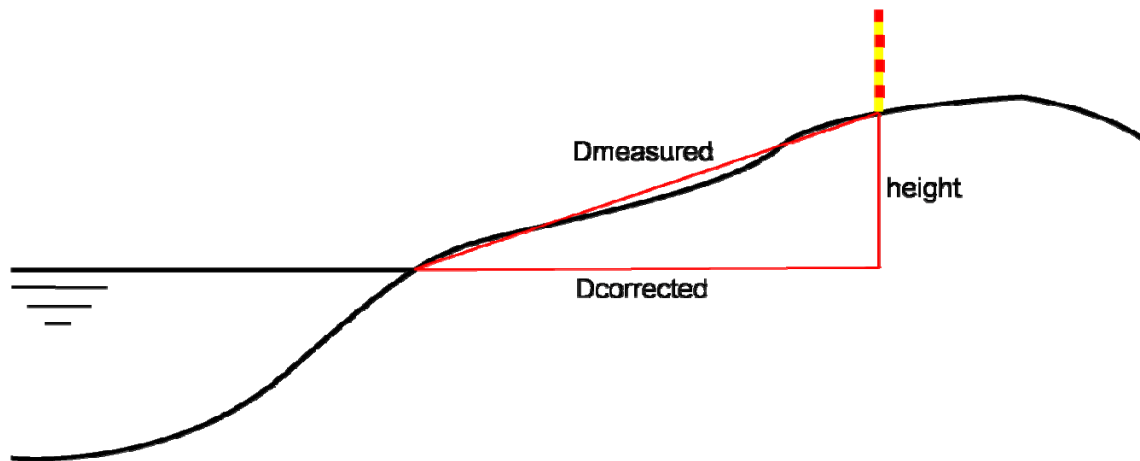

Fig. 3.2: Illustration of the difference between the measured distance from the waterline to a measurement location ($D_{measured}$) on a bar and the real distance ($D_{corrected}$).

48

3.2.3.5. Bank strength

Fig. 3.3: Location of the different shear vane measurement levels.

The lateral erodibility of the levees of the upper Columbia River was investigated by performing shear vane measurements. At each measurement location, the bank strength was measured close to the water level (level 1), in the strongly rooted part of the bank (level 3) and in between these levels (level 2) (figure 3.3), in order to address differences in bank strength between these levels.

3.2.3.6. Residual channels

The lithological sequence of residual channels was obtained by performing borings with an open gouge or vibra-corer in residual channels. The borings were performed in the lowest point of the residual channel. Sediments were sampled at each 10cm. For each sample, texture, amount of organic content, presence of plant remnants, colour, oxidation-reduction stage, percentage of gravel, presence of lime, presence of iron oxide and other details were determined. For sandy material, the median grain size, sorting and angularity were determined (method of Berendsen and Stouthamer, 2001). The borehole logs were documented in LLG 2008. This is a program designed by the department of Physical Geography of the Utrecht University for processing of borehole logs.

3.3. Results of fieldwork

Measurements have been performed on bifurcations, confluences, crevasses, sharp and gentle bends and residual channels. Additionally, bank strength and bed material have been measured at several locations along the river.

In section 3.3.1 a map is shown which indicates the location of the measurements. In section 3.3.2, the measurements on crevasses, bifurcations and confluences are presented. This section starts with a classification of the different types of bifurcations and confluences (section 3.3.2.1). In section 3.3.2.2, the crevasse, bifurcation and confluence measurements are described. The measurements on sharp and gentle bends are described in sections 3.3.3.1 and 3.3.3.2, respectively. In section 3.3.4, the bank strength measurements are presented. Finally, the residual channel measurements are described in section 3.3.5.

3.3.1. Measurement locations

The location of the measured bifurcations, confluences, crevasses, sharp and gentle bends, and residual channels, as well as locations where bank strength was measured and bed material was sampled are shown in figure 3.4.

3.3.2. Crevasses, bifurcations and confluences

3.3.2.1. Classification

In the upper Columbia River valley, four different types of bifurcations, and two types of confluences were distinguished. The four types of bifurcations were:

1.   Asymmetric discharge division, newly formed bifurcation; crevasse.
2a.   Asymmetric discharge division, relatively young bifurcation; growing minor bifurcate.
2b.   Asymmetric discharge division, relatively old bifurcation; growing major bifurcate.
3.   Symmetric discharge division, quasi-stable bifurcation; bifurcates approximately equal in size.

The two types of confluences were:

1.   Symmetric planform confluence; upstream channels with symmetric discharge division.
2.   Symmetric planform confluence; upstream channels with asymmetric discharge division.

During the fieldwork campaign, the overall planform and cross- and long-profiles were measured at two crevasses, five bifurcations and six confluences. At three bifurcations and confluences, the bifurcation followed within a short range of a confluence, consequently the bifurcation and confluence were measured as a single complex. In this section the overall planform and bathymetry of the measured crevasses, bifurcations and confluences is described.
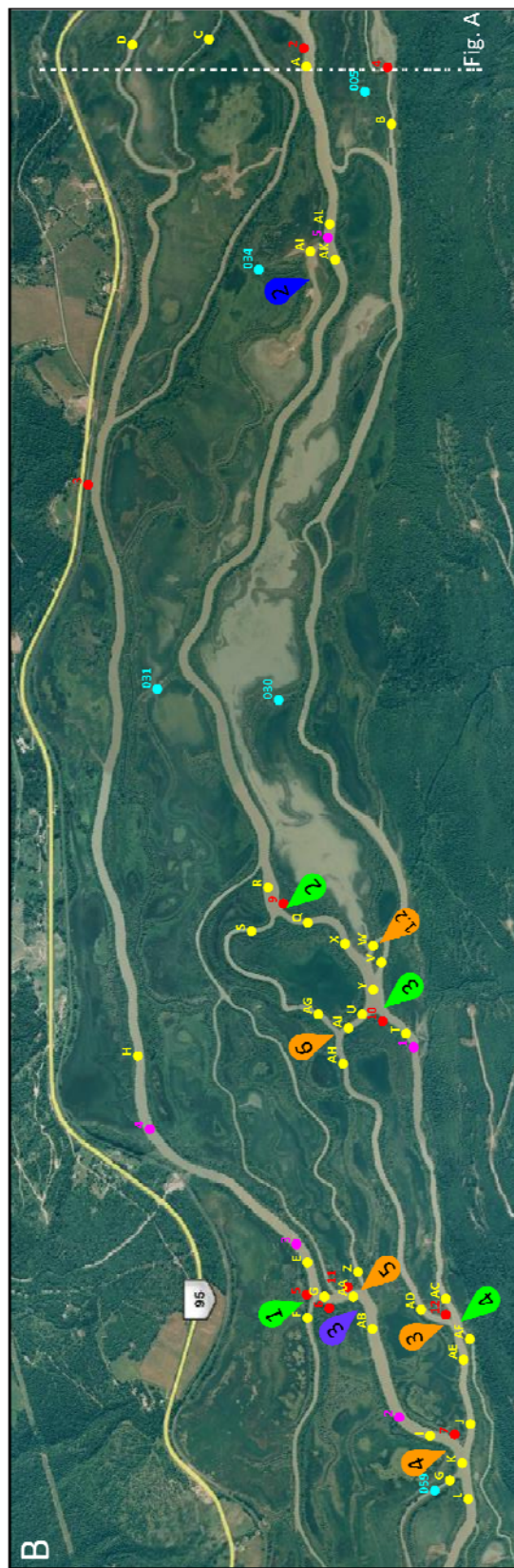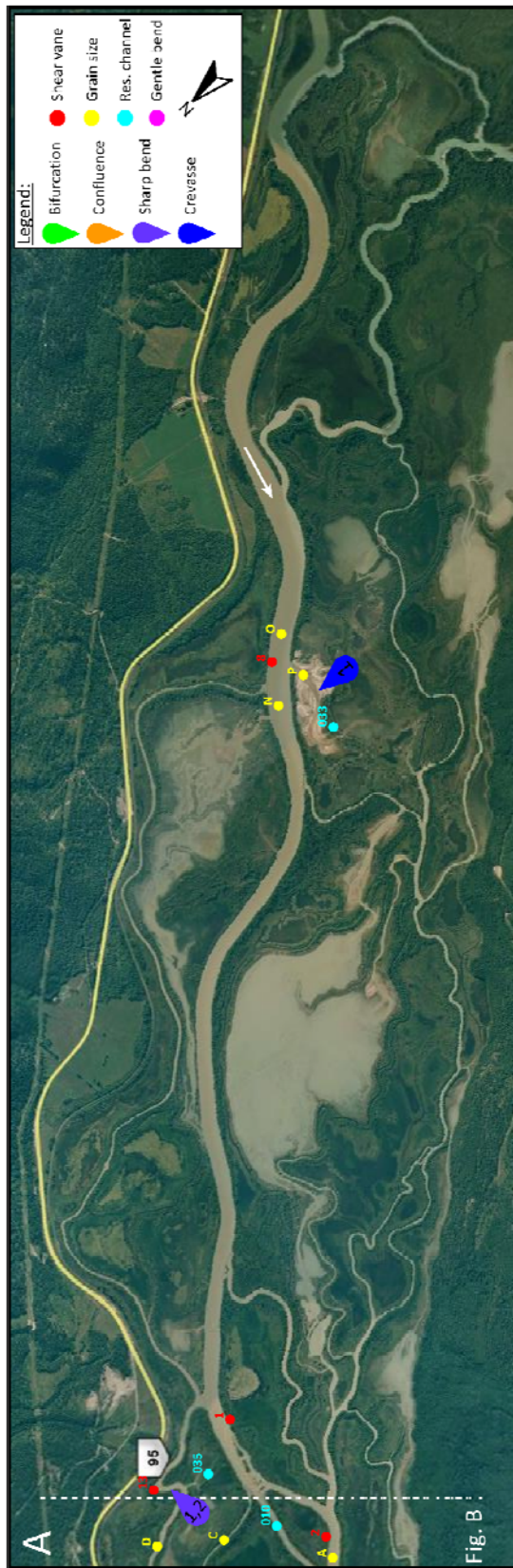
Fig. 3.4: Measurement locations.

52

3.3.2.2. Crevasses

Both crevasses can be described as newly formed bifurcations. Crevasse 1 and 2 are both characterized by a large body of sand, in which a small channel has formed. The entrance of both crevasses is relatively deep, and the cross-profiles are comparable to that of fully developed channels (figure 3.5; 3.8). However, within 50m of the crevasse entrance the bankfull water depth decreases to less than 1m (figure 3.6); only a small crevasse channel is present.

The entrance of crevasse 1 is completely blocked by a log-jam, consequently the long-profile stretches only to the crevasse entrance (figure 3.6). The median grain size in the main channel upstream of the crevasse entrance is 870μm, downstream of the crevasse entrance this is 720μm. The material is poorly sorted. The median grain size in the crevasse entrance is 1000μm, which is significantly coarser than the median grain size in the main channel. Note that the bed material grain size is highly variable, the three samples downstream of the crevasse entrance are; 420-600, 600-850 and 850-1000μm (table 3.3). The median grain size of the sample thus ranges between 420-1000μm.

The median grain size in crevasse 2 is 925μm. In the main channel, upstream of the crevasse (channel A), the median grain size is 580μm. Downstream of the crevasse the median grain size is 810μm. So both crevasse 1 and 2 trap coarse bed material. Both crevasse 1 and 2 (figure 3.7) are located in an outer bend. Note that the planform of crevasse 1 suggests an inner bend situation, but in the fieldwork period the thalweg was found to be located close to the crevasse entrance.
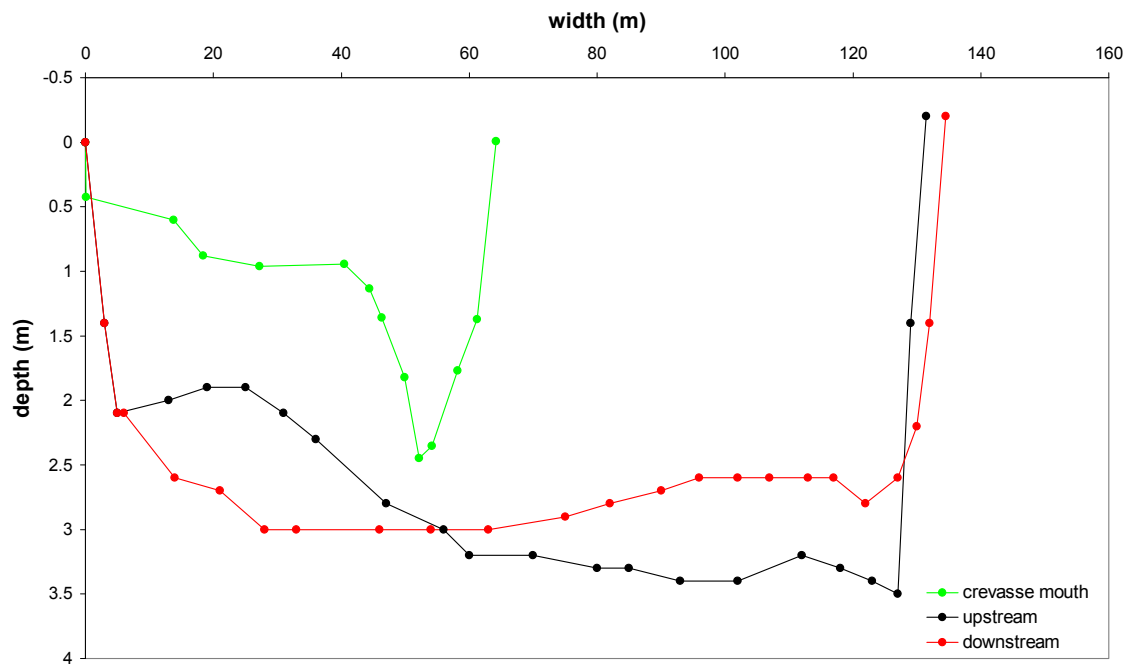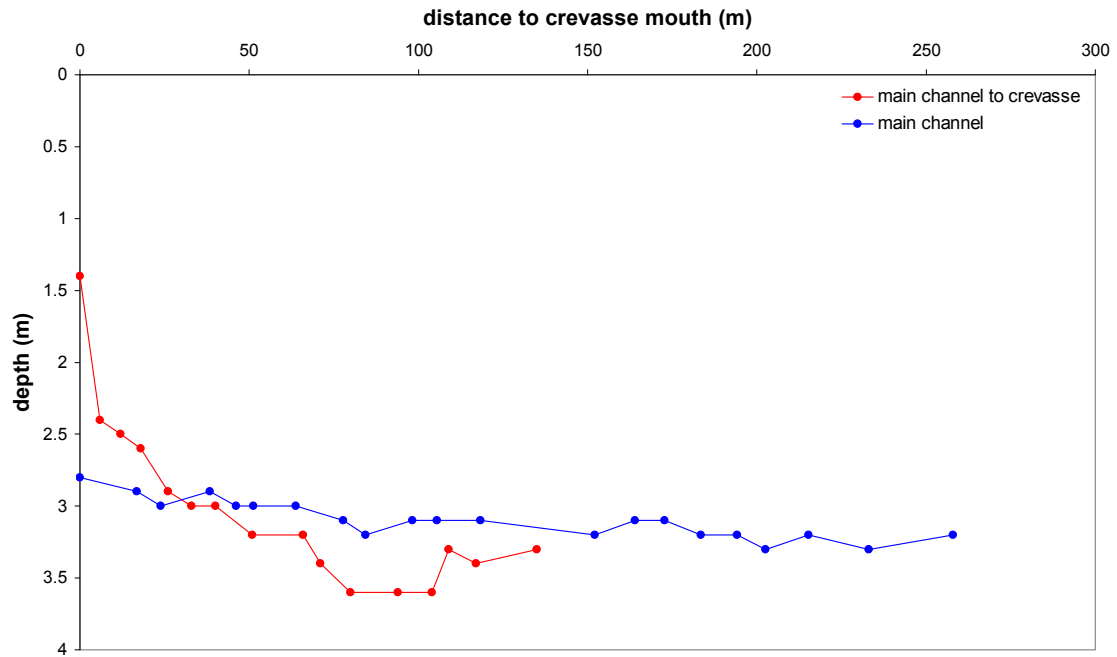

Fig. 3.5: Cross-profiles of crevasse 1.
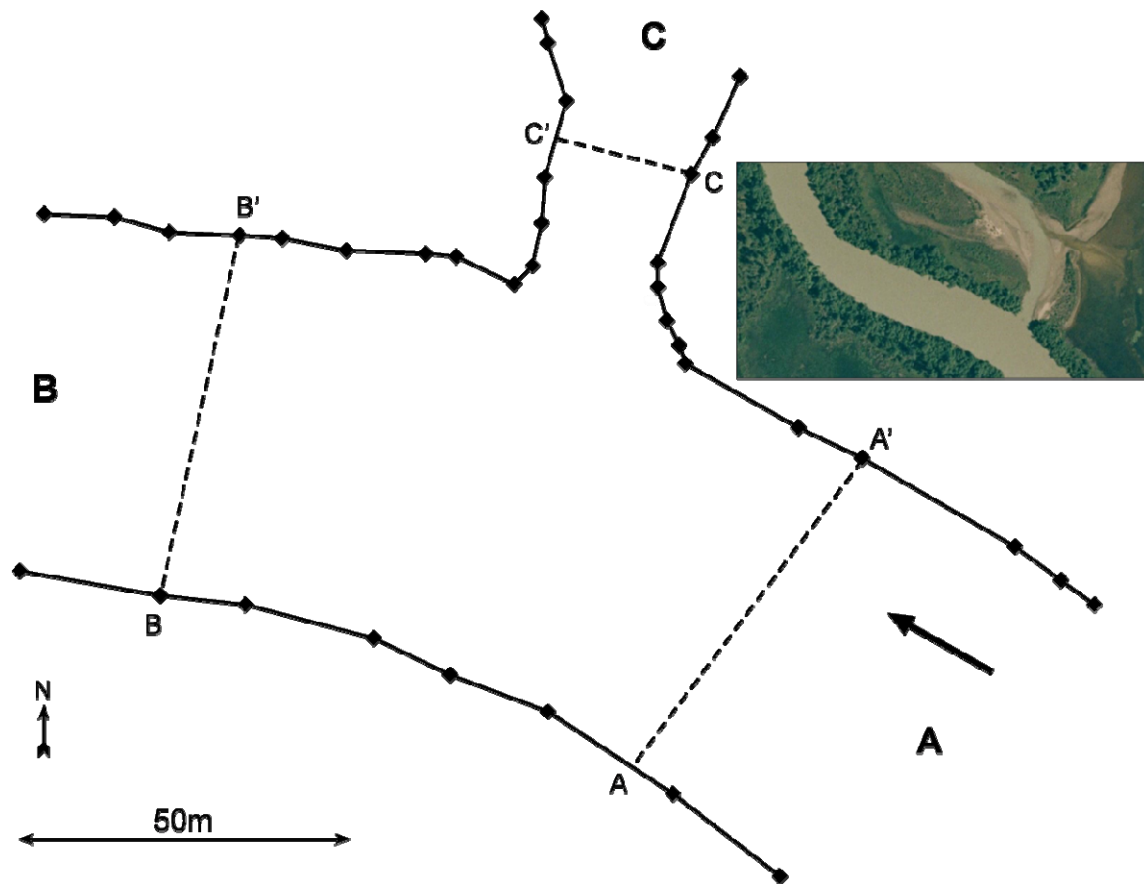
Fig. 3.6: Long profiles of crevasse 1.
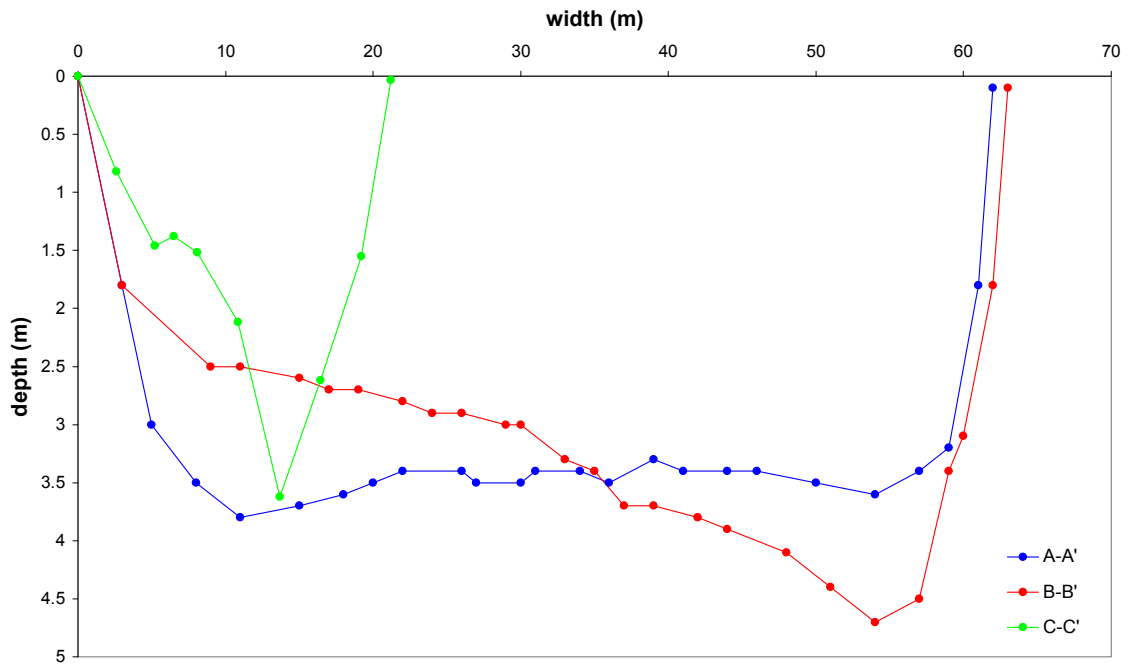

Fig. 3.7: Planform of crevasse 2.
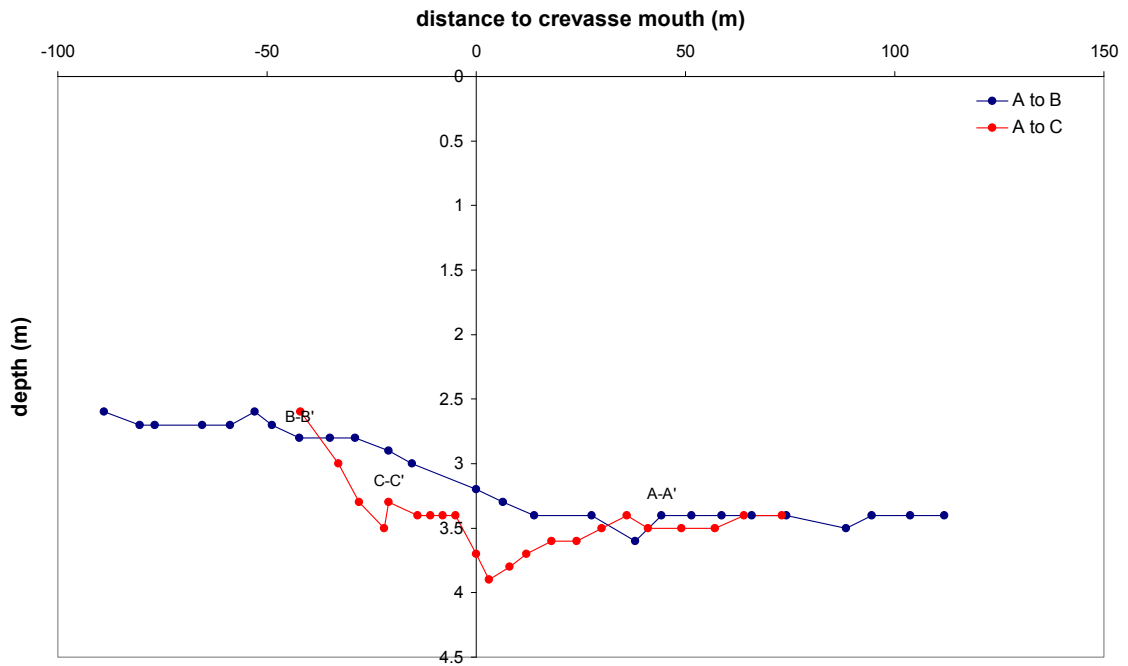
Fig. 3.8: Cross-profiles of crevasse 2.

Fig. 3.9: Long-profiles of crevasse 2.

3.3.2.3. Bifurcations and confluences

In this section the overall planform and cross- and long-profiles of the measured bifurcations and confluences is presented. In table 3.1 the bankfull width and flow area of the measured bifurcations and confluences as well as the non-dimensional inlet step (depth of the minor bifurcate divided by the depth of the upstream channel; h_2/h_{up}) of the measured bifurcations are summarized.

Table 3.1: Bankfull width and flow area in the upstream (W_{up}; A_{up}) from cross-profiles, major bifurcate (W_1; A_1) and minor bifurcate (W_2; A_2), bifurcation asymmetry (W_1/W_2; A_1/A_2) and non-dimensional inlet step (h_2/h_{up}) from long-profiles..

	W_{up}	W_1	W_2	W_2/W_1	A_{up}	A_1	A_2	A_2/A_1	h_2/h_{up}
Bifurcation	m	m	m	-	m²	m²	m²	-	-
1	55	56	31	0,55	165	141	65	0,46	0,51
2	87	37	30	0,82	225	112	74	0,67	-0,29
3	98	49	34	0,70	267	133	76	0,57	0,27
4	63	54	21	0,38	240	218	48	0,22	0,00
5	73	65	19	0,30	330	315	25	0,08	1,04
	W_{down}	W_1	W_2	W_1/W_2	A_{down}	A_1	A_2	A_1/A_2	
Confluence	m	m	m	-	m²	m²	m²	-	
1	73	54	26	0,48	190	143	63	0,44	
2	73	26	28	1,08	190	63	62	0,98	
3	63	43	41	0,95	240	138	119	0,86	
4	73	61	48	0,79	330	198	176	0,89	
5	68	61	25	0,42	195	184	56	0,30	
6	46	34	30	0,88	162	91	90	0,99	

Bifurcation 1

Bifurcation 1 is located in a bend (figure 3.10). The minor bifurcate (C) is located in the outer bend, the major bifurcate (B) is located in the inner bend. At the bifurcation point, a small log-jam is present, which is partially human induced since wooden poles are implemented to trap driftwood in order to maintain most of the discharge in the main channel. In the fieldwork period, a small bar was present in the inner bend. Just downstream of the bifurcation, a small channel connects to bifurcate B, forming a confluence.

Four cross-profiles are measured (figure 3.10; 3.11), one in the upstream channel (A-A'), one in both bifurcates (B-B'; C-C') and one in front of the bifurcation (D-D'). The width of the upstream channel and major bifurcate is approximately equal. The maximum depth of the major bifurcate exceeds the maximum depth of the upstream channel, this is caused by the fact that the cross-section in the major bifurcate is located in a bend, and consequently a deep outer bend pool is present. Due to the shallow water depth in the inner bend of the major bifurcate, the total flow area is largest in the upstream channel. The maximum water depth in the minor bifurcate is slightly smaller than the maximum water depth in the upstream channel and the major bifurcate. Its width is approximately half the width of the

major bifurcate, and hence its flow area is significantly smaller than the flow area of the major bifurcate. In the cross-profiles, no large alternating bars are present.

An inlet step of approximately 1.5m is present at the entrance of the minor bifurcate (figure 3.12). At 70-100m downstream of the bifurcation the water depth in the minor and major bifurcate is characterized by a sharp increase. In the major bifurcate this is caused by the fact that the water depth is not measured in the outer bend pool, but close to the inner bend.

Bifurcation 1 can be characterized as a type 2a bifurcation. Bifurcation 1 experiences an asymmetric discharge division. The inlet step indicates that the minor bifurcate is silting up, and thus closing.

The median grain size in channels A and B is 510μm, in channel C the median grain size is 180μm. The sediment samples in channel C are characterized by a large fraction of mud within the sand. The median grain size in the minor bifurcate is thus significantly smaller than in channels A and B.
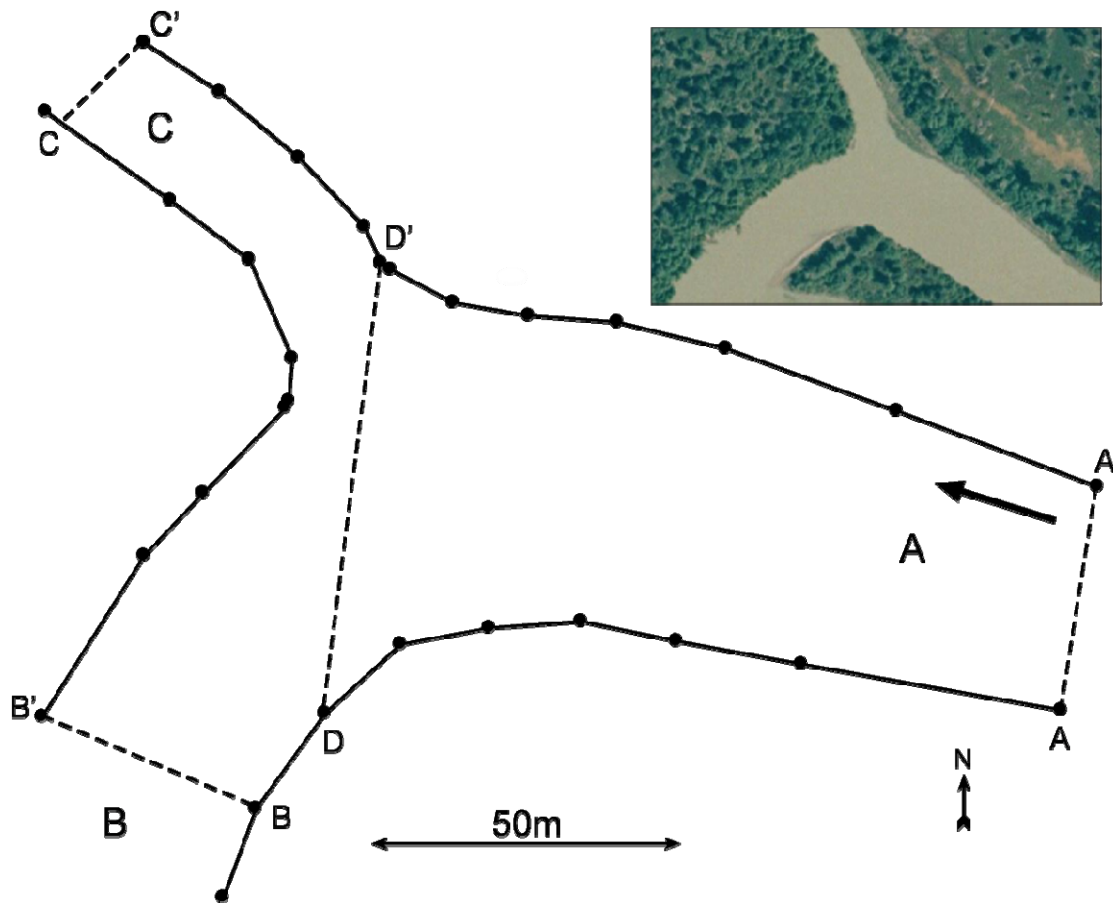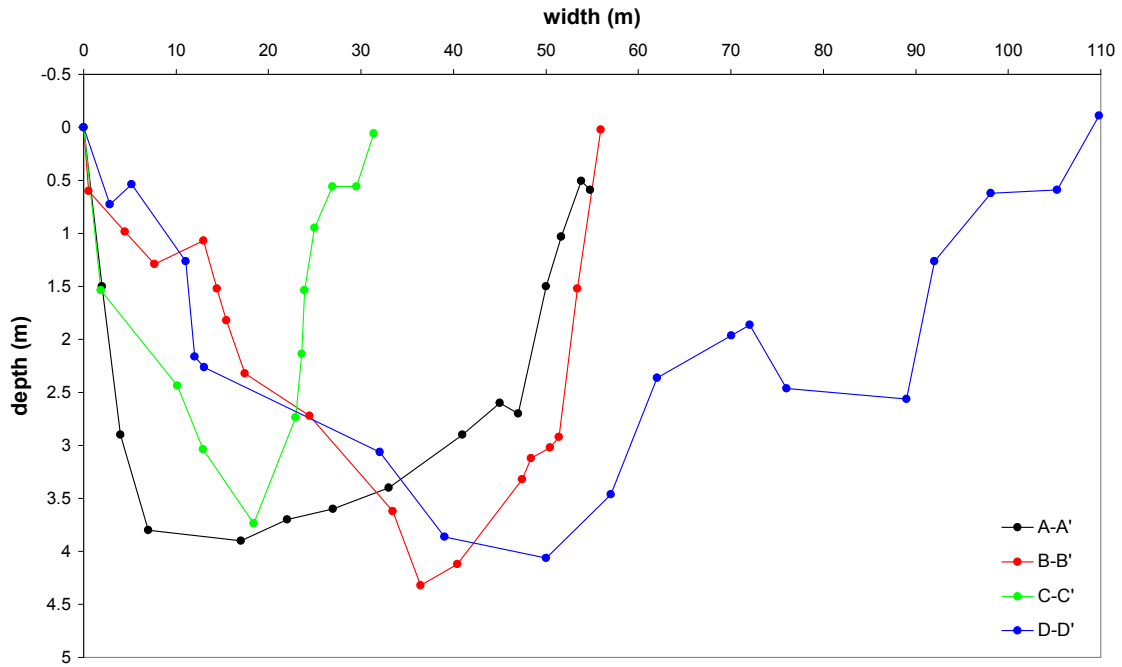

Fig.3.10: Planform of bifurcation 1.
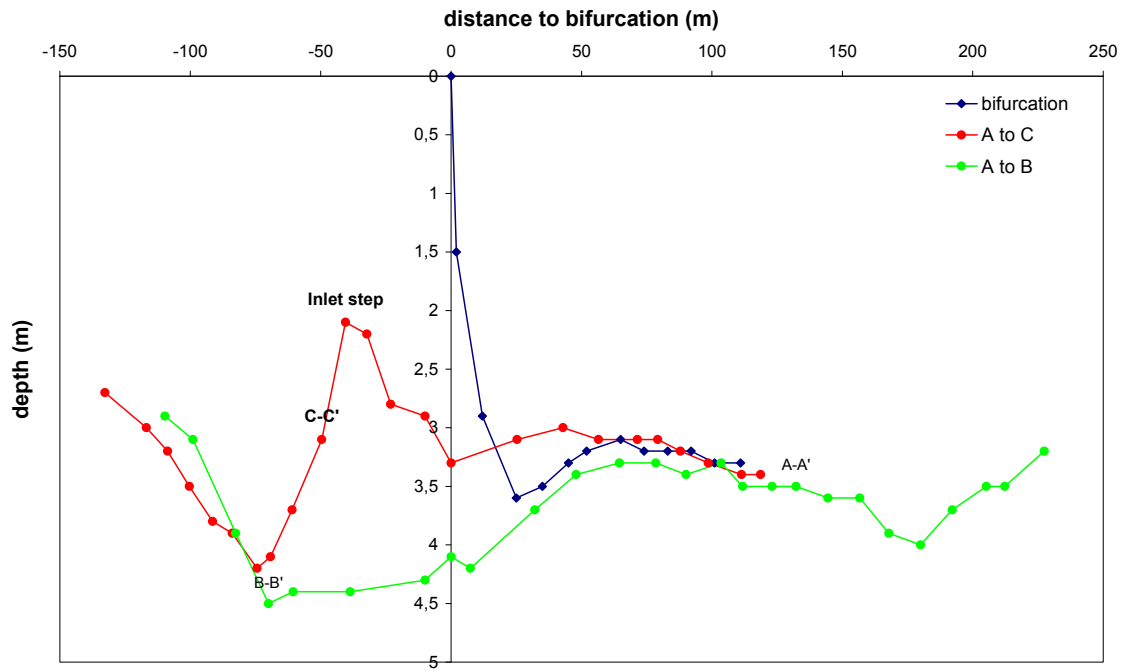
Fig. 3.11: Cross-profiles of bifurcation 1.

Fig. 3.12: Long-profiles of bifurcation 1.

Bifurcation 2

Bifurcation 2 is characterized by a gentle upstream bend (figure 3.13). Its most striking feature is that the sum of the widths of the bifurcates is smaller than the width in the upstream channel (figure 3.14), whereas in most bifurcates the sum of the widths of the bifurcates exceeds the width in the upstream channel (bifurcation 1, 4, 5). Both bifurcates are characterized by a sharp bend away from the main channel, causing them to direct their flow almost perpendicular to the flow direction in the main channel within 100m downstream of the bifurcation point.

Bifurcate B is slightly larger than bifurcate C. The depth of both bifurcates is larger than the depth in the upstream channel (figure 3.14; 3.15). This was caused by the decrease in width, which leads to an increase in depth if the flow velocity does not significantly increase. Flow velocity measured in the thalweg of the main channel and in both bifurcates, measured by boat drifting in the absence of wind is indeed approximately equal. Respectively, 0.83, 0.89 and 0.92m/s in the main channel, bifurcate B and bifurcate C. No inlet step is present at the entrance of the bifurcates (figure 3.15). As expected from the cross-profiles, the channel depth increases at the entrance of the bifurcates. The sharp increase in channel depth in channel B is caused by a deep outer bend pool. Since the flow area of both bifurcates is approximately equal, bifurcation 2 can be defined as a type 3 bifurcation. The median grain size of the bed material in channel A is 650μm, in channel B it is 790μm and in channel C it is 480μm. All samples are very poorly sorted.
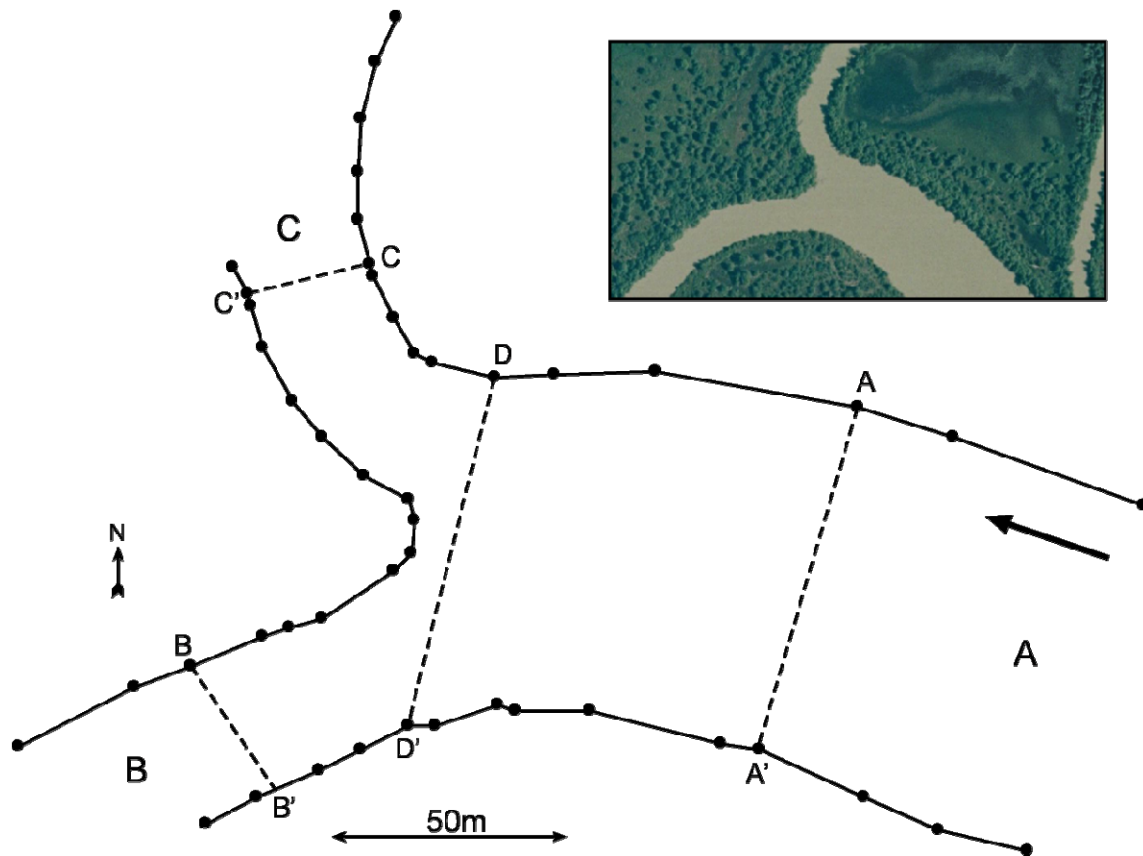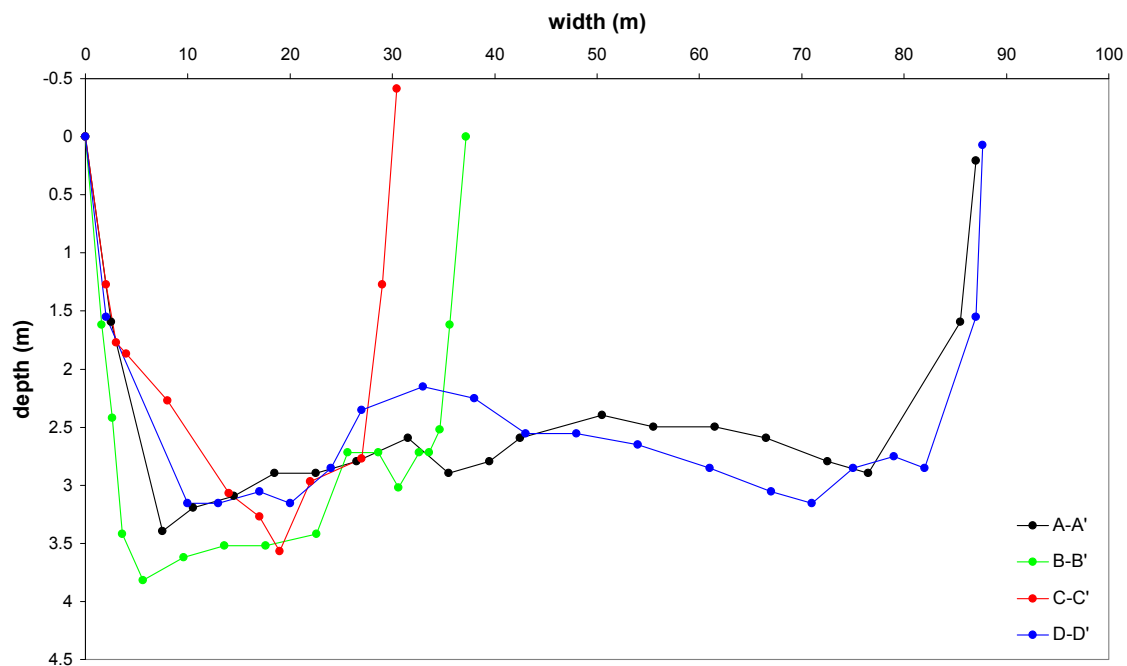
Fig. 3.13: Planform of bifurcation 2.
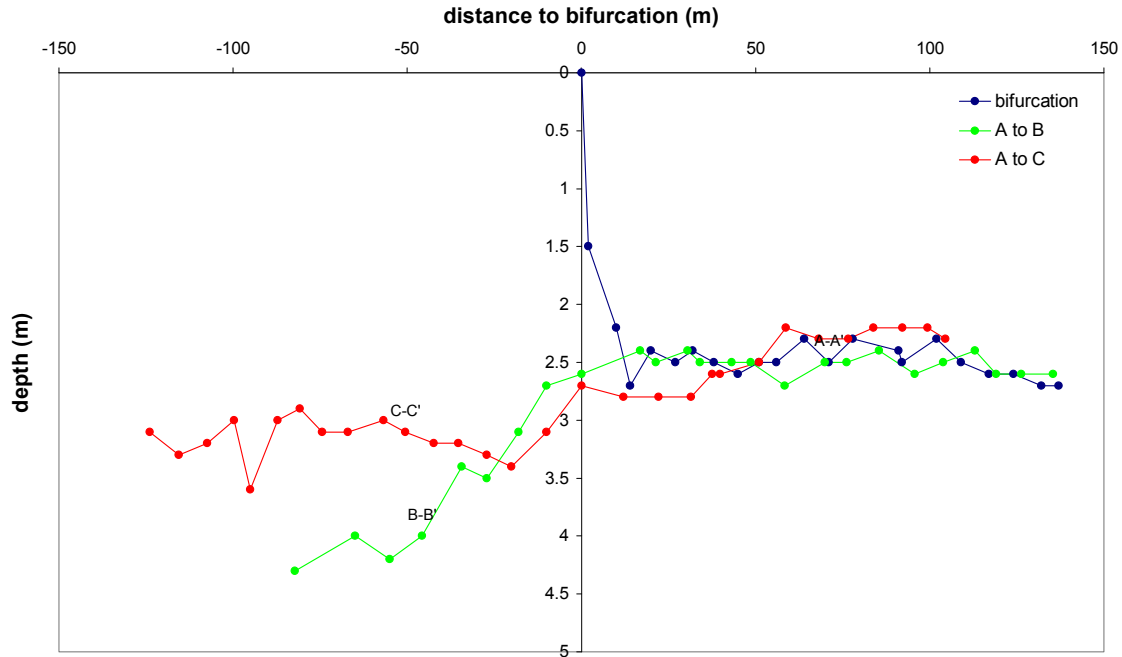

Fig. 3.14: Cross-profiles of bifurcation 2.

Fig. 3.15: Long-profiles of bifurcation 2.

Bifurcation 3, confluence 1,2

Bifurcation 3 is located downstream of two confluences (figure 3.16). The main upstream channel, channel E, is the downstream part of channel B of bifurcation 2. Channels C and D originate from the same channel, and are separated by a small island. Since channel E is the major channel, the thalweg is directed from channel E towards channel A, causing bifurcate B to be located in an 'inner bend'.

Bifurcate A is larger than bifurcate B (figure 3.17). The sum of the widths of bifurcate A and B is smaller than the width upstream of the bifurcation. The water depth in bifurcate A is approximately equal to the water depth in the upstream channel. Bifurcate B is characterized by an inlet step of approximately 0.7m. About 100m downstream of the bifurcation point, the water depth in bifurcate B is characterized by a sharp increase which is caused by a deep outer bend pool.

Bifurcation 3 can be defined as a transition from a type 3, to a type 2b. Bifurcate A is slightly larger than bifurcate B, and the inlet step in front of bifurcate B (figure 3.19) suggests that bifurcate B is silting up. The median grain size in channels A and B is respectively 600μm and 670μm. At the cross-section G-G', upstream of bifurcation 3 the median grain size is 760μm. The grain size division at the bifurcation is thus approximately equal. Channels C and D are characterized by a significantly smaller width than channel E (figure 3.18), whereas their maximum water depth is comparable. No significant scour holes are present at confluence 1 and 2 (figure 3.19). The confluence angle of confluence 1 is 59 degrees; the confluence angle of confluence 2 is 45 degrees. Both confluence 1 and 2 can be

61

characterized a type 2 confluence. The median grain size in channel C, D, and E, is respectively 720μm, 460μm, and 760μm.
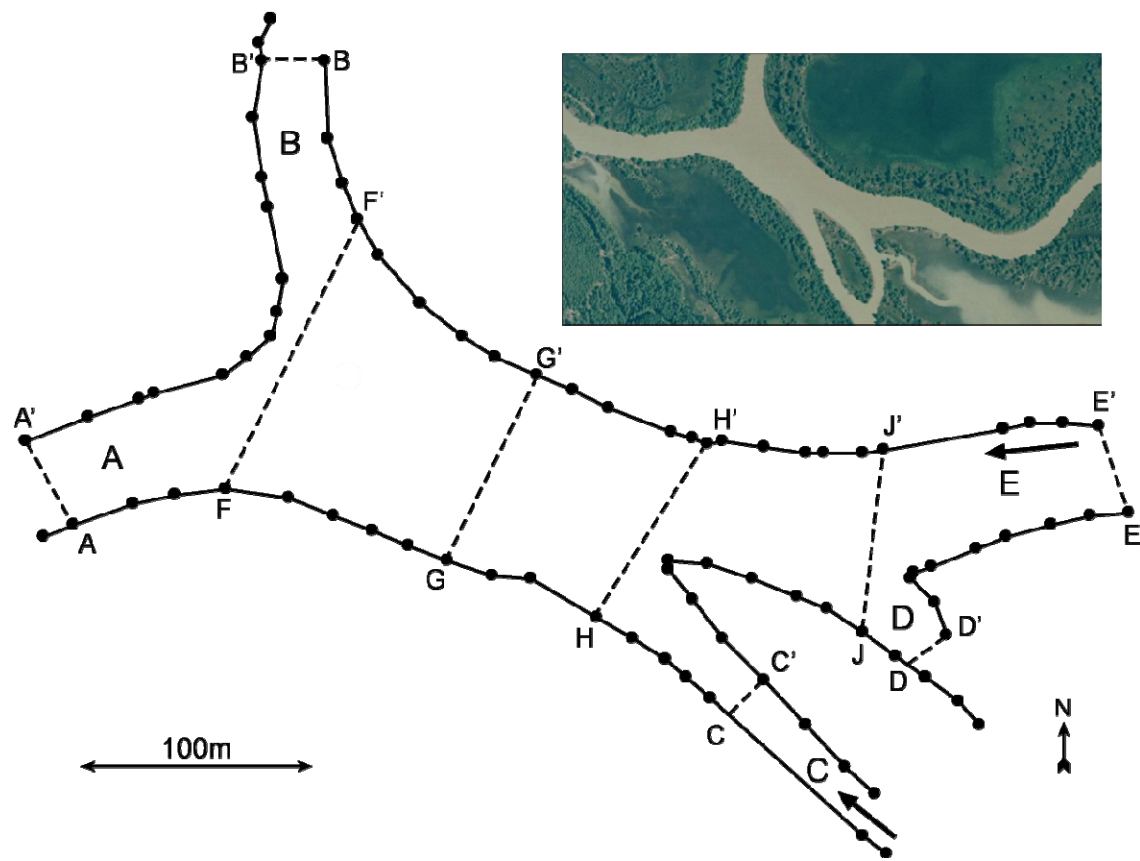

Fig. 3.16: Planform of bifurcation 3 and confluences 1 and 2.
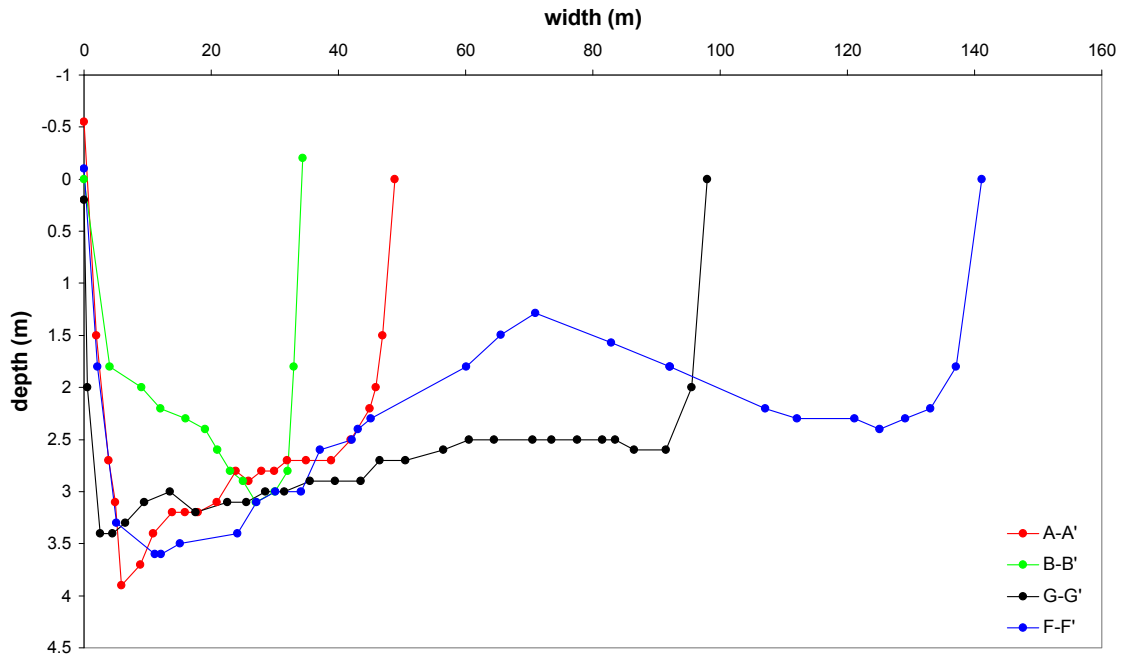
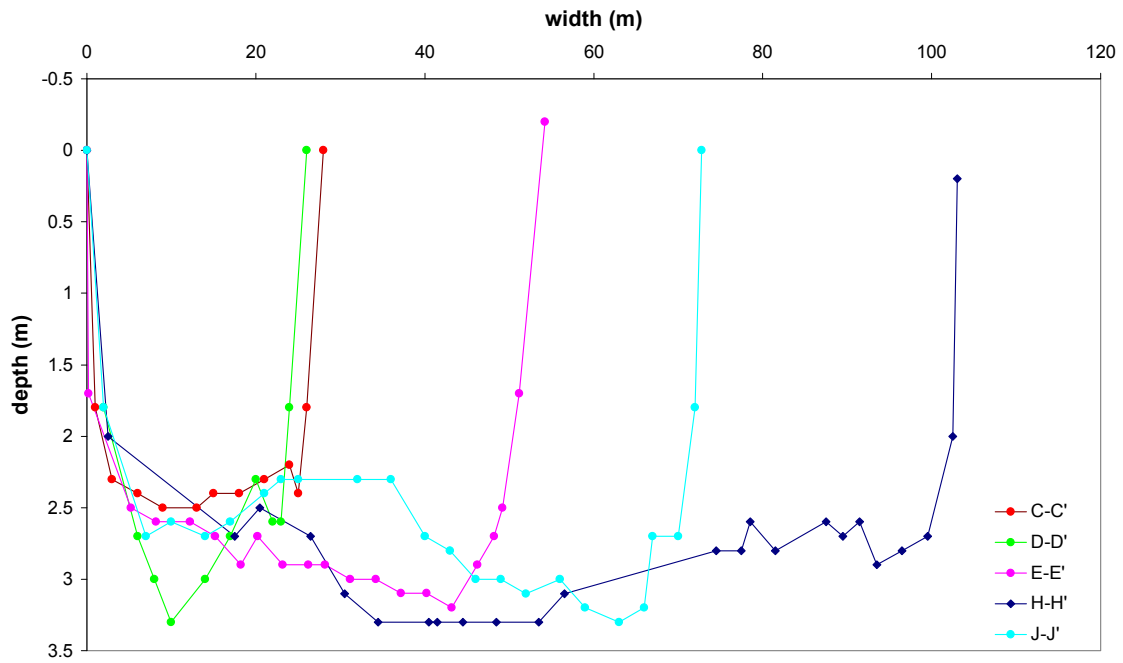*Fig. 3.17: Cross-profiles of bifurcation 2.*
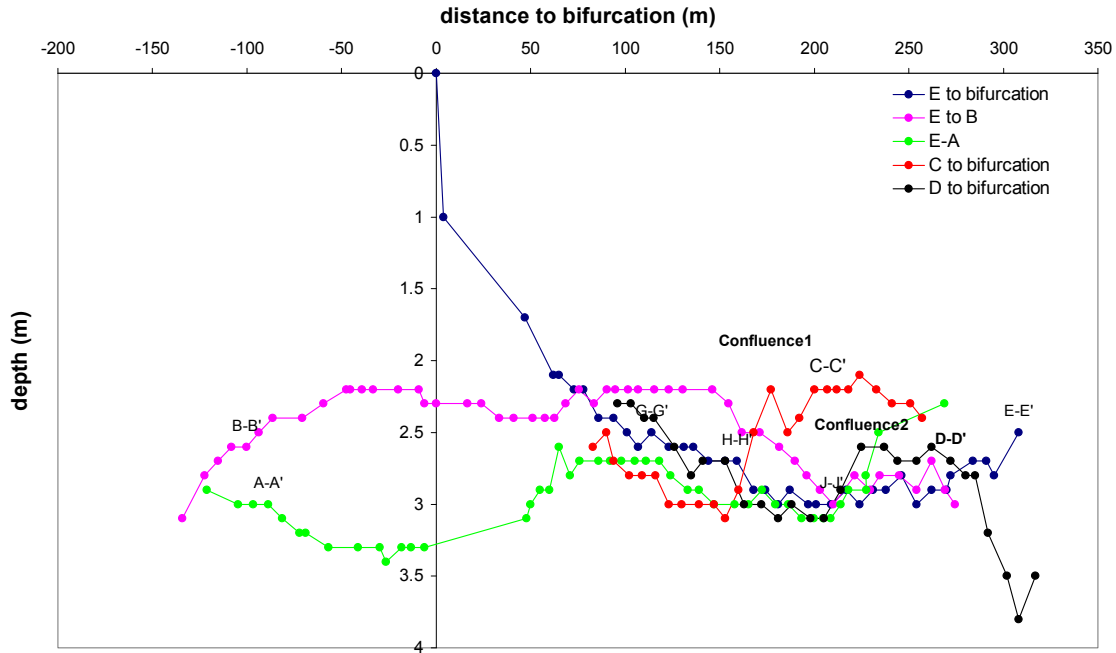

Fig. 3.18: Cross-profiles of confluence 1 and 2.

Fig. 3.19: Long-profiles of bifurcation 3 and confluence 1 and 2.

Bifurcation 4, confluence 3

Bifurcation 4 is characterized by the presence of a large upstream confluence. Channel B is the downstream part of channel A of bifurcation 3. Channel A is the downstream part of channel C of confluence 6. No upstream bend is present. In front of the bifurcation point, a large patch of woody debris is present (figure 3.20). This log-jam causes the actual point of flow division to be more upstream.

The major bifurcate (C) is significantly larger than the minor bifurcate (D). Its width is approximately 2 times larger, and its depth is approximately 1.5 times as large (figure 3.21). No inlet step is present in the minor bifurcate (figure 3.23). This may be caused by fact that bifurcation 4 is a type 2a bifurcation. Channel D is a young channel, which has favorable downstream conditions compared to channel C and is consequently growing (Makaske, personal communication), so that an inlet step is absent. The median grain size in channel C is 1000μm. This coarse median grain size is caused by a very coarse sample with a median grain size >2000μm. In channel D, the median grain size of the bed is 150μm, whilst the largest fraction of the material consists of mud.

Channels A and B are comparable in size. A deep scour hole is present downstream of the confluence. The depth of both channel A and B is approximately 3m (figure 3.22). The maximum depth of the scour hole is almost 7m. The median grain size of channel A and B is 650μm. The confluence angle is 62 degrees. Confluence 3 can be characterized as a type 1 confluence.
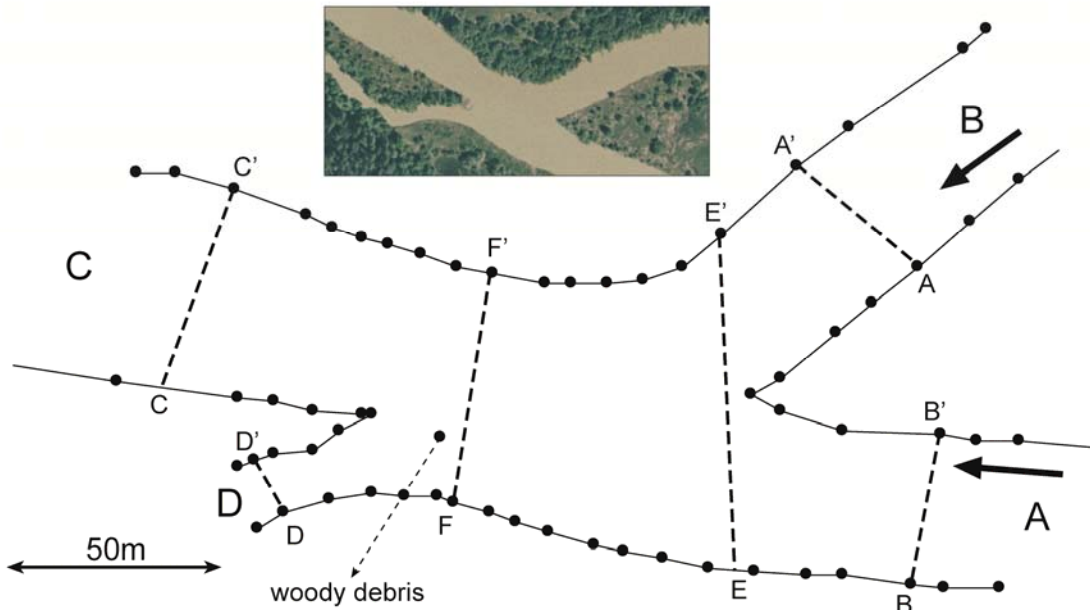
64

Fig. 3.20: Planform of bifurcation 4 and confluence 3.
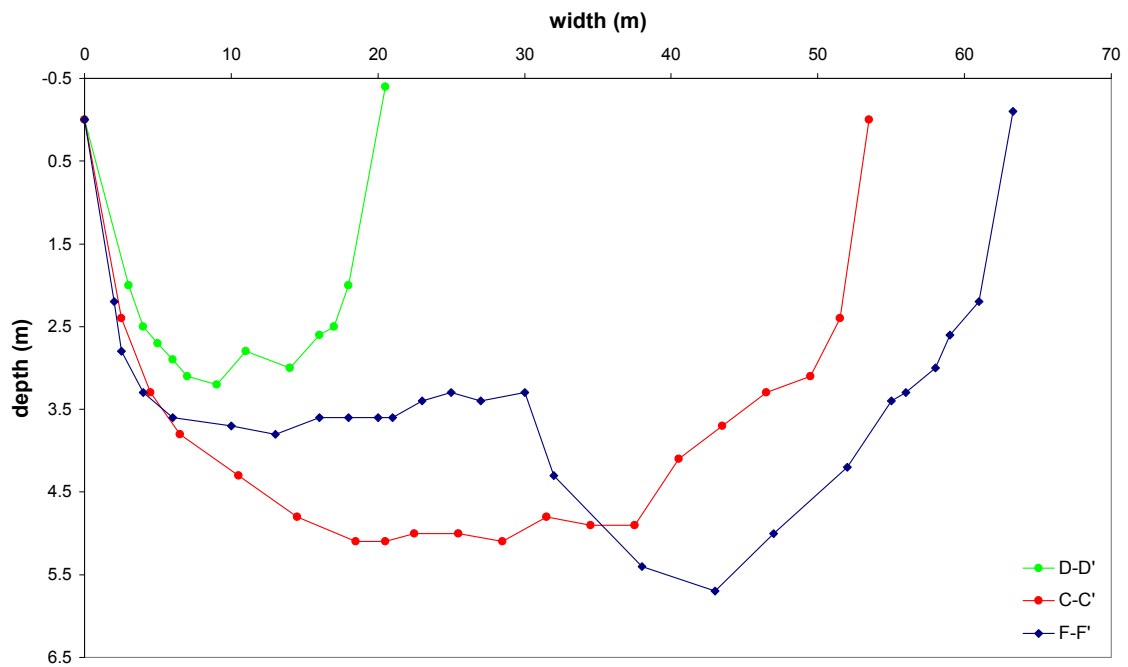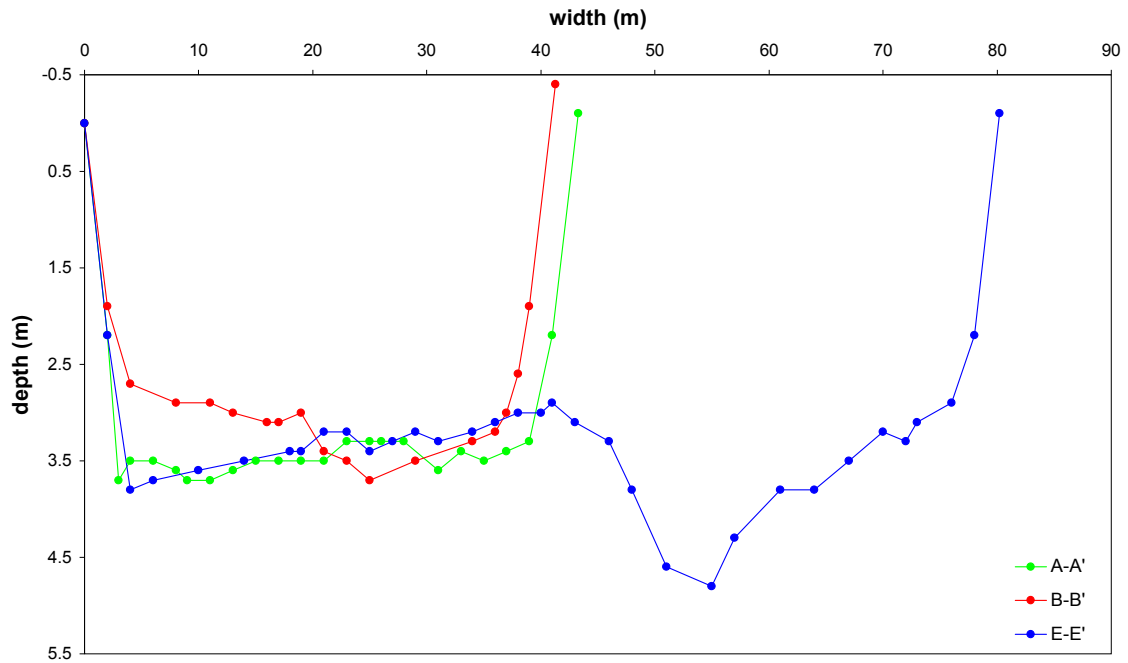

Fig. 3.21: Cross-profiles of bifurcation 4.
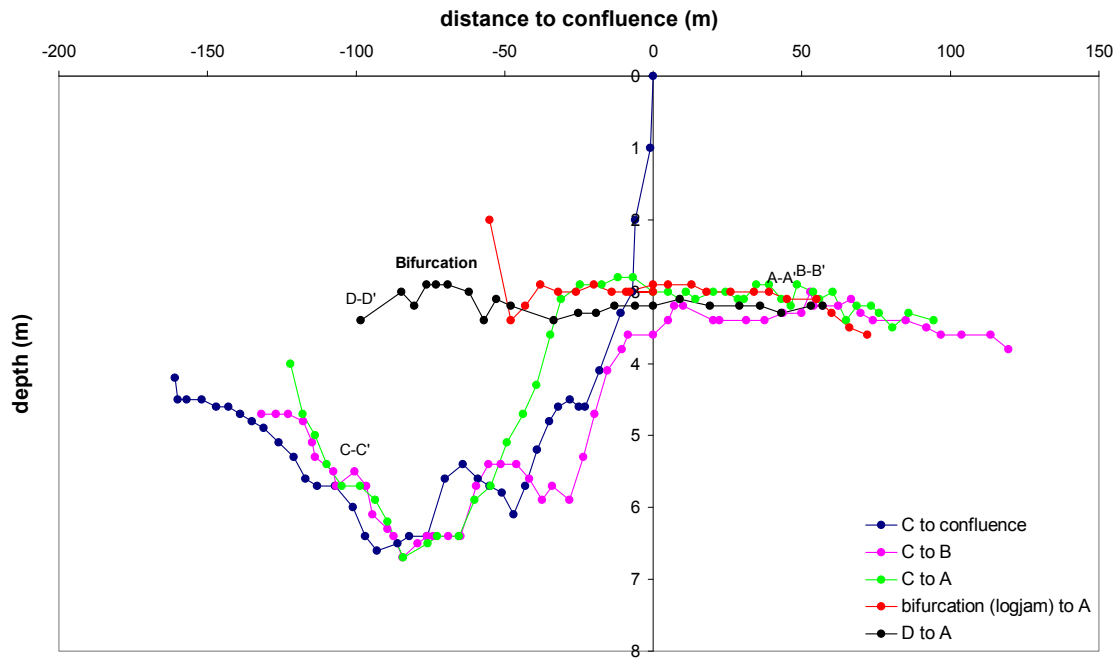
Fig. 3.22: Cross-profiles of confluence 3.

Fig. 3.23: Long-profiles of bifurcation 4 and confluence 3.

Bifurcation 5, confluence 4

Bifurcation 5 is characterized by an upstream confluence. The minor bifurcate is located in an inner bend (figure 3.24). Channel B is the downstream part of channel C of bifurcation 4.

The major bifurcate (C) is significantly larger than the minor bifurcate (D). The minor bifurcate has a depth of approximately 3m and a width of approximately 20m. The major bifurcate has a depth of approximately 6m and a width of approximately 65m (figure 3.25). The inlet step at the entrance of the minor bifurcate is almost 5m. For a small part this is caused by the upstream confluence, which forms a scour hole, which increases the water depth in front of the bifurcation. The bed in channel D is characterized by dunes or sand waves, which are approximately 1m high and 50m long. Such dunes or sand waves have also been identified by Makaske (1998) in a downstream part of the same channel.

Channel A approaches the confluence with a curve, consequently a nice transverse slope can be identified. The scour hole can be identified in cross-profile E-E'and F-F' (fig 3.26), so the turbulence induced at the confluence head spreads for more than 150m. The confluence angle is 59 degrees. The flow area of channel A and B is approximately equal, consequently confluence 4 is characterized as a type 1 confluence.

The median grain size in channel A, B, C, D and the middle at E-E' is respectively; 360μm, 580μm, 740μm, 255μm and 510μm. Channel D is covered with mud drape, which is deposited during moderate and low stage, and is probably removed during bankfull stage. The underlying material could not be sampled with a grab sampler. A vibracoring in channel D (boring 059) indicates that the median grain size beneath the mud drape is 'coarse sand'. Additionally, the vibracoring indicates that channel D had a maximum depth of 7.80m in the past. Consequently, channel D is a type 2b bifurcation.
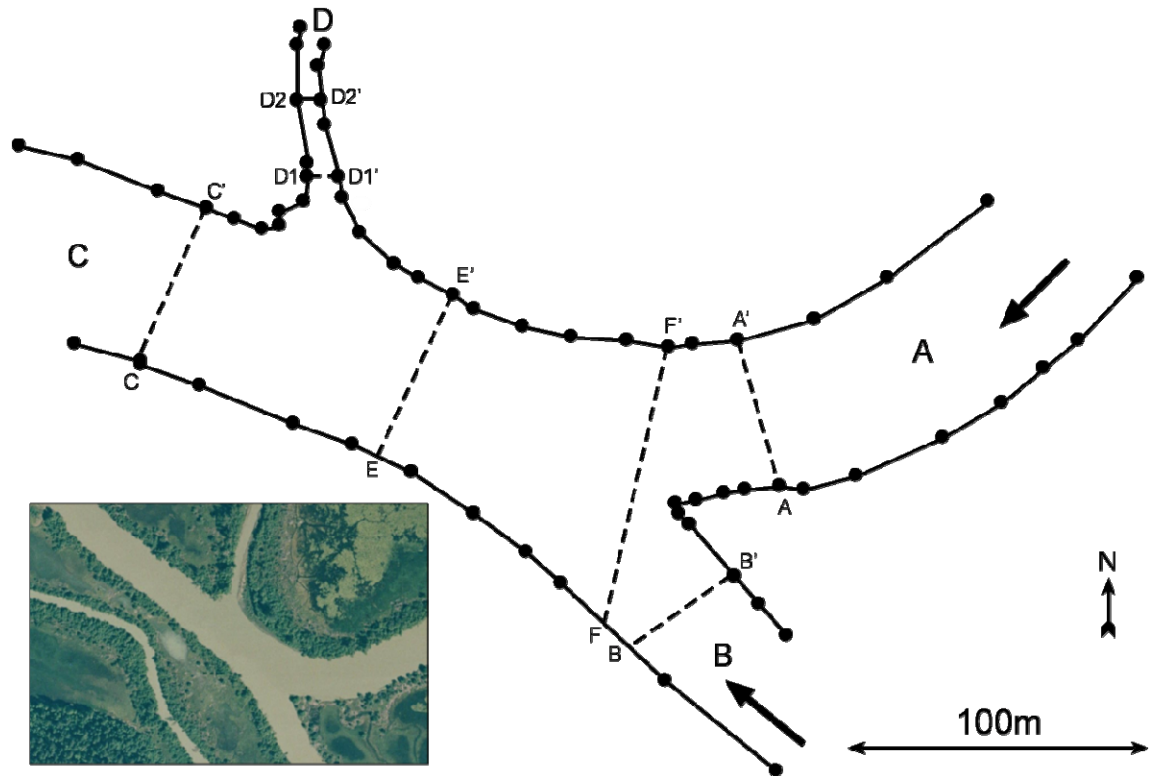
Fig. 3.24: Planform of bifurcation 5 and confluence 4.
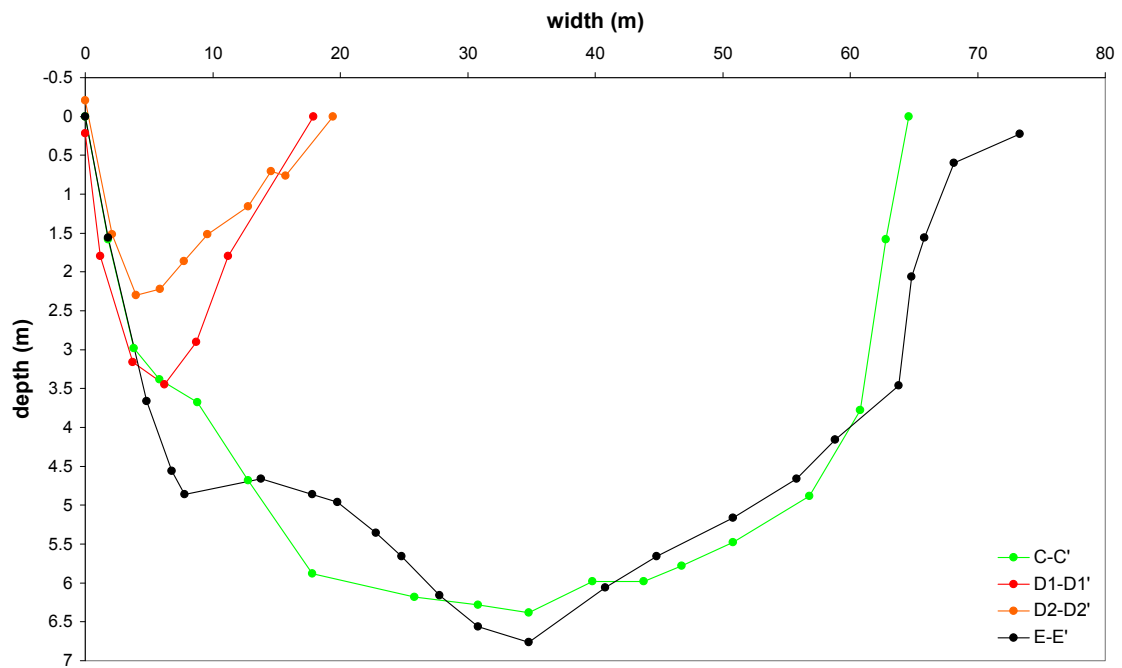
Fig. 3.25: Cross-profiles of bifurcation 5.
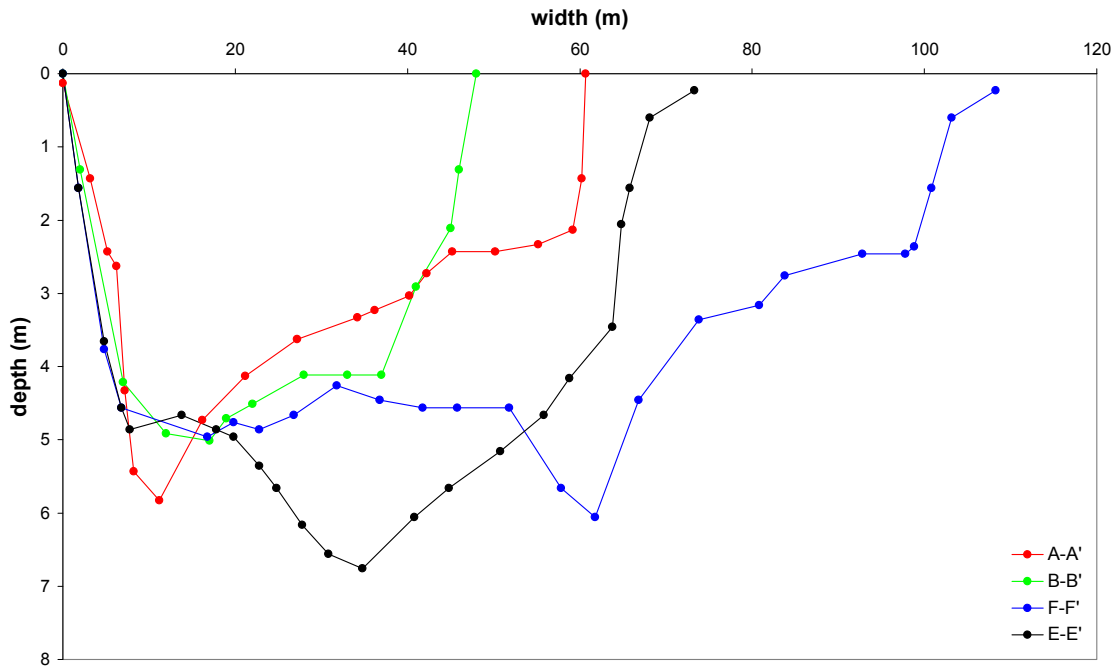
Fig. 3.26: Cross-profiles of confluence 4.
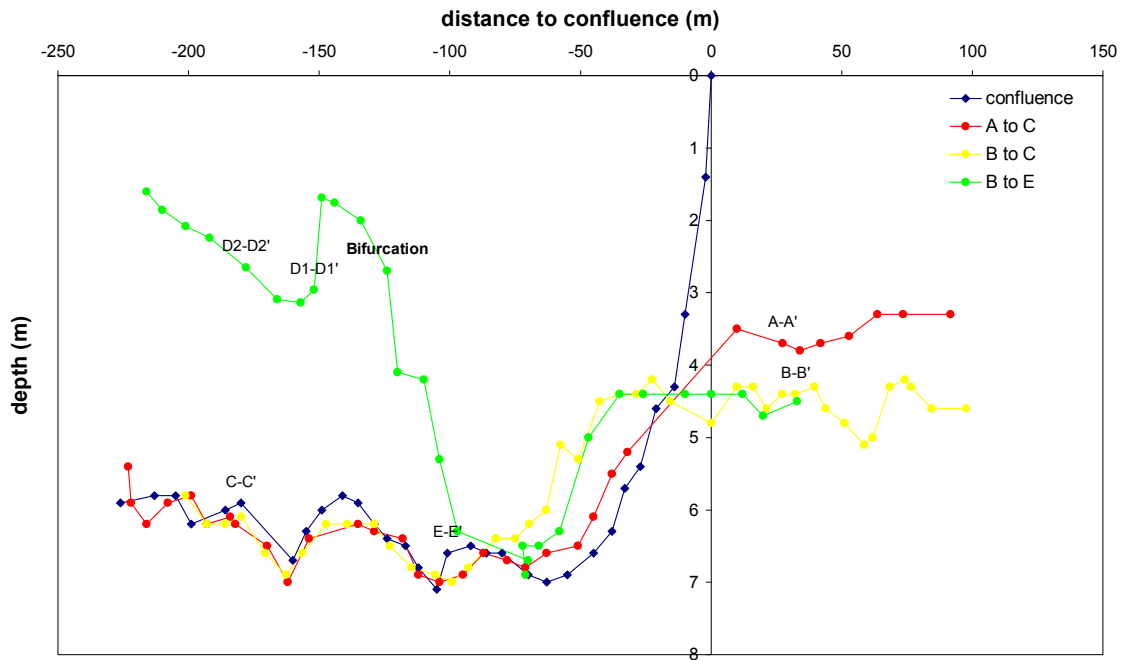
Fig. 3.27: Long-profiles of bifurcation 5 and confluence 4.

Confluence 5

At confluence 5, a small channel joins the main channel in the outer bend (figure 3.28). Channel C is the upstream part of channel A of confluence 4, while channel B is the downstream part of channel B of bifurcation 1. In the inner bend of the main channel, a bar is present, which is measured more extensively in section 3.3.3.1.

Channel A is a shallow channel, with a bankfull depth of only 2.5m and a width of 25m. The main channel is significantly larger and is characterized by a width of 60m and a depth of 4m (figure 3.29). Downstream of the confluence, at the bar, the bed is characterized by a transverse slope. This explains the differences in channel depth in the long-profiles (figure 3.30), with significantly smaller water depths close to the inner bend levee.

The median grain sizes in channel A, B and C are respectively 255μm, 740μm and 510μm. In channel B one coarse sample was collected with a median grain size of 1200μm. The confluence angle is 74 degrees. Confluence 5 is a type 2 confluence.
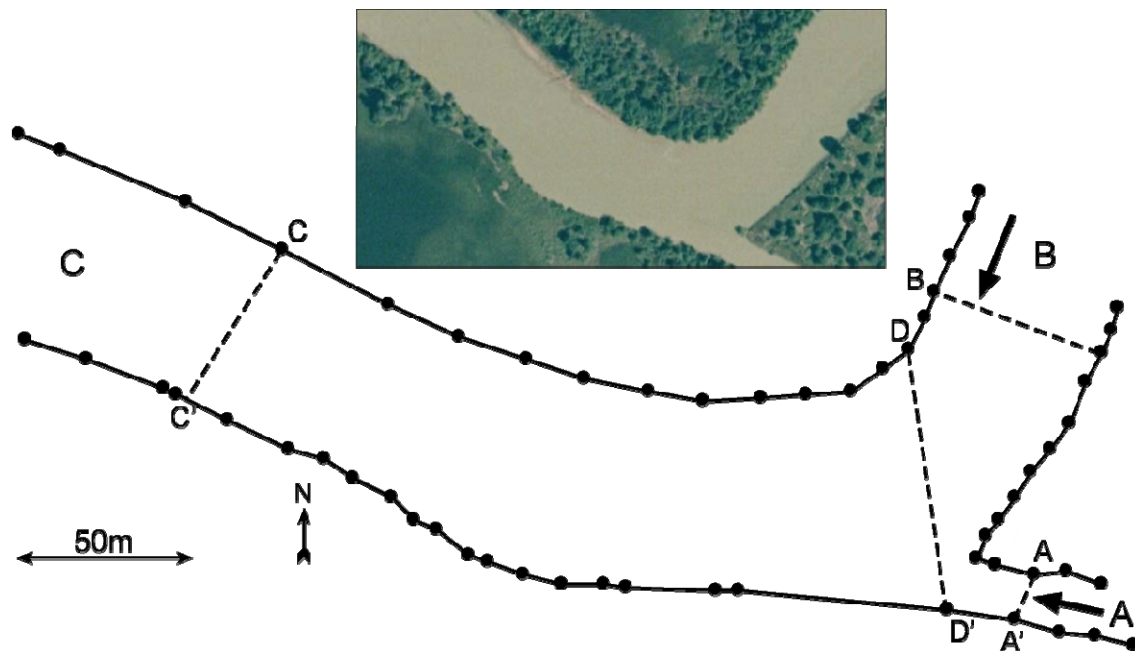
Fig. 3.28: Planform of confluence 5.
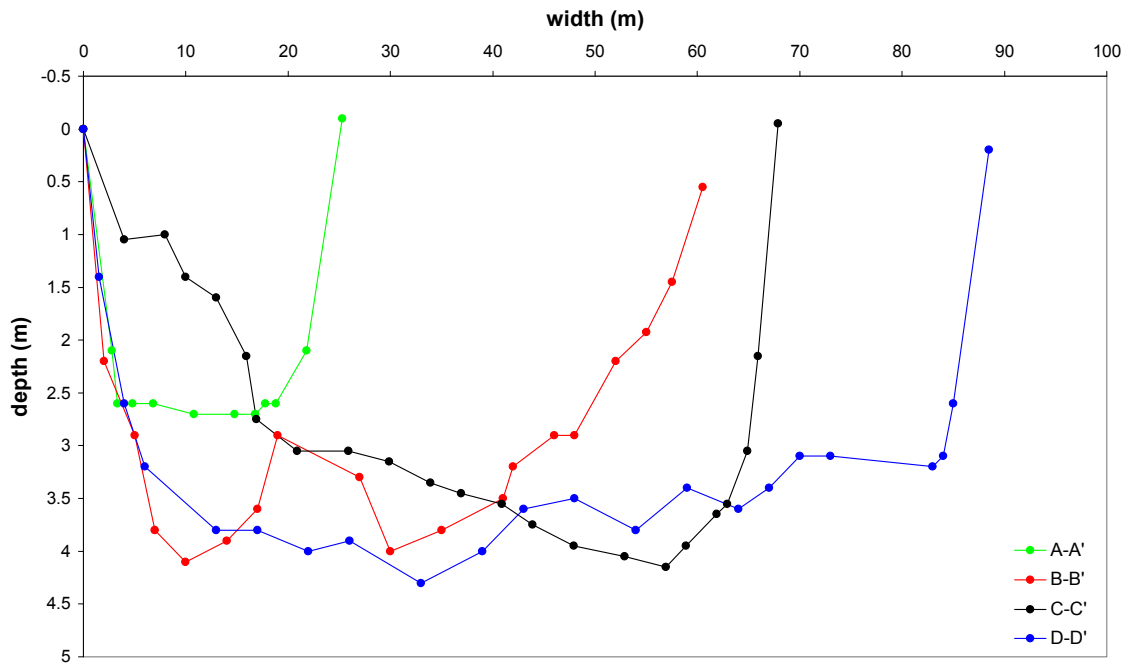
Fig. 3.29: Cross-profiles of confluence 5.

Fig. 3.30: Long-profiles of confluence 5.

71

Confluence 6

Channels A and B of confluence 6 (figure 3.31) are respectively the downstream parts of channel C from bifurcation 2 and Channel B from bifurcation 3. Channel B is slightly wider than channel A, but channel A on its turn is deeper so that the flow areas of both channels are comparable (figure 3.32). A scour hole of more than 6m (figure 3.33) deep originates from channels A and B, which have depths of approximately 4.5 and 3m.

The median grain sizes of channel A, B and C are respectively 340μm, 640μm and 255μm.

The confluence angle is 97 degrees. Confluence 6 is a type 1 confluence.

Fig. 3.31: Planform of confluence 6.
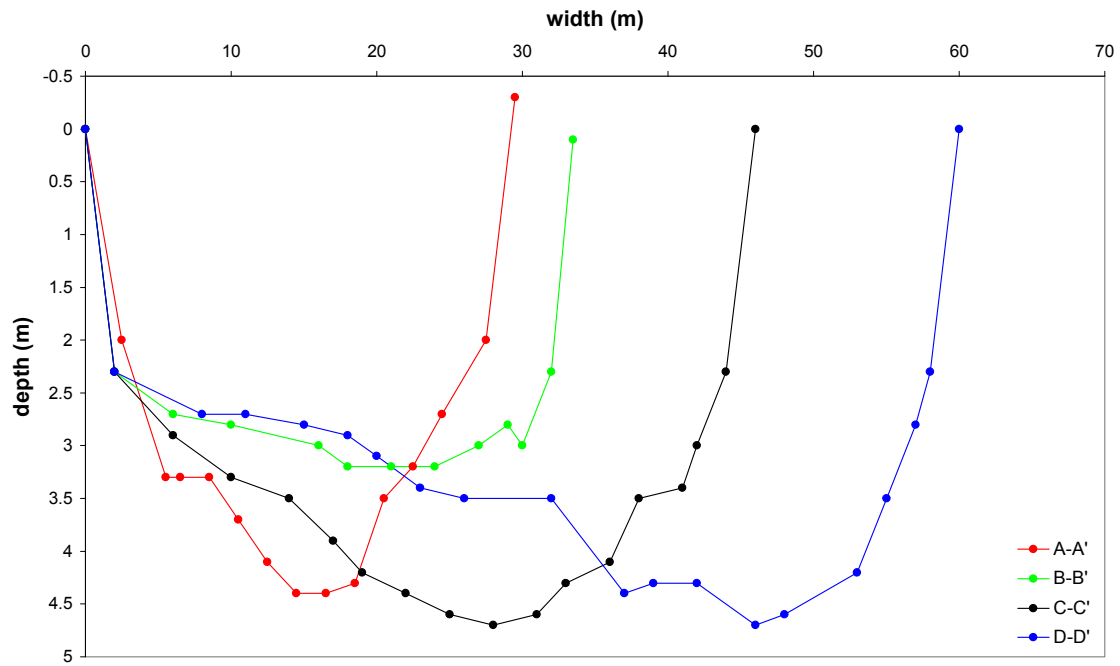
Fig. 3.32: Cross-profiles of confluence 6.

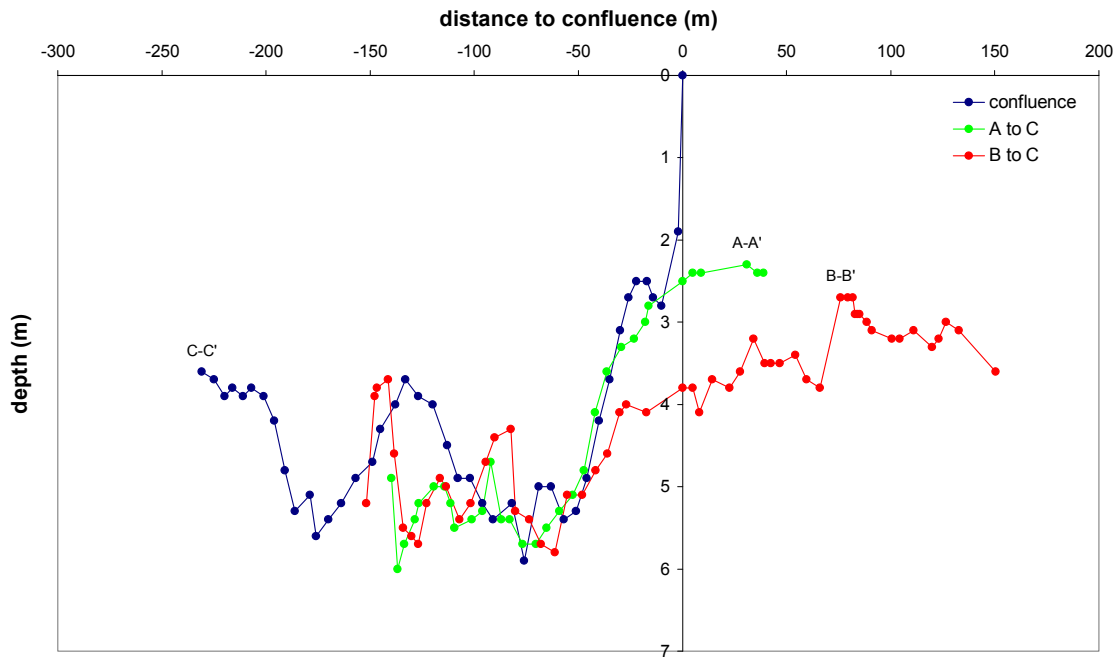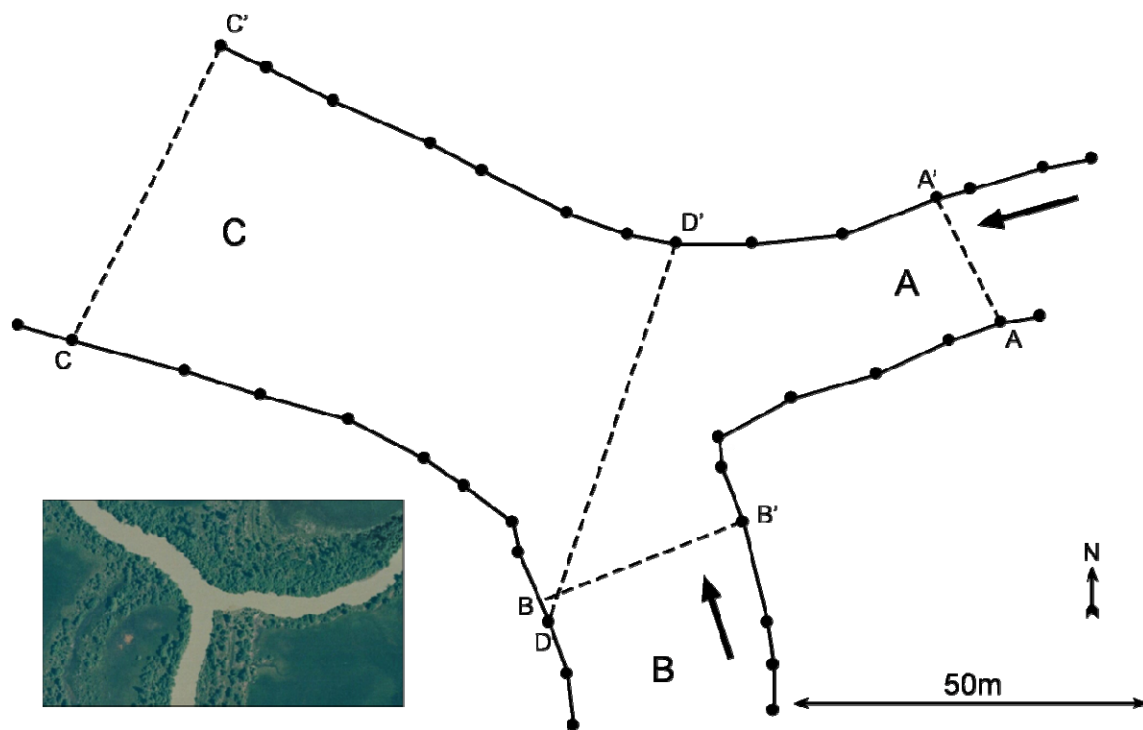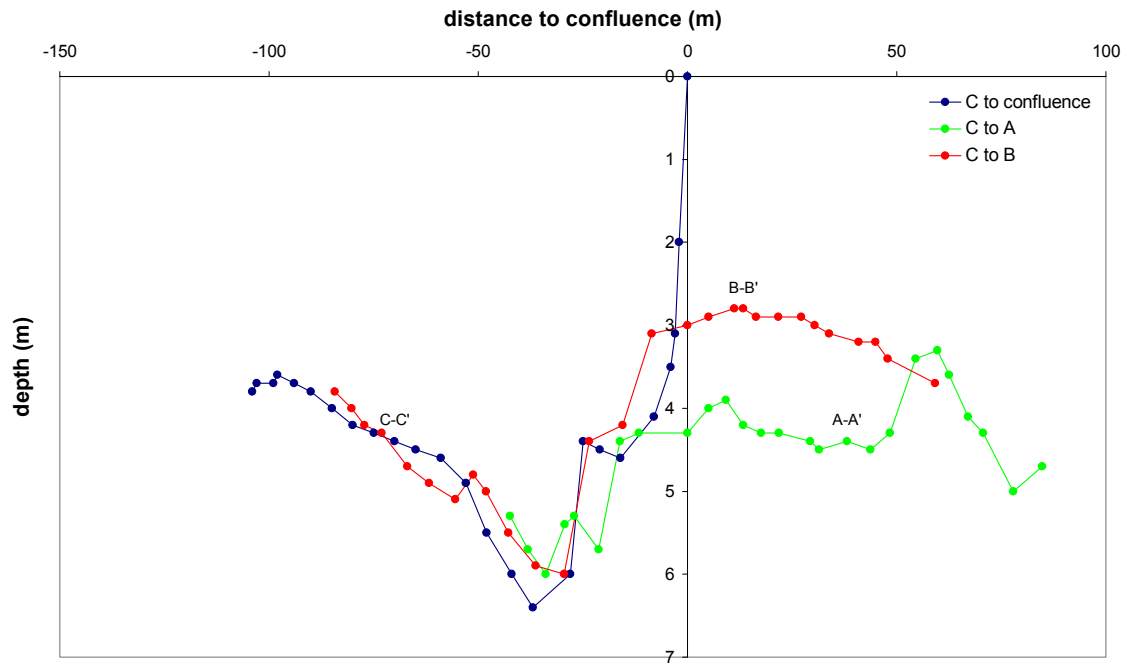*Fig. 3.33: Long-profiles of confluence 6.*

73

3.3.3 Transverse bed slope in sharp and gentle bends

In order to gain insight in the amount of spiral flow in the upper Columbia River, transverse slopes are measured in 4 sharp and 5 gentle bends (see figure 3.4 for locations). Cross-profiles of sharp bends are discussed in section 3.3.3.1, cross-profiles of gentle bends are discussed in section 3.3.3.2.

3.3.3.1 Sharp bends

During moderate flow stage in September, bars are present above the water table in sharp bends. The transverse bed slope continues up to the levee top. Five to six cross-profiles are measured at three sharp bends, named sharp bend 1, 2 and 3 (figure 3.34 and 3.37). Additionally, a single cross-section of the major bifurcate of bifurcation 1 (fig 3.11) is used, which is also located in a sharp bend. In this section the major bifurcate of bifurcation 1 will be referred to as sharp bend 4.

The bend radius of sharp bend 1 (figure 3.34) ranges between 60 and 69m. The bend radius of sharp bend 2 (figure 3.34) ranges between 59m and 83m. Sharp bend 3 (figure 3.37) has a bend radius between 137 and 180m. The bend radius of sharp bend 4 ranges between 136 and 163m.

In sharp bend 1 the thalweg is located in between the middle of the channel and the outer bank levee. However, the maximum water depth is located further away from the outer bend levee in the most upstream part than is the case in middle and downstream part (figure 3.35). This may be caused by flow separation, which is observed during the fieldwork by the author. Flow separation occurrs in all sharp bends but was most pronounced in sharp bend 1. The flow separation is characterized by the features described by Kleinhans et al. (2009) for sharp bends in tidal mudflats; flow separation occurs at the sharpest point at the inner bank, and a recirculation eddy is present. Additionally, a recirculation eddy is present at the outer bank. This outer bend eddy is observed in the area between A' and B' in figure 3.34, and may be the cause of the shallow area near the outer bend bank observed in cross-section A-A', since the recirculation in this part of the bend favors deposition. The transverse bed slope in gentle bend 1 ranges between 0.12 and 0.17m/m.

In sharp bend 2, a very deep outer bend pool is present in cross-section G-G' (figure 3.36), how this outer bend pool has formed is unknown. This deep outer bend pool leads to a transverse bed slope of 0.18m/m. In cross-profiles H-H' and J-J', a new levee is forming 2-10m in front of the former, highly vegetated levee. The transverse bed slope ranges between 0.08 and 0.18m/m. The average transverse bed slope is approximately 0.10m/m. Sharp bend 3 is characterized by a nice evolution of bathymetry along the bend (figure 3.38); the thalweg is located just in front of the outer bend levee. Initially, the depth of the outer bend pool gradually increases from A-A' to D-D', after which it gradually decreases from D-D' to F-F'. The transverse bed slope ranges between 0.07 and 0.11m/m. Sharp bend 4 is characterized by a transverse bed slope of 0.12m/m.

Although flow separation is observed in the inner part of the bends, and will probably be more pronounced during bankfull discharge, there are no indications that the bars in sharp bends are lee-side banks induced by flow separation. In that case a shallow area should be present at the location of the recirculation area, the dead zone. A sharp transition towards the outer part of the bend, which is not affected by the recirculation eddy, should be present in the form of a very steep bed slope towards the relatively deep outer bend. However, the bathymetry of all sharp bends shows a gradual deepening towards the outer bend. Only sharp bend 1 is characterized by the morphology described above, which might indicate that the morphology at sharp bend 1 is slightly influenced by flow separation.

3.3.3.2 Gentle bends

In the measured gentle bends, during moderate flow stage in September, no bars are present above the water surface. Two or three cross-profiles are measured in five gentle bends (see figure 3.4 for location). These cross-profiles are located in the upstream-, middle-, or downstream part of the bend.
In the middle-, and downstream part of gentle bend 1 a small transverse bed slope is present of approximately 0.04m/m (figure 3.39). In the upstream part a negative transverse bed slope is present, the water depth in the inner bend is larger than the water depth in the outer bend. Gentle bend 1 is located 200m downstream of the entrance of channel A of bifurcation 3 (figure 3.16). Water that flows into channel A at bifurcation 3 is directed against the most northern levee. Since flow needs time to adapt to a disturbance such as a meander bend or bifurcation, the thalweg is still located at the northern levee, which is the levee at the inner bend of gentle bend 1, causing the thalweg at the most upstream part of gentle bend 1 to be located in the inner bend, so that a negative transverse slope is formed.
In gentle bend 2 (figure 3.40), no transverse slope is present in the upstream-, and middle part of the bend. Only the downstream part has a transverse bed slope of 0.02m/m. Gentle bend 3 does not have a clear transverse bed slope (figure 3.41). A bar is present in the middle of the channel.
In gentle bend 4, the upstream- and middle part of the bend are characterized by a small transverse slope of 0.03m/m, in the downstream part of the bend, no clear downstream slope can be defined (figure 3.42). A small negative transverse bed slope is present. In gentle bend 5 a small negative bed slope is present in the upstream part of the bend, whilst in the downstream part of the bend a clear transverse bed slope can be distinguished of 0.06m/m (figure 3.43). The negative transverse bed slope is caused by an upstream meander bend, which directs the thalweg towards the inner bend of gentle bend 5.
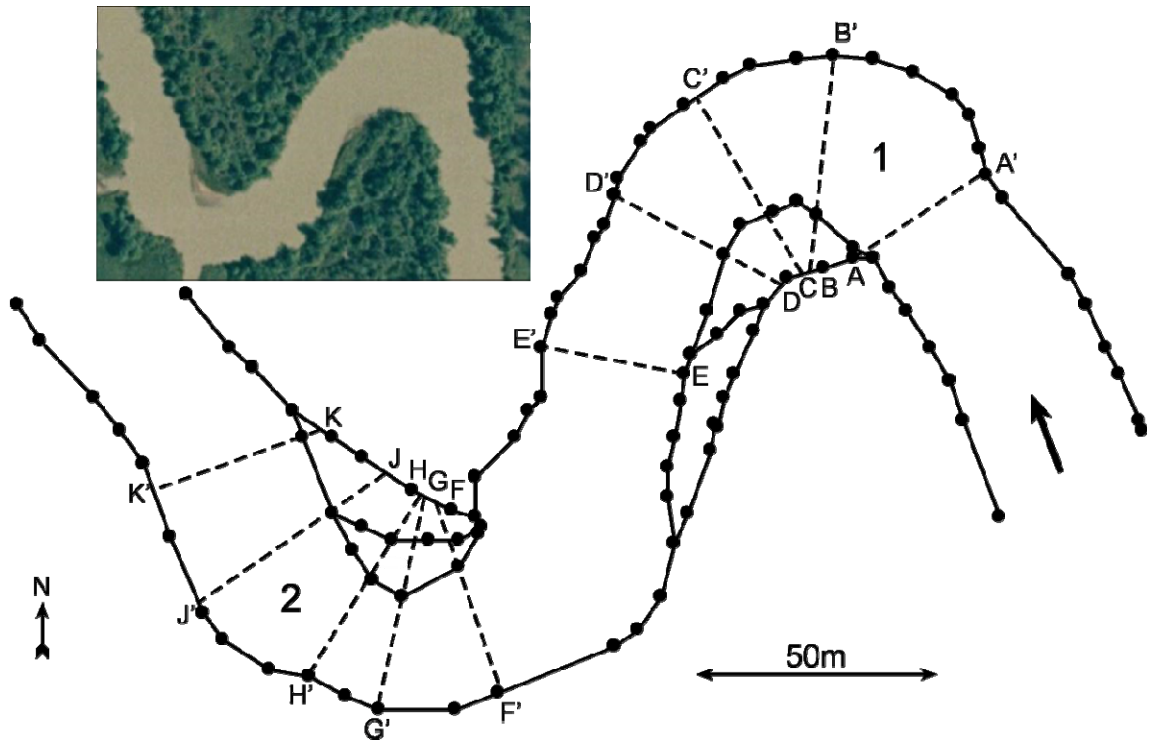
Fig. 3.34: Planform of sharp bend 1 and 2.
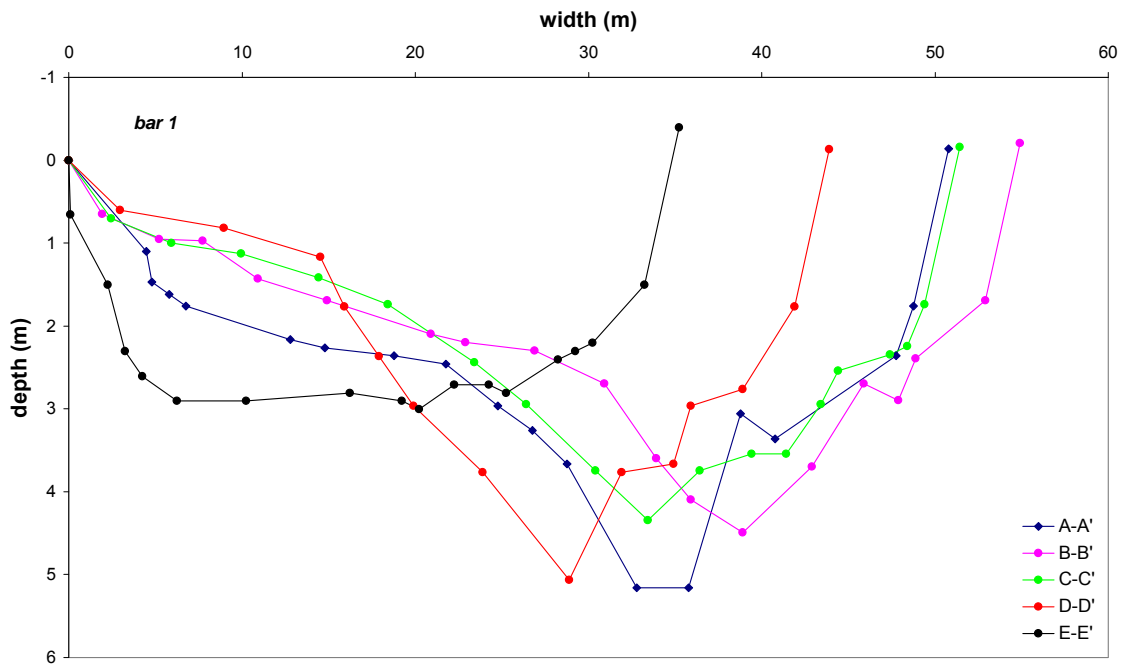
Fig. 3.35: Cross-profiles of sharp bend 1.
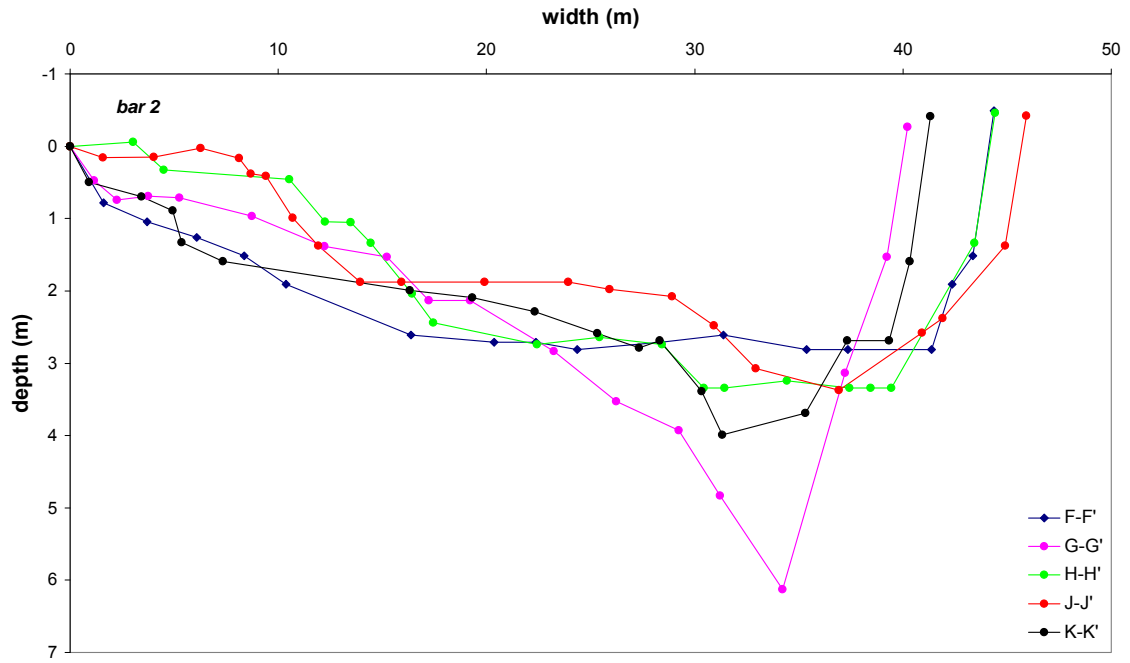
Fig. 3.36: Cross-profiles of sharp bend 2.
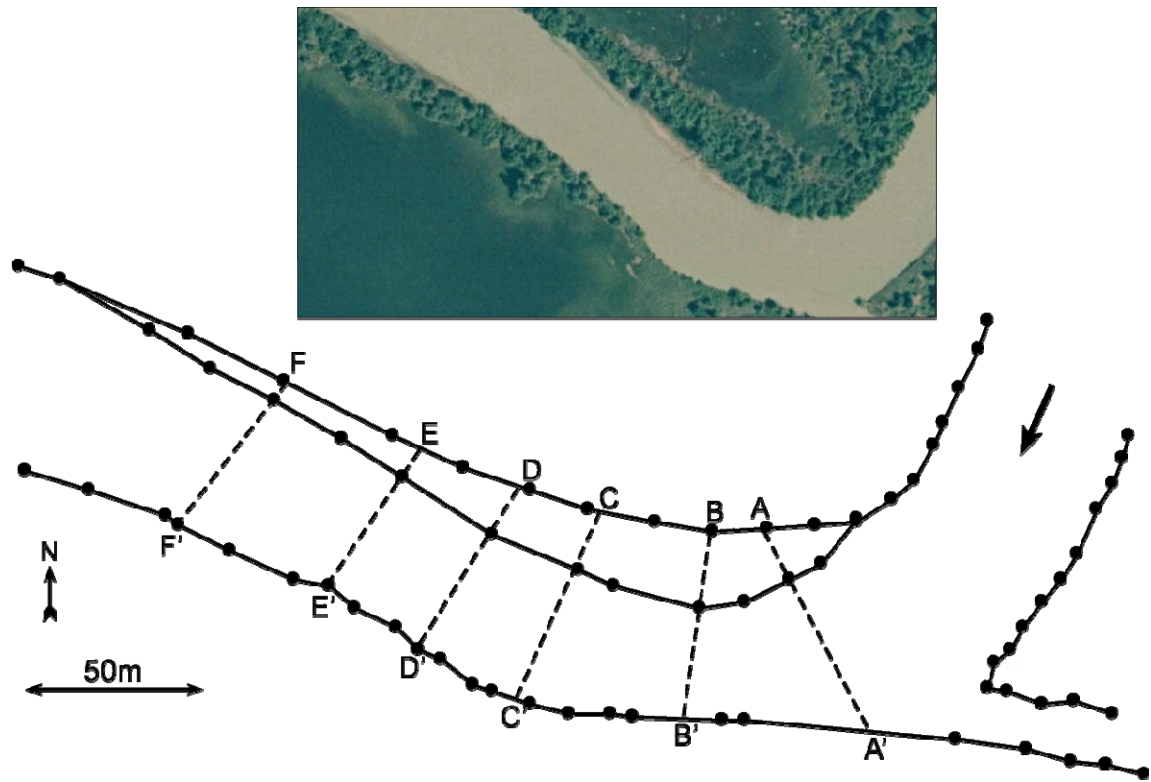
Fig. 3.37: Planform of sharp bend 3.
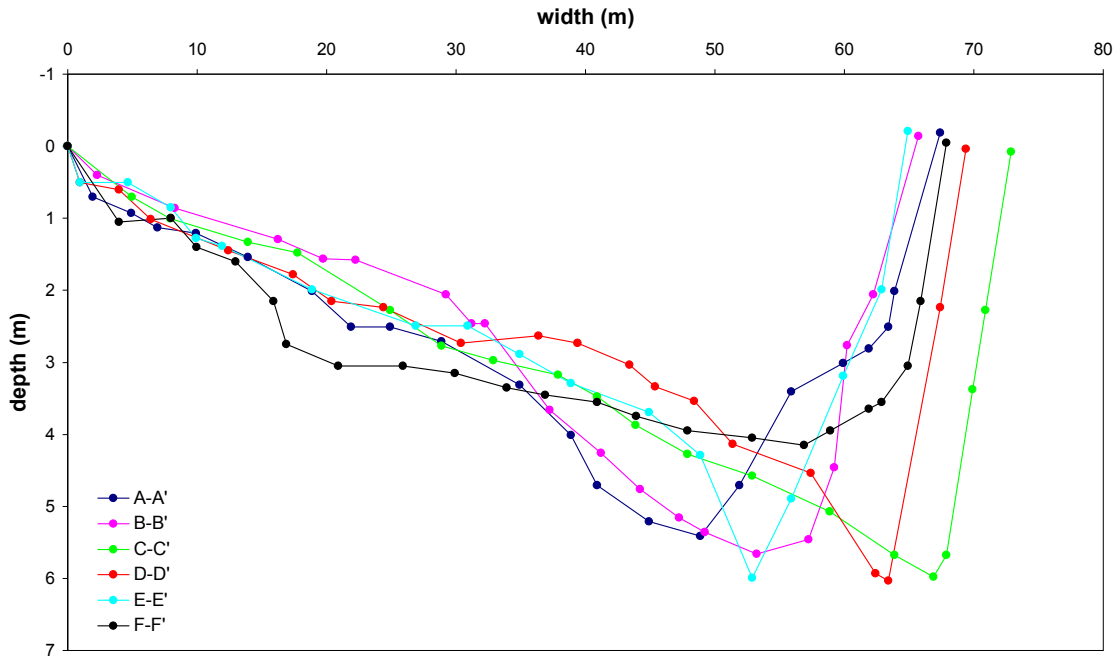
Fig. 3.38: Cross-profiles of sharp bend 3.
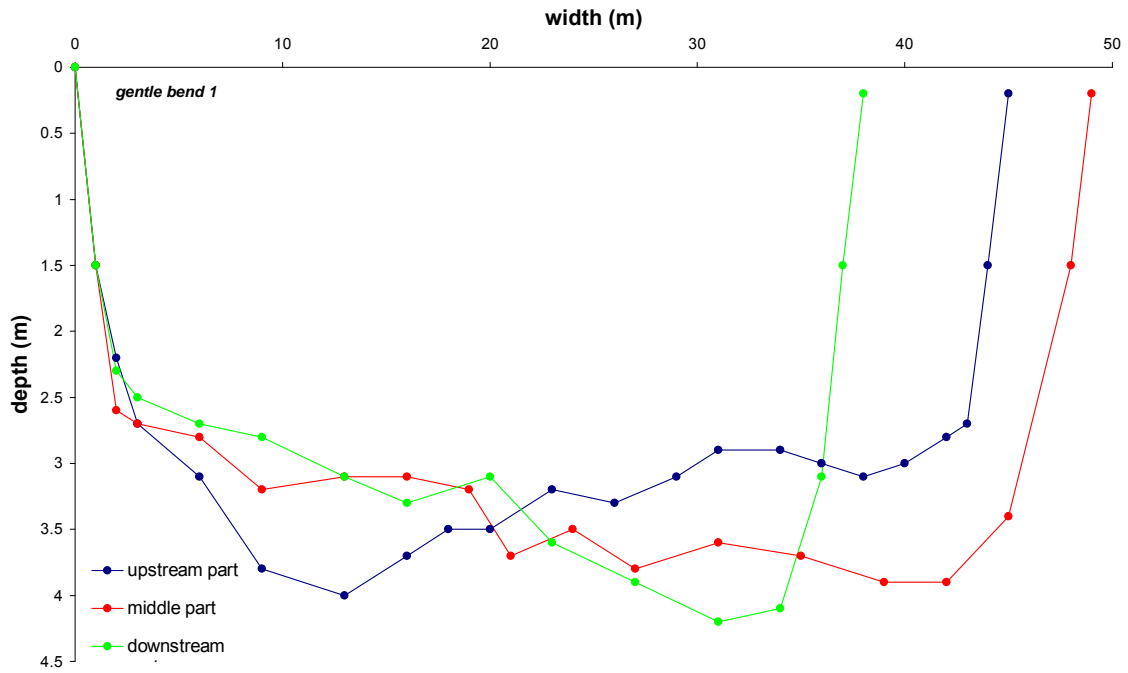
Fig. 3.39: Cross-profiles of gentle bend 1.
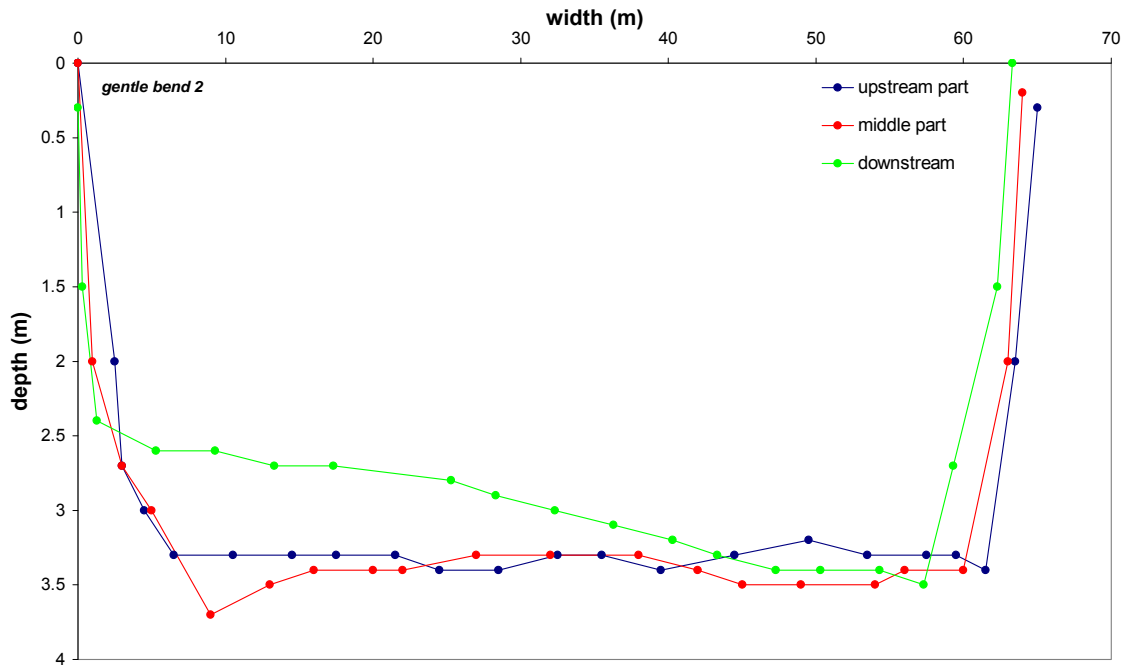
Fig. 3.40: Cross-profiles of gentle bend 2.
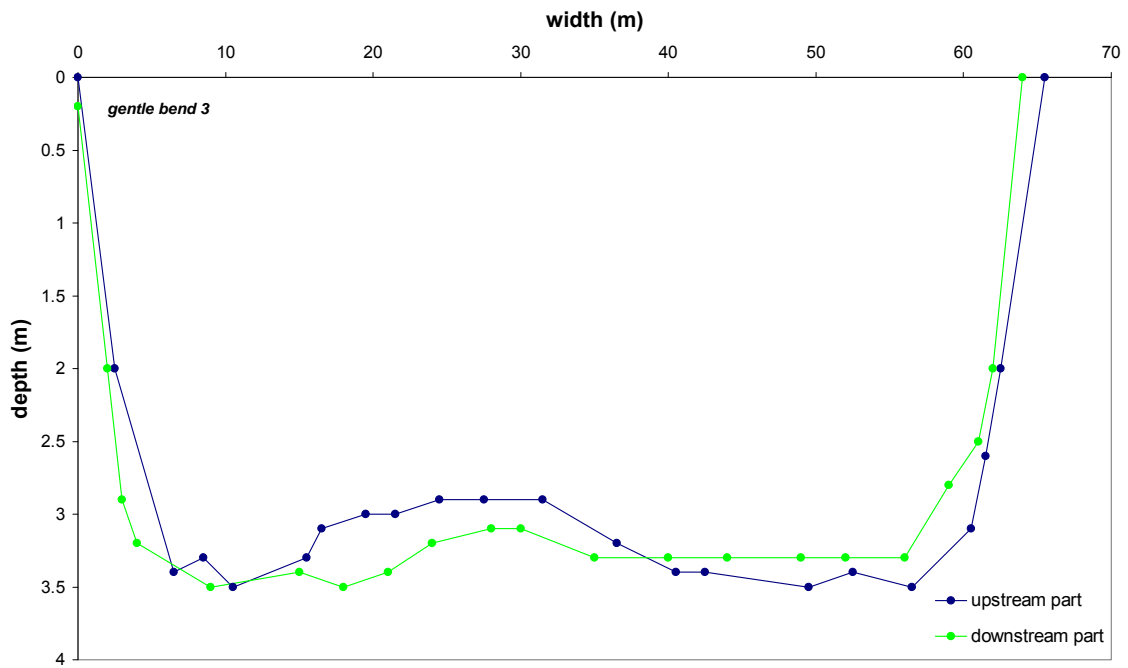
Fig. 3.41: Cross-profiles of gentle bend 3.
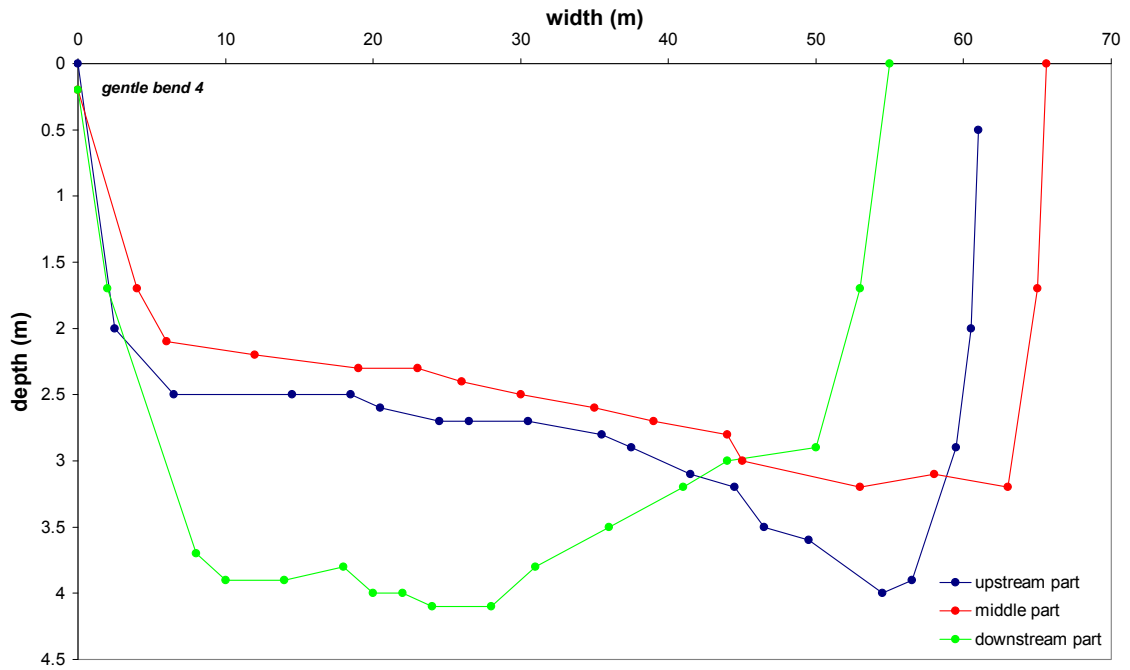
Fig. 3.42: Cross-profiles of gentle bend 4.
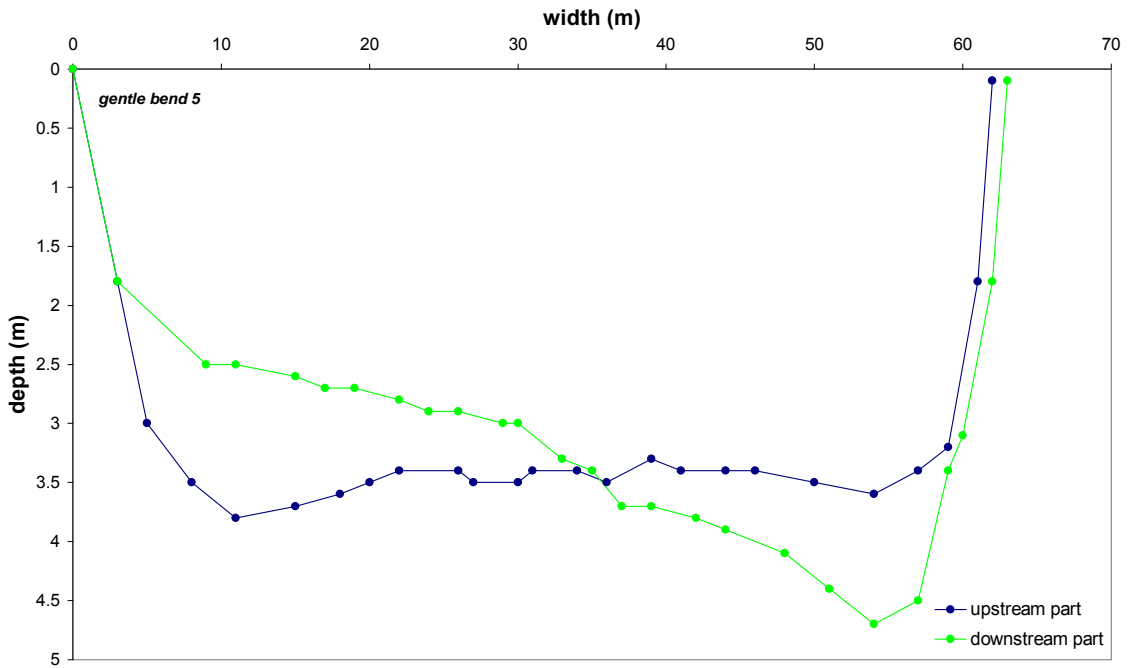
Fig. 3.43: Cross-profiles of gentle bend 5.

3.3.4. Bank strength

At thirteen locations in the studied reach (figure 3.4) the bank strength is measured. These measurements have been performed in order to obtain information about inter-channel, and along-channel differences in bank strength, and to gain insights in the ability of the upper Columbia River to erode its banks.

The measured bank strength values at thirteen locations along the upper Columbia River are presented in table 3.2. In figure 3.44 the bank strength values of the three different measurement levels (figure 3.3) are summarized as the median, 16 and 84 percent percentile. The bank strength varies between 5 and 40 kN/m^2 and is highest for level 3.
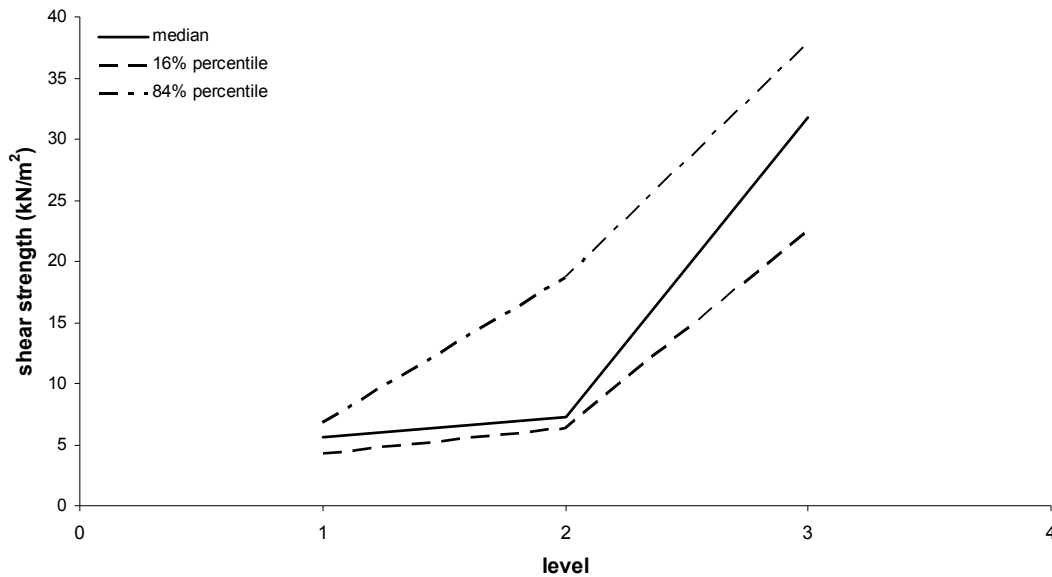
Fig. 3.44: Bank strength at the three different measurement levels (figure 3.3) summarized as the median, 16 percent percentile and the 84 percent percentile.

3.3.5. Residual channels

Borings have been performed in nine residual channels in the upper Columbia River. Numbering of the borings is conformable to the numbering employed by Lavooi (2010).

Borings 010 and 059 are performed by using a vibra-corer, the other borings are performed with an open gouge. Borings 005, 031, 033, 034 and 058 are all performed in outer bend residual channels. Boring 030 and 059 are performed in an inner bend residual channel. Boring 010 is performed in the middle channel of a trifurcation, the same probably holds for boring 035.

81

Boring 059 is performed by Prof. Derald Smith and is presented in the cross-valley transect of Makaske (1998), the borehole log is provided by Dr. Bart Makaske (personal communication).

The borehole logs can be found in appendix 1.

Tbl. 3.2: Measured bank strength. See figure 3.4 for locations. The table continues on the next page.

No.	level	shear strength kg/cm2	shear strength kN/m2	remarks	No.	level	shear strength kg/cm2	shear strength kN/m2	remarks
1	1	0.056	5.567	Aggrading levee,	8	1	0.031	3.071	Eroding levee.
		0.053	5.279	vegetation mostly			0.060	6.047	Material at level 2
		0.048	4.799	pioneer grasses			0.039	3.935	extremely dry.
	2	0.082	8.158	and mosses.		2	0.208	20.778	Small roots present
		0.073	7.294				0.164	16.404	at level 3.
		0.061	6.143				0.230	22.966	
	3	0.197	19.685			3	0.339	33.902	
		0.219	21.872				0.284	28.434	
		0.273	27.340				0.295	29.527	
2	1	0.043	4.319	Eroding levee.	9	1	0.067	6.719	Eroding levee.
		0.048	4.799				0.061	6.143	
		0.056	5.567				0.053	5.279	
	2/3	0.109	10.936			2	0.054	5.375	
		0.164	16.404				0.074	7.390	
		0.197	19.685				0.073	7.294	
3	1	0.043	4.319	Eroding levee.		3	0.230	22.966	
		0.082	8.158	Relatively high values			0.328	32.808	
		0.072	7.199	of shear strength			0.241	24.059	
	2/3	0.109	10.936	at level 1: caused by	10	1	0.031	3.071	Eroding levee.
		0.164	16.404	relatively "dry" loam.			0.068	6.815	
		0.219	21.872				0.051	5.087	level 3, mos
4	1	0.068	6.815	Eroding levee.		2	0.088	8.830	as vegetation.
		0.068	6.815	At the largest shear			0.081	8.062	
		0.086	8.638	strength at level 1, the			0.078	7.774	
	2	0.070	7.007	loam was more dry.		3	0.372	37.182	
		0.045	4.511	Pioneer vegetation at			0.437	43.744	
		0.086	8.638	level 2; mainly grass.			0.437	43.744	
5	1	0.058	5.759	Aggrading levee.	11	1	0.038	3.839	Eroding levee. Vegetation at level 3 is
		0.055	5.471				0.048	4.799	
		0.057	5.663				0.037	3.743	mainly grass.
	2	0.262	26.246			2	0.068	6.815	
		0.273	27.340				0.066	6.623	
		0.317	31.714				0.071	7.103	
6	1	0.068	6.815	Eroding levee.		3	0.361	36.089	
		0.063	6.335	Relatively high fraction			0.591	59.054	
		0.059	5.855	of sand in the bank			0.416	41.557	
	2	0.053	5.279	material at level 2.	12	1	0.062	6.239	Eroding levee. Vegetation at level 3 is
		0.065	6.527				0.042	4.223	
		0.096	9.598				0.058	5.759	mainly grass.
	3	0.175	17.498			2	0.076	7.582	
		0.175	17.498				0.068	6.815	
		0.208	20.778				0.070	7.007	
7	1	0.029	2.879	Eroding levee		3	0.317	31.714	
		0.046	4.607	Material at level 1 and 2			0.372	37.182	
		0.054	5.375	equal, at level 2 more			0.383	38.276	
	2	0.065	6.527	dry.	13	1	0.073	7.294	Eroding levee.
		0.068	6.815	Small roots present al			0.054	5.375	Some water plants at
		0.061	6.143	level 3.			0.083	8.254	level 1.

Tbl. 3.2: Measured bank strength. See figure 3.4 for locations.

7	3	0.306	30.621		13	2	0.219	21.872	Small roots present at
		0.328	32.808				0.230	22.966	level 3.
		0.350	34.995				0.219	21.872	
						3	0.328	32.808	
							0.317	31.714	
							0.361	36.089	

Tbl. 3.3: Measured median grain size. Under the header sorting, vps stands for very poorly sorted, ps stands for poorly sorted, ms stands for moderately sorted and mud indicates a large fraction of mud in the sample. See figure 3.4 for locations.

No	D_{50}	Sorting	No	D_{50}	Sorting	No	D_{50}	Sorting
	µm			µm			µm	
a	850-1000	vps	n	850-1000	ps	aa	420-600	ms
	850-1000	ms		420-600	ps		420-600	ps
	600-850	ms		600-850	ps		100-1400	vps
b	420-600	ms	o	1000-1400	ps	ab	420-600	ms
	420-600	ms		600-850	ps		420-601	ms
	mud			600-851	ms		420-602	ms
c	150-210	ps	p	850-1000	vps	ac	420-600	ms
	150-210	ps		1000-1400	vps		600-850	ms
	420-600	vps					600-850	ps
d	1000-1400	vps	q	600-850	vps	ad	600-850	vps
	1000-1400	vps		850-1000	vps		600-851	ps
	600-850	vps		600-850	vps		420-600	ps
e	420-600	ps	r	600-850	vps	ae	>2000	ms
	420-600	ps		420-600	vps		300-420	ms
	420-600	ps		600-850	vps		600-850	ps
f	150-210	mud	s	300-420	ms	af	mud	
	150-211	mud		600-850	vps		mud	
	mud			300-420	ms		mud	
g	420-600	ps	t	mud		ag	420-600	ms
	420-600	ps		420-600	ms		300-420	ps
	420-600	ms		420-600	ps		300-420	vps
h	420-600	ps	u	300-420	ms	ah	210-300	ws
	420-600	ps		850-1000	ps		210-300	ms
	300-420	ms		600-850	ps		210-300	ms
i	300-420	ps	v	600-850	ms	ai	600-850	vps
	300-420	ps		850-1000	ps		600-850	vps
	210-300	ms		420-600	ps		420-600	vps
j	600-850	ps	w	300-420	ms	aj	850-1000	ms
	420-600	ps		420-600	ps		850-1000	ms
	420-600	ms		420-600	ms		850-1000	ms
k	420-600	ps	x	300-420	ps	ak	1000-1400	vps
	420-600	ps		600-850	vps		420-600	vps
	420-600	ms		1000-1400	vps		600-850	vps
l	1000-1400	ps	y	300-420	ps	al	600-850	vps
	420-600	vps		1000-1400	vps		420-600	vps
	420-600	ms		600-850	vps		420-600	vps
m	210-300	ws	z	210-300				
	210-300	ms		210-300	ps			
	210-300	ms		mud				

3.4. Field data analysis

In this section, the field data described in section 3.3 is analysed. This analysis is performed to gain insight in the characteristics of the upper Columbia River. These insights can be used during modelling in order to determine input values and boundary conditions. Additionally, the results can be used for calibration and validation of the model.

In section 3.4.1 the implications of the measured bank strength on the rivers erodibility and dynamics is discussed. The inter-channel hydraulic geometry is investigated in section 3.4.2, by adding measurements of Makaske (1998) to the data of Tabata and Hickin (2003). The theory of Struiksma et al. (1985) is used to gain insight into the upper Columbia River's bar regime (section 3.4.3). Data of Locking (1983) is used to describe the mode of sediment transport in the upper Columbia River (section 3.4.4). The role of spiral flow in the upper Columbia River is investigated in section 3.4.5, by comparing measured transverse slope in bends with the theory of Struiksma et al. (1985) (section 3.4.5.1), and by investigating the fill of inner- and outer bend residual channels (section 3.4.5.2). Bifurcation equilibrium configurations are calculated in section 3.4.6. Finally, in section 3.4.7 the confluence scour depth is compared to the depth predicted by the predictors of Ashmore and Parker (1983), Best (1985) and Kjerve et al. (1979).

3.4.1. Bank strength

The bank strength measurements (table 3.1) indicate that at a site variation in bank strength is in the same order as the cross- and long-valley variation. The main reason for the differences in bank strength over the three different levels is the fraction of water contained by the different samples. At level 1 (figure 3.3), which is located close to the water surface, the samples contain a relatively large fraction of water. Consequently, the bank strength of these samples is relatively small (figure 3.44).

Level 1 and 2 are both not covered by vegetation. The bank material at both levels is comparable. Level 2 is more elevated and consequently samples taken from level 2 contain a smaller fraction of water. This automatically leads to a larger bank strength. At level 3, the samples contain a smaller fraction of water. Additionally, some vegetation is present. This vegetation contains mainly grass or moss. Due to the presence of vegetation, and thus small roots, the bank strength becomes larger.

The differences in bank strength at the different measurement locations are relatively small. The bank strength in the studied reach of the upper Columbia River is very high relative to the stream power of the channels. This explains the very limited lateral migration of the channels is marginal as suggested by the absence of meander bends with ridges and swales (Makaske et al., 2009).

3.4.2. Hydraulic geometry

Data of Tabata and Hickin (2003) and Makaske (1998) is combined to obtain hydraulic geometry relations. The hydraulic geometry relations obtained by Tabata and Hickin (2003) are described in section 2.2.2.

A new fit of a hydraulic geometry relation to the combined data of Tabata and Hickin (2003) and Makaske (1998) leads to the following geometry relations:

$$w_{bf} = 4.25 Q_{bf}^{0.56} \tag{3.2}$$

$$h_{bf} = 0.99 Q_{bf}^{0.23} \tag{3.3}$$

$$u_{bf} = 0.24 Q_{bf}^{0.21} \tag{3.4}$$

Including data of Makaske (1998) leads to a smaller power for bankfull width, and larger powers for bankfull depth and bankfull velocity compared to the hydraulic geometry relations of Tabata and Hickin (2003) (figure 3.44). The amount of scatter is larger for depth than for width and velocity.

Abbado et al. (2005) defined a gentle reach downstream of the entrance of the Spillimacheen River. Further downstream a steep reach is present, followed by a more gentle reach downstream of this steep reach which has a slope comparable to the slope of the upstream gentle-sloped reach (see section 2.2.2 and figure 2.6). Tabata and Hickin (2003) measured hydraulic geometry at several locations in the gentle reach downstream of the entrance of the Spillimacheen River and in the steep reach. Makaske (1998) measured hydraulic geometry in the gentle reach downstream of the steep reach. There is no difference in hydraulic geometry between the two gentle reaches and the steep reach (figure 3.44). Hydraulic geometry data for the steep and gentle reaches show approximately the same amount of scatter.

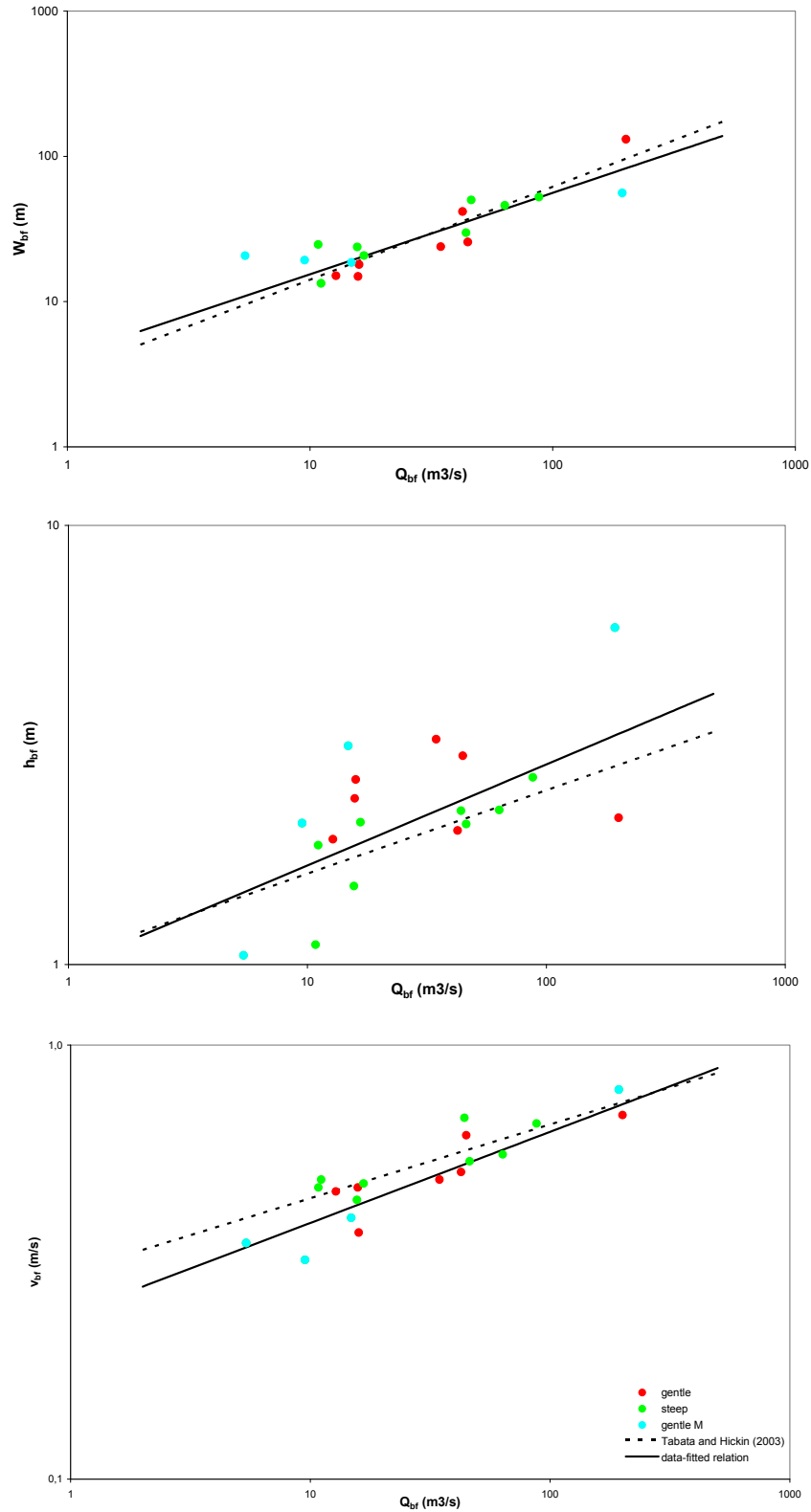*Fig. 3.44: Hydraulic geometry relations. The solid line indicates the fitted relation, the dashed line indicates the relation of Tabata and Hickin (2003). The green dots indicate measurements performed on the steep reach indicated by Abbado et al. (2005). The red dots indicate the upstream gentle reach, while the blue dots indicate the downstream gentle reach (measurements of Makaske et al. (2002)).*

3.4.3. Bar regime

As discussed in section 2.4.3.1, a river's bar regime is important for the applicability of 1D nodal point relations in predicting bifurcation evolution. For the two measuring locations of Locking (1983), Spillimacheen and Nicholson, the interaction parameter is calculated and compared to equation 2.26, in order to determine the bar regime of the upper Columbia River and to test the applicabilty of 1D nodal point relations in the upper Columbia River.

At Spillimacheen, the depth of the main channel is 3.19m, the width is 104m. The Chézy parameter is $55.8m^{0.5}/s$, the channel slope is $9.43.10^{-05}m/m$, the D_{50} is 0.71mm and n is 1.933. However, Struikma's theory only accounts for n > 3, therefore in the case of Spillimacheen, a power n of 3 is used in the calculations of the bar regime. This is justified by the fact that the sediment transport at Spillimacheen is strongly influenced by the Spillimacheen River, which delivers a large amount of sediment to the upper Columbia River (Locking, 1983; Makaske et al., 2002, 2009; Abbado et al., 2005). Therefore the n of 1.933 at Spillimacheen is debatable.

At Nicholson, the depth of the channel is 4.68m, the width is 83m. The Chézy parameter is $30.1m^{0.5}/s$, the channel slope is $1.65.10^{-4}m/m$, the D_{50} is 0.47mm and n is 3.52.

Applying these values to Struiksma's theory leads to an IP of 0.241 at Spillimacheen. The criterion for overdamped bars at Spillimacheen (equation 2.26a) is 0.244. Bars at Spillimacheen are thus slightly overdamped. At Nicholson the IP is 0.289. The criterion for overdamped bars at Nicholson is 0.222; the criterion for growing bars at Nicholson (equation 2.26c) is 3.92. Hence, the bars at Nicholson are slightly underdamped.

Note, that Locking (1983) performed her measurements both at Spillimacheen and Nicholson in the main channel. From figure 2.12, it becomes clear that bar regime is strongly dependent upon width/depth ratio. Decreasing the width/depth ratio forces the bar regime of a channel towards an overdamped regime. From the inter-channel hydraulic geometry relations of the upper Columbia River (section 5.3) it becomes clear that the width/depth ratio increases with increasing bankfull discharge, since the power of width versus discharge is 0.56 and the power of depth versus discharge is 0.23. Because the main channel at Spillimacheen and Nicholson experiences a bar regime close to the transition between an overdamped- and underdamped regime (a damped regime), the smaller, secondary, channels will definitely experience an overdamped bar regime since their width-depth ratio is smaller.

In summary, bar regime in the upper Columbia river is close to the overdamped- to underdamped regime transition in the main channel, in the smaller secondary channels the bar regime is overdamped. Hence, it can be concluded that alternating bars are absent in the upper Columbia River except immediately downstream of bends, so that bifurcations are not influenced by these alternating bars.

3.4.4. Sediment transport

In order to investigate the sediment transport mode in the upper Columbia River, sediment transport data of Locking (1983) is compared to several sediment transport predictors. Locking (1983) measured sediment transport in the months June, July and August, which corresponds with a decreasing discharge (figure 3.2). Unfortunately, Locking (1983) did not distinguish the difference between suspended and wash load, and consequently only measured bedload can be compared to calculated bedload.

The bed load transport predictors of Meyer-Peter and Mueller (1948) (MPM), Parker et al. (1982) (PaE), Van Rijn (1984) (VR) and Ribberink (1998) (Rib) are compared to measured bedload transport. In non-dimensional form the MPM predictor is as follows:

$$\phi_b = 8(\theta' - \theta_{cr})^{1.5} \tag{3.5}$$

wherein φ_b = the nondimensional sediment transport rate, θ' is the grain related Shields stress and θ_{cr} is the critical Shields stress for incipient motion (θ_{cr} = 0.03):
The MPM predictor was derived from flume experiments with well-sorted gravel near the beginning of motion. The PaE predictor was developed for gravel transport in natural streams near the beginning of motion, without bedforms. The equation is:

$$\phi_b = 11.2 \frac{(\theta' - \theta_{cr})^{4.5}}{\theta'^3} \tag{3.6}$$

The VR predictor was derived from calibrated predictors of the saltating motion of sand particles. The bed load equation is:

$$\phi_b = 0.1 \left(\frac{\theta' - \theta cr}{\theta'^3} \right)^{1.5} D*^{-0.3} \tag{3.7}$$

where D* is:

$$D^* = D_{50} \sqrt{\frac{(S-1)g}{v^2}} \tag{3.8}$$

89

where v is kinematic viscosity (m^2/s). The Rib predictor was carefully calibrated on a large amount of data in currents, waves, combined flow, mostly sand but also gravel, and in conditions near the beginning of motion and far into the sheet flow range (Kleinhans, 2005). The equation is:

$$\phi_b = 11\left(\theta' - \theta_{cr}\right)^{1.65}$$
(3.9)

The nondimensional bedload transport can be transformed to unit bedload transport by using equation 3.10:

$$\phi = \frac{q_{bors}}{\left((s-1)g\right)^{0.5} D_{50}^{1.5}}$$
(3.10)

where q_{bors} is the unit bedload or suspended sediment transport rate (m^2/s). The Engelund Hansen (1967) (EH) predictor for total transport was derived for suspended dominated conditions. It was based on energy considerations and calibrated on flume experiments:

$$\phi = \frac{0.1}{f} \theta^{2.5}$$
(3.11)

where φ is total transport and f is the Darcy-Weisbach coefficient related to total roughness which is related to the Chézy coefficient as:

$$f = \frac{8g}{C^2}$$
(3.12)

A sediment transport predictor based on grain-related Shields stress only is fitted to the bedload sediment transport data of Locking (1983), in order to overcome numerical errors in the network model (section 4). This equation reads as:

$$\phi_b = 5.62 \theta'^{1.66}$$
(3.13)

In figure 3.45, the Shields stress is plotted versus non-dimensional transport rate. The plus-signs indicate the measured sediment transport rate at Spillimacheen. The cross-signs indicate the measured sediment transport rate at Nicholson. In black they are based on grain-related Shields stress, in red they are based on total Shields stress. The EH sediment transport predictor is based on total Shields stress and should therefore be compared to the red plus-signs and cross-signs, while the MPM, Parker,

Rib, VR and fitted sediment transport predictor are based upon grain related Shields stress and should therefore be compared to the black plus-signs and cross-signs. For the EH sediment transport predictor two lines are plotted; one for the maximum Chézy value (measured at Spillimacheen) (EH Cmax), and one for the minimum Chézy value (measured at Nicholson) (EH Cmin). For the VR sediment transport predictor also two lines are plotted; one for the maximum $D*$ (measured at Spillimacheen) (VR $D*$max), and one for the minimum $D*$ (measured at Nicholson) (VR $D*$min). The difference in $D*$ has little effect on the predicted sediment transport, as can be seen in figure 3.45.

The PaE predictor underestimates the bedload transport rate, which is most likely caused by the fact that this predictor was developed for very different conditions. The MPM, VR and Rib predictors all predict approximately the same amount of bedload transport. The fitted function is approximately equal to the MPM, VR and Rib sediment transport rate predictor for the range of Shields stresses at Nicholson and Spillimacheen. For low Shields stress, it predicts a larger transport rate, since it does not take into account critical Shields stress.

The bedload transport rate measured at Nicholson is conform the MPM, VR and Rib predictor, despite the considerable scatter. The measured bedload transport rate at Spillimacheen is slightly higher than the bedload transport rate predicted by MPM, VR and Rib. This is most likely caused by the Spillimacheen River, which joins the upper Columbia River just upstream of the temporary gauging station of Locking (1983). The Spillimacheen River delivers a large amount of sediment into the upper Columbia River. This causes the measured bedload sediment transport rate to be higher than the predicted bedload transport rate.

The EH sediment predictor predicts the sediment transport rates less well than the MPM, VR, Rib and fitted predictors do. The sediment transport at Spillimacheen is underestimated, while the sediment transport at Nicholson is overestimated.

In conclusion, the sediment transport rate in the upper Columbia river is best predicted by grain-related Shields stress based sediment transport rate predictors. The PaE predictor underestimates sediment transport. The MPM, VR, Rib and fitted predictors are all able to predict the sediment transport with similar accuracy, given the measurements. The EH predictor does not predict the sediment transport rate accurately.
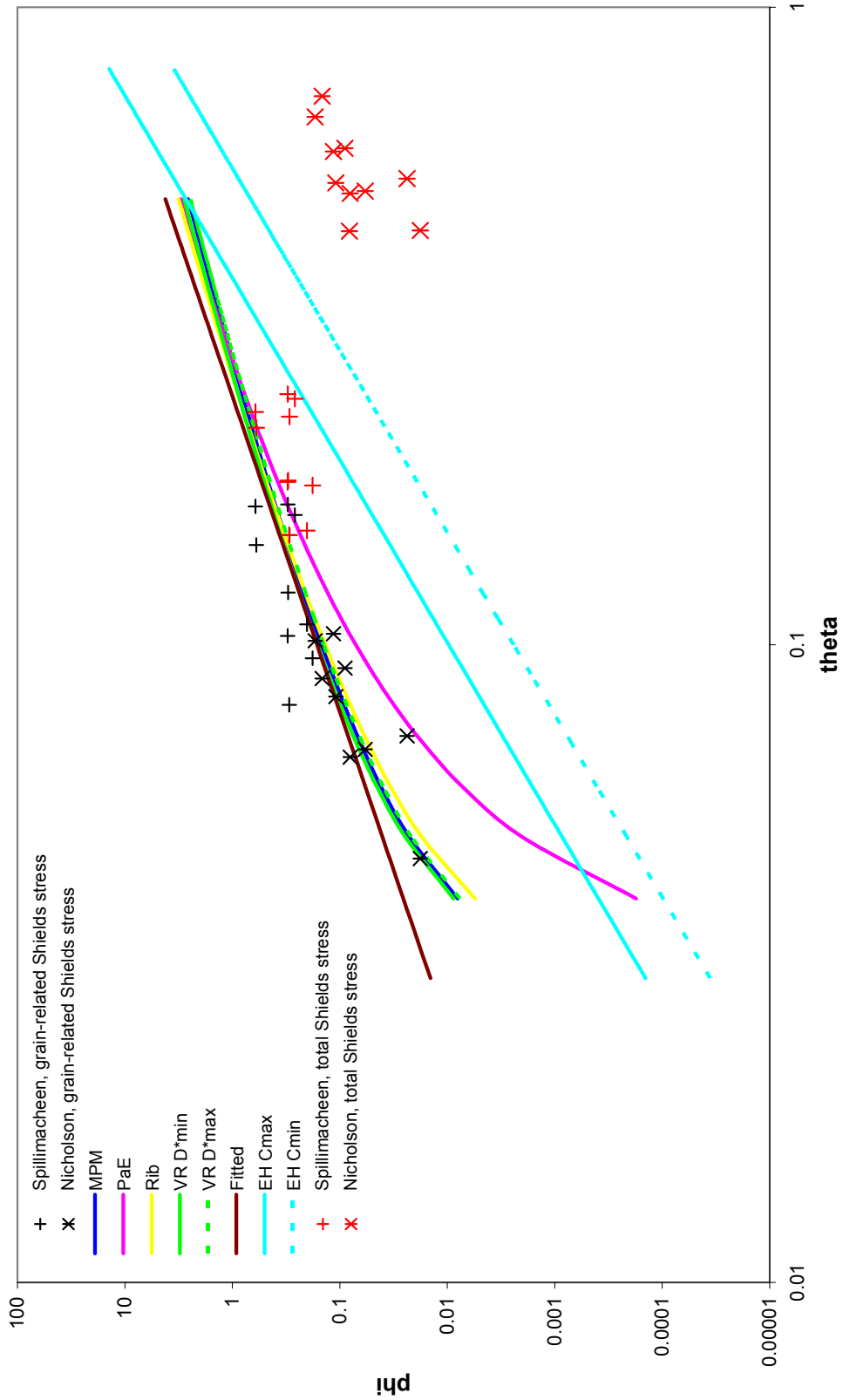
Fig. 3.45: Measured sediment transport rate at Spillimacheen and Nicholson compared to MPM, PaE, VR, EH and the fitted sediment transport predictor. See text for explanation of the symbols.

In order to obtain the amount of wash load relative to suspended sediment transport the Van Rijn (1984b) predictor is used to calculate the suspended sediment transport rate. For practical purposes Van Rijn (1984b) developed an analytical approximation accurate within 25%, which reads as:

$$q_s = Fuhc_a \tag{3.14}$$

wherein the reference concentration c_a is calculated as follows:

$$c_a = 0.015 \frac{D_{50}}{k_s} \left(\frac{\theta' - \theta_{cr}}{\theta_{cr}} \right)^{1.5} D*^{-0.3} \tag{3.15}$$

where F is:

$$F = \frac{(k_s/h)^Z - (k_s/h)^{1.2}}{(1 - k_s/h)^Z (1.2 - Z)} \tag{3.16}$$

where Z:

$$Z = \psi + \frac{w_s}{\gamma \kappa u*} \tag{3.17}$$

with ψ is stratification correction at large concentrations, here 0, γ is ratio of fluid and sediment mixing coefficient, here taken as 1. The settling velocity w_s is calculated as (Soulsby, 1997):

$$w_s = \frac{\nu}{D_{50}} \left(\sqrt{10.36^2 + 1.049 D*^3} - 10.36 \right) \tag{3.18}$$

and with u* (m/s) defined as:

$$u* = \sqrt{g R_r S} \tag{3.19}$$

When comparing the predicted suspended sediment transport rates with the measured suspended and wash load measurements by Locking (1983) it becomes clear that the wash load accounts for 98-99 percent of the total suspended and wash load. This is an extremely large fraction of washload. For example, the amount of wash load in the river Rhine can be up to 85 percent of the total suspended

93

and wash load (Asselman, 2000). Whetten et al. (1969) measured sediment grain size in seven reservoirs along the Columbia River. They found the finest sediment in the most upstream reservoir, the Grand Coulee Reservoir, which traps sediment from the upper Columbia River, the Kootenay River and the Clark Fork River (see figure 2 in Whetten et al., 1965). Most of Grand Coulee reservoir is filled with fine sand, silt and clay ranging in grain size from 0,0039 to > 0,125mm. About half of the reservoir is filled with sediment that has a grain size > 0.0039mm. In fact, the Grand Coulee Reservoir contains the finest material of all reservoirs, whilst it is the most upstream reservoir and is located in the most montane setting. This is caused by the fact that the most upstream sediment sources produce generally fine-grained sediments, such as the clays and silts from the glaciolacustrine sediments and loess deposits (Whetten et al., 1969) (section 2.2.1).

Wang and Dittrich (1992) suggested a critical Rouse number, Z_{cr}, of 0.06 for sediment transport. Note that the critical Rouse number of 0.06 suggested by Wang and Dittrich (1992), is suggested somewhat arbitrarily (Frings et al., 2008). Based on a Z_{cr} of 0.06, the corresponding wash load cut-off size for the upper Columbia River is 0.050mm. This means that silt and clay are transported as wash load in the upper Columbia River. Based on figure 10 in Whetten et al. (1969), it can be concluded that approximately 95 percent of the Grand Coulee Reservoir has bed sediment that is smaller in size than 0.050mm. This indicates that there is indeed a large amount of wash load in the upper Columbia River. In conclusion, the VR predictor for bed and suspended transport rate is used to compare the amounts of bed and suspended sediment transport. According to the VR predictors 93-95 percent of the total suspended and bedload transport in the upper Columbia River is bedload transport. The upper Columbia River is thus a bedload dominated river. This implicates that the sediment transport rate in the upper Columbia River can be modelled by using a bedload transport predictor only.

3.4.5. Spiral flow

In order to examine the role of spiral flow in the upper Columbia River, and thus the applicability of the nodal point relation of Kleinhans et al. (2008) to the upper Columbia River, the transverse bed slope is measured in gentle and sharp bends and compared to equation 3.20 (section 3.4.5.1) which is also employed in the Kleinhans et al. (2008) nodal point relation. Secondly, to test the role of spiral flow at bifurcations the lithological sequence in inner and outer bend residual channels is compared (section 3.4.5.2). This is done because due to the spiral flow effect induced by a bend upstream of a bifurcation inner bend residual channels are hypothesized to have a dominantly sandy fill, whereas the channel fill of outer bend residual channels is hypothesized to consist mainly of silt and clay.

3.4.5.1. Transverse bed slope

Kleinhans et al. (2008) state that on a sloping bed the direction of the sediment transport β_s deviates from that of the shear stress due to gravitational effects. This effect determines the morphology of a river bend. To account for the combination of gravitational effects and spiral flow Kleinhans et al. (2008) used equation 2.18 (section 2.4.3) (Struiksma et al., 1985).

In an infinitive long bend, or a bend with strongly damped morphology like the upper Columbia River (section 3.4.3), with a constant radius an axi-symmetric solution leads to a transverse slope that can be defined as follows:

$$\tan\left(\frac{\partial z}{\partial y}\right) = A f(\theta)\frac{h}{R} \tag{3.20}$$

The above equation is derived from equation 2.18 and 2.19, where an infinitively long bend implies $v/u = 0$. To determine whether spiral flow influences bifurcation evolution in anastomosing rivers, like the upper Columbia River, in the same manner as spiral flow influences bifurcation evolution in meandering rivers (Kleinhans et al., 2008) the transverse bed slope measured in five gentle bends and four sharp bends, (section 3.3.3) are compared to the transverse slope predicted by equation 3.20.

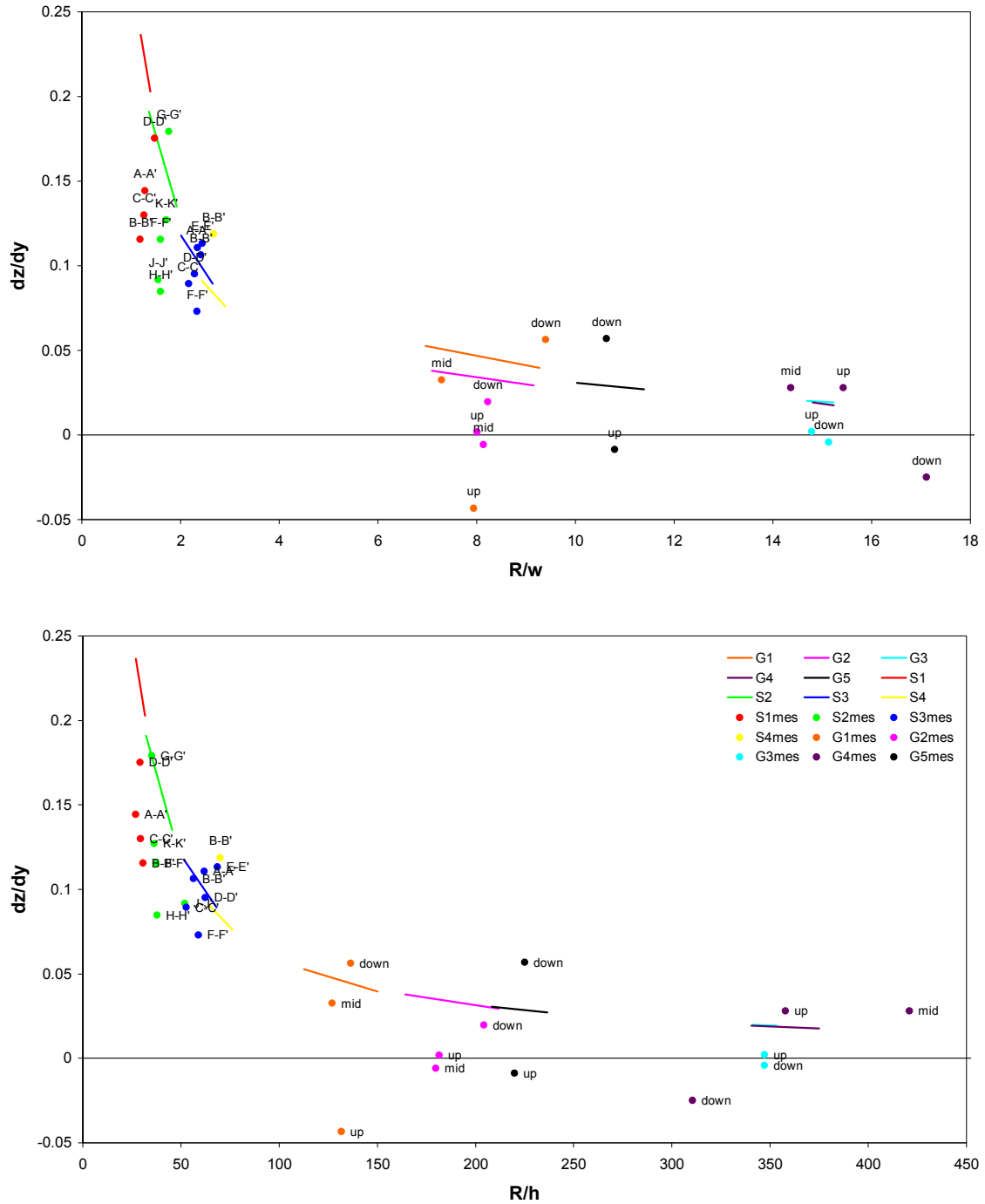*Fig. 3.46: Bend radius divided by channel width (R/w) (above) and channel depth (R/h) (below) plotted versus transverse bed slope. The lines indicate the transverse slope predicted with equation 3.20 for the smallest and largest measured bend radius. The dots indicate the measured bed slope of the sharp and gentle bends indicated in section 3.3.3. G1 to G5 indicate gentle bend 1 to 5. S1 to S4 indicate sharp bend 1 to 4.*

In figure 3.46, a plot of bend radius divided by channel width R/w and water depth R/h plotted versus transverse bed slope $\delta z/\delta y$ is shown. For each bend, the radius of the sharpest part of the bend and the average ratio of the bend are measured, a line is fitted between the transverse bed slope obtained by equation 3.20 for both bend radii. The measured transverse bed slopes are plotted as dots.

In general the sharper the bend, the larger the transverse bed slope. The transverse bed slope increases exponentially for small bend radii. This trend can be seen in both the modelled- and measured transverse bed slopes (figure 3.47). The fact that the transverse bed slope increases exponentially for small bend radii explains why bars with transverse slopes that continue up the levee height only occur in sharp bends. Since the upper Columbia River is characterized by a damped bar regime (section 3.3.3), a strong perturbation is needed for bars to fully develop up to levee height, such a perturbation is only generated by a sharp bend for which Struiksma's theory is invalid.

Despite the fact that the general trend of transverse bed slope versus bend radius divided by channel width and channel depth is reasonably well reproduced, the transverse bed slopes of the gentle bends are characterized by a significant amount of scatter (section 3.3.3.2). The transverse bed slope in the middle- and downstream part of gentle bend 1 corresponds with the predicted transverse bed slope. The upstream part of the bend is characterized by a negative transverse bed slope, and consequently does not correspond with the predicted transverse bed slope. The measured transverse bed slopes in gentle bend 2 are lower than the predicted transverse bed slopes. In the upstream- and middle part of the bend no significant transverse bed slope is present, while the transverse bed slope in the downstream part of the bend is only slightly lower than the predicted transverse bed slope. In gentle bend 3 no significant transverse bed slope is measured in both the up- and downstream part of the bend, a small transverse bed slope is predicted however. The measured transverse bed slope of the upstream and middle part of gentle bend 4 is slightly larger than the predicted transverse bed slope. The downstream part has a negative transverse bed slope (section 4.3.2). There is a large difference in transverse bed slope between the down- and upstream part of gentle bend 5. The predicted transverse bed slope is approximately the average bed slope of the down- and upstream part of the bend.
The measured transverse bed slope of both sharp bends 1 and 2 is lower than the predicted transverse bed slope. Only for G-G' of sharp bend 2 is the measured transverse bed slope equal to the predicted transverse bed slope. This is caused by the deep outer bend pool in G-G' (section 3.3.3.1, figure 3.36), which increases the transverse bed slope. The average measured transverse bed slope in outer bend 3 is approximately equal to the predicted transverse bed slope. Only one transverse bed slope is measured at sharp bend 4, this transverse bed slope is larger than the predicted transverse bed slope.
The scatter appears to be larger at gentle bends than at sharp bends. This is caused by the fact that in some parts of the gentle bends a transverse bed slope is absent or even negative. This is mainly caused by the influence of upstream perturbations, like an upstream bend or bifurcation (section 3.3.3.2).

In summary, the transverse bed slope can reasonably be predicted by using Struiksma's theory for spiral flow. This indicates that spiral flow is able to rework bed material to form transverse slopes which are comparable to the transverse slopes found by Struiksma et al. (1985) in meandering rivers. Since Kleinhans et al. (2008) characterize spiral flow at bifurcations with an upstream meander bend conform equation 2.18 and 2.19, it can be assumed that this nodal point relation is applicable to predict the evolution of the bifurcations in the upper Columbia River.

3.4.5.2. Residual channels

In the previous section the influence of spiral flow in the upper Columbia River system was investigated by inspecting the transverse slope in meander bends. The effect of spiral flow on sediment division at bifurcations is crucial for modelling the upper Columbia River network. If spiral flow indeed influences bifurcations with an upstream bend in the upper Columbia River, as indicated by Kleinhans et al. (2008) for meandering rivers there should be a pronounced difference in channel-fill of inner- and outer bend residual channels.

In the upper Columbia River, bedload is dominated by sandy material (Locking, 1983), while suspended and wash load is dominated by silt and clay (section 3.4.4). At bifurcations with an upstream meander bend, spiral flow forces bed material towards the inner bend bifurcate, while suspended and wash load are forced towards the outer bend by the centrifugal force. Hence, sandy material will mostly be trapped in inner bend residual channels and silt and clay mostly in outer bend residual channels.

To test this hypothesis borings are performed in nine residual channels (figure 3.4; 3.47; 3.48), five outer bend residual channels, two inner bend residual channels and two trifurcation residual channels. The origin of the residual channel that corresponds to boring 035 is not certain; it is hypothesized as a trifurcation residual channel (figure 3.47; 3.48).

The five outer bends all approximately show the same lithological sequence. A thick top layer consisting of clay and silt, and a thinner succession of sand and gravel below, mostly representing channel-lag deposits. The full channel-fill succession can only be seen in boring 005 and 031, where floodplain deposits are found, consisting of silt, clay and peat, beneath the sandy channel fill, indicating the base of the residual channel. The other three outer bend residual channels all show a thick succession of silt and clay on top of sandy bed material. However, the plug of clay and silt on top of this sandy bed material is significantly thicker than that of an inner bend residual channel.

The two inner bend bifurcates are fully filled with sand and gravel material, except for the top meter which is filled with silt. Sand is deposited in the residual channel, until the inlet step becomes too high

for spiral flow to force sand into the inner bend bifurcate, so that only some suspended and wash load is able to enter the inner bend bifurcate, causing the top meter to consist of silt.

Tbl. 3.3: Ratio of silt and clay divided by sand for inner and outer bend residual channels.

	outer bends		inner bends	
boring	5	31	30	59
ratio	1.11	3.8	0.42	0.15

When calculating the ratio of the thickness of the clay and silt succession divided by the thickness of the sand and gravel succession (table 3.3), it becomes clear that for outer bend residual channels this ratio is larger than 1, whereas the ratio is smaller than 1 for inner bend residual channels.

In conclusion, spiral flow effects the bifurcations in the upper Columbia River, causing inner bend residual channels to mainly fill with sandy material, and outer bend residual channels to mainly fill with silt and clay. Due to the pronounced effect of spiral flow at bifurcations in the upper Columbia River, the Kleinhans et al. (2008) nodal point relation is applicable for modelling the upper Columbia River network.

Outer bend residual channels

Inner bend residual channels

Trifurcation residual channels

Fig. 3.47: Upstream bends of residual channels. Flow carrying channels are indicated by solid lines, whereas residual channels are indicated by dotted lines.
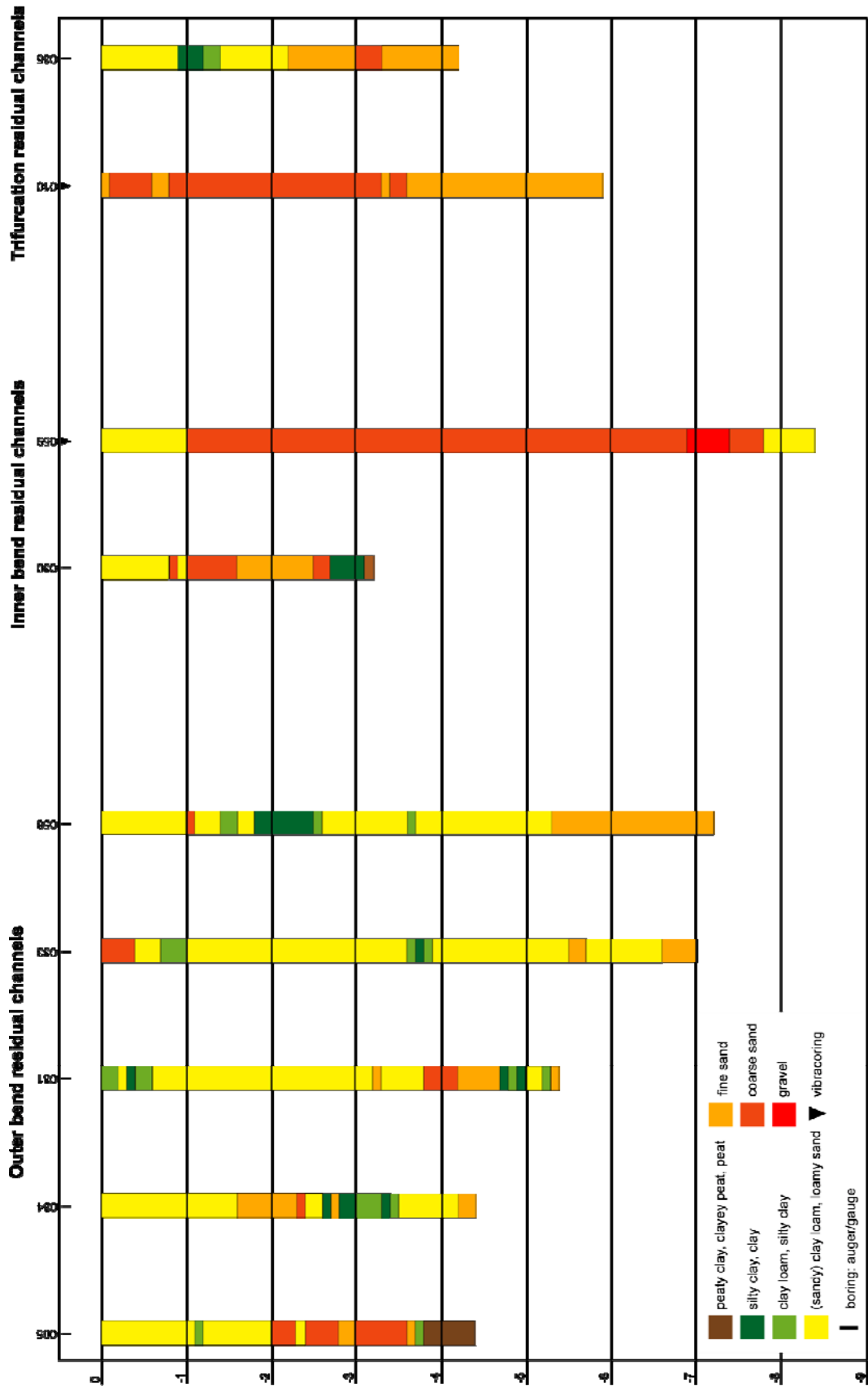
100

Fig. 3.48: Fill of residual channels indicated in figure 3.47.

3.4.6. Bifurcation equilibrium configurations

In order to investigate the effect of Shields stress and aspect ratio ($w_{up}/2h_{up}$) on bifurcation equilibrium configurations of the upper Columbia River the area ratio ($A_{minor\ bifurcate}/A_{major\ bifurcate}$) and the nondimensional inlet step of the bifurcates of the five measured bifurcations in the upper Columbia River (section 3.3.2.2) are plotted. To obtain a more general view on bifurcation equilibrium configuration of channels characterized by a small width/depth ratio and cohesive banks, four bifurcations from the Cumberland Marshes are also investigated. These data are provided by Dr. M.G. Kleinhans (personal communication).

Four figures are made: a graph of Shields stress versus area ratio (figure 3.49), a graph of aspect ratio versus area ratio (figure 3.50), a graph of Shields stress versus inlet step (figure 3.51) and a graph of aspect ratio versus inlet step (figure 3.52), as was also done by Bertoldi and Tubino (2005) on bifurcation equilibrium configurations of experimental braided river bifurcations (figure 2.9).

Data of the upper Columbia River and the Cumberland Marshes reveal the following trend. For increasing Shields stress the area ratio decreases, bifurcations become more asymmetric for higher values of Shields stress. For an increasing aspect ratio, the area ratio increases. This is caused by the fact that the Shields stress becomes larger, when the aspect ratio decreases. The plot of aspect ratio versus area ratio shows more scatter than the plot of Shields stress versus area ratio.

The plot of inlet step versus aspect ratio (figure 2.52) is not characterized by a clear trend, as is the case for area ratio (figure 3.50). When Shield stress is plotted against inlet step (figure 3.51), the inlet step would be expected to increase with increasing Shield stress, since inlet steps are highest for highly asymmetric bifurcations. Despite the large amount of scatter this trend can be distinguished. In the plot of aspect ratio versus inlet step no trend can be distinguished, whereas an increasing inlet step would be expected for decreasing aspect ratio, contrary to the trend measured in experimental braided rivers by Bertoldi and Tubino (2005).

In conclusion, bifurcations in channels characterized by a small width/depth ratio and cohesive banks become more asymmetric for increasing Shields stress. The inlet step height increases with increasing Shields stress, but the trend is obscured by a significant amount of scatter.
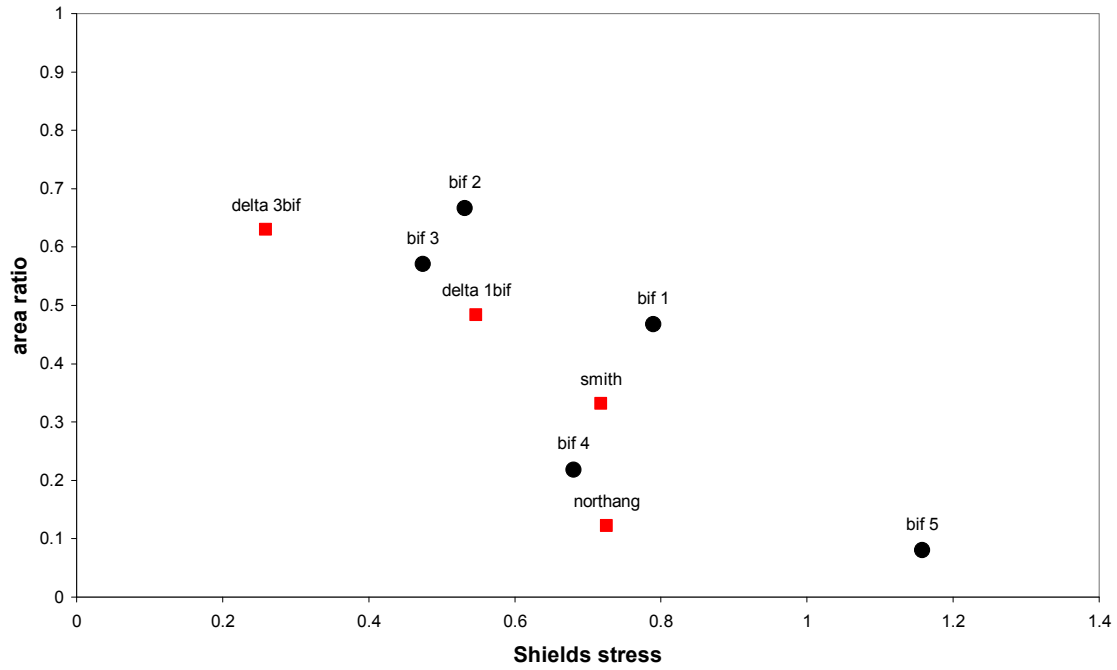
Fig. 3.49: Shield stress plotted versus area ratio for bifurcations in the upper Columbia River (black) and the Cumberland Marshes (red).

Fig. 3.50: Aspect ratio plotted versus area ratio for bifurcations in the upper Columbia River (black) and the Cumberland Marshes (red).

Fig. 3.51: Shields stress plotted versus nondimensional inlet step for bifurcations in the upper Columbia River (black) and the Cumberland Marshes (red).
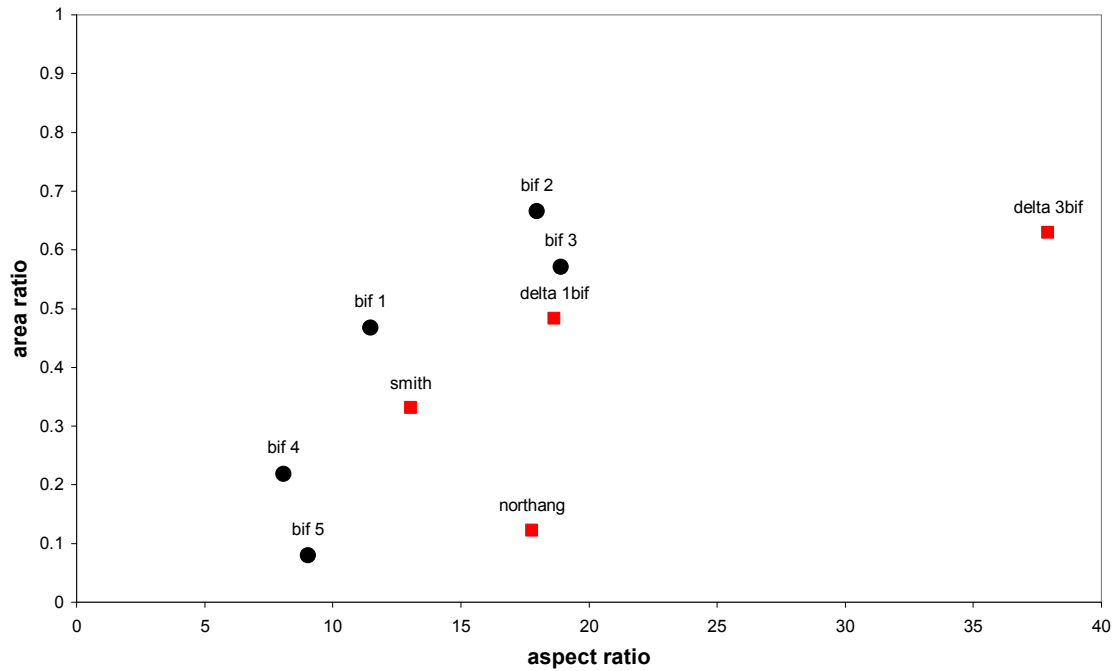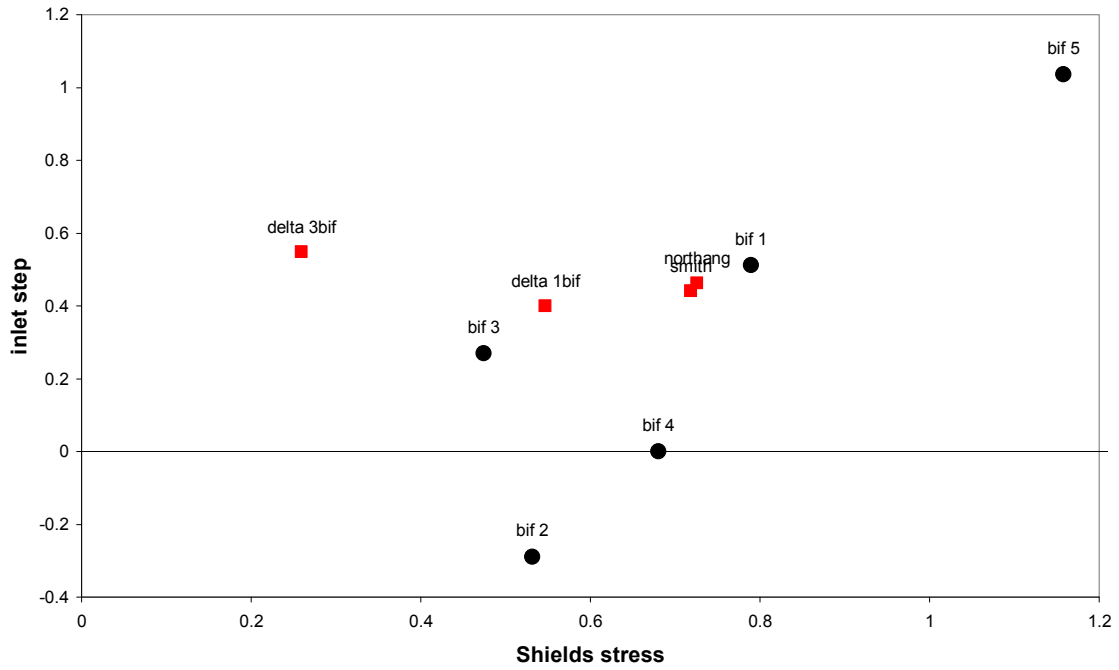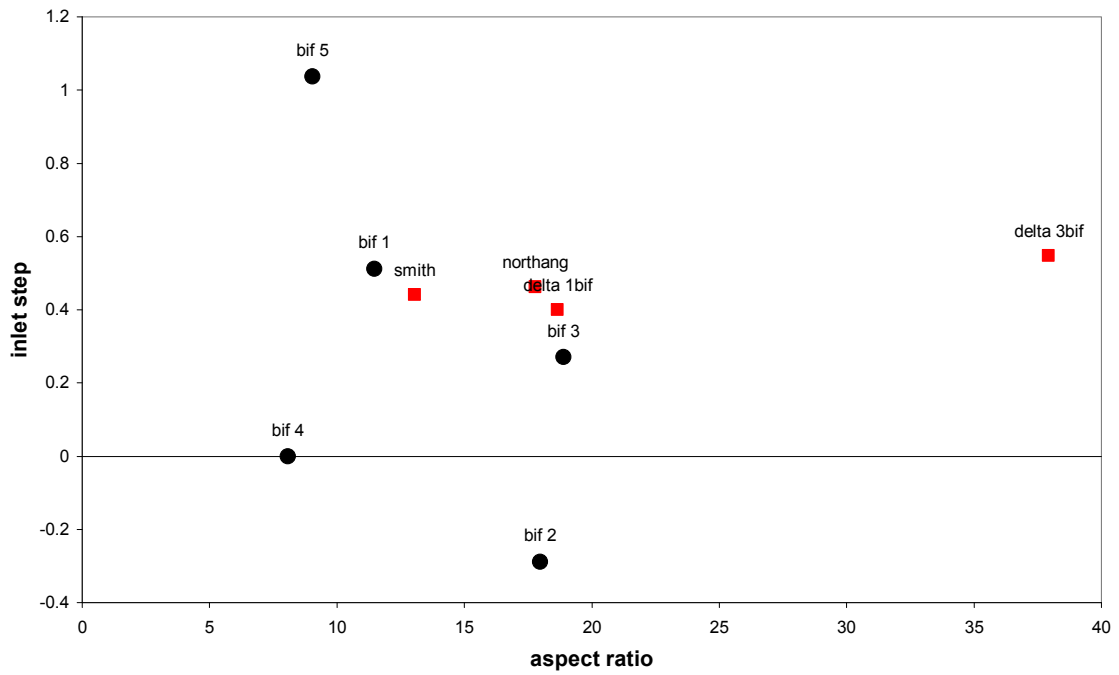

Fig. 3.52: Aspect ratio plotted versus nondimensional inlet step for bifurcations in the upper Columbia River (black) and the Cumberland Marshes (red).

3.4.7. Confluence scour depth

In figure 3.53, the nondimensional scour hole depth d_s of confluence 3, 4, 5 and 6 is compared to the scour hole depth predictors of Ashmore and Parker (1983), Best (1985) and Kjerve et al. (1979) (section 2.5). In the data of confluence 1 and 2, no scour hole can be distinguished. This might be caused by the fact that the cross- and long-profiles were not located at the scour hole, or more probably by the fact that indeed no scour hole was present.

The scour hole depth predictors tend to overpredict the scour hole depth of the confluences in the upper Columbia River (figure 3.53). Only the depth of the scour hole at confluence 3 is underpredicted by Kjerve et al. (1979), whilst it is still overpredicted by the other scour depth predictors.

Based on the measured confluences (section 3.3.3), the nondimensional scour hole depth does not seem to increase with confluence angle, but seems to stay constant at a value of $d_s = 2$.

This might be due to the lack of data, which might make it not possible to distinguish a clear trend. An other explanation might be that the cross- and long profiles at the confluences were not located at the deepest point of the scour hole, causing an underestimation of the scour hole depth and consequently an overestimation of the nondimensional scour hole depth by the scour hole depth predictors.

A last explanation might be the fact that the scour hole predictors are designed for braided river confluences, which generally have smaller water depth and less cohesive bed material than anastomosing river systems. The smaller water depth might increase the nondimensional scour hole depth since it is the scour hole depth divided the average depth of the upstream channels (equation 2.30). The fact that the bed material is less cohesive in braided rivers causes bed material to be more easily eroded by the vertical vortices created by the friction between the water masses of the upstream channels, and consequently the scour hole depth to become larger.
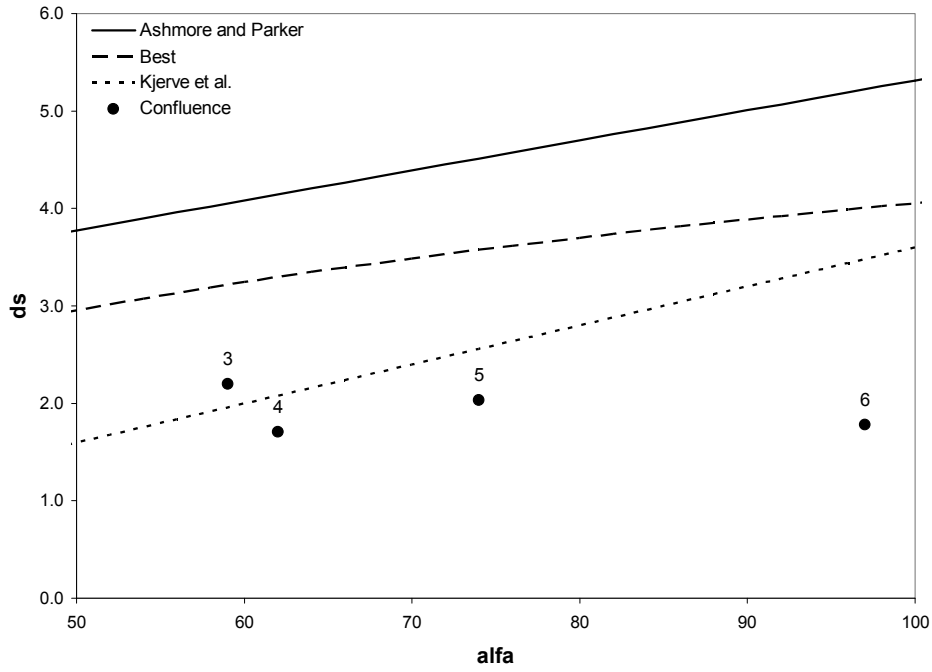
Fig. 3.53: Nondimensional scour hole depth versus confluence angle for the upper Columbia River confluences and the Ashmore and Parker (1983), Best (1985) and Kjerve et al. (1979) nondimensional scour hole depth predictors.

4. River network model

4.1. Introduction

In order to gain insight in river networks, especially the dominant processes that influence the evolution of such networks, idealized river networks are modelled during this research. In section 4.2, the model developed to fit this purpose is described. The model schematization, boundary- and initial conditions are described in section 4.3. Since bifurcations are the dominant features in a river network, a sensitivity analysis on bifurcations is performed in section 4.4.1. In section 4.4.2 bifurcation equilibrium configurations for a range of Shields stress are analysed. The dynamics of river networks is investigated in section 4.4.3 with idealized river networks. In section 4.4.4 the network of a highly-anastomosed reach of 21km of the upper Columbia River is modelled and analysed.

4.2. Model formulation

In this section, the river network model is described by describing the input needed, the equations used, the numerical scheme and the models critical assumptions and simplifications.

Network

The channel network has to be defined as model input, this is done as follows: the channel network is divided into several orders (figure 4.1). For each order, the numbers of the channels present in this order have to be defined. For each channel, the number(s) of the channel(s) that are connected to this channel at the up- and downstream boundary have to be defined. If two upstream channels are connected to a certain channel, a confluence is present. If two downstream channels are connected to a certain channel, a bifurcation is present. If a certain channel has one channel up- and downstream, a through-flow node is present for numerical reasons.

The height of each bifurcation and confluence has to be defined as well as the height of the upstream boundary. The height of each through-flow node can then be interpolated from the heights of the bifurcations and confluences.
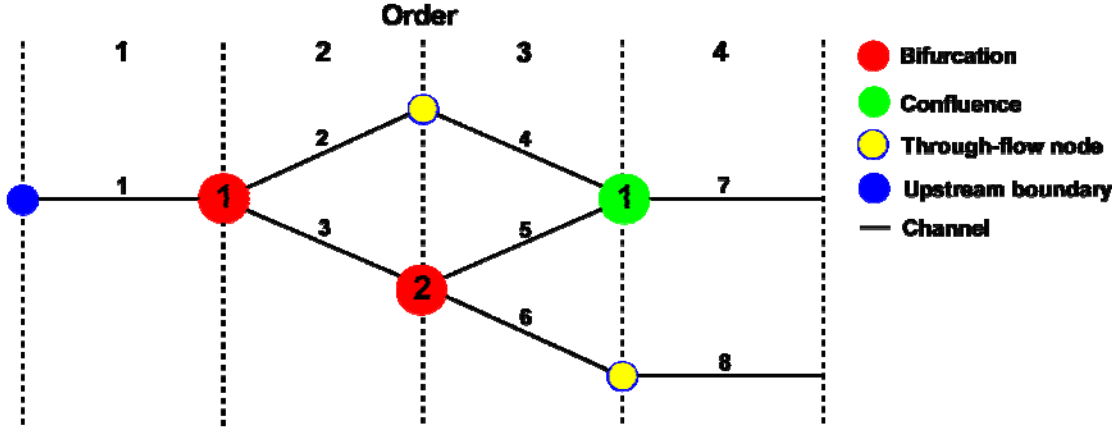
Fig. 4.1: Definition of network elements for the network in figures 4.10, 4.11, 4.12 and 4.13.

flow

The model used in this research computes variation in river bed level $\eta(x, t)$, where x denotes a streamwise coordinate and t denotes time. The model is characterized as a network of channels, where channels split at bifurcations and channels join at confluences.

The flow in a channel is computed using the backwater formulation for steady, gradually varied flow under the constraint of constant water discharge. The discretized backwater equation is:

$$\frac{\Delta h}{\Delta x} = \frac{S - S_f}{1 - Fr^2} \tag{4.1}$$

where the friction slope S_f (-) and Froude number Fr (-) are defined as:

$$S_f = \frac{g}{C} Fr^2 \tag{4.2}$$

$$Fr = \frac{u^2}{gh} \tag{4.3}$$

wherein the flow velocity u is given from continuity as:

$$u = \frac{Q}{wh} \tag{4.4}$$

The bed friction C used in the model is either set as a constant value or calculated by the Colebrook-White equation (equation 2.14) when a constant Nikuradse roughness height k_s is assumed. Subcritical flow $Fr < 1$, is considered in the model. This implies that integration of equation 4.1 must proceed upstream from $x = L$. The relation between bed slope and bed elevation is:

$$S = -\frac{\delta\eta}{\delta x} \qquad (4.5)$$

wherein η denotes bed elevation (m) and x is the along channel distance (m). Water surface elevation ξ (m) is given as

$$\xi = \eta + h \qquad (4.6)$$

where h is calculated by the numerical solution of equation 4.1 in upstream direction. The upstream end of the reach in question is at $x = 0$ and the downstream end is at $x = L$. For a specified bed elevation profile and specified water elevation at the downstream end of a channel, the backwater equations can be solved to calculate the water depth upstream of the downstream end of a channel. From the obtained upstream water levels the Shields stress is computed.

Sediment transport

The sediment transport is calculated by using either the EH, MPM, VR or the fitted sediment transport predictor (section 3.4).

The MPM and the VR sediment predictors are bedload transport predictors. These predictors are based upon the Shields stress, and the critical Shields stress for sediment motion. For flow conditions close the critical Shields stress for sediment motion, using the MPM or the VR sediment transport predictors leads to numerical instabilities in some networks. The EH sediment transport predictor is based on total roughness. It does not include a threshold for sediment motion. Therefore it does not lead to numerical instabilities, however, the EH sediment transport predictor does not lead to an accurate prediction of the transport rate in the upper Columbia River (section 3.4.4). The fitted sediment transport predictor is based on grain-related Shields stress only, and does lead to an accurate prediction of the transport rate in the upper Columbia River for moderate flow conditions; additionally it does not lead to numerical errors.

Flow division at bifurcations and confluences

At bifurcations, the division of flow and sediment can be obtained by using the nodal point relations of Wang et al. (1995), Bolla Pittaluga et al. (2003) or Kleinhans et al. (2008) (section 2.4.3). At confluences the flow and sediment load in the downstream channel is obtained by adding the flow and sediment load of the two upstream channels.

Morphological change

The Exner equation for sediment continuity is used for morphological change. The Exner equation of sediment continuity takes the form:

$$\left(1 - \lambda_p\right)\frac{\partial \eta}{\partial t} = -\frac{\partial q_t}{\partial x} \tag{4.7}$$

where λ_p denotes the porosity of the bed deposit, q denotes the unit water discharge (m²/s) and t denotes time. In words, the equation states that a change in bed elevation over time is induced by the gradient in sediment transport along the channels.

Additionally, not only the bed elevation is updated over time, also the channel is able to widen or narrow over time. The method obtained is loosely based upon the method proposed by Miori et al. (2006). The fraction of channel width that is able to deposit sediment on the levees is defined as:

$$L_f = \frac{w}{h} \tag{4.8}$$

The parameter L_f is introduced to overcome the following problem. Not all sediment that is being transported in a channel can be deposited on a channel levee, only the sediment that is transported within a certain range of the levee can. This range is defined as L_f. The relaxation time for the channel geometry to adjust to its equilibrium width is characterized as:

$$T_w = \frac{L_f h w}{q} \tag{4.9}$$

The equilibrium width of a channel follows from hydraulic geometry and is calculated as follows:

$$B_{eq} = aQ^b \tag{4.10}$$

where a is the coefficient and b is the power of hydraulic geometry. By combining the equilibrium width and the timescale of adaption of the channel to the equilibrium width, the actual channel width is calculated as follows:

$$B_t = B_{t-1} + \frac{B_{eq} - B_{t-1}}{T_w} \tag{4.11}$$

In order to test the situation where outer bend residual channels close by narrowing and inner bend residual channels close by vertical shallowing, an option is included wherein inner bend residual channels are allowed to adjust their width when growing, but are not allowed to adjust their width when narrowing, causing them to silt up vertically.

Numerical scheme

Each channel in the network is assumed to have a length L (m). This length is divided into M subreaches each with length Δx (m), where

$$\Delta x = \frac{L}{M} \tag{4.12}$$

This defines $M+1$ nodes with the positions:

$$x_i = (i-1)\Delta x, i = 1..M+1 \tag{4.13}$$

The first node is a ghost node. The ghost node is used for the flow distribution at bifurcations. As stated before, from the height of the bifurcations and confluences and the length of the channels, the slope of each channel is calculated. Hence, the initial bed elevations η_i at each note are denoted as:

$$\eta_i = S_i(L - x_i), i = 1..M+1 \tag{4.14}$$

The numerical implementation proceeds in two steps. First the backwater equation (equation 4.1) is solved over a known bed under the constraint of a specified, constant water surface elevation at the downstream end of each channel, so allowing the determination of the sediment transport at each node. Secondly, equation 4.7 is applied to find the new bed one time step later.

To solve the backwater equation, the depth h_{i+1} is supposed to be known, and the depth h_i at one node upstream is to be computed. The relation discretizes with the aid of equation 4.2, 4.3, 2.11 and 4.5 to give:

$$h_i = h_{i+1} - F_{back}(h)\Delta x \qquad (4.15)$$

where:

$$F_{back}(h) = \frac{\dfrac{\eta_i + 1 - \eta_i}{\Delta x} - C_f \dfrac{q^2}{gh^3}}{1 - \dfrac{q^2}{gh^3}} \qquad (4.16)$$

In the model a predictor-corrector scheme is used to solve for h;

$$h_{pred} = h_{i+1} - F_{back}(h_{i+1})\Delta x \qquad (4.17)$$

The predicted value of h, h_{pred}, is then used in equation 4.18 leading to a new value of F_{back}. So, two values of F_{back} are now attained; one by using the initial h, the predicted F_{back}, and one by using the predicted h, the corrected F_{back}. Now, the actual value of h can be solved by:

$$h_i = h_{i+1} - \frac{1}{2}\left[F_{back}(h_{pred}) + F_{back}(h_{i+1})\right]\Delta x \qquad (4.18)$$

After applying the above equation, the water level at all nodes in a single branch is known. However, the network model consists of a number of branches. Hence, the backwater curves have to be calculated for each branch separately. Since flow is assumed to be subcritical, e.g. $Fr < 1$, a disturbance travels upstream. For branches with an downstream confluence, through flow node, or boundary condition, the backwater curve can simply be applied. After each calculation, the computed water depth for the most upstream values of a branch, becomes the downstream boundary condition for the upstream branch. For branches that have an upstream bifurcation, a difference in water level at the most upstream node of both bifurcates may occur after applying the backwater curve. Consequently, iteration has to be performed to obtain equal water levels in both bifurcates at a bifurcation. In this iteration, the discharge is varied to obtain equal water levels.

Now h is known at all nodes in all the branches, so the Shields stress can be computed from equation 11. From the Shields number, the sediment transport $q_{t,1}$ can be computed from the applied sediment transport predictor. Additionally, the nodal point relations are applied to obtain the sediment division at bifurcations. The sediment into both bifurcates is appointed to a ghost node, a node that does not have an exact position, but is located upstream of $i = 1$. At confluences, the discharge and sediment transport in the upstream branches are added to obtain the discharge and sediment transport in the downstream branch. Now the amount of sediment transport is known for all nodes. The transport gradient is then calculated in a mixed upwind-downwind scheme:

$$\frac{\Delta Q}{\Delta x} = a_u \frac{Q_{t,i} - Q_{snode,t,i}}{\Delta x} + (1 - a_u)\frac{Q_{t,i+1} - Q_{t,i-1}}{\Delta x}, i = 1$$

$$\frac{\Delta Q}{\Delta x} = a_u \frac{Q_{t,i} - Q_{t,i-1}}{\Delta x} + (1 - a_u)\frac{Q_{t,i+1} - Q_{t,i-1}}{\Delta x}, i = 1..M \qquad (4.19)$$

$$\frac{\Delta Q}{\Delta x} = \frac{Q_{t,i} - Q_{t,i-1}}{\Delta x}, i = M + 1$$

The coefficient a_u can be set between 0 and 1. Setting a_u to 1 yields a pure upwinding scheme, which gives stability at the cost of accuracy. Setting a_u to 0.5 yields a central difference scheme, which gives accuracy at the cost of stability. Schemes using a backwater formulation are prone to numerical instability in the absence of at least some upwinding, so that a_u should be greater than 0.5.

The transport gradient in the most upstream node, $i = 1$, is calculated from the difference in sediment transport between the upstream ghost node and the downstream node. The upstream ghost node can be one or two upsteam channels in case of through-flow node or confluence, or a bifurcation, where the amount of sediment transport in the ghost node follows from the nodal point relation. For the nodes $i = 1..M$, the gradient follows from the difference between the up- and downstream node. At the last node, no downstream node is present, so that only node i and i-1 are used in transport gradient calculation. Finally, the new bed elevation at the next time step is given from a discretized version of (equation 4.17) which reads for a constant channel width:

$$\eta_{i,t+\Delta t} = \eta_{i,t} - \frac{1}{1 - \lambda_p}\frac{\Delta Q_{t,i}}{\Delta x}\frac{1}{w_{t,i}}\Delta t \qquad (4.20)$$

In the case of varying channel width, the width is obtained from equation 4.11. The discretized version of 4.20 then becomes:

$$\eta_{i,t+\Delta t} = \eta_{i,t} - \frac{1}{1 - \lambda_p}\frac{\Delta Q_{t,i}}{\Delta x}\frac{1}{w_{t,i}}\Delta t + \frac{(w_{t,i} - w_{t,i-1})h_{t,i}}{w_{t,i}} \qquad (4.21)$$

113

the second term is necessary to make sure that the sediment that is eroded/deposited from the levees of the river is deposited/eroded on the bed.

Spatial step and time step

When a very small time step is used in a mathematical model, the results obtained are more accurate than when a larger time step with a corresponding spatial step is applied. But, using a very small time step is time extensive. The application of a large time step is less time extensive, but might cause numerical instabilities. To make sure that the model will not produce incorrect results, but still uses a time step as large as possible to reduce the calculation time, the Courant condition is applied to calculate the time step. The Courant condition is characterized as follows:

$$C_r \frac{c * \partial t}{\partial x} \tag{4.22}$$

where C_r is the Courant criterion, c is the celerity of a bed disturbance x/t, t is the time step and x is the gridsize. As a corollary, when the grid point separation δx is reduced, the upper limit for the time step also decreases.

In the model a minimum time step is implemented, so that the time step induced by the Courant conditions cannot become infinitely small.

Assumptions

The network model is based on a the following simplifications and assumptions:
- Rectangular channel bathymetry
- One-dimensional flow and sediment transport
- Constant discharge
- Gradually varied flow
- No head loss at confluences
- Equal size of sediment fraction in bed and banks

4.3. Model schematization, boundary- and initial conditions

In this section, the general input parameters used in all model runs are described. Both their value and how this value is obtained are discussed. Case specific parameters will be described in the relevant section.

As indicated in section 4.2, the following parameters are required as input to the network model: topology, initial discharge and median grain size in the individual channels, the height above reference datum of bifurcations and confluences, the relative upstream bend radius of each bifurcation, the intermittency of the given discharge, the bed sediment porosity, the Nikuradse roughness height or Chézy roughness, the upstream width, the power on discharge to obtain hydraulic geometry width, the alpha parameter and the epsilon parameter from the Kleinhans et al. (2008) nodal point relation. Additionally, for each run the following assumptions have to be made: the channel width can either be kept fixed, or channels can be allowed to adjust their width to changing discharge. As a third option, channels can be allowed to widen for increasing discharge, but are not allowed to narrow for decreasing discharge. Second a choice of nodal point relation and sediment transport predictor has to be made.

In all model runs the Kleinhans et al. (2008) nodal point relation is used since this nodal point relation is especially designed for meandering rivers, and spiral flow is included. From section 3.4.5 it becomes clear that spiral flow has a large influence on bifurcations in the upper Columbia River. In all model runs the channel width is non-fixed, e.g. the channel width is able to adjust its width for in- and decreasing discharge. The choice of sediment transport predictor and bed roughness assumption is case specific and will therefore be defined in the relevant section.

The topology is either that of a Y-shaped bifurcation, simple network or a reach of the upper Columbia River of 21km with 99 branches. In the first two cases the topology is loosely based upon the channels of the upper Columbia River. The topology of the complete upper Columbia River is derived from sattelite images from Google Earth.

The upper Columbia River discharge is highly seasonal (figure 2.2). To overcome the large discharge variability, a channel forming discharge that transports the annual sediment load is used as input for the river network model. The channel forming discharge is calculated by using discharge data from the Nicholson gauging station and the flow and sediment transport data of Locking (1983) (table 2.3). Locking (1983) found that the discharge measured at Nicholson is five percent higher than the discharge at Spillimacheen due to some tributary channels entering the upper Columbia River between Spillimacheen and Nicholson. So, by using daily discharge measurements from the Nicholson gauging

station from 1917-2008 and extracting five percent, the daily discharge from 1917-2008 is known for the modelled upper Columbia River reach.

Based on discharge and sediment transport data of Locking (1983) measured at Nicholson, a discharge-unit sediment transport rate relation can be made. This relation reads as follows:

$$q_b = 4.00 * 10^{-10} Q^{1.6674}$$
(4.23)

By using the daily discharge from 1917-2008 at Spillimacheen and the discharge-unit sediment transport rate relation, the daily unit sediment transport rate for the period 1917-2008 can be calculated. Based on the total unit sediment transport in this period a corresponding constant discharge, which leads to exactly the same amount of total unit sediment transport for the period 1917-2008 is calculated: the channel forming discharge. The calculated channel forming discharge is 187 m^3/s. For simplicity, the channel forming discharge used as input for the model is 200 m^3/s. Since the input discharge is defined as the channel forming discharge, the intermittency can automatically be set to 1.

Locking (1983) measured a median grain size at Spillimacheen of 0.7mm. Median grain size measurements taken in the modelled reach are of comparable size (table 3.2). Consequently as input to the model runs, a median grain size of 0.7mm is used. For simplicity the median grain size is equal in all channels.

Abbado et al. (2005), measured the main channel slope in the upper Columbia River between Spillimacheen and Golden (section 2.2.2). They found that the modelled reach is characterized by an initially relatively gentle slope of 6.8*10^{-5}m/m, followed by a relatively steep sloped reach of 2.1*10^{-4} m/m, which is followed by a relatively gently sloped reach with an average slope of 6.8*10^{-5}m/m. Since the steep reach is characterized by the most pronounced anastomosis, the slope used for the sensitivity, equilibrium configurations and simple network analysis is the slope of the steep reach, rounded to 2*10^{-4}m/m.

In the analysis of a complete reach of the upper Columbia River, the elevation data of Abbado et al. (2005) is used to obtain the height of all bifurcations and confluences in this reach. This is done by assuming a uniform cross-valley elevation. A long-valley profile can be made based on the heights measured by Abbado et al. (2005). The heights of the bifurcations and confluences can then be interpolated based on their long-valley position.

Using data of Locking (1983) and slope measurements of Abbado et al. (2005), the Nikuradse roughness height can be calculated at Spillimacheen and Nicholson. Based on this data the Nikuradse roughness height at Spillimacheen and Nicholson is respectively approximately 0.03m and 1.20m. So there is a large unexplained difference in roughness height at Spillimacheen and Nicholson. This is most likely caused by the occurrence of large bed forms at Nicholson when the measurements of

Locking (1983) were taken. The Nikuradse roughness height used in the model runs is in between the values measured at Spillimacheen and Nicholson: 0.15m. This roughness height is assumed to be equal in all channels.

The α parameter, introduced by Bolla Pittaluga et al. (2003) in their nodal point relation, can be described as the length of upstream morphological change induced by a bifurcation divided by the channel width. According to Bolla Pittaluga et al. (2003) this length is the range 1-3. At bifurcation 1, 2 and 3 the length of upstream morphological change is measured (figure 3.12, 3.15 and 3.19). The corresponding values of α for bifurcation 1, 2 and 3 are respectively 0.47, 0.16 and 1.76. The α parameters is thus very small in the upper Columbia River in agreement with the damped bar regime. In the model, α is set to 1.

The relative bend radius is measured for each bifurcation separately, and is derived from Google Earth. The relative upstream bend radius is in this section defined as R/w, but for simplicity referred to as R. For the sensitivity analysis and the simple network runs, a representative bend radius is chosen.

The bed porosity is set at 0.35, the power on discharge for hydraulic geometry width is 0.56 (section 3.4.2), ε is set at 2. The general input parameters and the assumptions used in the model runs are summarized in table 4.1.

Tbl. 4.1: Values of general parameters and assumptions used during modelling.

General parameters			Settings and choices	
value		unit		
Qup	200	m^3/s	nodal point relation	Kleinhans et al. (2008)
D50	0.7	mm	sediment transport predictor	EH, MPM or F
ks	0.15	m	Upstream channel width	50-100 m
R	Inf-50	-	bed roughness	Constant C or ks
S	5.10^{-5} - 3.10^{-4}	-		
L	100-3000	m		
I	1	yr		
λ	0.35	-		
n	0.56	-		
α	1	-		
ε	2	-		

4.4 Modelling results

4.4.1 Introduction

In this section, first a sensitivity analysis is performed to gain insight in the effect of certain parameters on the evolution of bifurcations in a simple fork bifurcation (section 4.4.2). In section 4.4.3 the equilibrium configuration of bifurcations induced by a slope advantage in one of the bifurcates or by an upstream bend for a range of Shields stress is investigated to address the effect of Shields stress on bifurcation equilibrium configurations. In order to investigate river networks, the evolution of two simple river networks is analysed in section 4.4.4. The first river network consists of two bifurcations and six branches, the second river network consists of two bifurcations, one confluence and 8 branches. In section 4.4.5 a 21km reach of the upper Columbia River is modelled to investigate the dynamics of large river networks. The model outcomes are used to test the applicability of the network model to reproduce such river networks, to explain the bed configuration of the modelled upper Columbia River reach and to test the hypotheses on the origin of anastomosis in the upper Columbia River.

4.4.2 Sensitivity analysis

In the sensitivity analysis the following factors are analysed (figure 4.2 and 4.3): the effect of sediment transport predictor, nodal point relation, fixed- or non-fixed channel width, constant Chézy C or Nikuradse bed roughness k_s, the value of Nikuradse roughness height, relative upstream morphological influence of a bifurcation α, relative upstream bend radius R, a slope advantage in one of the bifurcates, length of the bifurcates and finally the fraction of the banks that a channel is able to erode T_f. This is done by analysing a simple Y-shaped bifurcation. The standard model run can be described as follows: the length of the upstream channel is 1000m, while the length of the two downstream bifurcates is 2000m. The slope is $2.0*10^{-4}$m/m in each channel. The upstream discharge is 200m^3/s, the discharge is equally distributed over the downstream bifurcates. The channels are allowed to adjust their width to the amount of discharge they receive. A constant C is used to indicate the bed roughness. The data-fitted sediment transport predictor is used as sediment transport predictor. As a perturbation, a relative upstream meander bend of $R = 15$ is used, or a slope advantage of 10 percent.
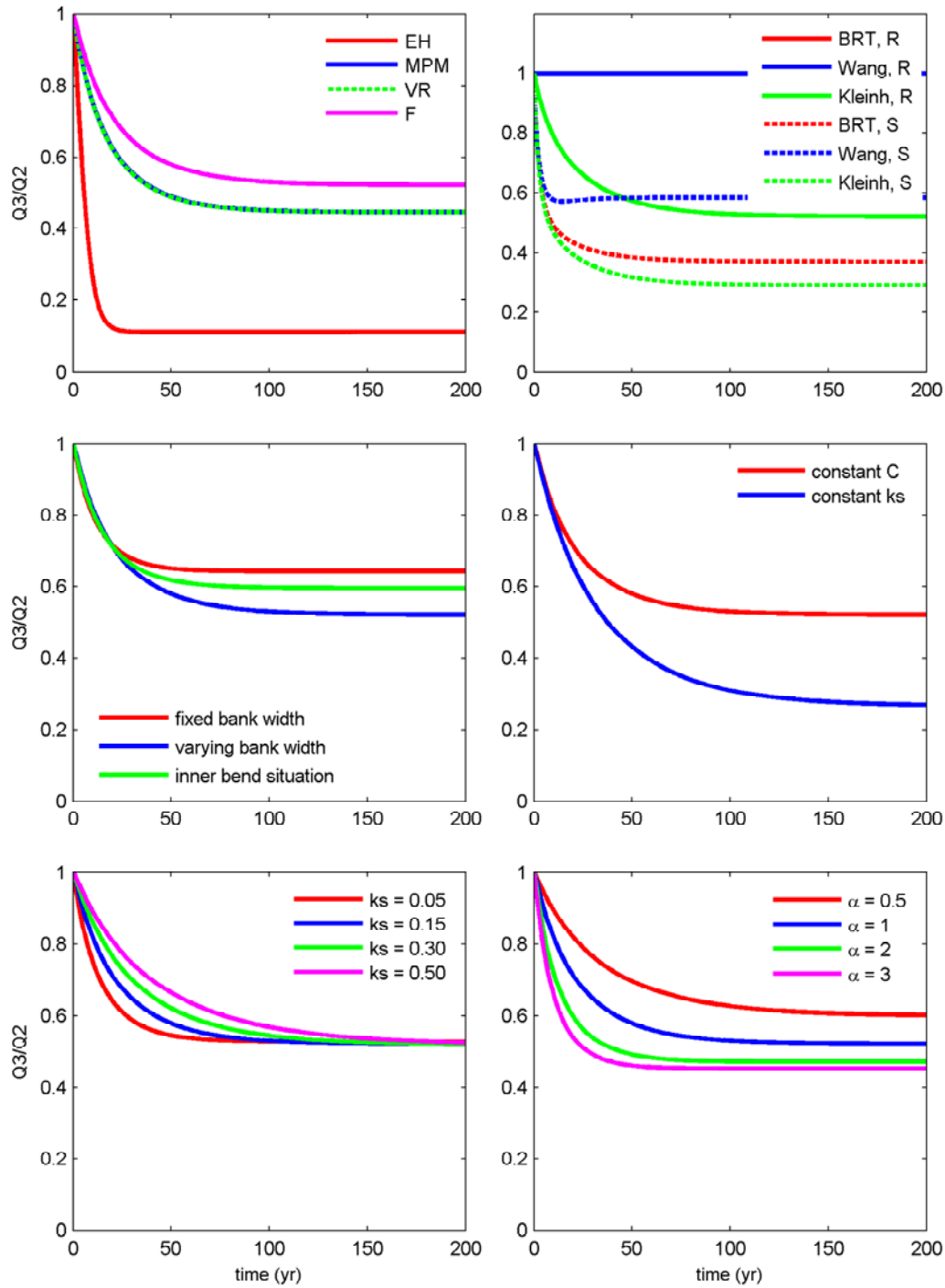
Fig. 4.2: Sensitivity analysis for sediment transport predictor, nodal point relation, fixed or varying channel width, constant Chézy roughness or constant Nikuradse roughness coefficient, total roughness coefficient and upstream morphological influence of a bifurcation. EH, MPM, VR and F stand for respectively the Engelund and Hansen (1967), Meyer-Peter and Mueller (1948), Van Rijn (1984a) and fitted sediment transport predictor. BRT, Wang and Kleinh respectively indicate the Bolla Pittaluga et al. (2003), Wang et al. (1995) and Kleinhans et al. (2008) nodal point relation, R indicates upstream bend perturbation, S indicates a slope advantage in one of the bifurcates. Varying channel width indicates that channels are able to grow and close according to the hydraulic geometry relations (equation 3.2, 3.3 and 3.4). Inner bend situations indicates that the outer bend channel grows according to hydraulic geometry, but the inner channel silts up vertically and is unable to narrow..

Fig. 4.3: Sensitivity analysis for relative bend radius, slope advantage in one of the bifurcates, different bifurcate length and different erosion fraction. R indicates a disturbance by an upstream bend, Sadv indicates a disturbance due to a slope advantage in one of the bifurcates, L indicates that the bifurcates are longer. Tf indicates the fraction of width that a channel is able to erode/deposit per timestep.
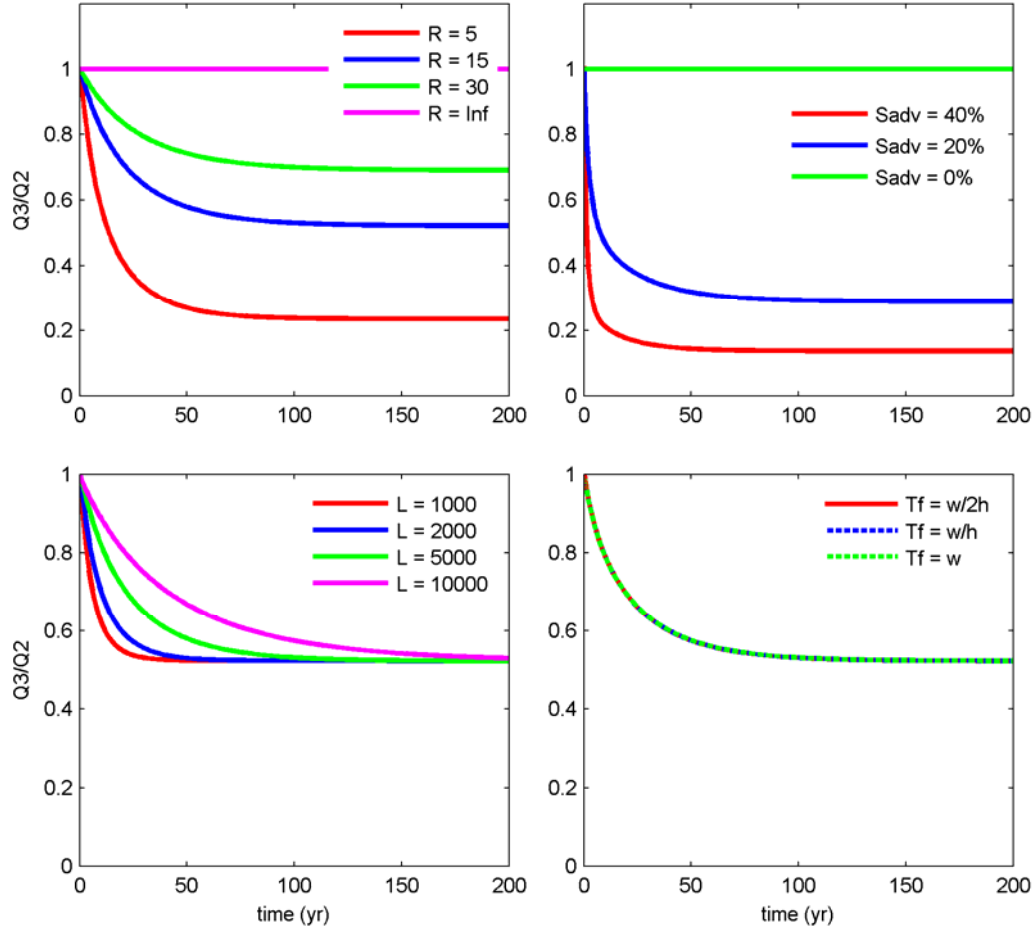
Sediment transport predictor

For the given conditions, the EH sediment transport predictor leads to a very asymmetric discharge division of $Q_3/Q_2 = 0.1$. The MPM and VR sediment transport predictors both lead to an equilibrium configuration of approximately $Q_3/Q_2 = 0.45$. An equilibrium is set once the division of sediment is in proportion with the division of flow at a bifurcation. The fitted sediment transport predictor leads to the most symmetric equilibrium configuration; $Q_3/Q_2 = 0.55$. The discharge division predicted by the EH predictor is in equilibrium within 30 years. The MPM, VR and fitted sediment transport predictors predict that an equilibrium is reached in about 150 years.

The EH predictor is based on total Shields stress, while the other predictors are based on the grain related Shields stress (section 3.4.4). In this case, the total Shields stress is larger than the grain related Shields stress. Therefore the EH predictor predicts a larger amount of sediment transport. Consequently, the minor bifurcate silts up faster, the major bifurcate erodes its bed faster and the

equilibrium situation is reached faster; additionally a more asymmetric equilibrium configuration is reached.

In contrast to the fitted sediment transport predictor, the MPM and VR sediment transport predictors take critical Shields stress into account. This leads to a deviation between the fitted and the MPM and VR predictor for Shield stress values close to critical Shields stress and values of relatively high Shields stress. For Shields stress close to critical Shields stress and at relatively high Shields stress, the fitted sediment transport predictor predicts a larger amount of sediment transport (figure 3.46). For most channels in the upper Columbia River, the amount of sediment transport predicted by the MPM and VR predictors is approximately equal to that predicted by the fitted predictor. Only for nearly closed bifurcates, the Shields stress is close to critical Shields stress, so that the fitted predictor predicts a larger amount of sediment transport than the MPM and the VR predictors. Application of the fitted predictor leads to a more symmetric equilibrium configuration, since the predicted amount of sediment transport is approximately equal for most of the first 150 years, the equilibrium configuration is reached in approximately the same time for the fitted and the MPM and VR sediment transport predictors.

Nodal point relation

At a bifurcation with equal conditions in both bifurcates, and an upstream bend causing a disturbance, the Wang et al. (1995) and Bolla Pittaluga et al. (2003) nodal point relations predict a symmetric discharge division since a perturbation by an upstream bend is not taken into account by both nodal point relations. The Kleinhans et al. (2008) nodal point relation does take the disturbance induced by an upstream bend into account. Consequently, an asymmetric discharge division is predicted by the Kleinhans et al. (2008) nodal point relation.

When no upstream bend is present all three nodal point relations predict an asymmetric discharge division at the bifurcation, when there is a 20 percent slope advantage in one of the bifurcates. The Kleinhans et al. (2008) nodal point relation predicts the most asymmetric discharge division, whilst the Wang et al. (1995) nodal point relation predicts the most symmetric discharge division. Since a k of 1 is used for the Wang et al. (1995) nodal point relation, the sediment division is equal to the discharge division at the bifurcation. The Bolla Pittaluga et al. (2003) and the Kleinhans et al. (2008) nodal point relations also take into account the transverse slope effect (section 2.4.3). The transverse slope effect initially enhances the growing bifurcate causing a more asymmetric equilibrium configuration to occur for the Bolla Pittaluga et al. (2003) and Kleinhans et al. (2008) nodal point relations. Although both the Bolla Pittaluga et al. (2003) and Kleinhans et al. (2008) nodal point relations take into account the transverse slope effect, application of the Kleinhans et al. (2008) nodal point relation leads to a more asymmetric discharge division than application of the Bolla Pittaluga et al. (2003) nodal point relation. This can be explained as follows: In both nodal point relations the transverse flux of sediment q_{sy} is

121

defined as equation 2.8. The direction of the sediment transport β_s is defined as equation 2.9 in Bolla Pittaluga et al. (2003) and as equation 2.18 in Kleinhans et al. (2008). In these equations, β_τ is defined as equation 2.10 in Bolla Pittaluga et al. (2003) and equation 2.19 in Kleinhans et al. (2008) since in the latter both the transverse slope and upstream bend radius effect is taken into account. For the situation without an upstream bend, equation 2.19 reduces to equation 2.10, so that β_τ is equal in both the Kleinhans et al. (2008) and the Bolla Pittaluga et al. (2003) nodal point relation. However, with β_τ equal, β_s still remains unequal. This causes the transverse flux of sediment q_{sy} to be larger for the Kleinhans et al. (2008) nodal point relation, causing the equilibrium configuration predicted by the Kleinhans et al. (2008) nodal point relation to be more asymmetric than the equilibrium configuration predicted by the Bolla Pittaluga et al. (2003) nodal point relation.

Fixed or non-fixed channel width

Allowing channels to adjust their width to an in-, or decrease of discharge leads to a more asymmetric discharge division, than keeping the width of the channels fixed. The ratio Q_3/Q_2 respectively becomes approximately 0.5 for varying channel width and 0.65 for fixed channel width. Due to a disturbance at a bifurcation, in this case a relative bend radius of 15, one of the bifurcates will start to silt up and will transport less discharge, whilst the other bifurcate erodes its bed and will transport more discharge. When the width of the minor bifurcate is fixed, the minor bifurcate rapidly becomes very shallow. When the width is allowed to deform, the minor bifurcate will also narrow, so that the depth stays larger. The transport capacity will thus stay larger. When the minor bifurcate for non-fixed width has become as shallow as the minor bifurcate with fixed banks, so that the bifurcation stabilizes, the minor bifurcate in the former case has a much smaller width, so that the flow area is smaller. Consequently, the equilibrium discharge division is more asymmetric in the former case.

Inner bend bifurcates in the upper Columbia River mainly silt up vertically, whilst outer bend bifurcates mainly silt up by narrowing and shallowing (section 3.4.5.2). The silting up of outer bend bifurcates is reproduced by allowing the channel width to deform in all channels. When growing bifurcates and closing outer bend bifurcates are allowed to adjust their channel width, but closing inner bend bifurcates are not allowed to narrow the following equilibrium configuration occurs: an equilibrium configuration occurs that is more symmetric than for the situation where all channels are allowed to adjust their width, and to an equilibrium configuration that is more asymmetric than for the situation where all channels have a fixed width occurs. This is caused by the fact that compared to the fixed width situation, the outer bend bifurcate is allowed to widen, so that this bifurcate is able to become larger, which causes the discharge division to become more asymmetric than the for the fixed width situation.

Roughness assumption

Bed roughness can be modelled based on two assumptions. The first assumption is a constant k_s. This allows C to increase in small channels, since these channels have a larger hydraulic radius than large channels, since the channel depth is larger relative to the channel width for small channels (section 3.4.2). This effect is justified by the fact that the influence of wall friction increases in small channels. The second assumption is to assume a constant C. This assumption can be justified by the fact that the dimensions of bedforms become larger for larger discharges, causing the total roughness to increase in large channels, so that the decrease in wall friction is balanced by the increase in bedforms dimension. Assuming k_s to be constant, leads to a more asymmetric discharge division. When one of the bifurcates starts silting up, and a constant k_s coefficient is assumed, the C in the closing bifurcate will increase, since the hydraulic radius increases. In the growing bifurcate, the exact opposite occurs; the hydraulic radius decreases, causing the C to decrease. Since the growing bifurcate experiences less friction than the closing bifurcate, flow through this bifurcate is more efficient. Causing the closing bifurcate to silt up even more. This leads to a positive feedback which causes the equilibrium configuration to become more asymmetric than for the situation with a constant C in both branches, where no positive feedback occurs.

Nikuradse roughness coefficient

A difference in total bed roughness does not lead to a difference in equilibrium configuration. For higher values of total bed roughness, the equilibrium configuration is reached later. This is caused by the fact that the bed roughness affects the grain-related Shields stress (equation 2.11). The larger the bed roughness, the smaller the amount of sediment transport, and consequently the longer the time before an equilibrium is reached. The equilibrium configuration is not affected since the roughness is equal over both bifurcates.

Upstream morphological influence of a bifurcation

An increase in upstream morphological influence of a bifurcation leads a more asymmetric discharge division at a bifurcation. Additionally, the equilibrium configuration is reached faster. This behaviour can be explained as follows: the larger the upstream morphological influence of a bifurcation, the larger the distance upstream over which a transverse slope is present, the larger the distance over which the division of flow and sediment occurs. Consequently, a larger asymmetry between the division of flow and sediment is able to occur in a certain amount of time. The equilibrium configuration will thus set earlier, and the equilibrium discharge division becomes more asymmetric.

This concept is incorporated in equation 2.15: for the same q_{sy}, the larger a_u, the larger the sediment flux in front of the bifurcation and thus the faster the equilibrium state is reached.

Relative upstream bend radius

An increase in upstream bend radius leads to a more asymmetric discharge division over the two bifurcates. At a bend with an infinitively long radius, in other words no upstream bend, the discharge division at the bifurcation is balanced. This is caused by the fact that in such a situation all conditions are equal; no perturbation is present.

The smaller relative bend radius becomes, the stronger the spiral flow becomes. So more sediment is forced into the minor bifurcate relative to flow; the minor bifurcate will silt up more, which causes the discharge division at the bifurcation to become more asymmetric.

Slope

The larger the slope advantage in one of the bifurcates, the more asymmetric the discharge division at the bifurcation becomes. This is caused by the fact that a larger slope in one of the bifurcates causes a larger total shear stress (equation 2.12), and a larger grain-related shear stress since the velocity is larger in a steeper channel (equation 2.11). The transport capacity is thus larger in the steeper bifurcate, causing this bifurcate to erode its bed. The larger the slope difference between the bifurcates, the larger the difference in transport capacity and thus the more asymmetric the discharge division at the bifurcation becomes.

Bifurcate length

Varying the length of both bifurcates does not lead to a different equilibrium configuration, only the time until an equilibrium configuration is reached increases with increasing bifurcate length. For a situation with bifurcates of 1000m, the equilibrium configuration is reached within 50 years whereas for a situation with bifurcates of 10000m, the equilibrium configuration is reached within 250 years. This behaviour can be explained as follows; in a short bifurcate that is silting up, only a short reach has to be filled with sediment before an equilibrium configuration is reached. In a long bifurcate that is silting up, a long reach has to be filled with sediment before an equilibrium configuration is reached. Logically, in the former case the equilibrium configuration is reached faster.

Fraction of channel width that is available for erosion

The fraction of width that a channel is able to erode does not have any effect on the bifurcation equilibrium configuration. This is caused by the fact that other parameters are limiting the amount of erosion per time step, so that the amount of erosion per time step is always smaller than the amount of potential bank erosion.

4.4.3. Bifurcation equilibrium configurations

In this section, bifurcation equilibrium configurations are calculated for a range of Shields stress in the upstream channel, as done by Bertoldi et al. (2005) for experimental braided rivers. This is done in order to explain the difference in the trend of discharge ratio plotted against Shields stress for the experimental braided rivers of Bertoldi et al. (2005), and the bifurcations in the Cumberland Marshes (Edmonds and Slingerland, 2008) and the upper Columbia River (section 3.4.6).

The Shields stress can be varied by varying discharge, slope and median grain size of the bed. In order to obtain the required range of Shields stress, the discharge is varied between 20 and 1200m^3/s. Slope is varied between $1.0*10^{-5}$ and $8.0*10^{-4}$m/m. The median grain size of the bed is varied between 0.7mm and 10mm.

The analysis is performed on a simple Y-shaped bifurcation. The standard situation can be described as follows: the length of the upstream channel is 1000m, while the length of the two downstream bifurcates is 5000m. The slope in all channels is $2.0*10^{-4}$m/m.

The width in the upstream channel is fixed at 80m, the downstream channels are allowed to adjust their width. An increase in discharge thus leads to an increase in hydraulic radius and thus an increase in Shields stress in the upstream channel. A constant C (figure 4.4) or a constant k_s (figure 4.5) is chosen to represent bed roughness.

A disturbance can be induced by an upstream bend radius or a slope difference between the bifurcates. For the upstream bend radius induced equilibrium configurations a R of 10 or 20 is used, for the slope induced equilibrium configurations a slope advantage in one of the bifurcates of 10 or 20 percent is used.

To establish the effect of critical Shields stress on bifurcation equilibrium configurations, equilibrium configurations are computed for the MPM sediment transport predictor, which takes into account critical Shields stress, and the fitted sediment transport predictor, which does not take into account critical Shields stress.

In figure 4.4 and 4.5, the equilibrium configurations for the modelled scenarios are shown. The dots indicate the individual model runs. The equilibrium configurations obtained with the fitted sediment

transport predictor are connected by a dashed line. The equilibrium configurations obtained with the MPM predictor are connected by a solid line.

In figure 4.4, where a constant C is chosen to represent bed roughness, when a disturbance is generated by an upstream bend (left part of figure 4.4, Rinduced), the equilibrium configurations obtained for a relative bend radius of 10 (blue, R10) and 20 (black, R20) are shown. When a disturbance is generated by a slope advantage in one of the bifurcates (right part of figure 4.4, Sinduced), the equilibrium configurations obtained for a slope advantage of 10 percent (black, Sadv 10%) and 20 percent (blue, Sadv 20%) are shown. In the two upper graphs the Shields stress is varied by varying discharge (Qvar), in the two middle graphs the Shields stress is varied by varying channel slope (Svar) and in the two lower graphs the Shields stress is varied by varying median grain size of the bed (Dvar). In the upper left graph, the equilibrium configuration obtained for a smaller width, 50m (w50), in the upstream channel is shown in green. In figure 4.5 the results obtained for a constant k_s are shown. The same scenarios as for a constant C are calculated, however only for a relative bend radius of 10 and a slope advantage of 20 percent.

In the case of a constant C, the general equilibrium configuration for the fitted sediment transport predictor is a decreasing area ratio for an increasing Shields stress. For low Shields stress the rate of decrease in area ratio is large. For higher Shields stress the rate of decrease in area ratio becomes very small. Eventually equilibrium is reached. This equilibrium occurs for Shields stress above approximately 1.5. The value of this final equilibrium area ratio is determined by the strength of the disturbance induced at the bifurcation. For R is 20, the equilibrium area ratio is approximately 0.6 whilst for R is 10 the equilibrium area ratio is approximately 0.4. For a 10 percent slope advantage in one of the bifurcates, the equilibrium area ratio is approximately 0.65 when the median grain size is varied to vary Shields stress, and approximately 0.5 when the bed slope is varied to vary Shields stress.

Using the MPM sediment transport predictor leads to a different equilibrium configuration than using the fitted sediment transport predictor. For Shields stresses above 0.8-1.0 the equilibrium configurations obtained by both sediment transport predictors are equal. Below this Shields stress, the MPM predictor predicts a more asymmetric equilibrium configuration than does the fitted predictor. However, there is still a decrease in area ratio for an increase in Shields stress. For even lower Shields stresses, there is a sharp decrease in area ratio for a decrease in Shields stress. Consequently there is an optimum Shields stress for which the smallest area ratio occurs. The Shields stress for which this optimum occurs varies between the discharge, slope and median grain size induced variations in Shields stress and for the R and slope induced equilibrium configurations. When the discharge is varied, and the disturbance is R induced, the optimum occurs for a Shields stress of approximately 0.5. When the slope is varied, the optimum occurs for a Shields stress of approximately 0.2, when the

disturbance is R and slope induced. When the median grain size is varied, the optimum occurs for a Shields stress of approximately 0.6 when the disturbance is R induced.

Fig. 4.4: Plot of equilibrium configurations of Shields stress versus Area ratio for a constant Chézy bed roughness. The Shields stress is varied by varying either discharge, slope or median grain size of the bed. A disturbance is either induced by an upstream bend of a slope advantage in one the bifurcates. See text for a more detailed explanation of the figures.
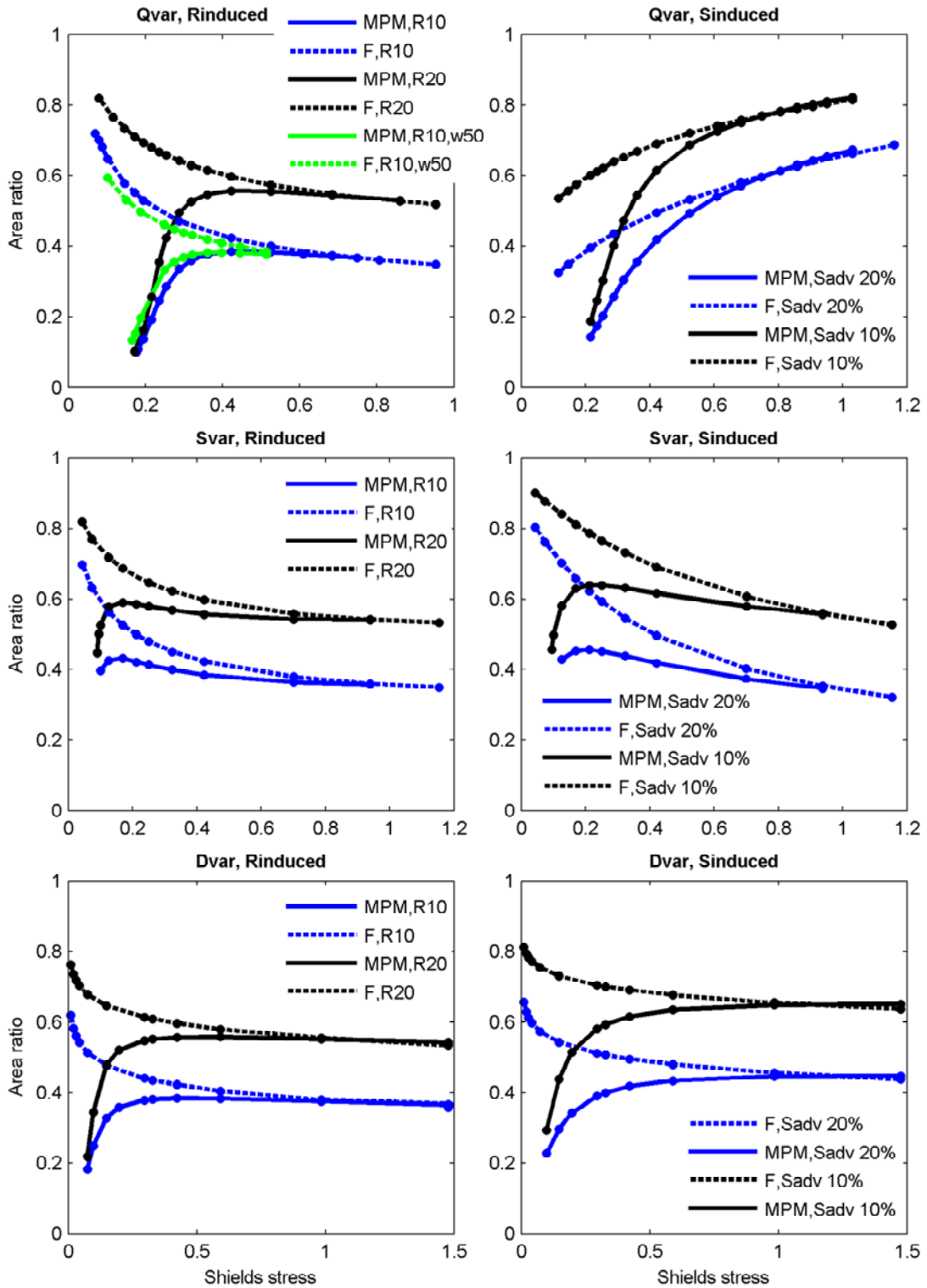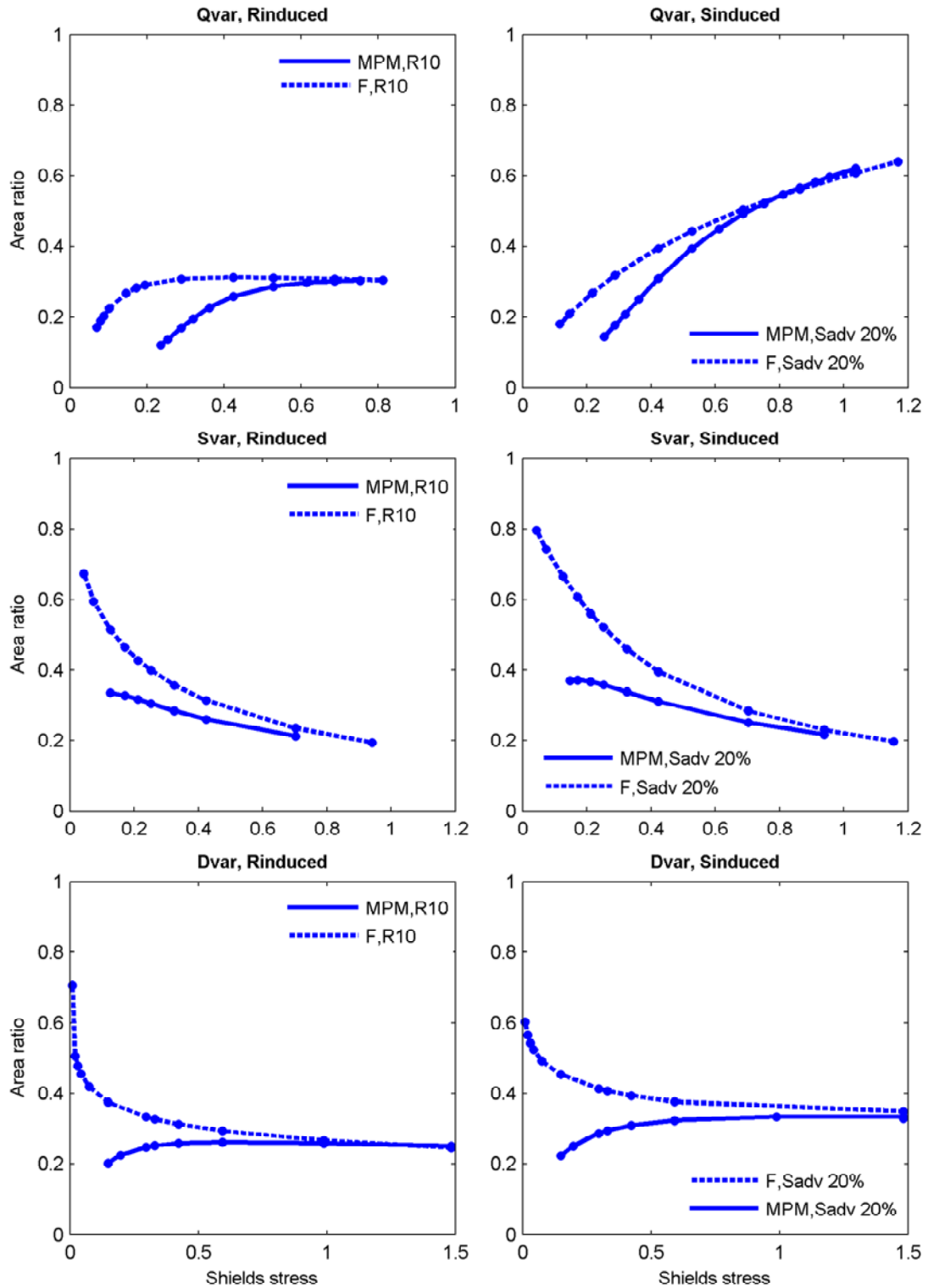
Fig. 4.5: Plot of equilibrium configurations of Shields stress versus Area ratio for a constant Nikuradse bed roughness. The Shields stress is varied by varying either discharge, slope or median grain size of the bed. A disturbance is either induced by an upstream bend of a slope advantage in one the bifurcates. See text for a more detailed explanation of the figures.

The optimum occurs at a Shields stress of 1.5 when the disturbance is slope induced. When the width of the upstream channel is reduced, the optimum shifts to a lower Shields stress.

The above described configuration is true for all situations, except one. When Shields stress is varied by varying discharge, and the disturbance at the bifurcation is slope induced a different equilibrium configuration occurs. In this case the area ratio increases for increasing Shields stress, both for the fitted and MPM sediment transport predictors. For Shields stresses of 0.6 and lower, the area ratio predicted by the MPM sediment transport predictor is smaller than the area ratio predicted by the fitted predictor. The rate of decrease in area ratio becomes larger at low Shields stress, both for the fitted and MPM sediment transport predictors.

In the case of a constant k_s assumption in general the overall equilibrium configuration is equal to that in the case of a constant C (figure 4.5). However, the equilibrium configurations for a constant k_s become more asymmetric. For a constant C for $R = 10$ the equilibrium area ratio is approximately 0.4, for a constant k_s the equilibrium area ratio is approximately 0.2. For a 20 percent slope advantage in one of the bifurcates, the equilibrium area ratio is approximately 0.4 for a constant C and approximately 0.2 for a constant k_s when the median grain size and the bed slope is varied to vary Shields stress. A more asymmetric discharge for a constant k_s than a constant C is exactly as expected from the results shown in figure 4.2.

When the discharge is varied to vary Shields stress, and a disturbance is induced by an upstream bend the general trend differs between a constant C and a constant k_s. For a constant C, the the equilibrium configuration becomes more asymmetric for increasing Shields stress in the case of the fitted sediment transport predictor. In the case of the MPM predictor an optimum Shields stress is present. For a constant k_s, both for the fitted and the MPM sediment transport predictor an optimum Shields stress is present. The equilibrium configuration is comparable to that where the discharge is varied to vary Shields stress and the disturbance is slope induced. A major difference however is that when the disturbance is induced by an upstream bend and a constant k_s is assumed an optimum is present at a relatively low Shields stress, whereas no optimum is present for relatively low Shields stress when the disturbance is slope induced for both a constant C and k_s.

The difference in general equilibrium configuration for the fitted sediment transport predictor and the MPM sediment transport predictor is explained as follows: just in front of the bifurcation point, the sediment is divided into the two bifurcates. Whether a bifurcate silts up or erodes depends on the transport capacity. Is the transport capacity larger then the amount of sediment forced into this bifurcate, erosion occurs. When the transport capacity is smaller than the amount of sediment forced into this bifurcate, deposition occurs.

The largest difference in the transport capacity predicted by the fitted and the MPM sediment transport predictors is close to critical Shields stress. Since the MPM predictor takes critical Shields stress into

account the sediment transport capacity close to critical Shields stress is very small. The fitted predictor predicts a larger transport capacity close to incipient motion, since critical Shields stress is not taken into account.

Once a bifurcate is silting up, its width and depth decreases. Consequently, the transport capacity in this bifurcate decreases. The fitted transport predictor predicts more sediment transport in a closing bifurcate, where the Shields stress is close to critical Shields stress, than the MPM transport predictor. The gradient between the sediment transport in the main channel just upstream of the bifurcation and at the entrance of the closing bifurcate is thus larger for the MPM predictor than for the fitted predictor. Consequently the discharge division becomes more asymmetric for the MPM predictor.

This difference only holds when the Shields stress in the upstream channel is relatively low. When the Shields stress in the upstream channel is relatively high, it follows that the Shields stress is also relatively high in both bifurcates. When the Shields stress in the closing bifurcate is relatively high, the sediment transport predicted by the fitted and the MPM predictor is approximately equal, so that the transport capacity predicted by both predictors is approximately equal. For high Shields stress the equilibrium configurations predicted by both predictors are thus approximately equal, as can be observed in figure 4.4 and 4.5.

For a relatively low Shields stress, the difference in transport gradient between the fitted and the MPM predictor thus explains the difference in equilibrium configuration between these two predictors. The difference can be illustrated by the power n on Shields stress in both predictors (figure 4.6). Since the fitted predictor does not take into account critical Shields stress, the power n is always 1.5. For Shields stress above 0.6, the power n in the MPM predictor is approximately equal to the power n in the fitted predictor; 1.5. For Shields stress below 0.6, the sediment transport predicted by the MPM predictor is influenced by the critical Shields stress. In figure 4.6, this effect is illustrated: the sediment transport predicted by the MPM predictor is an asymptotic function wherein the value of critical Shields stress is the asymptote. The power n shows a large increase close to critical Shields stress. Very close to critical Shields stress the power is above 100.
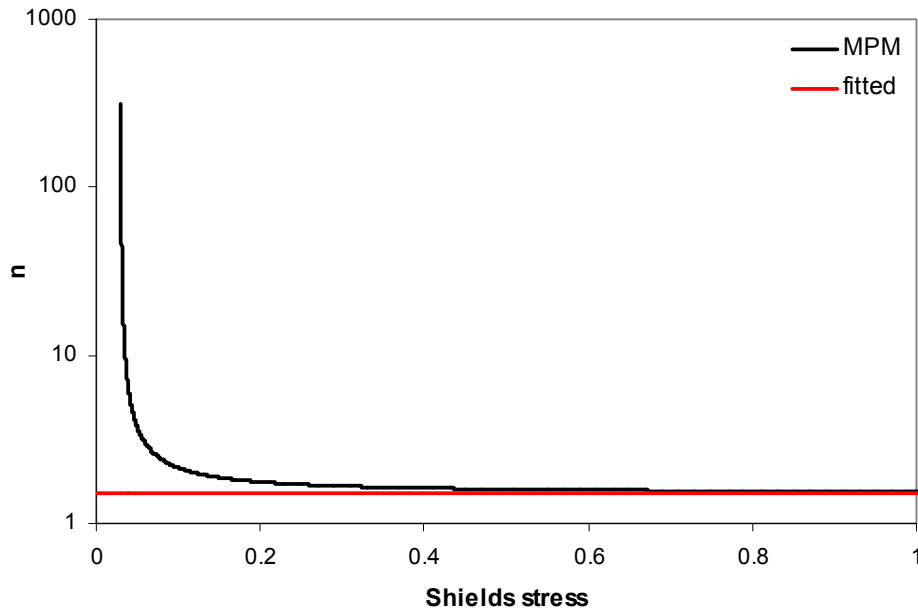
Fig. 4.6: Shields stress plotted versus power n for the MPM and fitted transport predictors.

The discharge division at low Shields stress for the MPM predictor becomes more asymmetric since the gradient in sediment transport between the entrance of the closing bifurcate just upstream of the bifurcation becomes larger for low Shields stress due to the above described asymptotic behaviour of the MPM predictor. Since this effect is significant only for low Shields stress, an optimum Shields stress is present, where the equilibrium configuration is most symmetric.

As noted above, both for a constant C and k_s when Shields stress is varied by varying discharge and the disturbance at the bifurcation is slope induced a different equilibrium configuration occurs. In this case the MPM and the fitted predictor become more symmetric for higher Shields stress. For low Shields stress the MPM predictor predicts a more asymmetric area ratio than the fitted predictor due to the asymptotic behaviour of the former predictor. The same trend is distinguished when the Shields stress is varied by varying discharge and the disturbance is induced by an upstream bend for a constant k_s, with the difference that an optimum is present for relatively low Shields stress.

In contrast to the other equilibrium configurations of the fitted predictor, in this case the area ratio does not become more asymmetric for increasing Shields stress, but becomes more symmetric for increasing discharge. Additionally, in the equilibrium configuration predicted by the MPM predictor the optimum Shields stress is absent when the disturbance is slope induced.

This difference can be explained as follows, for the situation where the disturbance is slope induced: When discharge is varied to vary Shields stress, the water depth increases for increasing Shields stress. Consequently, the backwater adaptation length ($\approx h/3S$) becomes smaller when the Shields stress becomes smaller. This leads to a relatively steep gradient in water level at the entrance of the bifurcates for low Shields stress.

Since the slope in the growing bifurcate is larger, the backwater adaptation length in this bifurcate is larger than the backwater adaptation length in the closing bifurcate. The effect of the steep gradient at the entrance of the bifurcates induced by a short backwater adaptation length is thus larger in the closing bifurcate. This causes more sediment to enter the closing bifurcate causing the bifurcation to become more asymmetric.

For comparison, when the slope is varied to vary Shields stress the backwater adaptation length becomes larger for smaller Shields stress, since the slope is smaller for smaller Shields stress. So there is little difference in water level gradient at the entrance of the two bifurcates. So that the above described process is not valid and the equilibrium configurations are conform the general equilibrium configurations.

4.4.4. Simple networks

In order to gain insight in the dynamics of river networks, in particular the role of bifurcations, confluences and number of channels, two simple networks are analysed. The first network is designed to evaluate the role of bifurcations in a river network. The network starts as a single channel ending at a bifurcation, one of the bifurcates flows straight to the downsteam boundary, whilst the other splits at a second bifurcation after which the two bifurcates originating from the second bifurcation end in the sea. The second network is designed to test the role of confluences in a river network. The network is comparable to the first network, with the exception that a bifurcate originating from the first bifurcation and a bifurcate originating from the second bifurcation join at a confluence.

The boundary conditions are equal in all channels. The slope in the channels is $2.0*10^{-4}$m/m, the length of the channels is 2000m. The initial discharge of 200 m^3/s in the upstream channel is divided equally over the bifurcates. The network evolution is computed for the EH, MPM and the fitted sediment transport predictor, in order to investigate the influence of sediment transport predictors on the evolution of channel networks. This is done for both a situation where all bifurcations have no upstream bend and a situation when the most upstream bifurcation has a R of 30. When an upstream bend is present, this bend in all cases leads to enlargement of the outer bend bifurcate. This is done for bed roughness defined as a constant C and for bed roughness defined as a constant k_s.

4.4.4.1. River network with two bifurcations

The MPM and the fitted sediment transport predictors lead to a similar network evolution. When all conditions are equal and a constant C is assumed (figure 4.7), the bifurcate originating from the most upstream bifurcation that is characterized by a downstream bifurcation (bifurcate 3) is slightly growing, while the other bifurcate (bifurcate 2) becomes sligthly smaller. This is caused by the fact that when a constant C is assumed that is equal for all the channels, it is more efficient to transport flow and sediment through multiple small channels than through less larger channels.

When a constant k_s is assumed (figure 4.9), the bifurcate originating from the most upstream bifurcation that is characterized by a downstream bifurcation becomes smaller (bifurcate 3), whilst the other bifurcate is growing (bifurcate 2). When a constant k_s is assumed, C is allowed to vary with the hydraulic radius of channels (equation 2.14). From the hydraulic geometry relations of the upper Columbia River (section 3.4.2), it follows that the hydraulic radius of small channels is larger than the hydraulic radius for large channels. Consequently, the Chézy roughness in small channels is larger than the Chézy roughness in large channels. This causes flow and sediment transport through multiple small channels to be less efficient than through less larger channels.

The effect of a constant k_s appears to be larger than the effect of a constant C. Assuming a constant C and applying the MPM predictor leads to a Q_{down}/Q_{up} of 0.52 in bifurcate 3 and a Q_{down}/Q_{up} of 0.48 in bifurcate 2. The fitted predictor leads to a Q_{down}/Q_{up} of 0.56 in bifurcate 3 and a Q_{down}/Q_{up} of 0.44 in bifurcate 2.

Assuming a constant k_s and applying the MPM predictor leads to a Q_{down}/Q_{up} of 0.18 in bifurcate 3 and a Q_{down}/Q_{up} of 0.82 in bifurcate 2. The fitted predictor leads to a Q_{down}/Q_{up} of 0.62 in bifurcate 3 and a Q_{down}/Q_{up} of 0.38 in bifurcate 2.

The above described configuration does not hold for the EH predictor. When this predictor is used, both for a constant C and a constant k_s the bifurcate originating from the most upstream bifurcation that is characterized by a downstream bifurcation (bifurcate 3) becomes smaller. Additionally, the EH predictor predicts a more asymmetric configuration. For both roughness assumptions the following discharge division holds; Q_{down}/Q_{up} in bifurcate 2 is 0.87, in bifurcate 3 the ratio Q_{down}/Q_{up} is 0.13.

An upstream bend of $R = 30$ at the upstream bifurcation favouring bifurcate 3 has a larger effect than has the efficiency effect for the MPM and fitted predictor. For the situation with a constant k_s and applying the MPM predictor Q_{down}/Q_{up} in bifurcate 3 becomes 0.77 and Q_{down}/Q_{up} in bifurcate 2 becomes 0.33. The fitted predictor leads to a Q_{down}/Q_{up} of 0.65 in bifurcate 3 and a Q_{down}/Q_{up} of 0.35 in bifurcate 2 (figure 4.10).

For a constant C the MPM predictor leads to a Q_{down}/Q_{up} in bifurcate 3 of 0.61 and a Q_{down}/Q_{up} in bifurcate 2 of 0.39. The fitted predictor leads to a Q_{down}/Q_{up} of 0.58 in bifurcate 3 and a Q_{down}/Q_{up} of 0.42 in bifurcate 2 (figure 4.8). For both situations, the efficiency effect is balanced by a relative bend radius in the range 40-50.

When the EH predictor is applied, the efficiency effect is larger than the the effect of a R of 30. The amount of asymmetry at the bifurcation is equal with or without an upstream bend. Only the time until an equilibrium discharge division is reached increases.

Fig. 4.7: Evolution of a river network with 2 bifurcations, for the Engelund and Hansen (EH), Meyer-Peter and Mueller (MPM) and fitted sediment transport predictor (F). The bed roughness is defined by a constant Chézy roughness coefficient (C), no upstream bend (R) is present.

Fig. 4.8: Evolution of a river network with 2 bifurcations, with a relative bend radius (R) of 30 at the first bifurcation that favors the bifurate that is closing for a situation without a relative bend radius, for the Engelund and Hansen (EH), Meyer-Peter and Mueller (MPM) and fitted sediment transport predictor (F). The bed roughness is defined by a constant Chézy roughness coefficient (C).
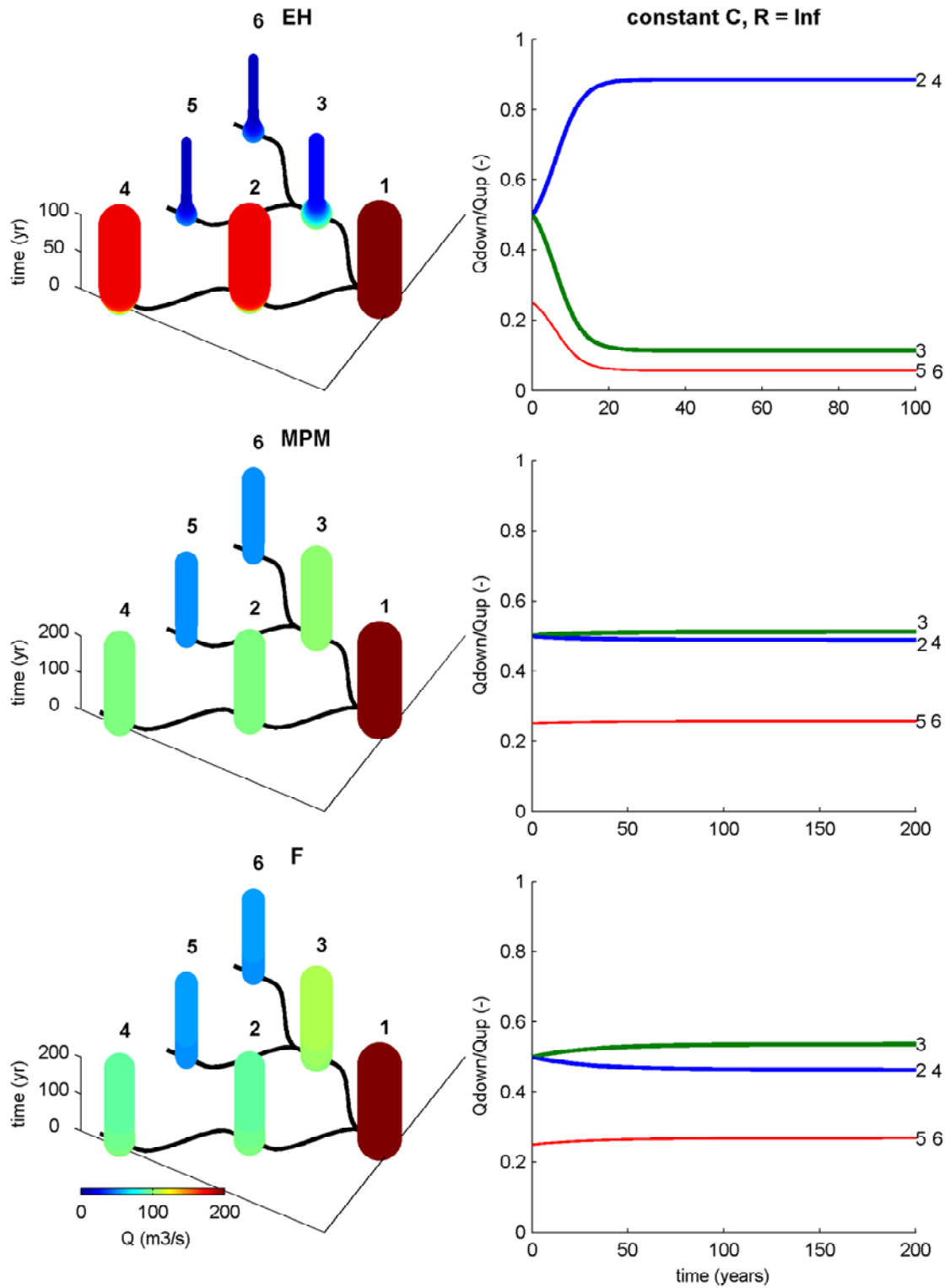
137

Fig. 4.9: Evolution of a river network with 2 bifurcations, for the Engelund and Hansen (EH), Meyer-Peter and Mueller (MPM) and fitted sediment transport predictor (F). The bed roughness is defined by a constant Nikuradse roughness coefficient (k_s), no upstream bend (R) is present.

Fig. 4.10: Evolution of a river network with 2 bifurcations, with a relative bend radius (R) of 30 at the first bifurcation that favors the bifurate that is closing for a situation without a relative bend radius, for the Engelund and Hansen (EH), Meyer-Peter and Mueller (MPM) and fitted sediment transport predictor (F). The bed roughness is defined by a constant Nikuradse roughness coefficient (k_s).

In a river network with 2 bifurcations and 1 confluence the MPM and the fitted sediment transport predictors lead to similar results. When a constant C is assumed, the channels that are connected to a downstream confluence (2,4,5) become smaller. The channels that are not connected to the confluence (3,6,8) become larger. When a constant k_s is assumed the opposite holds. The channels that are connected to the downstream confluence (2,4 and 5) become larger.

As is the case in a network with 2 bifurcations, the effect of a constant k_s appears to be larger than the effect of a constant Chézy. Assuming a constant Chézy and applying the MPM predictor leads to a $Q_{\mathrm{down}}/Q_{\mathrm{up}}$ of 0.54 in bifurcate 3 and a $Q_{\mathrm{down}}/Q_{\mathrm{up}}$ of 0.46 in bifurcate 2. The fitted predictor leads to a $Q_{\mathrm{down}}/Q_{\mathrm{up}}$ of 0.58 in bifurcate 3 and a $Q_{\mathrm{down}}/Q_{\mathrm{up}}$ of 0.42 in bifurcate 2 (figure 4.11).

Assuming a constant k_s and applying the MPM predictor leads to a $Q_{\mathrm{down}}/Q_{\mathrm{up}}$ of 0.22 in bifurcate 3 and a $Q_{\mathrm{down}}/Q_{\mathrm{up}}$ of 0.78 in bifurcate 2. The fitted predictor leads to a $Q_{\mathrm{down}}/Q_{\mathrm{up}}$ of 0.64 in bifurcate 3 and a $Q_{\mathrm{down}}/Q_{\mathrm{up}}$ of 0.36 in bifurcate 2 (figure 4.13).

An upstream bend of R is 30 at the upstream bifurcation favoring bifurcate 3 has a larger effect than has the efficiency effect. For the situation with a constant k_s and applying the MPM predictor $Q_{\mathrm{down}}/Q_{\mathrm{up}}$ in bifurcate 3 becomes 0.72 and Qdown/Qup in bifurcate 2 becomes 0.28. The fitted predictor leads to a $Q_{\mathrm{down}}/Q_{\mathrm{up}}$ of 0.64 in bifurcate 3 and a $Q_{\mathrm{down}}/Q_{\mathrm{up}}$ of 0.36 in bifurcate 2 (figure 4.14). For the situation with a constant Chézy roughness and applying the MPM predictor $Q_{\mathrm{down}}/Q_{\mathrm{up}}$ in bifurcate 3 becomes 0.64 and $Q_{\mathrm{down}}/Q_{\mathrm{up}}$ in bifurcate 2 becomes 0.36. The fitted predictor leads to a $Q_{\mathrm{down}}/Q_{\mathrm{up}}$ of 0.62 in bifurcate 3 and a $Q_{\mathrm{down}}/Q_{\mathrm{up}}$ of 0.38 in bifurcate 2 (figure 4.12).

The above described observations can be explained by the same mechanism as valid for the river network with 2 bifurcations. A bifurcation increases the amount of channels, making flow and sediment transport more efficient through the bifurcated path when assuming a constant C, and making flow and sediment transport less efficient when a constant k_s is assumed. Similarly, a confluence decreases the amount of channels, making flow and sediment transport less efficient through the confluenced path when assuming a constant C, and making flow and sediment transport more efficient when a constant k_s is assumed.

As is the case for the network with 2 bifurcations, application of the EH predictor leads to similar behaviour for the situation with a constant C and the situation with a constant k_s. Assuming a constant Chézy or Nikuradse roughness in both cases leads to approximately the same configuration; a $Q_{\mathrm{down}}/Q_{\mathrm{up}}$ of 0.85 in bifurcate 2 and a $Q_{\mathrm{down}}/Q_{\mathrm{up}}$ of 0.186 in bifurcate 3. Additionally, a relative upstream bend radius of 30 is not able to counteract the efficiency effect.
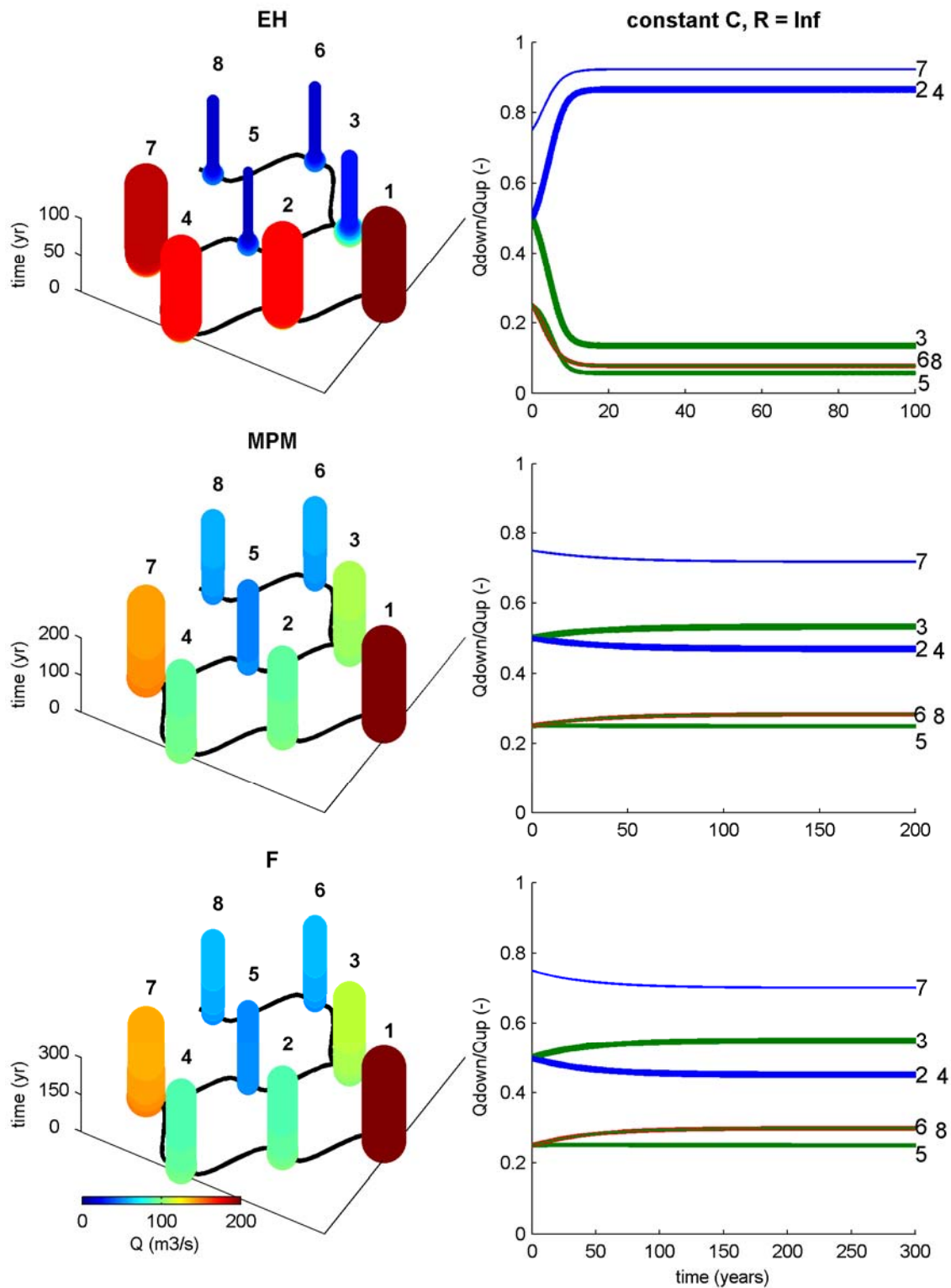
Fig. 4.11: Evolution of a river network with 2 bifurcations and 1 confluence, for the Engelund and Hansen (EH), Meyer-Peter and Mueller (MPM) and fitted sediment transport predictor (F). The bed roughness is defined by a constant Chézy roughness coefficient (C), no upstream bend (R) is present.
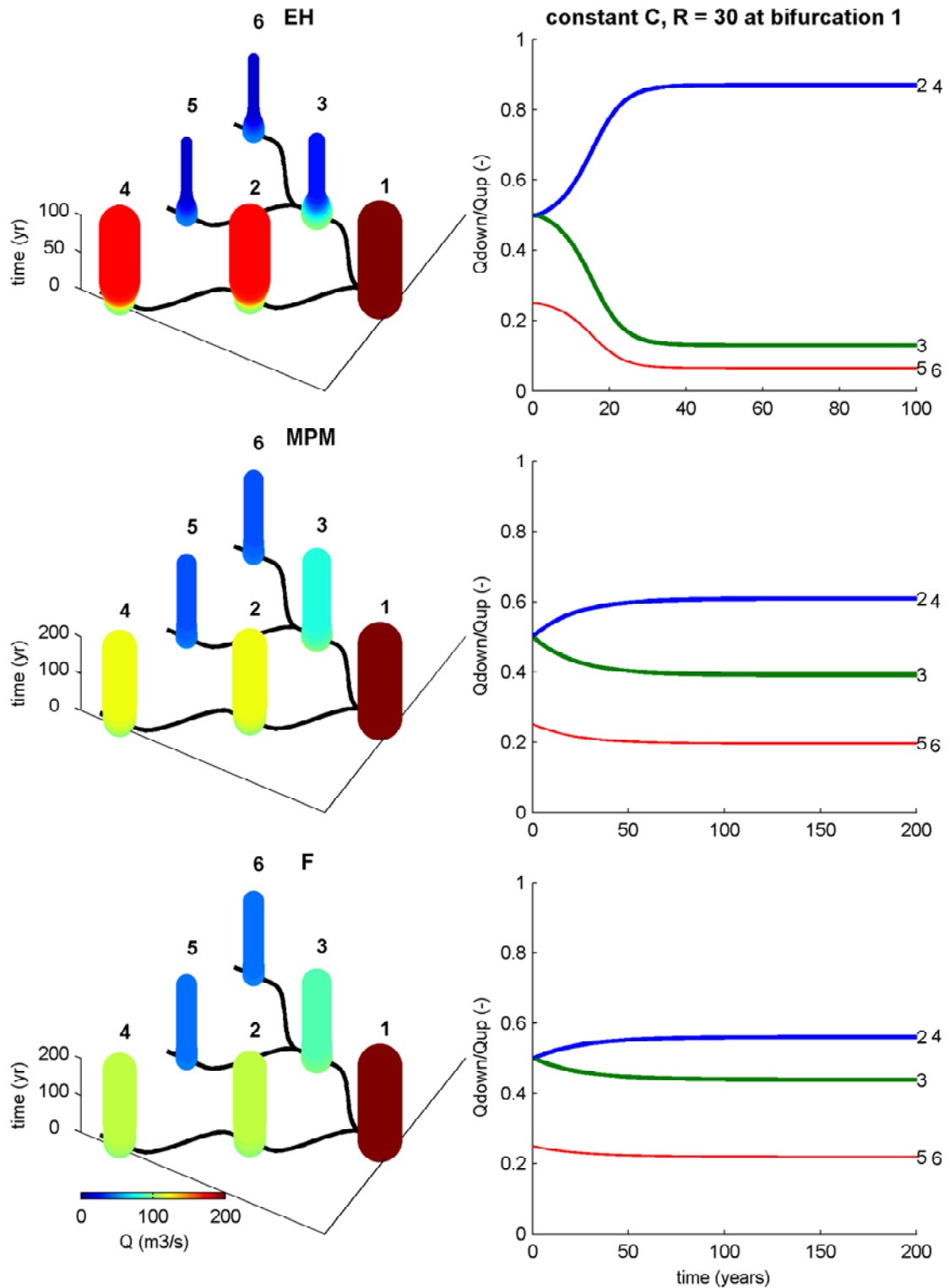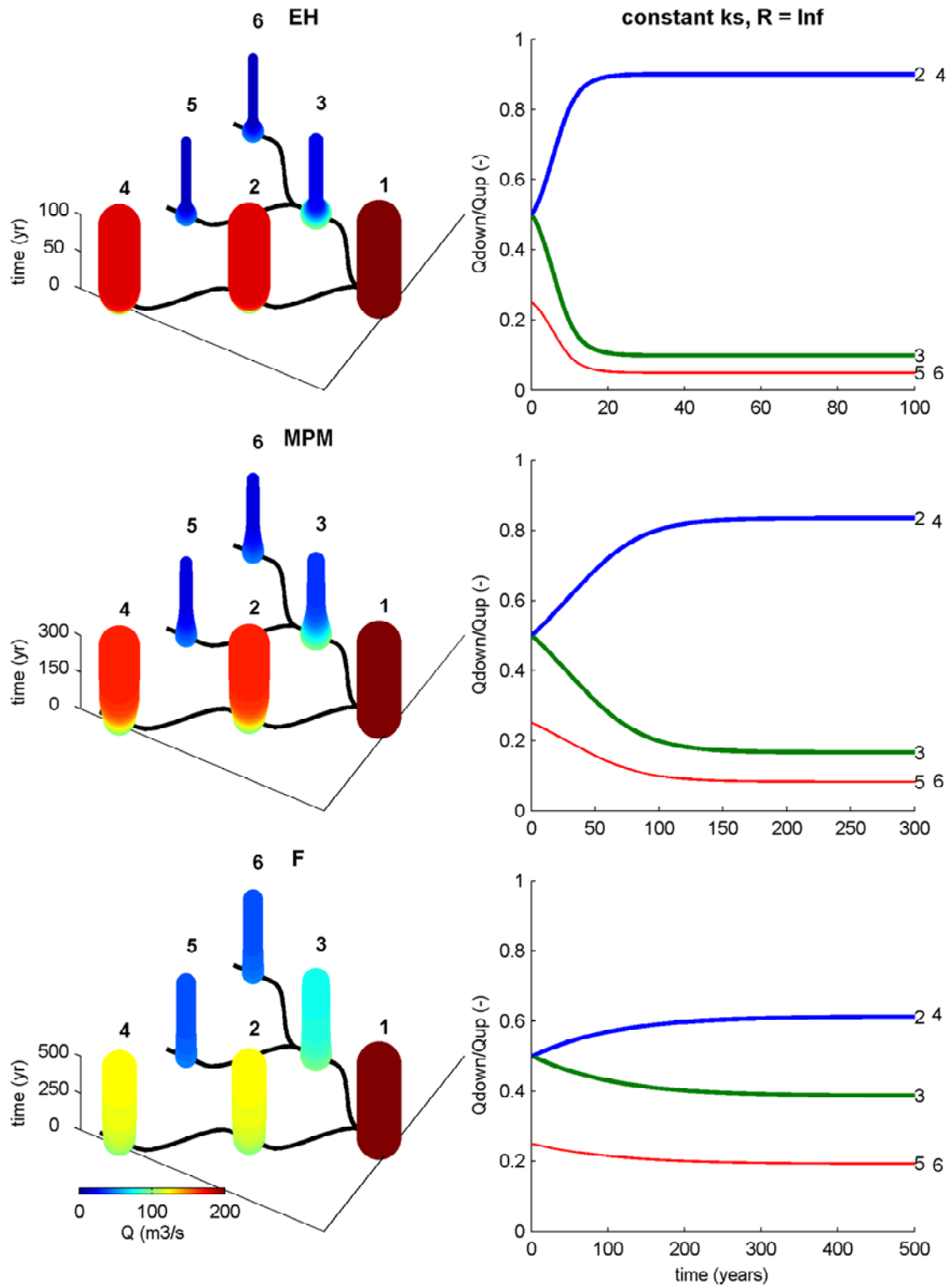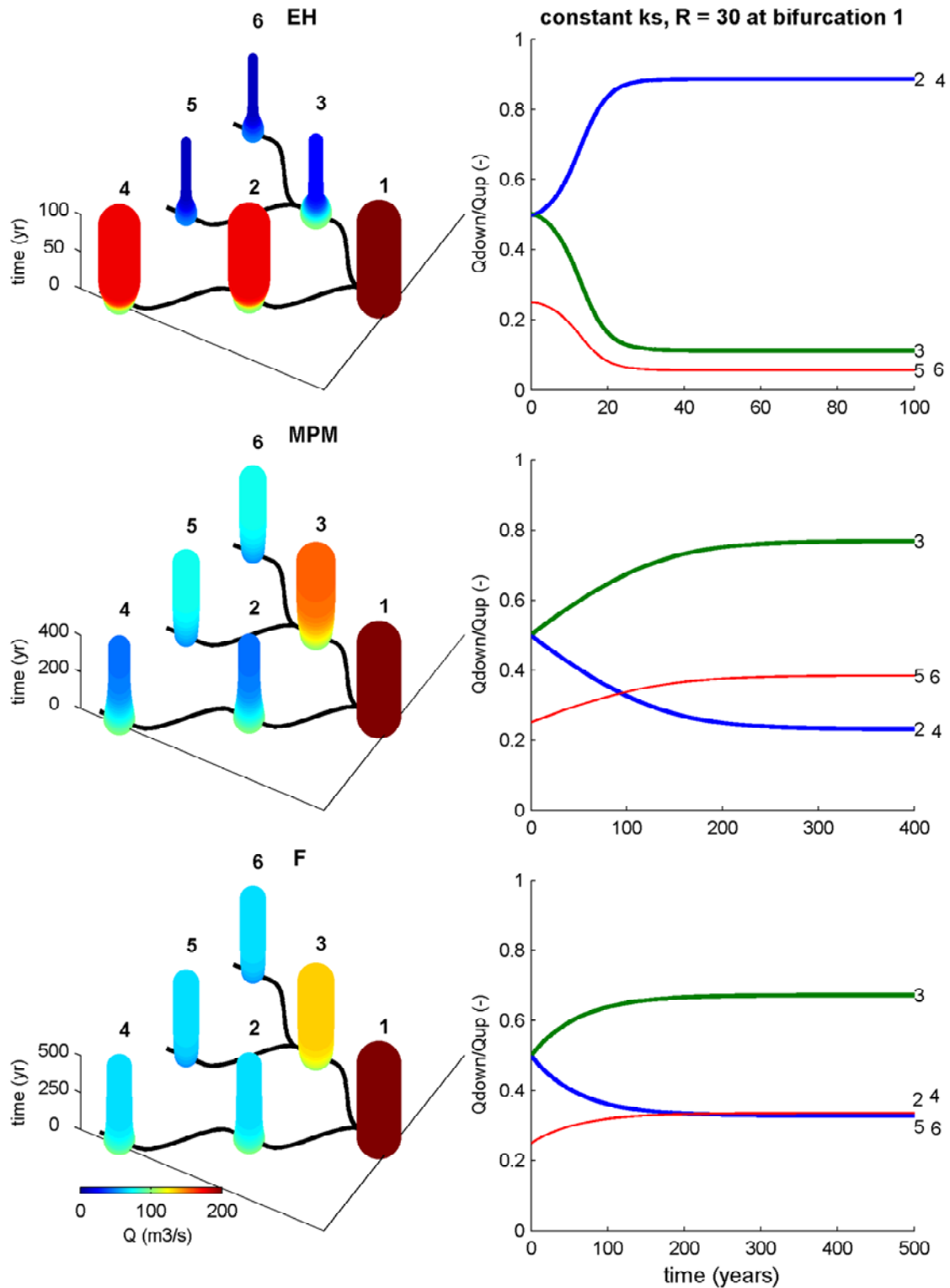
Fig. 4.12: Evolution of a river network with 2 bifurcations and 1 confluence, with a relative bend radius (R) of 30 at the first bifurcation that favors the bifurate that is closing for a situation without a relative bend radius, for the Engelund and Hansen (EH), Meyer-Peter and Mueller (MPM) and fitted sediment transport predictor (F). The bed roughness is defined by a constant Chézy roughness coefficient (C).
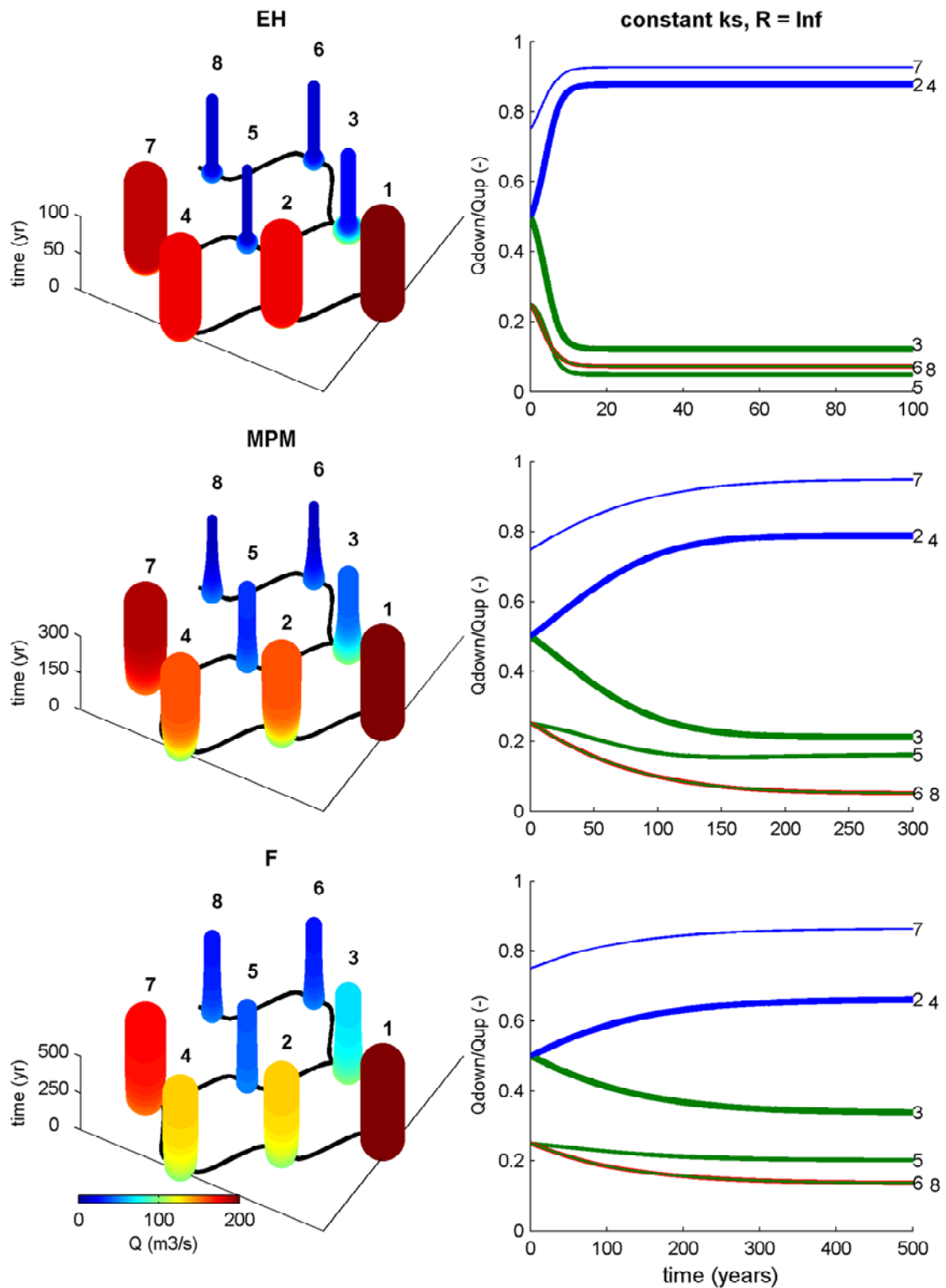
Fig. 4.13: Evolution of a river network with 2 bifurcations and 1 confluence, for the Engelund and Hansen (EH), Meyer-Peter and Mueller (MPM) and fitted sediment transport predictor (F). The bed roughness is defined by a constant Nikuradse roughness coefficient (k_s), no upstream bend (R) is present.

143

Fig. 4.14: Evolution of a river network with 2 bifurcations and 1 confluence, with a relative bend radius (R) of 30 at the first bifurcation that favors the bifurate that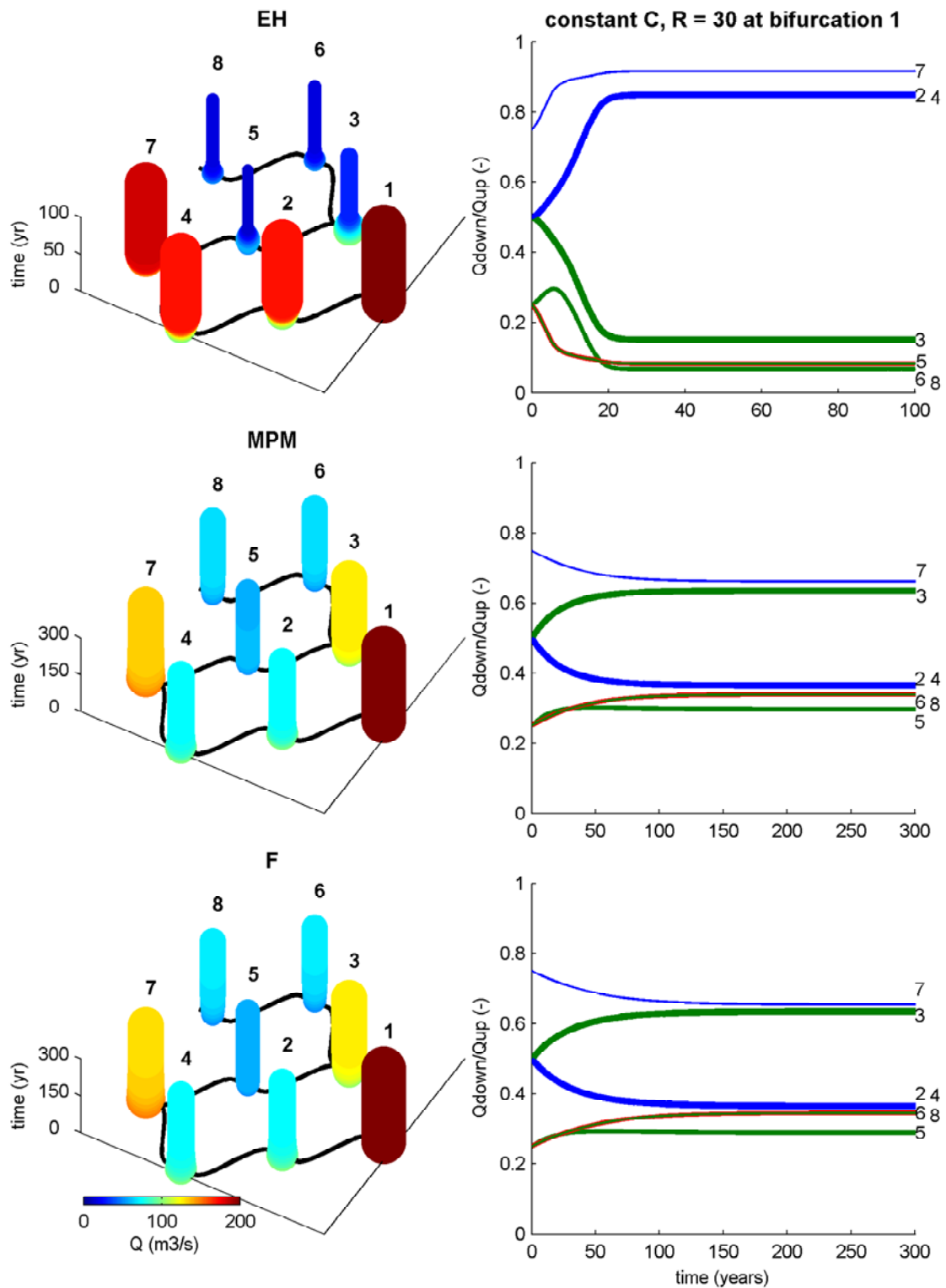 is closing for a situation without a relative bend radius, for the Engelund and Hansen (EH), Meyer-Peter and Mueller (MPM) and fitted sediment transport predictor (F). The bed roughness is defined by a constant Nikuradse roughness coefficient (k_s).
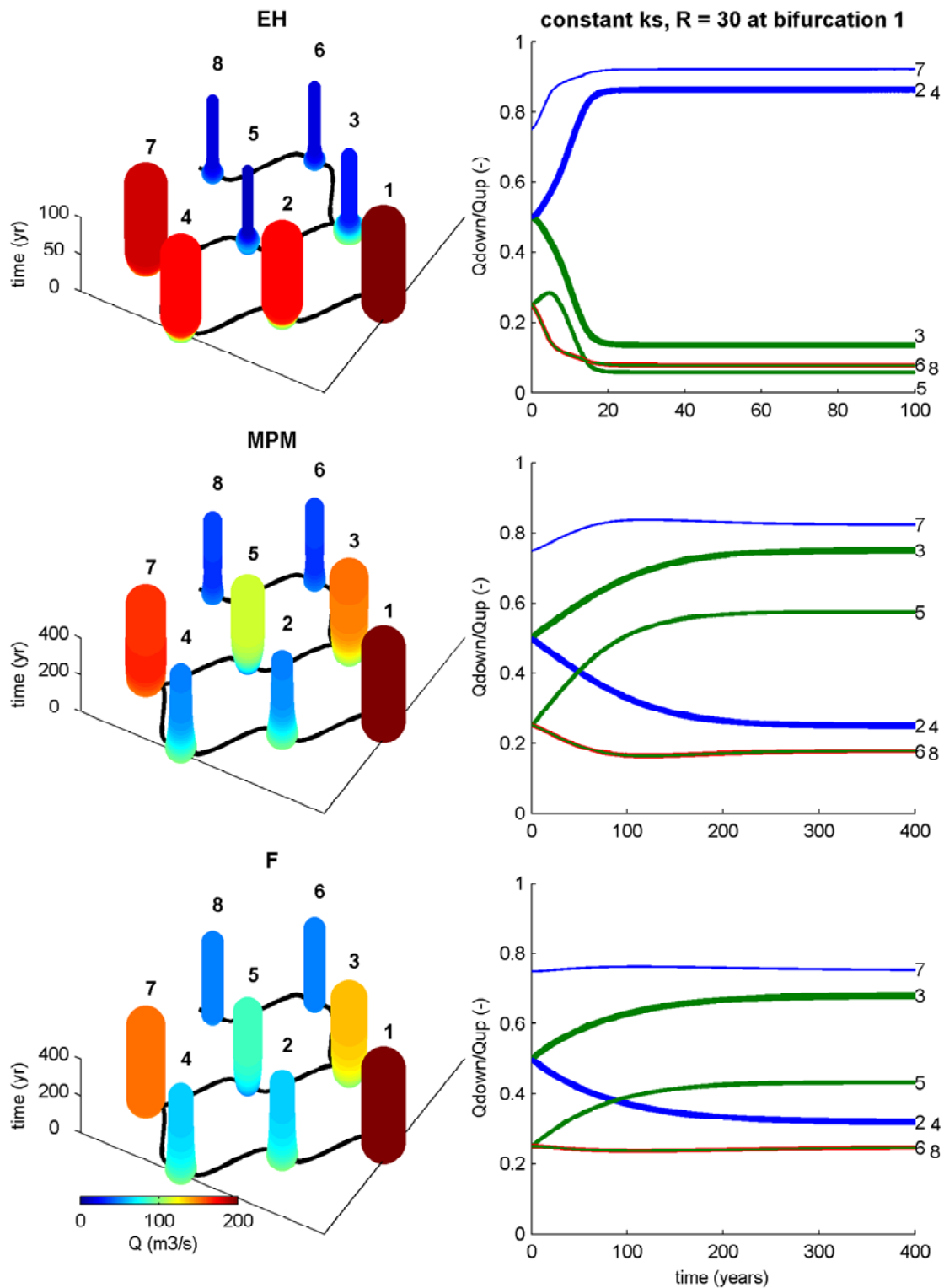
4.4.5. Total reach

In order to explain the dynamics of the upper Columbia River, and to establish to what extent the river network model is able to reproduce the present day discharge configuration of the upper Columbia River, the discharge division of a 21 kilometer reach of the Columbia River is modelled and compared to the observed discharge division. The reach is modelled with and without taking into account upstream bends in order to investigate the influence of bends in the upper Columbia River network.

In this section, first the modelled reach is described and the schematized river network of this reach is discussed (section 4.4.5.1). In section 4.4.5.2 the current configuration of the modelled upper Columbia River reach is described. The configuration predicted by the network model without implementation of upstream bends is described in section 4.4.5.3. In section 4.4.5.4 the configuration predicted by the network model with implementation of upstream bends is discussed. The model performance in quantified in section 4.4.5.5. In section 4.4.5.6, the results of section 4.4.5.2, 3, 4 and 5 are used to describe the dynamics of the modelled upper Columbia River reach. Finally, the evolution of the bed profile is discussed (section 4.4.5.7).

4.4.5.1. Schematization of the upper Columbia River reach

The modelled reach of the upper Columbia River stretches from just downstream of Spillimacheen to 5km downstream of Castledale (figure 4.15). The upstream boundary is placed just downstream of the place where the main tributary of the Spillimacheen flows into the upper Columbia River. A minor tributary of the Spillimacheen River flows into the modelled reach between bifurcation 2 and 4. However, according to Locking (1983) this tributary transports less than five percent of the total discharge of the Spillimacheen River. For simplicity, this tributary is neglected. The downstream boundary is placed at the position where all tributaries of the upper Columbia River have connected to a single channel. The reach includes the complete steep reach as described by Abbado et al. (2005) (section 2.2.2). The exact location of this steep reach is indicated in figure 2.16 and 4.15. In figure 4.15, the locations of the bifurcations and confluences in the modelled reach are indicated in a Google Earth satellite image. Additionally, the schematized river network of the modelled reach is shown.

The height of each bifurcation and confluence is calculated using data of Abbado et al. (2005). The slope in each channel follows from the elevation of each bifurcation and confluence. The length of each channel in the river network, and the relative bend radius upstream of each bifurcation is derived from Google Earth. The upstream discharge is 200 m^3/s. Initially, the discharge is equally divided at each bifurcation. The median grain size in each channel is 0.7mm. A constant k_s is assumed to represent bed roughness. In order to prevent numerical errors, the fitted sediment transport predictor is used. The relative bend radii of the 15 bifurcations are given in table 4.2.

145

Tbl. 4.2: Relative upstream bend radii of the 15 bifurcations in the modelled reach (figure 4.15). Inf stands for infinitive. A partial log-jam indicates that a patch of woody debris in front of a bifurcation which is not blocking the entire entrance of a bifurcate. The correspondence between the bifurcations indicated in figure 4.15 and the measured bifurcations (section 3.3.2.2) is indicated by the number in between brackets.

Bifurcation	1	2	3	4	5	6	7	8
R	23	35	41	48	38	Inf	Inf	25
log-jam	yes	yes	yes	no	partial	yes	yes	partial
Bifurcation	9	10 (2)	11	12 (3)	13 (1)	14 (4)	15 (5)	
R	24	37	Inf	35	6	Inf	17	
log-jam	partial	no	no	no	partial	partial	partial	

4.4.5.2. Observed discharge division

The current discharge division through the network is reconstructed in this section based on measurements of Makaske (1998), Tabata and Hickin (2003) and Abbado et al. (2005) (see figure 3.5 and table 1) of bankfull channel width and depth, the bifurcation and confluence measurements performed on this research and a Google Earth image of the modelled reach.

In the most upstream part of the reach, there is one clearly dominant waterway. In the schematization of the reach, this main waterway comprises channel 1, 3, 5, 8 and 11. The other channels flowing parallel to the main waterway are all relatively small. To the north of the main channel a small waterway comprising channel 2, 4 and 7 flows parallel to the main channel. To the south of the main waterway, two small waterways are present, these channels originate from the main waterway at bifurcation 2 and 3.

In the middle part of the reach (steep reach) no clearly dominant waterway is present. There are two main waterways flowing through this reach, of which the waterway flowing through the northern part of the river valley in the steep reach is the largest. The first large waterway comprises channel 15, 20, 25, 31, 36, 41, 44, 48, 53, 58 and 64. This waterway is fed by two sub-waterways, that originate from a trifurcation. Since no nodal point relation exists for trifurcations, this trifurcation is schematized by two bifurcations; bifurcation 6 and 7. From bifurcation 6, the waterway comprising channel 21, 26 and 32 mounts in the first large waterway. From bifurcation 7, the waterway comprising channel 27, 33 and 37 mounts in the first large waterway. However, the third channel, channel 28, originating from the trifurcation is by far the largest. The waterway comprising channels 21, 26 and 32 is relatively small. The waterway comprising channel 27, 33 and 37 is characterized by a large width; consequently on the Google Earth images it appears to be a large channel.
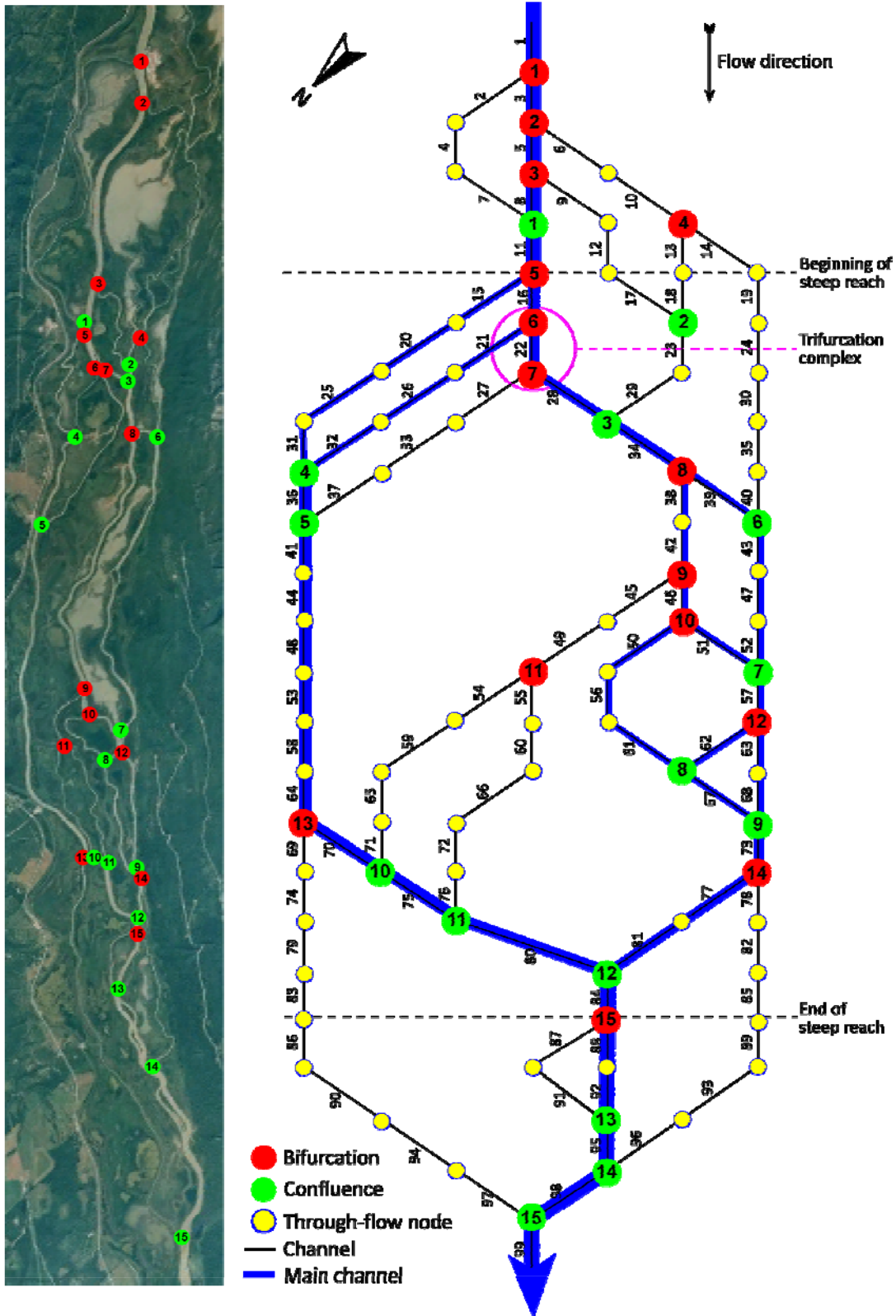
146

Fig. 4.15: Schematization of the modelled upper Columbia River reach. On the Google Earth image on the left the actual locations of the bifurcations and confluences are shown. The length of the reach is approximately 21km.

However, field observations and borings (section 3.4.5.2) show that this channel used to be large with a depth of more than 6 meter (boring 059 in figure 3.49). Nowadays this channel is completely silted up so that only a small amount of discharge is transported through this waterway.

The discharge through channel 28 combines with the bulk of the discharge transported through the two small waterways flowing south of the main waterway at the upstream gentle reach. This forms a large channel (34), which then splits its discharge at bifurcation 8 forming a waterway comprising channel 38 and 42, and a waterway comprising channel 39, 43, 47 and 52. The waterway comprising channel 14, 19, 24, 30, 35 and 40 mounts in the latter waterway. This waterway does not transport a large amount of discharge however. The former channel transports the largest amount of discharge. Consequently, this is the second main waterway through the steep reach. On the Google Earth image, both waterways appear comparable in size. However, the former channel is characterized by a significantly larger width and depth, and consequently transports more discharge (see measuring location 23 and 27 in table 1 and figure 3.5). The former channel splits at bifurcation 9, to form the waterway containing channel 45 and 49, which splits later on. This channel contains a small amount of discharge. The bulk of the discharge flows through channel 46 and then splits in two channels: channel 51 and a waterway comprising channel 50, 56, and 61. The former channel transports slightly more discharge. Additionally this channel joins with the waterway comprising channel 43, 47 and 52, and consequently forms a large channel: channel 57. Within 100m, this channel splits again at bifurcation 12, forming channel 62 and the waterway containing channel 63 and 68, which transport most of the discharge. The former channel joins with the waterway comprising channel 50, 56 and 61 to form channel 67. Channel 67 and the waterway comprising channel 63 and 68 become comparable in size. These channels join at confluence 9, but within 100m they divide their discharge again at bifurcation 14. At this bifurcation a minor part of the flow is transported into the waterway comprising channel 78, 82, 85, 89, 93 and 96. The bulk of the discharge is transported into the waterway comprising channel 77 and 81. As indicated in section 3.3.2.6, the waterway comprising channel 78, 82, 85, 89, 93 and 96 at bifurcation 14 is a young growing waterway. Consequently, the conditions might be in favor of this waterway, so that this waterway might ultimately become more dominant than the waterway comprising channel 77 and 81.

The waterway comprising channel 77 and 81 joins at confluence 12 with channel 80 to form a large channel (84). Channel 80 originates from bifurcation 13, where the first main waterway of the gentle reach (channel 41, 44, 48, 53, 58 and 64) splits into a long waterway comprising channel 69, 74, 79, 83, 86, 90, 94 and 97 and the waterway comprising channel 70, 75 and 80. In the latter, two small channels mount that originate from the waterway comprising channel 45 and 49. At bifurcation 13, the bulk of the discharge is transported into the waterway comprising channel 70, 75 and 80. In the other channel originating at bifurcation 13 (bifurcation 1 in section 3.3.2), an inlet step is present which indicates that this channel is indeed silting up, causing the bulk of the discharge to be transported through the other waterway. At channel 84 the transition from steep to gentle reach is present.

Downstream of this point, there is a distinct main channel present, namely the waterway comprising channel 84, 88, 92, 95, 98 and 99. Channel 84 splits at bifurcation 15 into channel 88, 92 and 87, 91. The latter waterway is transporting far less discharge however, which is illustrated by the large inlet step at this bifurcation and small area ratio compared to the main channel (figure 3.27). The waterway originating from channel 84 becomes even more enhanced by the fact that both the waterway comprising channel 69, 74, 79, 83, 86, 90, 94 and 97 and the waterway comprising channel 78, 82, 85, 89, 93 and 96 mount in the main waterway ultimately forming a large, single channel (channel 99).

In summary, in the upstream part of the reach, there is a distinct main waterway comprising the channels 1, 3, 5, 8 and 11. Downstream of channel 11 the gentle slope of the upstream part of the reach becomes steep. Downstream of this transition there is not a distinct main channel, but two main waterways. The first follows a course that comprises the channels 15, 20, 25, 31, 36, 41, 44, 48, 53, 58, 64, 70, 75, and 80, whilst the second follows a course that comprises the channels 16, 22, 28, 34, 38, 42, 46, 51, 57, 63, 68, 73, 77, and 81. Note that the latter course temporarily becomes less distinct, from channel 46 to 73, since it splits in multiple small channels. At channel 84, at the transition from the steep to gentle sloped reach, both waterways join to form a single main waterway again, which comprises channel 84, 88, 92, 95, 98 and 99.

An important note has to be made concerning the present configuration of the channels in the network. Human interference has led to several artificial induced log-jams at bifurcations concerning the main channel, in order to stimulate discharge into the main channel at these bifurcations. These log-jams are induced by implementing poles vertically into the bed at the entrance of the minor bifurcates, so that driftwood is trapped between these poles causing log-jams to block the entrance of the minor bifurcates. These artificially induced log-jams have been observed at bifurcation 1, 2, 3, 5, (6, 7; the trifurcation), 8, 9, 13, 14 and 15. One of the most pronounced examples is the log-jam in front of bifurcation 3, which has completely blocked the minor bifurcate (the waterway comprising channel 9, 12, 17), except for a small breach in the log-jam (figure 4.16), in favor of the main channel.

Fig. 4.16: Human induced log-jam at bifurcation 3. The log-jam almost completely blocks the entrance of the minor bifurcate (upper picture), except for a small breach in the log-jam (lower picture). Note the remnant of one of the vertical poles on the lower picture, as well as the difference in water level in front and behind the log-jam, indicating the backwater effect induced by the log-jam.

The implementation of the human induced log-jams most likely originates from the early 1900's, when steamboats were the only mode of transportation through the Columbia River. Since this river is highly dynamic, parts of the main navigating channel most likely started silting up, for example the waterway containing channel 27, 33 and 37, which used to be a large channel but has nowadays completely silted up. The log-jams at the trifurcation are implemented in front of the other two trifurcates, in order to favor discharge into this waterway.

4.4.5.3. Modelled discharge division without taking into account upstream bends

When comparing the modelled discharge division without upstream bends (figure 4.17) with the observed discharge division (section 4.4.5.2), it becomes clear that the main waterway following the north of the river valley in the steep reach, e.g. the waterway comprising the following channels: 1, 3, 5, 8, 11, 15, 20, 25, 31, 36, 41, 44, 48, 53, 58, 64, 70, 75, 80, 84, 88, 92, 95, 98 and 99 is reproduced. At bifurcation 5, the waterway comprising channel 15, 20, 25 and 31 transports more discharge than channel 16 does, which is opposite to the natural configuration. Due to the division of the main channel discharge over multiple channels, the discharge through the waterway comprising channel 15, 20, 25 and 31 is smaller than the discharge trough the upstream part of the main waterway. However, when both the waterway comprising channel 21, 26 and 32 and the waterway comprising channel 27, 33 and 37 have delivered their discharge to the northern main channel, from channel 41 in downstream direction, this channel becomes large again, as is the case in the present-day configuration of the upper Columbia River.

At bifurcation 13, most of the discharge is transported into the waterway comprising channel 70, 75 and 90, as observed in nature. When this waterway joins its discharge with the discharge of the waterway comprising channel 77 and 81, indeed a distinct main channel is formed following the waterway comprising channel 84, 88, 92, 95, 98 and 99 as is the case in the current upper Columbia River. In nature, the waterway comprising channel 88 and 92 transports far more discharge than the waterway comprising channel 87 and 91. In the modelled river network, the former waterway indeed transports most of the discharge. In nature the division is far more asymmetric however.

The main waterway following the south of the river valley in the steep reach is reproduced less accurate by the river network model than is the main waterway following the north of the river valley. At bifurcation 6, most of the discharge is conveyed into the waterway comprising channel 21, 26 and 32. Consequently, only little discharge is conveyed into channel 22. At the downstream end of this channel, at bifurcation 7, the discharge is approximately equally divided over the waterway comprising channel 27, 33 and 37 and channel 28. Consequently, very little discharge is transported through channel 28. As described in the previous section, in the current upper Columbia River only few discharge is transported through the waterway comprising channel 21, 26 and 32 and the waterway comprising channel 27, 33 and 37 so that most of the discharge is transported through channel 28.

After channel 28 has joined with the waterway comprising channel 23 and 29, the discharge transported through channel 34 is relatively large. In reality, the discharge transported through channel 28 and the waterway comprising channel 23 and 29 is approximately equal. In the modelled network, the amount of discharge transported through the waterway comprising channel 23 and 29 is

overestimated. This happens because the amount of discharge transported through the waterway comprising channel 9, 12 and 17 is overestimated since in reality a large log-jam at bifurcation 3 blocks the entire entrance of this waterway (figure 4.16). This causes less discharge to enter the waterway comprising channel 9, 12 and 17, leading to less discharge in the waterway comprising channel 23 and 29 in nature.

At the downstream end of channel 34, at bifurcation 8, the waterway comprising channel 39, 43, 47 and 52 transports more discharge than the waterway comprising channel 38 and 42. This is opposite to the division of discharge observed in nature. Consequently, the former waterway is the main waterway following the south of the river valley in the steep reach. At the downstream end of the latter waterway, channel 46 transports most of the discharge divided at bifurcation 9, as observed in nature. Once the waterway comprising channel 43, 47 and 52 joins with channel 51 in channel 57 the configuration becomes similar to that observed in nature again. The amount of transported discharge through channel 67 and the waterway comprising channel 63 and 68 is approximately equal as observed in nature. At bifurcation 14, most of the discharge is transported into the waterway comprising channel 77 and 81, as is currently the case. The waterway comprising the channels 78, 82, 85, 89, 93, 96 stays relatively small. This leads to the prediction that this waterway, which during the field campaign was addressed to be a young, growing channel, will not grow to be a new major channel.

In summary, the present day discharge division in the upper Columbia River is reasonably well predicted by the river network model without upstream bends. The main waterway following the north of the river valley in the steep reach is completely reproduced. The main waterway following the south of the river valley in the steep reach is not accurately reproduced. This is caused by a wrong discharge division at bifurcation 6 and 7 and bifurcation 8. At bifurcation 6 and 7, which in nature is a trifurcation, in nature most of the discharge is transported through channel 28. However, when the trifurcation is represented by two bifurcations following each other within a short distance, only a minor amount of the discharge is transported into channel 28. Consequently, the amount of discharge transported into the southern part of the valley is too small. At bifurcation 8, most of the discharge is transported into the waterway comprising channel 39, 43, 47 and 52, whereas in nature most of the discharge is transported into the waterway comprising channel 38 and 42.

4.4.5.4. Modelled discharge division with taking into account upstream bends

The main differences in river network configuration when the relative bend radius upstream of the bifurcations is taken into account (figure 4.18) compared to the river network configuration of the reach without taking into account relative bend radius (figure 4.17) are described in this section.

At bifurcation 1, the waterway comprising channel 2, 4 and 7 is located in an outer bend. Consequently, this waterway transports more discharge than in the situation without bend radii. Compared to nature, the modelled discharge is too large. The situation without bend radii for this bifurcation leads to a more accurate prediction at this bifurcation. However, it should be noted that in nature this waterway is in nature partly blocked by a human induced log-jam, leading to less discharge into this waterway than would normally be the case.

At bifurcation 5, the waterway comprising channel 15, 20, 25 and 31 is favoured by the upstream bend. Consequently, even more discharge is transported through the main waterway following the north of the river valley in the steep reach.

At bifurcation 8, the waterway containing channel 38 and 42 is slightly favoured by the upstream bend. The advantage generated by the bend is not large enough to become the main waterway through the southern part of river valley in the steep reach.

At bifurcation 13, the waterway comprising channel 69, 74, 79, 83, 86, 90, 94 and 97 is favoured by a relatively sharp upstream bend. Consequently most of the discharge is transported through this waterway; this is not conform the situation in nature. Here, the situation is predicted better when the upstream bend radius is not taken into account.

Due to an upstream bend radius at bifurcation 15, the discharge division over the waterway comprising channel 87 and 91 and the waterway comprising channel 88 and 92 becomes more asymmetric than for the situation without upstream bend radii. In this case the former situation leads to a more accurate prediction.

In conclusion, the general network configuration does not differ a lot between the situation with or without upstream bend radii. For some channels the former, and for some channels the latter situation is the most accurate. Since most relative bend radii are within the range 30-50 the effect of these bends is mostly counteracted by the amount of downstream bifurcations and confluences. Indeed, the bifurcations described above where a different discharge division occurred are all characterized by a relative bend radius smaller than 25. Bifurcation 13, where the largest difference occurred after implementation of upstream bends, is characterized by the smallest R; namely 6. Additionally, the (partial) log-jams might alter the discharge division at the bifurcations in the upper Columbia river. The effect of the log-jams might be almost as important as the bend effects. This could explain the remaining discrepancies.
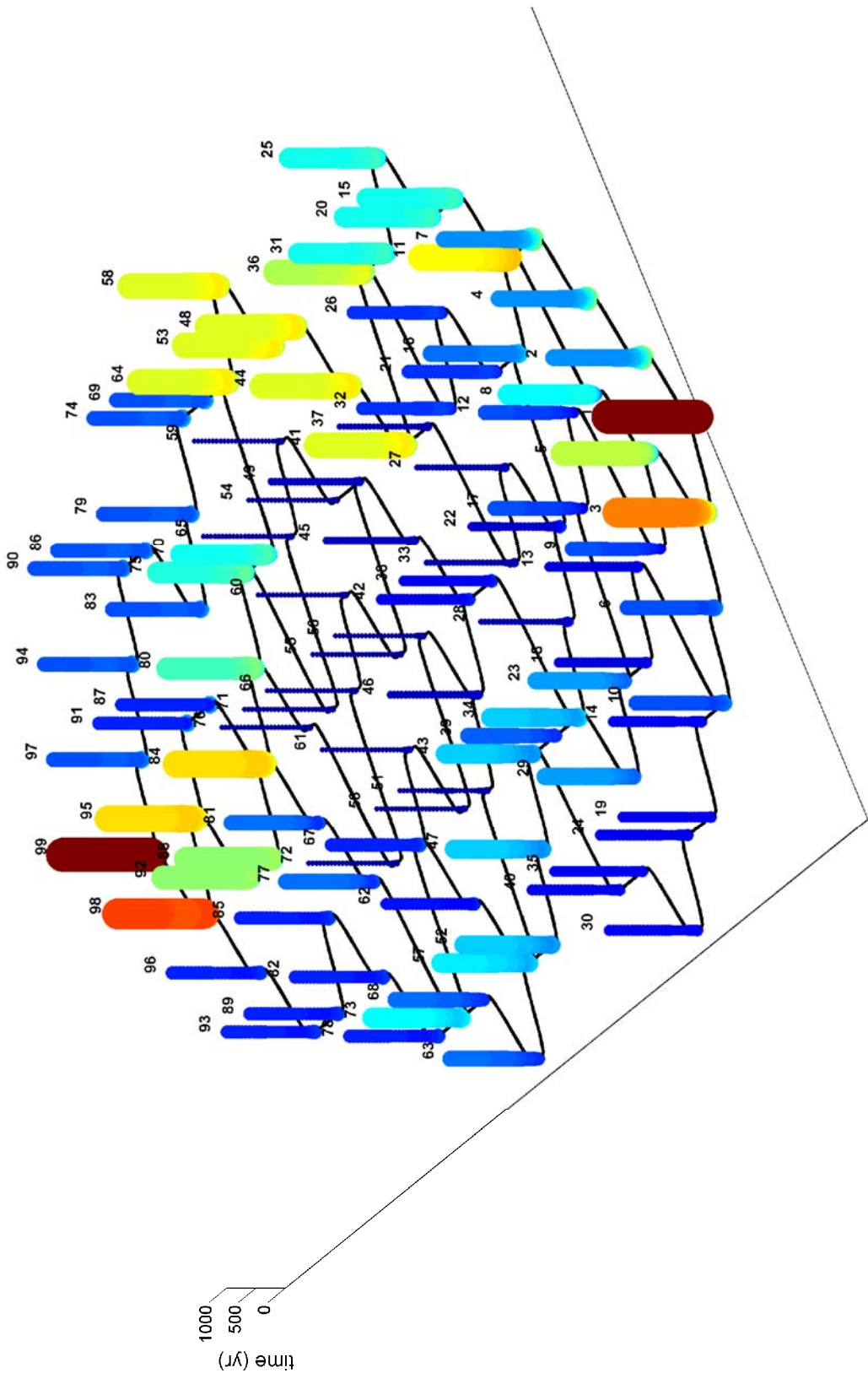
Fig. 4.17: Modelled discharge division of the Columbia River network without taking into account upstream bends.
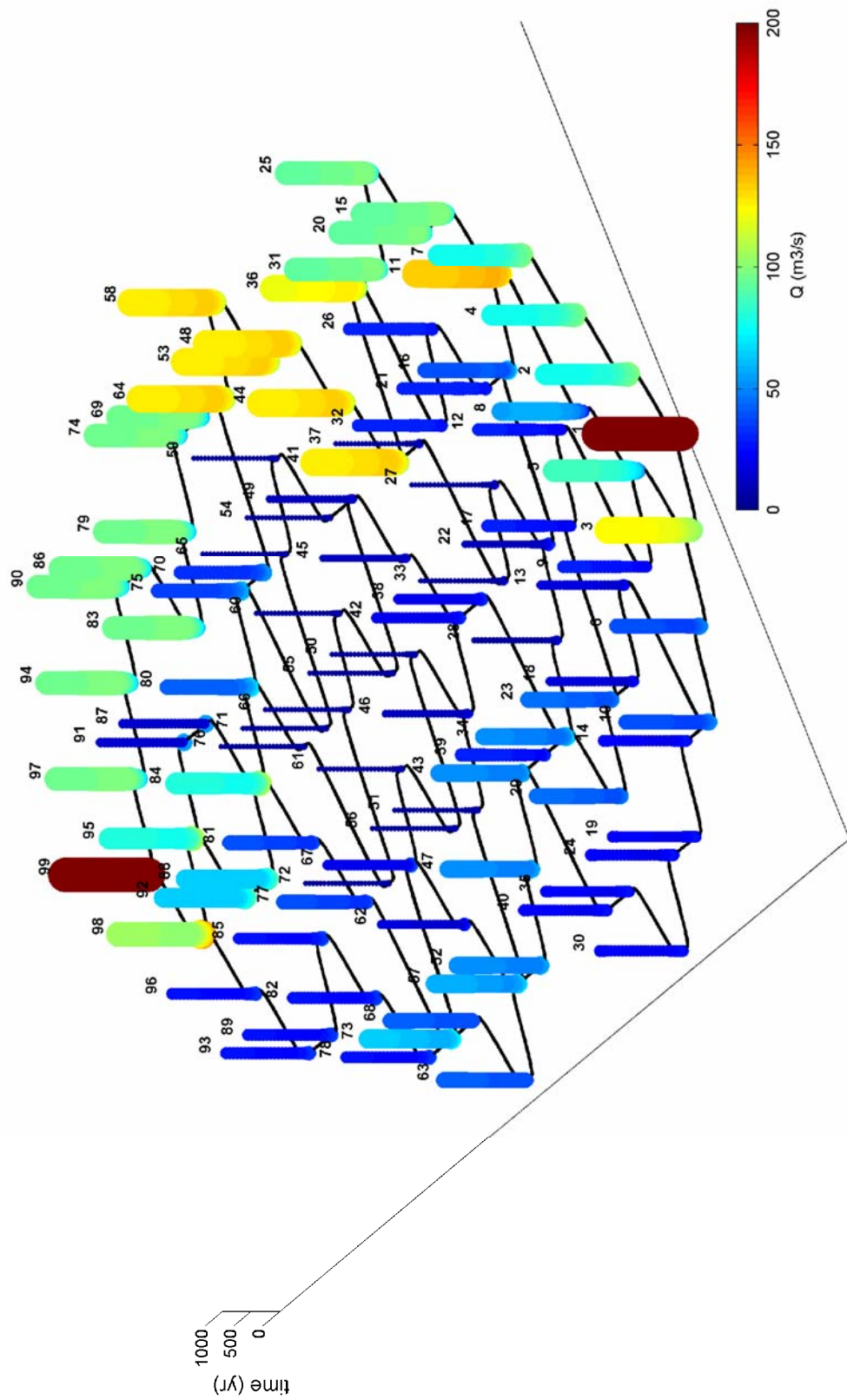
154

Fig. 4.18: Modelled discharge division of the Columbia River network when taking into account upstream bends.

4.4.5.5. Overall model performance

To quantify the model performance, in figure 4.19 the measured discharge shown in table 2.1 and figure 2.6 is compared to the modelled discharge in the corresponding channels. The correspondence between the discharge measurements shown in figure 2.6 and table 2.1 and the channels shown in figure 4.15 is shown in table 4.3. The discharge measurements have been performed for bankfull stage, whereas discharge in the model is the channel forming discharge. The bankfull discharge in the upper Columbia River is 250 m^3/s (figure 2.2), the channel forming discharge is 200 m^3/s. Therefore a systematic deviation between the measured and modelled discharge might be present.
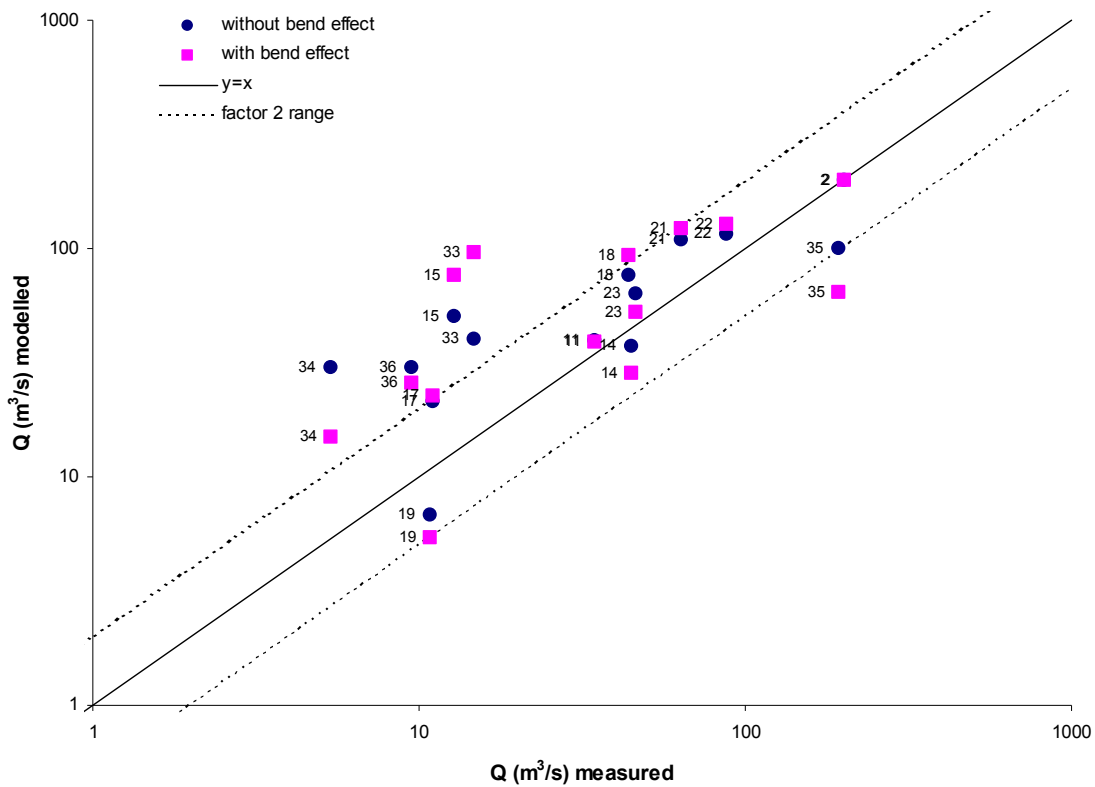
Fig. 4.19: Measured discharge compared to modelled discharge for the upper Columbia River. The numbers indicate the measurement numbers in figure 2.6 and table 2.1. The channel(s) as shown in figure 4.15 that correspond(s) to these measurements are shown in table 4.3.

Tbl. 4.3: Correspondence of measurement numbers shown in figure 2.6 and table 2.1 with the channel numbers as shown in figure 4.15.

Figure 2.6	no.	2	11	14	15	17	18	19
Figure 4.15	branch	1	6, 10	9, 12, 17	2, 4, 7	14, 19,…40	15, 20,…31	27, 33, 37
Figure 2.6	no.	21	22	23	33	34	35	36
Figure 4.15	branch	36	41, 44,…64	43, 47, 52	69, 74, 97	87, 91	88, 92	78, 82,…96

Despite the significant scatter, the model is able to reproduce the discharge in the upper Columbia River reasonably well. The channels that are the largest in reality also become the largest channels in the model. Channels that are the smallest in reality become the smallest channels in the model.

The model tends to overestimate the discharge. This is most pronounced in relatively small channels. The scatter is largest for relatively small channels. This might be caused by the fact that in reality some small channels completely close off to become residual channels, whereas in the model small channels do not completely close off.

The model performance appears to be approximately equal with or without inclusion of the bend effect. In some channels the bend effect deteriorates the model predictions (e.g. 15, 33), whereas in other channels the bend effect improves the model predictions (e.g. 23, 34).

It can be concluded that the network model is able to qualitatively reproduce the discharge in the upper Columbia River channels. For a quantitative reproduction of the discharge in the channels there is too much scatter. This is caused by the high rate of complexity of large river networks. There are many factors that might negatively influence the discharge division through the network, e.g. (partial) log-jams, alternating bars, the presence of a trifurcation. Additionally the direction of information propagation is very important. A deviation between measured and modelled discharge upstream in the network, affects the discharge prediction in all connected downstream channels.

4.4.5.6. Factors controlling the evolution of the upper Columbia River

As becomes clear from the previous sections, the river network model is able to qualitatively reproduce the discharge division of the current upper Columbia River. Consequently, the model results can be used to gain insight into the dynamics of large river networks, and to address the factors controlling the evolution of the upper Columbia River.

The modelled reach of the upper Columbia River reaches its equilibrium within approximately 1000yr. Some bifurcations reach their equilibrium configuration relatively fast, whilst other bifurcations reach their equilibrium configuration relatively slow. This phenomenon has large consequences for the evolution of discharge division at downstream bifurcations. For example, in figure 4.17 it can be seen that the discharge in the waterway comprising channel 69, 74, 79, 83, 86, 90, 94 and 97 initially decreases, then increases, after which the discharge decreases again. This phenomenon can be seen in most of the waterways in the river network, especially those located downstream in the network. This behaviour can be explained as follows: due to the complexity of the river network, the discharge of a certain waterway, especially if it is located downstream in the network, might be affected by the discharge division at two or more bifurcations. Suppose that the evolution of one of the bifurcations is relatively fast whilst the evolution of the other bifurcation is relatively slow, and the evolution of the first bifurcation enhances the discharge in the downstream waterway whilst the evolution of the second bifurcate frustrates the downstream waterway. In this situation, the discharge in the downstream waterway will initially increase, due to the fast evolution of the first bifurcation and after a while the discharge will decrease again, due to the fact that the discharge division in the second bifurcation has become more asymmetric which frustrates the discharge through the downstream waterway.

The division of discharge over the modelled reach of the upper Columbia River is mainly explained by the network topology and gradients. As initial guess, the discharge is equally divided at all bifurcation. Consequently, channels that have many upstream bifurcations are relatively small, since flow is divided over many channels. The opposite holds for channels that have few upstream bifurcations. The initial guess already represents the present-day configuration of the modelled reach relatively accurate. Based on disturbances induced by downstream slope differences, backwater effects and upstream bend radii the discharge in certain channels becomes larger or smaller than the discharge appointed in the initial guess. Due to the relatively gentle slope of the upper Columbia River valley, slope differences between different channels are in most cases marginal. Most relative upstream bend radii are relatively small. Differences in downstream friction induced by the amount of downstream channels (section 4.4.4) also only cause a small disturbance. Consequently, the disturbances leading to an asymmetric discharge division at bifurcations are relatively small, so that the discharge division at most bifurcations does not become very asymmetric. Therefore it can be concluded that the discharge

division over the network is for the largest part induced by the network topology. This effect is illustrated by the fact that the largest waterway through the steep reach is the waterway comprising channel 41, 44, 48, 53, 58, 64, 75 and 80. This waterway is simply the largest waterway because it is fed by four waterways, namely at confluence 4, 5, 10 and 11, whilst it only divides its discharge at one bifurcation (13). This has two advantages: firstly, the discharge in a channel increases as the discharge of another channel is added to this channel at a confluence, and secondly it is more efficient to transport flow through a confluenced pathway (section 4.4.4.2). The main waterway flowing through the south of the steep reach is characterized by many bifurcations and consequently the discharge has to be divided over many channels, causing these channels to transport less discharge than the above described main waterway flowing through the north of the steep reach.

The more upstream a bifurcation is located in a river network, the more important this bifurcation is for the network evolution, since the more upstream a bifurcation is located in a network, the more channels and bifurcations are influenced by the discharge division at this bifurcation. In the modelled reach of the upper Columbia River, the trifurcation is the most important discharge divider since it divides the discharge of the main channel of the upstream gentle reach over the southern and northern waterway through the steep reach. As becomes clear in section 4.4.5.3 and 4.4.5.4, the discharge through the southern pathway is underpredicted, because the discharge through channel 28 is underestimated. This is caused by the fact that the implementation of two bifurcations in order to reproduce the trifurcation does not lead to the discharge division observed in reality.

Another important assumption that might significantly influence the modelled network configuration is the usage of the fitted predictor in order to overcome numerical instabilities. The fitted predictor predicts a fairly symmetric discharge division at low Shields stresses, whilst the MPM or VR predictor would have predicted a more asymmetric discharge division (figure 4.2). Additionally, the channel thalweg was observed to not always follow the bend radius (section 3.3.3.2) due to upstream disturbances to which the flow was not able to adjust fast enough, such as the presence of a bend upstream. This might have pronounced effects on the spiral flow in certain bends, which might affect the equilibrium configurations of bifurcations that have an upstream bend.

4.4.5.7. Bed evolution

In order to establish whether the bed configuration of the modelled upper Columbia River reach, characterized by the transition from a gentle to a steep slope and back to a gentle slope again, as described by Abbado et al. (2005), is an equilibrium configuration, the bed evolution of the upper Columbia River is analysed in this section.

In figure 4.21 the bed evolution of the upper Columbia River of the model run without upstream bends (upper graph) where the upstream sediment feed is equal to the transport capacity of the upstream channel, is plotted for the network shown in figure 4.17. Second, a situation characterized by a sudden sediment pulse of on average three times the upstream sediment capacity from t = 200 to t = 350yr (lower graph) is shown.

For the situation without a sudden sediment pulse, the bed rapidly adjusts its slope until an equilibrium slope is reached. The equilibrium slope of $7.6*10^{-5}$m/m is reached within 200yr. This equilibrium slope is approximately equal to the measured slope of the gentle reach between Castledale and Golden of $6.8*10^{-5}$m/m. Consequently, it can be concluded that the gentle reach of the current upper Columbia River is the river's equilibrium slope, whilst the presence of the steep slope is not an equilibrium situation. This hypothesis is emphasized by the fact that in order to reach the equilibrium slope of the modelled reach, net erosion occurs and by the fact that the measured sediment transport at Spillimacheen (Locking, 1983) is larger than the predicted sediment transport capacity (section 3.4.4).

To obtain the present day bed configuration of the modelled reach, indicated by the bed configuration at t = 0yr, aggradation has to occur in the reach. This can only happen when more sediment enters the reach than can be transported. Just upstream of the modelled reach, the Spillimacheen River enters the Columbia River. Since the slope of the Spillimacheen River is larger than the slope of the upper Columbia River the transport capacity of the former river is significantly larger. Additionally, a lot of sediment is available from the mountains, consequently the Spillimacheen River transports more sediment than the upper Columbia River does. Due to the gentle slope of the upper Columbia River the transport capacity is relatively small. Not all sediment entering the modelled reach can thus be transported, causing aggradation, which on its turn causes the bed slope to become steeper.

However, the steep reach does not start at the point where the Spillimacheen River joins the upper Columbia River, but approximately 7 km downstream. This bed configuration can be reproduced by implementing a sudden sediment pulse into the modelled reach. The lower graph in figure 4.21 displays the effect of a sudden sediment pulse. In the first 200yr of this sediment pulse, the upstream sediment feed is equal to the transport capacity. Consequently, in the first 200yr the bed evolution is equal to the bed evolution in the upper graph of figure 4.21. From 200 to 250yr, the upstream sediment feed is twice the transport capacity, from 250 to 300yr the upstream sediment feed is three times the

transport capacity and from 300-350yr the upstream sediment feed is four times the transport capacity. From t = 350yr onwards in time the upstream sediment feed is equal to the transport capacity again (figure 4.20) .
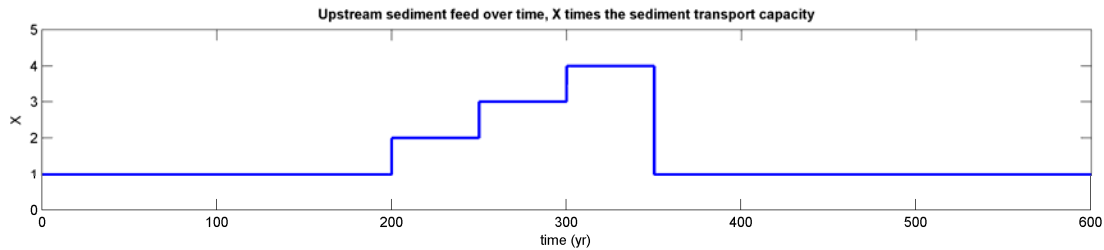

Fig. 4.20: Upstream sediment feed over time, expressed as X times the upstream sediment transport capacity.

At t = 240yr, more sediment has entered the reach than can be transported for 40 years. This sediment is deposited in the upstream part of the reach. Consequently the slope in the upstream part of the reach increases, which causes the sediment transport capacity in the upstream part of the reach to increase. Consequently, more sediment is transported along this newly formed steep reach. This sediment is then deposited at the downstream end of this steep reach. So, as time passes, the steep reach expands itself until finally in the entire modelled reach a steeper bed slope has formed.

At t = 350, the upstream sediment feed decreases to the original transport capacity. However, since the new equilibrium slope is steeper than the original equilibrium slope, the transport capacity is larger than is the upstream sediment feed; this causes erosion. Initially, the bed in the upstream part of the steep reach is eroded and the bed slope in this part of the reach adjusts itself to the new upstream sediment feed. Consequently, the transport capacity in this part of the reach becomes in equilibrium with the sediment transport. Now, the erosion mainly occurs more downstream, where the slope is still steeper and where erosion still occurs. This process continues until finally the bed of the entire reach is in equilibrium with the upstream sediment feed.

At t = 390yr, the implication of the above described process on the present day bed configuration of the upper Columbia River is illustrated. At this time, in the upstream 7km of the modelled reach the bed slope is already almost adjusted to the new, reduced, upstream sediment feed, whilst downstream the bed slope is still mainly conform the bed slope induced by the sudden sediment pulse. This causes a break in slope at a distance of approximately 7km along the river. Upstream of this point the slope is relatively gentle, and downstream of this point the slope is relatively steep.

In a qualitative way, the bed configuration at t = 390yr is equal to the present-day bed configuration, which is also characterized by a transition from gentle to steep slope at a distance of 7km downstream of the point where the sudden sediment pulse is induced. In reality the break in slope is more sudden. Additionally, in the modelled reach the downstream break in slope between the steep reach and the

161

downstream gentle reach is not reproduced. This might be explained by the fact that in reality many avulsions most likely occurred during the sediment pulse.
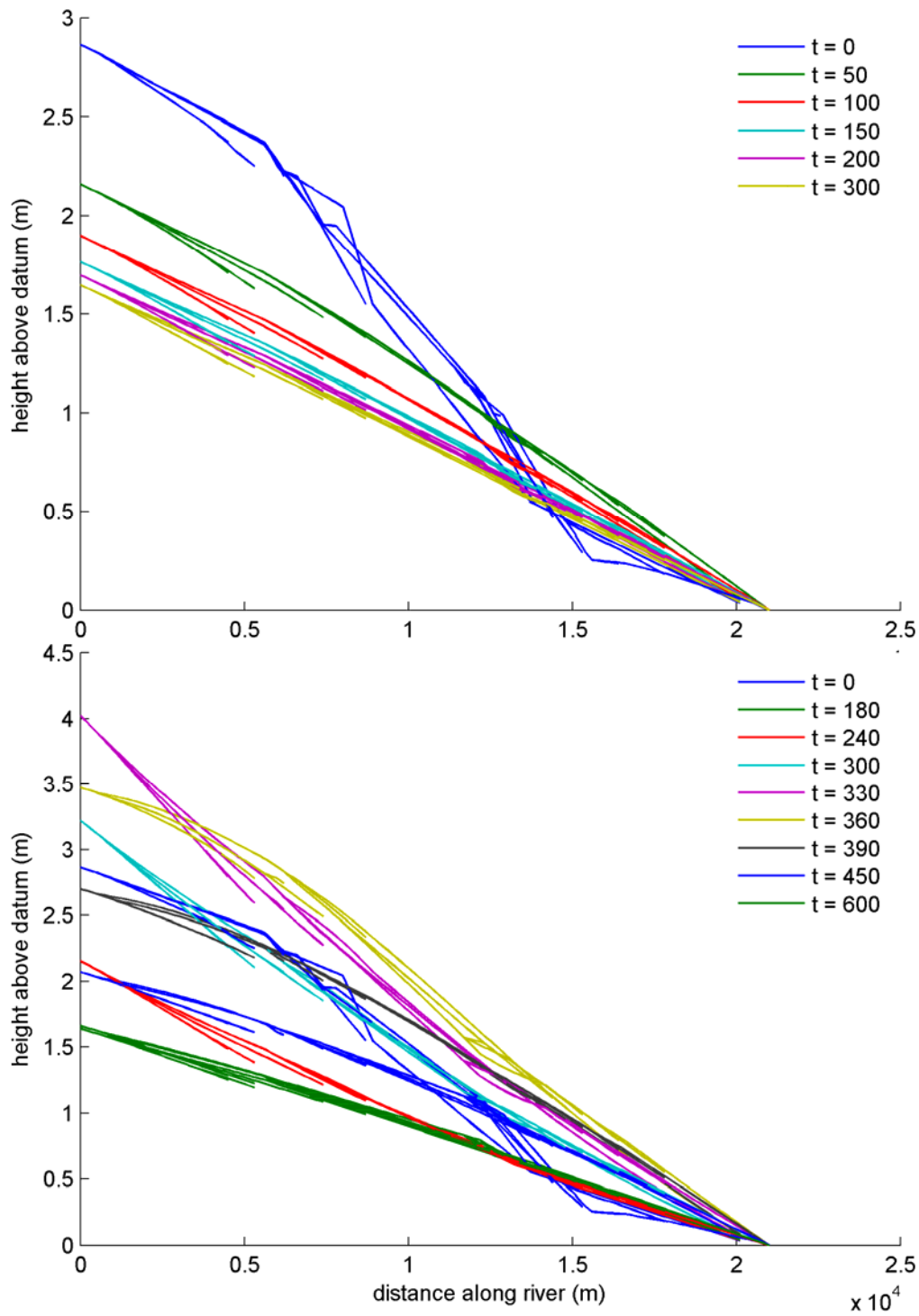

Fig. 4.21: Bed evolution of the upper Columbia River without (upper image), and with a sediment pulse of on average three times the transport capacity of 150 year (lower image).

5. Discussion of field and modelling results

5.1. Introduction

In this section, results of the literature research, fieldwork and modelling are combined and discussed. The different types of residual channels, observed by Makaske et al. (2002) are correlated with the observed channel-fill of inner- and outer bend residual channels (section 3.4.5.2) in section 5.2. The equilibrium configurations of the experimental braided rivers of Bertoldi and Tubino (2005) and the equilibrium configurations of bifurcations in the upper Columbia River and the Cumberland Marshes (Edmonds and Slingerland, 2008) are compared to the modelled equilibrium configurations (section 4.4.3) in section 5.3. In section 5.4, the dynamics of river networks, obtained in section 4.4 are discussed. In section 5.5, the two main hypothesis on the the origin of anastomosis are discussed and the origin of anastomosis in the upper Columbia River is explained.

5.2. Residual channels

Based on morphological observations and chronological data, Makaske et al. (2002) proposed a four-stage model for channel evolution in the upper Columbia River (figure 2.5). For clarity the channel evolution model will be briefly discussed again.

The first stage in the model is the formation of a shallow channel on a crevasse splay. The second stage is reached when the channel has become deep enough and the banks have become steep enough to allow widening of the channel by bank slumping next to continued bank-toe bed scour. In the third stage, in-channel sedimentation becomes dominant. Two different stages of channel-filling were observed by Makaske et al. (2002) in the upper Columbia River. In gradually abandoning channels, which are inadequately supplied with coarse bedload, channel narrowing by lateral accretion of banks is the primary channel process (C_1). This narrowing might cause very low width/depth ratios. Alternatively, where abundant coarse traction load is available, old channel reaches may fill vertically with sand and become shallow (C_2). This type of channel-filling might lead to a high width/depth ratio. The fourth stage is that of fully abandoned channels, in which only suspended/wash load deposition takes place, termed residual channels.

The two different modes of channel-filling observed by Makaske et al. (2002) can be correlated by the differences in inner- and outer bend residual channels described in section 3.4.5.2. It can be concluded that the gradually abandoning channels, which are inadequately supplied with coarse bedload (C_1) are outer bend residual channels. The residual channels where abundant coarse traction load is available (C_2) are inner bend residual channels. This can be explained with the bend effect described in

Kleinhans et al. (2008). At bifurcations with an upstream bend, spiral flow forces bed material towards the inner bend bifurcate, while suspended sediment and wash load are forced towards the outer bend by the centrifugal force. Hence, sandy material is mainly trapped in inner bend residual channels and silt and clay mainly in outer bend residual channels. This effect is clearly illustrated in figures 3.48 and 3.49. The thickness of the clay and silt succession divided by the thickness of the sand succession in inner bend residual channel appears to be smaller then 1, whereas in outer bend residual channels this ratio is larger than 1.

The difference indicated by Makaske et al. (2002) in final stage between outer bend residual channels (D_1) and inner bend residual channels (D_2), can be seen in the present-day appearance of residual channels. The appearance of an outer bend residual channel described by Makaske et al. (2002) is conform the appearance of outer bend residual channels observed by the author (figure 2.5); highly vegetated levees with a small channel containing stagnant water. The appearence of inner bend residual channels described by Makaske et al. (2002) is not conform the appearance of the residual channels observed by the author (figure 5.1). The inner bend residual channels are not fully vegetated with trees; trees only grow on the levee, while the residual channel is vegetated with grass and Cyperacea (figure 5.2). The residual channel is located approximately one meter below the top of the levees, instead of located at the same level as the levees. A small channel containing stagnant water is indeed absent.

The appearance of inner bend residual channel might on the distance from the bifurcation point. Possibly only the entrance of an inner bend residual channel has a sandy fill, since all sand is deposited at the entrance of a closing bifurcate where the transport capacity significantly decreases. Downstream of the sandy fill the residual channel will then mainly consist of clay and silt. It follows that in this part of the inner bend residual channel the appearance will be comparable to that of an outer bend residual channel.

The outcome of this analysis is that the difference in channel-fill of outer and inner bend residual channels should be taken into account in further research to residual channels. When analysing different residual channels, the origin of the residual channel, and in inner bend residual channels the distance from the bifurcations, are factors that should be taken into account, since inner-bend residual channels contain far more sandy material than outer bend residual channels.

Further research is needed to test the above described hypothesis on the difference in inner- and outer bend residual channels. First of all, the above described findings need to be placed in a broader perspective. The residual channel-fill of several inner and outer bend residual channels should be compared for different rivers, and different river systems.

Fig. 5.1: Present-day appearance of outer-bend residual channel 034. See figure 3.4 for location.

Fig. 5.1: Present-day appearance of inner-bend residual channel 059. See figure 3.4 for location.

5.3. Equilibrium configurations

Bertoldi and Tubino (2005) found that the discharge ratio at experimental braided river bifurcations increases with increasing Shields stress (section 2.4.2). Edmonds and Slingerland (2008) found an opposite trend: in the Mossey delta of the Cumberland Marshes, the discharge ratio decreases with increasing Shields stress. Measurements of the area ratio in the upper Columbia River and bifurcations in the Cumberland Marshes performed for this research show the same trend as observed by Edmonds and Slingerland (2008) (section 3.4.6). The equilibrium configurations of the experimental braided river bifurcations of Bertoldi and Tubino (2005), and measurements on bifurcations in the Upper Columbia River and the Cumberland Marshes (section 3.4.6) are plotted together in figure 5.3. The bifurcations of Edmonds and Slingerland are not suitable to be plotted in the same figure. Note that the experimental braided river bifurcation asymmetry is characterized by a discharge ratio, whereas the bifurcation asymmetry in the upper Columbia River and the Cumberland Marshes is characterized by an area ratio. An estimation of the flow velocity with the Chézy equation in the upper Columbia River and the Cumberland Marshes indicates that the area ratio is approximately equal to the discharge ratio in the latter two rivers. Therefore the different measurements can be compared.
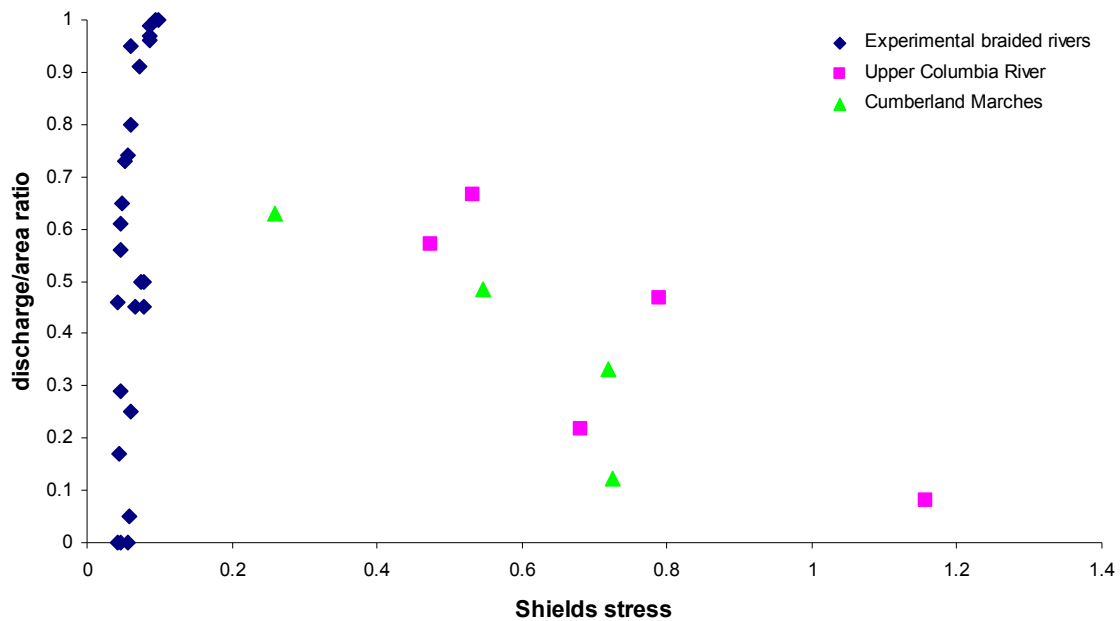
Fig. 5.3: Measured discharge/area ratio of experimental braided rivers of Bertoldi and Tubino (2005) (discharge ratio), the Upper Columbia River and the Cumberland Marshes (section 3.4.6) (area ratio).

Braided rivers are characterized by wide and shallow channels. Additionally, braided rivers have a bed containing mainly sand, gravel and boulders. This causes braided rivers to generally be characterized by low Shields stress. In the experiments of Bertoldi and Tubino (2005), the Shields stress was in the range of 0.04 to 0.1.

166

The channels in the upper Columbia River and Cumberland Marshes are relatively deep and narrow. The bed material is dominantly sandy. Compared to braided rivers, these river systems experience a relatively high Shields stress. The Shields stress at the measured bifurcations in the upper Columbia River and Cumberland Marshes employed in this research is in the range of 0.2 to 1.2.

Modelling results (section 4.4.3) indicate that when critical Shields stress is taken into account in the calculation of transport capacity, which is conform the natural situation, there is an optimum Shields stress for which the discharge division at a bifurcation is the least asymmetric. Depending on the disturbance, and the parameter varied to vary Shields stress, this optimum is located at a Shields stress in the range of 0.15 to 0.5. At Shields stresses lower than this optimum, the discharge ratio decreases for decreasing Shields stress, as observed by Bertoldi et al. (2005). At Shields stress higher than this optimum, the discharge ratio decreases for increasing Shields stress, as observed in the upper Columbia River and the Cumberland Marshes. In general, braided rivers experience Shields stresses lower than the optimum Shields stress and anastomosing and meandering rivers experience Shields stresses higher than the optimum Shields stress. Therefore the difference in response of discharge ratio on Shields stress between these river systems is explained by the presence of a critical Shields stress for sediment motion.

A second theory on the difference in response of braided, anastomosing and meandering river systems on Shields stress is also provided by the modelling results described in section 4.4.3. When the perturbance causing a bifurcation to become asymmetric is induced by a slope difference, a constant C is assumed to represent bed roughness, the perturbation is induced by the bend effect or a downstream slope difference between the two downstream bifurcates, a constant k_s is assumed to represent bed roughness and when the Shields stress is varied by varying discharge and thus water depth no optimum value of Shields stress is present for Shields stresses lower than 1.5. When all the above described criteria are fulfilled, the discharge ratio decreases for increasing Shields stress for the entire Shields stress range for both the fitted and MPM sediment transport predictors.

This response of discharge ratio on Shields stress is equal to the response of the experimental braided river bifurcations of Bertoldi and Tubino (2005). In braided rivers a disturbance causing a bifurcation to become asymmetric is mostly induced by a slope advantage and corresponding backwater effect in one of the bifurcates. Additionally, due to the montane setting of most braided rivers, these rivers respond quickly to rainfall and snow melt events causing the discharge in these river systems to be highly variable. In contrast the upper Columbia River is located in a gentle-sloped valley, consequently slope differences between different channels are marginal. The difference in response of braided rivers and anastomosing and meandering river systems on Shields stress might thus also be explained by the fact that in braided rivers the discharge is highly variable and the slope difference between bifurcates is relatively large.

167

It should be noted that for Shields stresses above the optimum Shields stress, the modelled decrease in discharge ratio for increasing Shields stress is not as strong as the decrease in discharge ratio measured in the upper Columbia River and the Cumberland Marshes. In the modelled results, the increase seems to be restricted by the strength of the disturbance. Modelling results indicate that when 3D effects, such as bar formation, are included in a model a bifurcation tends to become more asymmetric (Kleinhans et al., 2008). It might therefore be plausible that when a 3D model is applied to model the bifurcation asymmetry for a range of Shields stresses, there is a more abrupt decrease in discharge ratio for increasing Shields stress.

In order to test the hypotheses on the difference in response of braided rivers and anastomosing and meandering river systems on Shields stress, additional measurements and modelling on the influence of Shields stress on bifurcation equilibrium configurations in braided, anastomosing and meandering rivers have to be performed. Especially experiments and/or detailed 3D models covering the entire range of Shields stresses might provide useful information on the equilibrium configuration of braided, meandering and anastomosing rivers.

5.4. Network dynamics of anastomosing rivers

The evolution of river networks is mainly determined by the topology. Waterways through a network that are characterized by less bifurcations than confluences automatically become large waterways. This is clarified by the fact that the more a channel splits into two channels, the smaller the discharge through each channel becomes. Additionally, under the assumption of a constant k_s, it is hydraulically less efficient to transport flow and sediment in multiple channels than in a single channel. Confluences thus attract flow in a river network. Further, the division of flow and sediment is determined by the local parameters at a bifurcation, such as an upstream bend and a slope advantage in one of the bifurcates. It should be noted, however, that the mixing of the flow of the two channels that join at a confluence forms a shear layer which on its turn causes head loss at a confluence. This might damp the efficiency advantage of a confluence waterway. It is unknown which of these factors is the most important. Most likely, the influence of the efficiency advantage will be larger than the influence of the head loss. In particular, this appears to be true for the upper Columbia River, since the scour hole depth of confluences in this river is smaller than the depth predicted by scour hole depth predictors (figure 3.54), which indicates relatively little head loss. In order to quantify the efficiency effect relative to the head loss effect, flume experiments on river networks should be performed.

Since the channels in the upper Columbia River are hardly able to erode their banks, their positions are fixed. The position of the channels is mainly determined during their formation. The formation of a new channel originates from a crevasse. Eventually, the crevasse evolves into a throughflowing channel. The position of the crevasse thus determines the position of the later channel in the network, since the channel is hardly able to adjusts its position by lateral erosion. Once the newly formed channel connects to a downstream channel, it has become linked in the network. Additionally, this might affect the network in a different way; in the upper Columbia River, a significant amount of bifurcations occurs within a short range (0-300m) of a confluence. In the Spillimacheen-Castledale reach, this is the case for bifurcation 5, 12, 14 and 15 in figure 4.15. This can be explained as follows. At a confluence, due to secondary flow induced by the mixing of the flow of the two upstream channels, a scour hole is formed. The sediment eroded from this scour hole, is deposited slightly downstream forming a bar (figure 2.13). In anastomosing rivers, such as the upper Columbia River, lateral erodibility is very small. Consequently, the bar is the shallowest point in the channel. This causes this position to be vulnerable for avulsion. So, due to the formation of a bar downstream of confluences, a relatively large amount of avulsions occur just downstream of confluences and consequently a large amount of bifurcations occurs within a short range of a confluence.

5.5. Origin of anastomosis

There are two main hypotheses on the origin of anastomosis (section 2.3.2). For clarity, both hypotheses are briefly discussed again.

Nanson and Knighton (1996) state that a river in a state of dynamic equilibrium adjusts its channel pattern, cross-sectional geometry, slope and roughness in order to balance the available sediment load with the ability to transport this load. Therefore, the temporal and spatial persistence of anabranching systems indicates that in certain situations they must exhibit considerable advantages over their single-thread counterparts.

In cases where rivers gradients cannot easily be increased or sinuosity can be reduced to carry a larger sediment load, then an increase in the sediment/water discharge ratio must be accommodated by an increase in the rate of work being done per unit area of the bed. This can be accomplished by a shift from single to multiple channels, which, according to them, leads to an increase in sediment transport rate per unit water (Nanson and Knighton, 1996).

The second hypothesis on the origin of anastomosis is that of Makaske (2001). Makaske (2001) states that frequent avulsion and/or slow abandonment of old channels lead to continuing coexistence of younger deepening channels and old vertically infilling channels, composing an anastomosing system. Thus, if the avulsion duration exceeds the interavulsion period multiple channels (anastomosis) will occur. Abbado et al. (2005) and Makaske et al. (2009) indicate that avulsion of the upper Columbia River is mainly caused by the large upstream sediment supply, caused by tributaries such as the Spillimacheen River.

The Nanson and Knighton (1996) hypothesis on the origin of anastomosis implicates that anastomosis is an equilibrium channel pattern, whereas Makaske (2001) states that it is a disequilibrium channel pattern.

Results of the simple network analysis in section 4.4.4 indicate that when a constant C is assumed, it is hydraulically more efficient to transport flow and sediment over multiple channels. When a constant k_s is assumed, it is hydraulically less efficient to transport flow and sediment over multiple channels. Both roughness assumptions can be justified. A shift from a single channel to multiple channels causes the wall friction to increase since from hydraulic geometry (section 3.4.2) it follows that the hydraulic radius increases when channels transport less discharge. Consequently, in this case it becomes hydraulically less efficient to transport flow and sediment through multiple channels. On the other hand, bedform dimensions are larger in large channels than they are in small channels. This might counteract the effect of an increase in wall friction for a shift from a single to multiple channels, causing C to be equal in small and large channels.

In the latter case, the hypothesis proposed by Nanson and Knighton (1996) holds. However, in nature bed roughness is not characterized by a constant C or k_s, but the truth lays somewhere in between. Results of the simple network analysis indicate that the effect of a constant k_s on the difference in flow efficiency over a single channel and multiple channels is larger than the effect of a constant C. Hence it is concluded that an increase from a single to multiple channels is hydraulically less efficient. Therefore the Nanson and Knighton (1996) hypothesis does not explain anastomosis in the upper Columbia River. This agrees with Tabata and Hickin (2003) and Abbado et al. (2005) who concluded the same, but by means of different analyses.

According to the Makaske (2001) hypothesis, frequent avulsion and/or slow abandonment of old channels lead to the coexistence of multiple channels. Frequent avulsion is caused by a high channel bed aggradation rate. Makaske et al. (2009) indicated that the cause of the well-developed anastomosis between Spillimacheen and Castledale is caused by a high aggradation rate induced by the large sediment feed of the Spillimacheen River.

Modelling results of a 21km reach of the upper Columbia River, comprising the reach characterized by the well developed anastomosis between Spillimacheen and Castledale, indicate that there is, indeed, a high aggradation rate in this reach due to the large sediment feed of the Spillimacheen River (section 4.4.5.6). The modelling results indicate that the gentle slope measured in most of the upper Columbia River is the equilibrium slope of this river. The steep slope between Spillimacheen and Castledale measured by Abbado et al. (2005) is a disequilibrium slope. When a sediment pulse of on average three times the transport capacity is fed into the modelled upper Columbia River reach for 150yr, the bed slope measured by Abbado et al. (2005) is reproduced. It follows that the well developed anastomosis between Spillimacheen and Castedale is caused by a sediment pulse from the Spillimacheen River, since a high channel bed aggradation rate causes a high avulsion frequency and thus the coexistence of multiple channels. After this pulse the network will most likely evolve towards a single main channel again in the absence of a new sediment pulse.

This implicates that anastomosis in the upper Columbia River is a disequilibrium channel pattern. However, results of the network model applied to the Spillimachine-Castledale (section 4.4.5.4) indicate that the river network is in equilibrium after approximately 1000yr. This is caused by the facts that (1) avulsion is not able to occur in the network model and (2) that closing bifurcates do not close off completely to become residual channels.

A sediment pulse of 150yr of on average 3 times the transport capacity is applied since it leads to the best possible reproduction of the upper Columbia River valley slope. However, the magnitude and duration of the sediment overload pulse might possibly deviate up to a factor three. Additionally, the time that it takes for the upstream part of the Spillimachine-Castledale reach to adjust its slope to the initial equilibrium slope after the pulse might deviate by a factor three. The sediment pulse might for example be caused by an increase in logging activity in the source area of a tributary.

Observations indicate that the crevasse and avulsion activity the upper Columbia River has significantly decreased over the last decades (prof. Derald G. Smith, personal communication). This agrees with the sediment pulse hypothesis. During the sediment pulse the crevasse and avulsion activity is relatively high. After the sediment pulse, the crevasse and avulsion activity decreases. The modelling results indicate that it takes approximately 60yr to adjust the valley slope to match the current measured valley slope. This corresponds to the observed decrease in crevasse and avulsion activity over the last decades.

In conclusion, the origin of anastomosis in the upper Columbia River is explained by the Makaske (2001) hypothesis. Anastomosis in the upper Columbia River is a disequilibrium form. Frequent avulsion leads to continuing coextistence of multiple channels on the floodplain. Frequent avulsion in the upper Columbia River is induced by a sediment pulse.

The cause of anastomosis in other anastomosing river systems (Makaske, 1998) might possibly also be a constant overload of sediment or a temporary sediment pulse. Since bifurcations are unstable, river networks are unstable, therefore without a perturbation (high upstream sediment supply, either constant or with a pulse) a single channel will be present in stead of an anastomosing channel pattern.

6. Conclusions

Results of a literature research, fieldwork and modelling are combined to explain the network dynamics and the origin of anastomosis of the upper Columbia River. The main conclusions are the following:

- At bifurcations the division of flow and sediment is mainly induced by a slope advantage in one of the bifurcates or an upstream bend. An upstream bend forces bedload into the inner bend bifurcate and suspended load into the outer bend bifurcate. Therefore, inner bend bifurcates mainly fill with sand and gravel, whilst outer bend bifurcates mainly fill with clay and silt. The ratio of the thickness of the clay and silt succession divided by the thickness of the sand and gravel succession is larger than 1 for outer bend residual channels, and smaller than 1 for inner bend residual channels.

- In natural bifurcations, there appears to be an optimum Shields stress for which the discharge division at a bifurcation is most symmetric. This optimum is in the range of 0.15 to 0.5. For Shields stress lower than the optimum value, the bifurcation becomes more asymmetric with decreasing Shields stress. For Shields stress higher than the optimum value, the bifurcation becomes more asymmetric with increasing Shields stress. In general, braided rivers have Shields stresses lower than the optimum value, whereas meandering and anastomosing rivers have Shields stress larger than the optimum value.

- When a constant C is assumed to represent bed roughness, it is more efficient to transport flow and sediment in multiple channels than in a single channel. When a constant k_s is assumed to represent bed roughness, it is more efficient to transport flow and sediment in a single channel than in multiple channels. The effect of the latter roughness assumption is the largest.

- The discharge division in large river networks appears to be mainly determined by the topology, the more bifurcations a channel has upstream, the more the discharge is divided over multiple channels so the less discharge is transported through this channel. Additionally, the discharge configuration is slightly influenced by the amount of downstream confluences and bifurcations and the slope in the bifurcates, which affect the backwater curve in both bifurcates and thus the discharge division at the bifurcation. Finally, an upstream bend influences the discharge division at a bifurcation, and therefore the discharge configuration in a river network.

- If the bed roughness in a natural river network is characterized by a constant C, the Nanson and Knighton (1996) hypothesis on the origin of anastomosis is plausible. If the bed roughness in a natural river network is characterized by a constant k_s, the Makaske (2001) hypothesis on the origin of anastomosis is the most plausible. Since the effect of a constant k_s on the difference in flow efficiency between a single and multiple channels is significantly larger

then the effect of a constant *C*, in nature the hypothesis of Makaske (2001) is the most plausible.

- The well-developed anastomosis in the Spillimacheen-Castledale reach is caused by a sediment pulse from the Spillimacheen River. By imitating the Spillimacheen-Castledale reach by a model the steep slope of this reach can be reproduced by a pulse of 150yr with a sediment feed of on average three times the transport capacity. It follows that the Makaske (2001) hypothesis on the origin of anastomosis explains anastomosis in the upper Columbia River. Sediment pulses induce a high avulsion rate, and therefore cause the coexistence of multiple channels on the floodplain. In the absence of a new sediment pulse the river network will most likely evolve towards a single main channel again. Consequently anastomosis in the upper Columbia River is a disequilibrium channel pattern.

References

Abbado, D., Slingerland, R., Smith, N.D., 2005. Origin of anastomosis in the upper Columbia river, British Columbia, Canada. Special publications international association of sedimentologists 35, 3-15.

Ashmore, P., Parker, G., 1983. Confluence scour in coarse braided streams. Water resources research 19, 392-402.

Asselman, N.E.M., 2000. Fitting and interpretation of sediment rating curves. Journal of Hydrology 234, 228-248.

Bagnold, R.A., 1977. Bed load transport by natural rivers. In Abbado, D., Slingerland, R., Smith, N.D., 2005. Origin of anastomosis in the upper Columbia River, British Columbia, Canada. Special publications international association of sedimentologists 35, 3-15.

Berendsen, H.J.A., Stouthamer, E., 2001. Palaeogeographical development of the Rhine-Meuse delta, The Netherlands. Assen: Koninklijke Van Gorcum, 268.

Bertoldi, W., Tubino, M., Zolezzi, G., 2001. Laboratory measurements on channel bifurcation. 2nd International symposium on River, Coastal and Estuarine processes.

Bertoldi, W., Tubino, M., Zolezzi, G., 2002. Experimental observations of River bifurcations with uniform and graded sediments. River flow, Louvain le Neauve.

Bertoldi, W., Tubino, M., 2005. Bed and bank evolution of bifurcating channels. Water Resources Research 41, W07001, doi:10.1029/2004WR003333.

Bertoldi, W., Tubino, M., 2007. River bifurcations: Experimental observation on equilibrium configurations. Water Resources Research 43, W10437, doi:10.1029/2007WR005907.

Best, J.L., Reid, I., 1985. Seperation zone at open-channel junctions. Journal of hydraulic engineering 110, 1588-1594.

Best, J.L., 1986. The morphology of river channel confluences. Progress in physical geography 10, 157-174.

Best, J.L., Roy, A.G., 1991. Mixing-layer distortion at the confluence of channels of different depth. Nature 350, 411-413.

Biron, P.M., Richer, A., Kirkbride, A.D., Roy, A.G., Sangsoo Han, 2002. Spatial patterns of water surface topography at a river confluence. Earth surface processes and landforms 27, 913-928.

Biron, P.M., Ramamurthy, A.S., Sangsoo Han, 2004. Three-Dimensional numerical modelling of mixing at river confluences. Journal of hydraulic engineering 130, 243-253.

Blanckaert, K., De Vriend, H.J., 2003. Nonlinear modelling of mean flow redistribution in curved channels. Water resources research 39, 1375, doi: 10.1029/2003/WR002068.

Bolla Pittaluga, M., Repetto, R., Tubino, M., 2003. Channel bifurcation in braided rivers: equilibrium configurations and stability. Water resources research 39, 1046.

Bulle, H., 1926. Untersuchungen über die geschiebeableitung bei der spaltung von wasserläufen. Technical report, VDI Verlag, Berlin.

De Heer, A.F.M., Mosselman, E., 2004. Flow structure and bedload distribution at alluvial diversions. Proceedings of "River Flow 2004" (Napoli, Italy) 1, 801-806.

Edmonds, D.A., Slingerland, R.L., 2008. Stability of delta distributary networks and their bifurcations. Water resources research 44, W09426, doi:10.1029/2008WR006992.

Engelund, F., Hansen, E., 1967. A monograph on sediment transport in alluvial streams. Teknisk Forlag, Kobenhavn, Denmark.

Ferguson, R.I., Parsons, D.R., 2003. Flow in meander bends with recirculation at the inner bank. Water resources research 39, doi: 10.1029/2003WR001965.

Frings, R.M., Kleinhans, M.G., Vollmer, S., 2008. Discriminating between pore-filling load and bed-structure load: a new porosity-based method, exemplified for the river Rhine. Sedimentology 55, 1571-1593.

Hirose, K., Hasegaw, K., Meguro, H., 2003. Experiment and analysis of mainstream alternation in a bifurcated channel in mountain rivers. Proceedings of "3rd IAHR symposium RCEM"(Barcelona, Spain), vol. 1, edited by A. Sanchez-Arcilla and A. Bateman, pp. 571-583.

Huang, H.Q., Nanson, G.C., 2007. Why some alluvial rivers develop an anabranching pattern. Water resources research 43, 1-12.

Kjerve, B., Shao, C.C., Stapor, F.W., 1979. Formation of deep scour holes at the junction of tidal creeks: a hypothesis. Marine geology 33, 9-14.

Kleinhans, M.G., Jagers, H,R,A., Mosselman, E., Sloff, C.J., 2006. Effect of upstream meanders on bifurcation stability and sediment division in 1D, 2D and 3D models. River Flow 2006, 1355-1362.

Kleinhans, M.G., 2005. Flow discharge and sediment transport models for estimating a minimum timescale of hydrological activity and channel and delta formation on Mars. Journal of geophysical research 10, E12003, doi:10.1029/2005JE002521.

Kleinhans, M.G., Jagers, H.R.A., Mosselman, E., Sloff, C.J., 2008. Bifurcation dynamics and avulsion duration in meandering rivers by one-dimensional and three-dimensional models. Water resources research 44, 1-31.

Kleinhans, M.G., Schuurman, P., Bakx, W., Markies, H., 2009. Meandering channel dynamics in highly cohesive sediment on an intertidal mud flat in the Westerschelde estuary, the Netherlands. Geomorphology 105, 261-276.

Locking, T., 1983. Hydrology and sediment transport in an anastomoing reach of the upper Columbia River, B.C. MSc. thesis, Department of Geography, University of Calgary, Alberta, Canada.

Makaske, B., 1998. Anastomosing rivers; forms, processes and sediments. Netherlands Geographical Studies, 249, 1-298.

Makaske, B., 2001. Anastomosing rivers: a review of their classification, origin and
 sedimentary products. Earth-science reviews 53, 149-196

Makaske, B., Smith, D.G., Berendsen, H.J.A., 2002. Avulsions, channel evolution and floodplain
 sedimentation rates of the anastomosing upper Columbia River, British Columbia, Canada.
 Sedimentology 49, 1049-1071.

Makaske, B., Smith, D.G., Berendsen, H.J.A., de Boer, A.G., van Nielen-Kiezebrink, M.F., Locking, T.,
 2009. Hydraulic and sedimentary processes causing anastomosing morphology of the upper
 Columbia River, British Columbia, Canada. Geomorphology 111, 194-205.

Meyer-Peter, E., Mueller, R., 1948. Formulas for bed-load transport. Proceedings 2nd
 meeting, 39-64, International association for hydraulic structures research, Stockholm.

Miori, S., Repetto, R., Tubino, M., 2006. A one-dimensional model of bifurcations in gravel
 bed channels with erodible banks. Water resources research 42, W11413,
 doi:10.1029/2006WR004863.

Nanson, G.C., Huang, H.Q., 1999. Aabranching rivers: divided efficiency leading to fluvial diversity.
 Varieties of fluvial forms, 477-494.

Nanson, G.C., Knighton, A.D., 1996. Anabranching rivers: their cause, character and
 classification. Earth surface processes and landforms 21, 217-239.

Parker, G., Klingeman, P., McLean, D., 1982. Bedload and size distribution in paved gravel-bed
 streams. Journal of hydraulic engineering 108, 544-571.

Rhoads, B.L., Kenworthy, S.T., 1998. Time-averaged flow structure in the centsral region of a stream
 confluence. Earth surface processes and landforms 23, 171-191.

Ribberink, J.S., 1998. Bed-load transport for steady flows and unsteady oscillatory flows. Coastal
 Engineering 34, 59-82.

Rouse, H., 1937. Modern conceptions of mechanics of fluid turbulence. In Abbado, D.,
 Slingerland, R., Smith, N.D., 2005. Origin of anastomosis in the upper Columbia
 river, British Columbia, Canada. Special publications international association of
 sedimentologists 35, 3-15.

Slingerland, R., Smith, N.D., 1998. Necessary conditions for a meandering-river avulsion.
 Geology 26, 435-438.

Slingerland, R., Smith, N.D., 2004. River avulsions and their deposits. Annual reviews of earth
 science 32, 257-285.

Smith, D.G., 1983. Anastomosed fluvial deposits: modern examples from Western Canada.
 Special publications international association of sedimentologists 6, 155-168.

Soulsby, R., 1997. Dynamics of marine Sands, 215., Thomas Telford, London.

Stouthamer, E., Berendsen, H.J.A., 2000. Factors controlling the Holocene avulsion history of
 the Rhine-Meuse delta. Journal of sedimentary research 70, 1051-1064.

Stuiksma, N., Olesen, K., Flokstra, C., de Vriend, H., 1985. Bed deformation in curved alluvial channels. Journal of hydraulic research 23, 57-79.

Tabata, K.K., Hickin, E.J., 2003. Interchannel hydraulic geometry and hydraulic efficiency of the anastomosing Columbia River, Southeastern British Columbia, Canada. Earth surface processes and landforms 28, 837-852.

Törnqvist, T.E., 1994. Middle and late Holocene avulsion history of the river Rhine (Rhine-Meuse delta Netherlands). Geology 22, 711-714.

Van Rijn, L.C., 1984a. Sediment transport, part I. Bed load transport. Journal of hydraulic engineering 110, 1431-1456.

Van Rijn, L.C., 1984b. Sediment transport, part II. Suspended load transport. Journal of hydraulic engineering 110, 1613-1641.

Wang, Z., Dittrich, A., 1992. A study on problems in suspended sediment transportation. In; 2nd International conference on hydraulic and environmental modelling of coastal, estuarine and river waters, university of Bradford, UK.

Wang, Z., Fokkink, R., de Vries, M., Langerak, A., 1995. Stability of river bifurcations in 1d morphodynamic models. Journal of hydraulic research 33, 739-750.

Whetten, J.T., Kelley, J.C., Hanson, L.G., 1969. Characteristics of Columbia River sediment and sediment transport. Journal of Sedimentary Petrology 39, 1149-1166.